

THE UNIVERSITY *of* EDINBURGH

This thesis has been submitted in fulfilment of the requirements for a postgraduate degree (e.g. PhD, MPhil, DClinPsychol) at the University of Edinburgh. Please note the following terms and conditions of use:
This work is protected by copyright and other intellectual property rights, which are retained by the thesis author unless otherwise stated.
A copy can be downloaded for personal non-commercial research or study, without prior permission or charge.
This thesis cannot be reproduced or quoted extensively without first obtaining permission in writing from the author.
The content must not be changed in any way or sold commercially in any format or medium without the formal permission of the author.
When referring to this work, full bibliographic details including the author, title, awarding institution and date of the thesis must be given.

The effect of extracellular vesicles on the acquisition of radiotherapy resistance in triple-negative human breast cancer and canine mammary carcinoma

By Chantell Payton

This thesis is presented for the degree of Doctor of Philosophy at the University of Edinb



THE UNIVERSITY *of* EDINBURGH

Declaration

I declare that I have composed this thesis and that the work presented here is my own, except where acknowledgment has been made in the text. This work has not been submitted for any other degree or professional qualification at any other University.

Chantell Payton

Acknowledgments

Firstly, I would like to thank Prof. David Argyle for accepting me for this project and Dr.Lisa Pang for ensuring I made it to the end! A huge thank you to everyone in the Argyle group, especially Rhona Muirhead for the endless hour of Ultra-centrifugation and getting half-naked in air showers to help me irradiate endless boxes of plates. I would also like to thank Bob Fleming, Graeme Robertson, Steve Mitchell and Dr Anna Raper, without their patience and positivity during my many bioimaging hours, my experience would have been very different!

Secondly, I want to thank those responsible for allowing me to develop my skillsets that contributed to my entry to this PhD. Therefore, I want to thank Prof. Colin Butter, Prof. Lisa Collins and Dr Matthew Simmonds who taught me how to begin to navigate the scientific research world ever since my first few months as a baby-faced scientist at the University of Lincoln, right through to the end where I was interviewing for PhD positions. I especially want to thank Dr Stefan Milson, who at no benefit to himself, ensured I had whatever research experience was attainable to make sure my career goals would never be out of reach.

Thirdly, to my Roslin friends that provided motivation during the tough times; Dr Jo Stevens, Charlotte Woolley, Tom Watson, Jordan Mitchell, Susan Dan-Jumbo, and my dearest Dr Giulia Ferrari, you were there for me to vent and show my ugly western blots to, but also to coax me along (and drag me to the gym) when I was running out of PhD energy. I also want to thank my close friends outside of Roslin; Daniel Scott, Sarah Barker, Erin Ffur, Robin and Hayley Broadbent, Mathew Caird, Derek Warriner, Ruari Blake and Peter Alexander. Without all your support my life in Edinburgh would have been considerably different, especially through the rougher times, if it weren't I would not be where I am today. I want to say a final thank you to my parents, my brother and my partner Alessandro for their constant enthusiasm while celebrating my successful experiments with me, even when they weren't quite sure of the experiments we were celebrating. The support from my family and

friends cannot be understated during this PhD, as nobody would have predicted a literal world pandemic would happen partway through my studies. Without you all, my time at Edinburgh would have been considerably more stressful if I hadn't had your support.

I am especially grateful to Prof. Argyle for allowing me to do this project, as I feel the life-changing abilities our pets have on our day-to-day life mental health are immeasurable, but this is suddenly overlooked when it comes to promoting funding for research in veterinary medicine. This project uses canine and human breast cancer cell lines in parallel, allowing the molecular features of these cell lines to be compared. My personal motivation for this project was to provide building blocks to show dogs are not only "models" for human medicine, but to emphasise how life-altering cancer treatment used in human medicine could apply to veterinary cancer patients, and I hope that findings from this project may contribute, even if only slightly, to advancements in veterinary oncology.

I dedicate this thesis to my best friend for over half of my life; my golden retriever Angel, who died of cancer in April 2020.

Lay Summary

Radiotherapy is used to treat breast cancer, but cancer cells can become tolerant to doses of radiotherapy that should be lethal, known as radioresistance. Once cancer cells become radioresistant, they can survive radiotherapy, allowing cancer to regrow and spread around the body, which greatly increases the chances of the patient dying. This study looks at how cancer cells can become radioresistant in human breast cancer and canine mammary carcinoma. Extracellular vesicles (EVs) are incredibly small spherical bubbles (30 – 150 nm) that are produced by most cells. In healthy cells, EVs are used for cell to cell communication. The cell that makes EVs (parental cell) can pack specific molecular content from within their cell, which translates in to a message which is read when taken up by another cell (recipient cell). Studies have shown that EVs produced by cancerous cells, contain messages that can advise the recipient cell how to alter cellular pathways to grow quicker and become motile, which can lead to cancer cells spreading around the body, often proving fatal for the patient (Arscott *et al.,* 2013; Mutschelknaus *et al.,* 2017). Therefore, the working hypothesis for this project is that EVs from radioresistant cancer cells can cause non-radioresistant cells to develop radioresistance. To identify if this is biologically possible, EVs were isolated from non-radioresistant cells and radioresistant cells to use them in experiments to observe the effects of the EVs on cells that received chemotherapy and radiotherapy. If EVs from radioresistant cells could confer radioresistance to other cells, EVs could be broken open to read any potential messages that could be sent to recipient cells. This would allow future studies to block or interfere with the messages that advise how to become radioresistant, which could inhibit radioresistance developing in human and canine breast cancer.

The findings of this project showed EVs from radioresistant cancer cells could increase the growth rate, chemoresistance and radioresistance in recipient cancer cells with and without radioresistance. This project investigated the effect of EVs on cancer stem cells (a subpopulation of cells inside a tumour that are naturally

resistant to cancer therapies), and EVs from radioresistant cancer cells could promote the growth of cancer stem cells and further enhance cancer stem cell survival after chemotherapy and radiotherapy treatment.

To identify potential messages inside EVs produced from radioresistant cells, EVs derived from non-radioresistant and radioresistant cells were isolated and their proteins messages compared to identify potential new drug targets or biomarkers of radioresistance. The message revealed two key proteins as drivers of radioresistance; serine/threonine kinase (AKT) and Cyclin D1 (CCND1). In non=-cancerous cells, AKT regulates cell growth, proliferation, movement and plays a role in deciding if cells will die in a controlled manner called apoptosis. In non-cancerous cells, CCDN1 can help fix DNA damage and tightly regulates the cell cycle, deciding if and when cells can divide and grow. It was found that the EVs derived from radioresistant cancer cells had increased expression of AKT, potentially encouraging radioresistant cells to grow faster, prevents programmed cell death and activates cell motility. Secondly, an increased expression of CCND1 was identified to drive radioresistance. Normally, cells have a fixed timeframe to repair any (Deoxyribonucleic acid) DNA damage and if they fail to do so, they proceed to programmed cell death, this is how radiotherapy works – radiotherapy causes DNA damage in cancer cells at a rate they cannot repair and they proceed to cell programmed death. However, manipulation of CCDN1 allows radioresistant cells to increase the time they have to repair their DNA damage and survive a dose of radiotherapy that should result in programmed cell death. Interestingly, in published literature, these two proteins are also potential drivers of therapeutic resistance seen in cancer stem cells.

The similar molecular biology in the canine cancer cells and human cancer cells used in this project highlights the feasibility of using radioresistant canine cancer patients to further knowledge of human cancer and applying promising human therapies in veterinary medicine. This information could be used to advance and/or personalise

cancer treatment plans in both human and veterinary medicine. Future research could investigate using AKT and CCND1 inhibitors in patients with suspected radioresistance, as this may radiosensitise cancer cells and cancer stem cells, increasing the effectiveness of chemotherapy and radiotherapy to increase survival rates in human and veterinary patients with radioresistant cancer.

Abstract

Radiotherapy resistance is a significant challenge in the treatment of recurrent, advanced, and metastatic breast cancer in both humans and canines. Tumours are composed of a mixture of cell populations and can potentiate their own survival by fostering a highly dynamic microenvironment, of which extracellular vesicles (EVs) are emerging as important mediators of cellular communication. EVs are double membrane nanovesicles (30-150 nm) and their content reflects the cell of origin. EVs have active protein, nucleic acid and lipid content that can influence recipient cells proteome, and phenotype. The hypothesis of this project is that EVs derived from radioresistant cancer cells can confer resistance to recipient cells and profiling EV protein content will reveal how they influence oncogenic development, which may lead to the identification of novel targets for anti-cancer intervention. In this project, a panel of radioresistant cell lines derived from human and canine breast cancer cells were characterised, EVs were isolated from these cells and effects of these EVs on recipient cells were analysed. The data showed that EVs derived from radioresistant cells are more readily taken up, and can increase cell viability, colony forming ability, chemoresistance and radioresistance of recipient cells. EVs derived from radioresistant cancer cells could also increase the growth and proliferation of cancer stem cells and further enhance their chemotherapy and radioresistance in both human and canine cancer stem cell populations. To identify potential therapeutic targets or biomarkers of radioresistance, mass spectrometry analyses of protein content from EVs isolated from radioresistant and non-radioresistant breast cancer cells were analysed by bioinformatics. Results showed that overall, the protein content in EVs from radioresistant cells had higher expression of proteins associated with cell growth, proliferation and survival when compared to EVs derived from non-radioresistant cancer cells. Network analyses indicated AKT and CCND1 are potential drivers of radioresistance in both human and canine breast cancer, and theoretical downregulation of these molecules could inhibit the radioresistant phenotype. Biomarker analyses also predicted AKT and cell cycle regulator CCNH as potential biomarkers of radioresistance. These findings could be

used as building blocks for the advancement and/or personalisation of cancer treatment plans in human and veterinary medicine. In principle, dual AKT and CCND1 inhibitors could attenuate therapy resistance in radioresistant cells and cancer stem cells. This could mean that the effectiveness chemotherapy and radiotherapy may be increased; therefore, increasing overall survival and lifespan in human and veterinary patients with suspected radioresistance.

Abbreviations

AKT – serine/threonine kinase

ALDH - aldehyde dehydrogenase

ALK - Anaplastic lymphoma kinase

Alpha - α

APC - Antigen presenting cell

APOC1 - Apolipoprotein C1

ATM - Ataxia telangiectasia mutated

Beta - β

B cell - B lymphocyte

BC - Human breast cancer

BIRC - Baculoviral IAP repeat- containing

BSA – Bovine Serum Albumin

CAF - Cancer-associated fibroblast

CCND1 – Cyclin D1

CCNH – Cyclin H

CDE - Caveolin-dependent endocytosis

CMC - Canine mammary carcinoma

CME - Clathrin-mediated endocytosis

CO_2 – Carbon dioxide

COL1A1 – Collagen type 1 alpha 1 chain

DCIS – Ductal carcinoma *in situ*

DDR - DNA damage repair

DMEM – Dulbecco's modified Eagles medium

DMSO – Dimethl sulfoxide

DNA - Deoxyribonucleotide nucleic acid

DSBs - Double stranded breaks

DTT – Dithiothreitol

EMT - Epithelial to mesenchymal transition

ERα - Estrogen receptor

ERB2 - Human epidermal growth factor

ESCRT - Endosome sorting complex required for transport

ESR1 - Estrogen hormone receptor

FBS – Fetal bovine serum

FSC – Forward scatter

G1 - Gap 1

G2 - Gap 2

Gray - Gy

HIF1- α - Hypoxia inducible factor 1

HR - Homologous recombination

HRP – Horseradish peroxidase

HSP - Heat shock protein

IDs – Identifiers

IHC - Immunohistochemistry

ILV - Intra-luminal vesicle

IPA – Ingenuity pathway analysis

kDa - Kilo dalton

lcRNA - Long coding RNA

M - Mitotic phase

MET - Mesenchymal to epithelial transition

MFI – median fluorescence intensity

miRNA - Micro RNA

MISEV – Minimum information for studies of extracellular vesicles

mL – Millilitre

mM Millimolar

MMR - Mismatch repair

mRNA - Messenger RNA

mtDNA - Mitochondrial DNA

MVB - Multi-vesicular bodies

ncRNA - Non coding RNA

NHEJ - Non-homologous end joining

NK - Natural killer

nL - nanolitre

nM - Nanomolar

NonRR – non-radioresistant

nt - Nucleotide

NTA – Nanosight tracking analysis

P - Phosphorylated

PAGE – Polyacrylamide gel electrophoresis

PBS – Phosphate buffered saline

PHDs – Prolyl hydrolase

PR - Progesterone receptor

RHOGDI – Rho GDP-dissociation inhibitor

RIBE - Radiation induced bystander effect

RNA - Ribonucleotide acid

ROS - Reactive oxygen species

RR - radioresistant

rRNA - Ribosomal RNA

RT – Room temperature

S - Synthetic

SASP - Senescent-associated secretory phenotype

SD – standard deviation

SDS – Sodium dodecyl sulphate

SETX - Sentataxin

snRNA - Small nuclear RNA

SSBs - Single stranded breaks

SSC – Side scatter

TEAB - Triethylamonium bicarbonate

T cell - T lymphocyte

TEM – Transmission electron microscopy

TME - Tumour microenvironment

Tregs – Regulatory T cells

tRNA - Transfer RNA

TSG101 – Tumour suppressor gene 101

µL – Microlitre

µM – Micromolar

Contents

Declaration i
Lay Summary iv
Abstract vii
Abbreviations ix
List of Figures xvii
List of Tables xix
Chapter 1: Introduction 1
1.1. Cancer 1
1.2. Tumour microenvironment 1
1.3. Breast cancer in human and veterinary medicine 5
1.3.1. Breast cancer subtypes 6
1.4. Incidence and risk factors 10
1.4.1. Incidence 10
1.4.2. Gender 11
1.4.3. Age 11
1.4.4. Genetic factors 11
1.4.5. Obesity 12
1.5. Advantages of studying CMC in relation to human breast cancer 13
1.6. Breast cancer staging 14
1.7. Breast cancer treatment 16
1.7.1 Types of breast cancer removal surgery 17
1.7.2 Endocrine therapy for treatment of breast cancer 18
1.7.3 Chemotherapy treatment for breast cancer 19
1.7.3.1 Doxorubicin treatment for breast cancer 19
1.7.3.2 Immunotherapy for breast cancer 20
1.7.3.3 The use of PARP inhibitors for breast cancer treatment 21
1.7.4 Recent developments in breast cancer treatment 22
1.7.5 Radiotherapy treatment for breast cancer 23
1.7.6. Cancer stem cells 26
1.8. Radioresistance 27
1.8.1. Oxidative Stress 28
1.8.2. Hypoxia 28
1.8.3. Cell cycle and DNA damage response 29
1.9. Extracellular Vesicles 30

1.9.1 Current advancements in the use of EVs in clinical medicine 30
1.9.2 Current EV modification techniques.....33
1.9.3. EV biogenesis and formation..... 34
1.9.4 Formation, processing and packaging of ILVs within the MVB..... 37
1.9.5. Docking of MVBs at the cell membrane and release of EVs..... 40
1.9.6. EV uptake 42
1.9.7. EV composition 46
1.9.7.1 Protein content of EVs.....48
1.9.7.2 Nucleic Acid content of EVs.....50
1.9.7.3 Lipid content of EVs.....52
1.10. Role of EVs in cancer 53
1.10.1. Role of EVs in the tumour microenvironment..... 53
1.10.1.1 The role of EVs in the nurturing of developing cancer cells..... 54
1.10.1.2 The role of EVs in tumour-protective immune suppression 55
1.10.2. The role of EVs in the formation of pre-metastatic niches and distal metastasis 56
1.10.3. The role of EVs in the acquisition of radioresistance..... 57
1.10.4. Hypoxia and EVs 59
1.10.5. Radiation induced bystander effects..... 60
1.11.The rationale of the study: Hypothesis, aims and objectives 62
Chapter 2: Materials and Methods 65
2.1. General materials and methods..... 65
2.2. Tissue culture of cell lines 65
2.2.1. Maintenance of cell lines 66
2.2.2. Passaging of Adherent cells..... 66
2.2.3. Counting cells 66
2.2.4. Isolation of breast CSCs 67
2.2.5. Freezing and thawing cells 67
2.2.6. Maintenance of radioresistant phenotype..... 68
2.2.7. Preparation of EV depleted media 68
2.2.8. EV isolation via QIAGEN Exo-easy kit..... 69
2.2.9. EV isolation via ultracentrifugation 69
2.2.10. Transmission electron microscopy 70
2.2.11. Nanosight tracking analysis 70
2.2.12. Lysis and quantification of EV protein content..... 71
2.2.13. Fluorescent staining of EVs 71

2.2.14. Live imaging of EV uptake by recipient cells 72
2.2.15. Analysis of EV uptake via flow cytometry. 72
2.3. Protein methods 73
2.3.1. Harvesting and lysis of cell pellets 73
2.3.2. Quantification of protein concentration 73
2.3.3. SDS PAGE 74
2.3.4. Western blotting 74
2.3.5. Antibodies 75
2.3.6. Fluorescent detection of protein via the LICOR Odyssey 76
2.4. Cell cycle analysis 77
2.5. Migration assay 77
2.6. Colony formation assays with EV dose titrations 78
2.7. Colony formation assays after irradiation 79
2.8. Chemosensitivity assays 79
2.9. Tumoursphere formation assay 80
2.10.Cell viability 81
2.11.Analysis of EV content for mass spectrometry 82
2.11.1. Preparation of EV samples 82
2.11.2. Quantification of EVs samples by micro bicichoninic acid assay 82
2.11.3. EV protein digestion 83
2.11.4. Elution of EV peptides 83
2.11.5. Protein digestion, dimethyl labelling and liquid chromatography tandem mass spectrometry 84
2.12 Bioinformatic Analysis of Mass spectrometry data ..... Error! Bookmark not defined.
2.12.1 Analysis of EV protein content via Ingenuity Pathway Analysis 85
2.13 Statistical Analyses 86
2.13.1 Analyses of data to determine statistical significance 86
2.13.2 Analyses of protein data in IPA 86
Chapter 3: Characterisation of non-radioresistant and radioresistant cancer cells and optimisation of EV isolation 89
3.1 Introduction 89
3.2 Results 91
3.2.1 Radioresistant cells have a more spindle-like morphology than non-radioresistant cancer cells 91
3.2.2 Radioresistant REM134 RR and MDA-MB-231 RR breast cancer cells have a more mesenchymal phenotype 93

3.2.3 Radioresistant cell lines have a faster migration rate than non-radioresistant cell lines 95
3.2.4 Radioresistant cell lines have a higher percentage of cells in the G2 phase 97
3.2.5 Optimisation of EV isolation, quantification and visualisation 100
3.3 Discussion 105
Chapter 4: EVs derived from RR cancer cells can transfer radioresistance to recipient non-CSC and CSCs 113
4.1 Introduction 113
4.2 Results 115
4.2.1 EVs derived from RR cells increase cell viability of all recipient cells 115
4.2.2 EVs derived from RR cells have a greater rate of uptake 118
4.2.3 EVs derived from RR cells can increase the rate of migration of recipient breast cancer cells 121
4.2.4 EVs derived from RR cells can increase the chemoresistance of all naïve recipient cells and increase radioresistance of recipient cells 127
4.2.5 EVs derived from RR breast cancer cells can increase radioresistance of naïve and radioresistant recipient cancer cells 129
4.2.6 EVs derived from RR cells can increase chemotherapy resistance in recipient breast cancer stem cells 132
4.2.7 EVs derived from RR cells can increase radiotherapy resistance in recipient breast cancer stem cells 134
4.2.8 EVs derived from RR cells can increase the size and number of tumourspheres formed 136
4.3 Discussion 142
5 Chapter 5: Comparative analysis of the protein cargo of EVs derived from nonRR and RR cancer cell lines 150
5.1 Introduction 150
5.2 Results ..... Error! Bookmark not defined.
5.2.1 EVs derived from REM134 RR and MDA-MB-231 RR cell lines have higher expression of pro-oncogenic content and decreased expression of tumour and CSC suppressors when compared to their corresponding nonRR cancer cell lines ..... Error! Bookmark not defined.
5.2.1.1 Analysis of protein expression in EVs derived from REM134 RR cells 157
5.2.1.2 Analysis of protein expression in EVs derived from MDA-MB-231 RR cells 159
5.2.2 Functional analyses indicated enrichment of protein content associated with a more aggressive phenotype of cell growth, proliferation and migration and in the EVs derived from RR cells. 162

5.2.3 Analysis of canonical pathway activation indicated similarities in increased and decreased protein expression between the EVs derived from REM134 RR and MDA-MB-23 RR cell lines. 165

5.2.4 Potential novel targets of radioresistance could be cell cycle regulators and cell proliferation/migration proteins. 174

5.2.5 CCNH, COL1A1, CSTB, AKT1, ALK and APOC1 could be potential biomarkers of radioresistance 179

5.3 Discussion 182

5.3.1 EVs derived from REM134 RR and MDA-MB-231 RR breast cancer cells have increased expression of pro-survival and CSC proteins and decreased expression of tumour suppressor proteins 182

5.3.2 Networks associated with radioresistance in REM134 RR and MDA-MB-231 RR breast were highly similar and indicated the involvement of CSCs, cell cycle manipulation and proteins associated with EMT 187

5.3.3 IPA identified six potential biomarkers of radioresistance in REM134 RR and MDA-MB-231 RR breast cancer cells including AKT, COL1A1, APOC1, CCNH, ALK and CSTB 190

6 Chapter 6: Discussion 194

6.1 Radioresistant REM134 RR and MDA-MB-231 RR breast cancer cells have increased rates of migration and altered cell cycle distributions compared to their nonRR counterparts 195

6.2 EVs derived from REM134 RR and MDA-MB-231 RR breast cancer cells can induce chemotherapy and radiotherapy resistance potentially by promoting growth and proliferation of breast CSCs 196

6.3 Networks associated with radioresistance are DDR, CSCs and the AKT pathway 203

6.4 Biomarkers of radioresistance are associated with pathways such as DDR, AKT and CSCs 207

6.5 Future studies and directions 209

6.6 Limitations of this study 213

6.7 Conclusion 216

Chapter 7: References 219

Chapter 8: Appendix 266

Chapter 9: Publications 269

LIST OF FIGURES

FIGURE 1.1 SCHEMATIC OF THE TME. 3
FIGURE 1.3 HISTOLOGICAL STAINING OF TUMOURS FROM BC AND CMC DUCTAL CARCINOMA IN SITU (DCIS) 9
FIGURE 1.4 SUMMARY OF PATHWAYS ASSOCIATED WITH DNA REPAIR 25
FIGURE 1.5 A SUMMARY OF THE USES OF EVS IN HUMAN MEDICINE. 32
FIGURE 1.6 AN OVERVIEW OF EV FORMATION AND DEGRADATION/RELEASE.....36
FIGURE 1.7 THE ESCRT DEPENDENT PATHWAY. 37
FIGURE 1.8 THE ESCRT INDEPENDENT PATHWAY.. 38
FIGURE 1.9 LIPID RAFT DEPENDANT ILV FORMATION. 39
FIGURE 1.10 ILV FORMATION VIA THE CD63 TETRASPANINS AND FLOTILLINS. 40
FIGURE 1.11 SUMMARY OF THE MECHANISMS OF EV UPTAKE. 43
FIGURE 1.12 SUMMARY OF THE PROTEIN, NUCLEOTIDE AND LIPID CONTENT OF EVS 48
FIGURE 3.1 THE REM134 RR CELL LINE HAS A MORE MESENCHYMAL PHENOTYPE THAN REM134 CELLS. 92
FIGURE 3.2 ADHERENT BREAST CSCS DERIVED FROM RR CELL LINES HAVE A MORE MESENCHYMAL STEM TYPE 93
FIGURE 3.3 WESTERN BLOTS OF MARKERS OF EMT SHOW THAT THE RR CELL LINES HAVE AN INCREASED EXPRESSION OF MESENCHYMAL MARKERS. 94
FIGURE 3.4 RR CELL TYPES HAVE A FASTER MIGRATION RATE COMPARED TO THE NONRR CELL LINES.. 96
FIGURE 3.5 WORKFLOW FOR CELL CYCLE ANALYSIS. 98
FIGURE 3.6 RR CELL LINES HAVE A HIGHER PERCENTAGE OF CELLS IN THE G2 PHASE OF THE CELL CYCLE 99
FIGURE 3.7 WORKFLOW UTILISED TO ISOLATE, VISUALISE AND QUANTIFY EVS. 101
FIGURE 3.8 SIZE DISTRIBUTION OF VESICLES AFTER USING THE EXO-EASY ISOLATION KIT WITH AND WITHOUT UC. 102
FIGURE 3.9 ISOLATION OF EVS FROM ALL CELL LINES.. 104
FIGURE 4.1 WORKFLOW USED TO DETERMINE THE EFFECTS OF EVS ON RECIPIENT CELLS. 114
FIGURE 4.2 EVS DERIVED FROM REM134 RR AND MDA-MB-231 RR CELLS INCREASE THE CELL VIABILITY OF RECIPIENT CELLS. 115
FIGURE 4.3 EVS FROM REM134 RR AND MDA-MB-231 RR CELLS SIGNIFICANTLY INCREASE COLONY FORMING ABILITY 116
FIGURE 4.4 EVS FROM REM134 RR AND MDA-MB-231 RR CELLS SIGNIFICANTLY INCREASE COLONY FORMING ABILITY 117
FIIGURE 4.5 FLOW CYTOMETRY WORKFLOW TO QUANTIFY EV UPTAKE.....119
FIGURE 4.6 EVS DERIVED FROM REM134 RR AND MDA-MB-231 RR CELLS ARE MORE READILY TAKEN UP BY BOTH NONRR AND RR CANCER CELLS 120
FIGURE 4.7 EVS DERIVED FROM REM134 RR AND MDA-MB-231 RR CANCER CELLS INCREASE THE MIGRATION RATE OF ALL RECIPIENT CELLS. 125
FIGURE 4.8 EVS DERIVED FROM REM134 RR AND MDA-MB-231 RR CELLS INCREASED CHEMORESISTANCE IN RECIPIENT CELLS. 128
FIGURE 4.9 EVS DERIVED FROM REM134 RR AND MDA-MB-231 RR CELLS CAN INCREASE RECIPIENT CELL SURVIVAL FOLLOWING IRRADIATION 130

FIGURE 4.10 EVS DERIVED FROM REM134 RR AND MDA-MB-231 RR BREAST CANCER CELLS INCREASE THE CELL VIABILITY OF CHEMOTHERAPY NAÏVE BREAST CSCS 133
FIGURE 4.11 EVS DERIVED FROM MDA-MB-231 RR AND REM134 RR CELLS INCREASE THE BREAST CSC SURVIVAL FOLLOWING IRRADIATION 134
FIGURE 4.12 EVS DERIVED FROM NONRR AND RR CELL LINE CAN INCREASE THE NUMBER OF TUMOURSPHERES FORMED 137
FIGURE 5.1 PRELIMINARY HEATMAP ANALYSES SHOWED THAT EVS FROM THE REM134 RR AND MDA-MB-231 RR CANCER CELLS HAD MORE UPREGULATED PROTEINS THAN THEIR NONRR COUNTERPARTS..... 152
FIGURE 5.2 THE QUANTITY OF OVERLAPPING PROTEINS ASSOCIATED WITH RADIORESISTANCE WAS DETERMINED BY IPA CORE ANALYSES..... 153
FIGURE 5.3 FUNCTIONAL EXPRESSION ANALYSIS SHOWED EVS DERIVED FROM RR CELLS CONTAINED PROTEINS ASSOCIATED WITH A MORE AGGRESSIVE CELL PHENOTYPE. 165
FIGURE 5.4 CANONICAL PATHWAYS POTENTIALLY ACTIVATED BY EVS DERIVED FROM REM134 RR CELL LINE..... 168
FIGURE 5.5 EVS DERIVED FROM MDA-MB-231 RR CELLS POTENTIALLY ACTIVATE CANONICAL PATHWAYS ASSOCIATED WITH INCREASED CELL MIGRATION, SURVIVABILITY, PROLIFERATION AND DNA DAMAGE REPAIR..... 171
FIGURE 5.6 CANONICAL PATHWAY ENRICHMENT WAS SIMILAR WHEN COMPARING THE EV PROTEIN CONTENT DERIVED FROM THE REM134 RR AND THE MDA-MB-231 RR CELL LINES..... 174
FIGURE 5.7 NETWORKS ASSOCIATED WITH RADIORESISTANCE WERE SIMILAR BETWEEN THE EV CARGO DERIVED FROM REM134 RR AND MDA-MB-231 RR CELL LINES..... 177
FIGURE 5.8 DECREASING EXPRESSION OF CCND1 AND AKT COULD POTENTIALLY INHIBIT RADIORESISTANCE..... 179
FIGURE 5.9. CCNH, COL1A1, CSTB, AKT1, ALK AND APOC1 WERE IDENTIFIED AS POTENTIAL BIOMARKERS FOLLOWING IPA ANALYSES..... 180
FIGURE 6.1 EVS DERIVED FROM RADIORESISTANT BREAST CANCER CELLS CAN INDUCE RADIORESISTANCE IN RECIPIENT CELLS 202
FIGURE 6.2 TRANSFER OF EVS FROM RADIORESISTANT BREAST CANCER CELLS APPEARS TO BE ASSOCIATED WITH THE INDUCTION OF CANCER STEM CELLS..... 208

List of Tables

TABLE 1.1 CMC STAGING IN FEMALE CANINES……15
TABLE 1.2 BC STAGING IN HUMANS……16
TABLE 1.3 SUMMARY OF SURGICAL OPTIONS FOR THE REMOVAL OF BC……17

TABLE 2.1 THE TABLE OF PRIMARY ANTIBODIES USED WITH THE EXPECTED BAND SIZE IN KDA AND THE WORKING DILUTION FACTOR……75
TABLE 2.2 TABLE OF SECONDARY ANTIBODIES WITH THEIR WORKING DILUTION ALONG WITH THE COMPANY AND CATALOGUE NUMBER……76

TABLE 3.1 REM134 RR AND MDA-MB-231 RR CELL LINES HAVE ALMOST DOUBLE THE PERCENTAGE OF CELLS IN THE G2 PHASE OF THE CELL CYCLE ……100
TABLE 3.2 RAW NTA DATA SHOWED THAT UC RESULTED IN A HIGHER CONCENTRATION OF VESICLES AT A LOWER SIZE RANGE COMPARED TO THE OTHER METHODS TRIALLED……103
TABLE 5.1 THE CONTENT FOUND IN EVS WERE MOSTLY LOCATED IN THE CELL CYTOPLASM…… ……154
TABLE 5.2 THE OVERLAPPING MOLECULES IN THE EVS DERIVED FROM THE RR CELL LINES……157
TABLE 5.3 MOLECULES WITH THE HIGHEST FOLD CHANGE IN THE EVS FROM REM134 RR CELLS WERE ASSOCIATED WITH EMT AND DNA DAMAGE REPAIR……157
TABLE 5.4 PROTEINS WITH DECREASED EXPRESSION FOLD CHANGE FROM THE REM134 RR CELLS INCLUDED TUMOUR SUPPRESSORS AND STEM-CELL INHIBITORS……158
TABLE 5.5 PROTEINS WITH INCREASED EXPRESSION FOLD CHANGE IN THE EVS DERIVED FROM MDA-MB-231 RR CELLS WERE ASSOCIATED WITH THE CELL CYCLE AND ALTERED MITOCHONDRIA……160
TABLE 5.6 PROTEINS WITH DECREASED EXPRESSION FOLD CHANGE IN EVS FROM MDA-MB-231 RR CELLS WERE ASSOCIATED WITH TUMOUR SUPPRESSION AND INCREASED CANCER RESISTANCE……16

Chapter 1: Introduction

1.1. Cancer

Cancer is the aberrant proliferation of cells that can metastasise to secondary sites, with this metastasis typically resulting in increased morbidity and decreased lifespan. The characteristics of cancer cells alter upon the acquisition of a malignant phenotype which results in enhanced survival; these characteristics have been termed “the hallmarks of cancer” in a seminal review (Hanahan and Weinberg, 2011, Hanahan and Weinberg, 2000). These hallmarks describe the changes that occur in cancer cells that dictate the growth, development and metastasis of cancer cells including: resisting cell death; deregulating cellular energetics; avoiding immune detection; tumour promoting inflammation; activating invasion and metastasis; genome instability and mutation; inducing angiogenesis; sustaining proliferative signalling; evading growth suppressors; invasion and metastasis; and immortality. These hallmarks of cancer rely on the composition and signalling from within the tumour microenvironment (TME) to facilitate the development of non-cancerous cells towards tumourigenesis and then a malignant phenotype.

1.2. Tumour microenvironment

The TME is composed of several cell types including fibroblasts; macrophages; dendritic cells; T cells; cytokines; epithelial cells and the extracellular matrix (ECM) (Belli *et al.,* 2022). The communication between the tumour and stroma plays a role in the modification of the stroma, which can aid the development of a tumour within the microbiological niche (Sağlam-Uçar *et al.,* 2022). The developing tumour can reprogramme cellular constituents of the TME such as alteration of the blood vasculature, myeloid cells and tumour regulated cells (Tregs) which contribute towards initial immune system evasion (Datta *et al*., 2019). To begin invasion, the malignant tumour cells must first break through the basement membrane by the

release of proteases (Chang *et al.,* 2022). This allows malignant cells to utilise tethered growth factors within the ECM whilst simultaneously promoting angiogenesis (Gaiko-Shcherbak *et al.,* 2022). The TME undergoes a transition during invasive growth by malignant cells which then supports the developing tumour (Guo *et al.,* 2022). In 1889, Paget proposed the seed and soil hypothesis, identifying the need for malignant tumour cells to communicate with the TME of the secondary site to metastasise.

Under a non-diseased state, a substantial blood supply provides nutrients and oxygen, and removes waste metabolites from cells; however, in a growing tumour, there is an increased demand for oxygen due to the rapidly proliferating cells present this increases the production of waste metabolites, creating a requirement for increased blood circulation (Westbrooke *et al.,* 2022). The increase in demand is achieved by the initiation of angiogenesis, potentiated by cellular communication mediated by cells including fibroblasts; cancer-associated fibroblasts; endothelial cells; and immune cells (Han *et al.*, 2022). Fibroblasts can become cancer-associated fibroblasts (CAFs) upon reprogramming by cancer cells (Ahn *et al.,* 2022). Upon transitioning to CAF cell type, CAFs possess tumour-promoting abilities, primarily via the remodelling of the ECM (Zhang *et al.,* 2022). Endothelial cells typically remain in a quiescent state in healthy adults, with a turnover rate of approximately 150 days (Hida *et al*., 2018), their turnover rate can increase from 20-2,000 times in the TME (Dudley, A. 2012). Further to increasing turnover rate, endothelial cells within a tumour can promptly respond to pro-angiogenic cues from tumour cells to contribute to new blood vessel formation (Zecchin *et al*., 2017). Examples of these pro-angiogenic cues include the secretion of growth factors to promote the proliferation of endothelial cells in capillary walls in the surrounding TME resulting in the outward growth of new capillaries to support the developing tumour (Oberkersch *et al.,* 2022). However, new blood vessel growth is slower than tumour growth due to high proliferation rates, leading to increased production of waste metabolites and a resulting acidic environment, which is not optimal for immune cells, aiding tumour evasion of the immune system (Worsley *et al.,* 2022). Such accelerated growth of endothelial cells in developing blood vessels means that they

do not fully mature, resulting in abnormal and leaky blood vessels, also hindering immune cell infiltration (van Beijnum *et al.,* 2022). Immune cells in the microenvironment include T and B cells, natural killer cells and antigen presenting cells such as macrophages and dendritic cells (Figure 1.1) (Belli *et al.,* 2022).

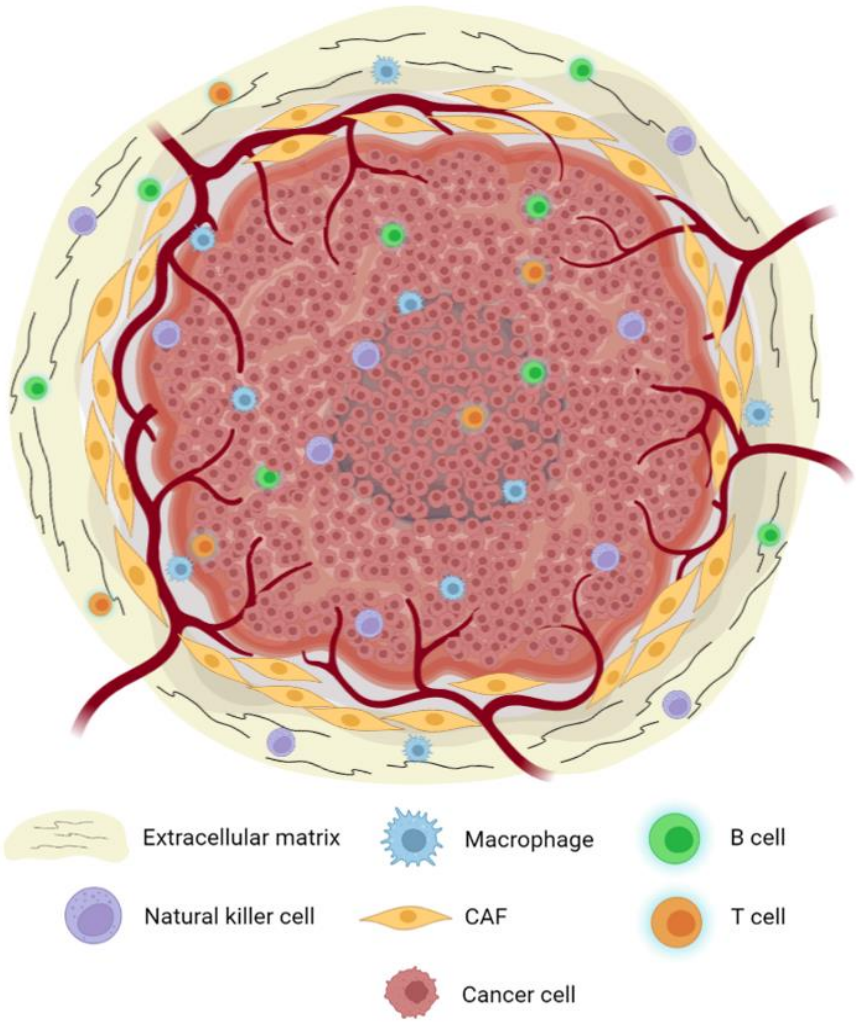


Figure 1.1 Schematic of the TME. *The cancer cells account for most of the tumour, and their growth develops a hypoxic centre (grey region) which then triggers angiogenesis to result in the formation of blood vessels to nurture the developing tumour. The tumour is surrounded by the extracellular matrix which is infiltrated by immune cells such as natural killer cells (NK cells), B and T lymphocytes (B and T cell), macrophages and CAFs (Adapted from Asgharzadeh et al., 2017 - Created in BioRender.com).*

Cancer cells can evade the immune system as the hypoxic environment impairs the ability of CD8 T cells and T helper cells to recognise and kill cancer cells (Zamarron and Chen, 2011). It has been found that CD4 T cells can be drawn to the TME by tumour-produced chemokines and are converted into immune-suppressing Treg cells (Curiel *et al.,* 2004). Tumours also evade the immune system via

downregulating the antigen processing of immune cells by the downregulation of antigen presenting MHC I molecules, and up-regulation of invariant chain protein, masking the presence of the few MHC proteins that are present on the surface of tumour cells (Dhatchinamoorthy *et al*., 2021). This evasion of the immune system aids the growth and spread of tumours to distal sites (Elder *et al.,* 2022).

The initiation of tumour propagation at a distal site requires the formation of a pre-metastatic niche (Qi *et al.,* 2022). To migrate, cancer cells undergo epithelial to mesenchymal transition (EMT) to travel throughout the body, many of these cells die via shear stress or anoikis (cell stress caused by detachment from the ECM) (Khan *et al.,* 2022). Cells that survive undergo mesenchymal to epithelial transition (MET) which is induced via activation of downstream signalling of STAT3 and c-MYC allowing cells to attach at a distant site (Figure 1.2) (Li *et al.,* 2022).

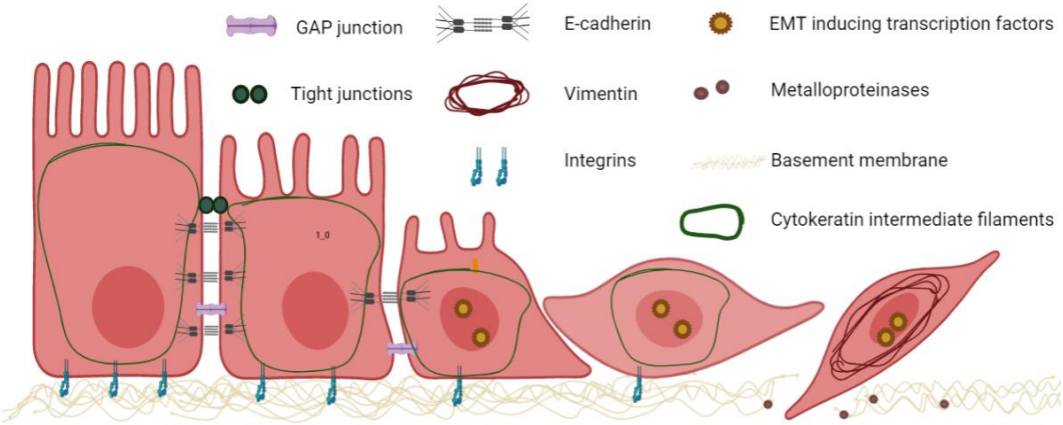


Figure 1.2 The process of Epithelial to Mesenchymal Transition. *The process depicts the differentiation that occurs upon the phenotype switch from an epithelial phenotype (left) to a mesenchymal phenotype (right). An epithelial phenotype is associated with the structured polarity of epithelial cells attached to the basement membrane with cell to cell junction proteins and tight junctions. A mesenchymal phenotype is the association of a change in cells after receiving signals from EMT transcription factors causing cells to detach from the basement membrane due to the production of matrix metalloproteinases (Adapted from Vaquero et al., 2017 - Created in BioRender.com).*

Therefore, upon the acquisition of a mesenchymal phenotype expression of the epithelial cell to cell junction marker E-cadherin would decrease, and mesenchymal markers such as β-catenin and vimentin would increase (Subbalakshmi *et al.,* 2022. EMT inducing transcription factors (Figure 1.2) include slug and snail which would

have increased expression as they are direct repressors of E-cadherin (Nakamura et al., 2018).

The propagating tumour cells begin to remodel the pre-metastatic niche to favour the growth of a new tumour (Elder *et al.,* 2022). Changes made include an increase in inflammation at the local TME site; induction of immune suppression and/or surveillance and an increase in angiogenesis and vascular permeability to support the proliferating tumour cells (Yang *et al.,* 2021).

1.3. Breast cancer in human and veterinary medicine

Human breast cancer (BC) is the leading cause of female mortality in 54% of the countries in the world, and the mortality rate of advanced BC is 80% within 5 years of diagnosis and most patients will eventually die of the disease (Bonotto *et al.,* 2014; Sorenmo *et al.,* 2020). This is an improvement of a mere 3% compared with a 30% improvement in the other stages of BC over the last 30 years. In 2020 ~2.3 million women were diagnosed with breast cancer, with this number expected to rise to ~3 million a year by 2040 (Sung *et al.,* 2021). Breast cancer is the most commonly diagnosed cancer in women, with triple-ngeative breast cancer accounting for 10-20% of breast cancer cases (Bray *et al.,* 2018; Fayaz *et al.,* 2019). Triple-negative breast cancer is more likely to metastasise and has a worse prognosis compared to receptor positive breast cancer subtypes (Ovcaricek *et al.,* 2011).

Likewise, canine mammary tumours are the most prevalent malignancies in intact older female dogs (Siegel *et al.,* 2019). Although canine mammary carcinomas (CMC) are not as widely researched as BC, the current data implies that the survival rates are like humans for canines with advanced solid tumours (Varallo *et al.,* 2019). However, 50% of CMC cases are malignant and will metastasise and result in death of the patient within one year (Misdorp *et al.,* 1999; Simon *et al.,* 2006). A study by Tran *et al.,* (2016) showed that invasive CMC treatment with adjunct chemotherapy

did not improve survival. Therefore, there is a need to improve clinical outcomes in veterinary and human patients by increasing the number of prognostic markers and novel therapies (Rasotto *et al.,* 2017). These high similarities, albeit with recognised differences, were the reason for the creation of the 'one health initiative' in the mid-1800s where human and veterinary medicine worked collaboratively to increase the rate of research advancements in medicine (Rushton *et al.,* 2018). In the 20th Century, the one health initiative is continued by veterinary medicine trialling and observing results for pre-clinical treatments, and benefiting from new medicines developed that were not beneficial for humans (Ogunseitan, 2022). The world of human medicine benefits from the biological and pharmacokinetic knowledge gained that can be utilised for novel treatment due to the high similarities between humans and canines (Garden *et al.,* 2018).

1.3.1. Breast cancer subtypes

BC is categorised into three main subtypes on the presence or absence of molecular markers; progesterone receptor (PR), estrogen receptor (ER) and human epidermal growth factor (ERB2) formerly HER2 (Shah *et al.,* 2022). Tumours lacking all three markers are termed "triple-negative". Hormone receptor status is used for prognostic and therapeutic purposes in BC and is associated with survival rates due to treatment availability, with triple-negative BC having larger tumour sizes of 5.2 cm, almost 2 cm larger than all other breast cancer subtypes, and the highest mortality rate due to limited treatment options (Sharma *et al.,* 2014; Howlader *et al.,* 2018). There are six subtypes of triple-negative breast cancer, two are categorised as basal with one being associated with BRCA mutations, pathways associated with cell cycle and division, and the second basal subtype being associated with growth factor signalling (Hubalek *et al.,* 2017). There is one immunomodulatory subtype associated with antigen processing and T cell functioning, and one mesenchymal which is enriched in pathways associated with cell differentiation pathways and cell motility (Hubalek *et al.,* 2017). Another mesenchymal stem-like subtype has similar features to the mesenchymal subtype but has processes linked to growth factor signalling (Kumar *et al.,* 2021). Finally,

there is one luminal androgen receptor subtype which is ER^- but genetic analyses have showed signalling heavily associated with hormonally regulated pathways (Harano *et al.,* 2018). The luminal androgen receptor subtype has up to ten times higher expression of androgen receptor expression compared to the other five subtypes (Lehmann *et al*., 2011). The subtype to be used in this study is the MDA-MB-231 triple-negative breast cancer cell line which is part of the mesenchymal stem-like subtype (Tseng *et al.,* 2017).

In cases of CMC, receptor status is increasingly researched but is not utilised in veterinary medicine as hormonal treatment is not used, as the primary treatment modality is mastectomy to remove the bulk tumour, followed by chemotherapy or radiotherapy to treat distant metastasis (Ežerskytė *et al.,* 2011; de Andrés *et al.,* 2022). REM134 is a CMC cell line established by (Else *et al*., 1982). REM134 is ER^- PR^- $HER2^+$, as they had the most similar receptor status compared to the MDA-MB-231 human breast cancer cell line of ER^- PR^- $HER2^+$. REM134 and MDA-MB-231 also have the most similar ER gene expression signature and are highly similar in cancer pathways such as KRAS, PTEN, WNT and MAPK (Gray *et al.,* 2020). Due to their high similarity, these two cells lines were chosen to be used in this project. MDA-MB-231 is derived from a patient with late stage metastatsis; however, the REM134 canine mammary carcinoma is yet to be further categorised. To date, the only information known of the cell line is the original tumour had a malignant phenotype, as the bitch was euthanised one month after the biopsy was taken due to metastases (Else *et al.,* 1982).

In veterinary medicine, immunohistochemistry (IHC) is performed to obtain a prognosis for CMC by observing how differentiated the tumour is to the original tissue type. If the morphology of the tumour is poorly differentiated, i.e. looks very different compared to original tissue type, this indicates an invasive CMC (Tavasloy *et al.,* 2013). Other IHC markers may be used such as myoepithelial marker p63, cells surrounded by a layer of p63 means the cancer is benign/*in situ*, the lack of a continuous layer indicates the cancer is invasive (Chocteau *et al*., 2019). Basal cell

markers such as cytokeratin 5 and 6 may be used, as these are high molecular weight proteins that can identify tumour types, positive staining with these markers also results in a tumour being categorised as “basal-like” (Walens *et al*., 2021). Triple-negative breast cancers can be termed “basal-like” which is identified by the appearance of cells following staining by immunohistochemistry (IHC), whereby cytokeratins such as CK5/6 are found, with high degrees of mitotic activity and necrosis (Buishand *et al.,* 2010). Basal-like IHC is associated with high-grade cancers that at ER^- and have a high proliferative rate; therefore, have a poorer survival rate (Wang *et al.,* 2021). Between 50-86% of triple-negative breast cancer is classified as basal by genetic analyses (Prat *et al.,* 2013; Garrido- Castro *et al.,* 2019). Additionally, Ki67 is a tumour proliferation marker that can be assessed by IHC in CMC with <33% cells staining positive is considered “high” and is associated with a higher histological grade which has also found to identify higher grade BC when used in human IHC (Brunetti *et al.*, 2021). There are recent studies which have identified a correlation between increased expression of senescence markers such as p16 and p21 in cases of tumour therapy resistance (Kavanagh *et al.,* 2017; Ionkina *et al.,* 2015); however, a study that in 1,140 cases, only 26.6% of triple-negative breast cancer cases were identified as p16 positive (Park *et al.,* 2021). The potential of p16 as a senescence marker may have the ability to indicate cells that are therapy resistant, but large scale studies would have to confirm this across different cancer types and species.

The classification of BC and CMC also depends on the grading, which is determined by cell morphology in terms of how abnormal the cells look compared to non-malignant cells. IHC is widely used in human and veterinary medicine and some of the IHC markers used show high similarity between human and veterinary patients (Figure 1.3).

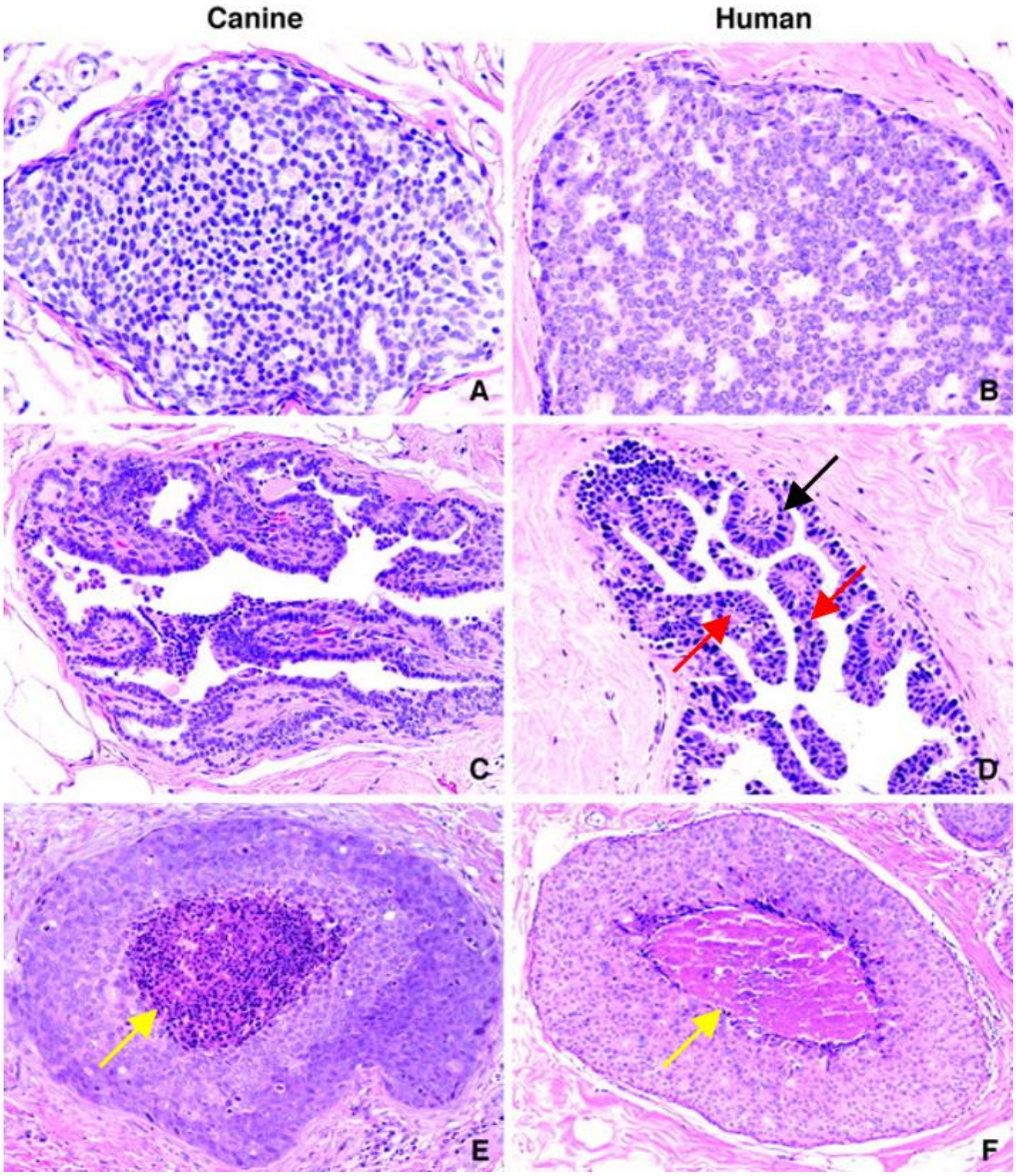


Figure 1.3 Histological staining of tumours from BC and CMC Ductal Carcinoma In Situ (DCIS). *Cases of low-grade DCIS in canines* ***A)*** *and human* ***B)*** *typically exhibit a cribriform pattern, a monomorphic cell population, and few features of nuclear atypia (mitotic figures, anisokaryosis).* ***(C, D)*** *shows Intermediate-grade DCIS. These samples exhibit papillary projections (black arrow), and moderate ansiokaryosis (red arrows). High-grade DCIS* ***(E, F)*** *is densely cellular and often has a central core of necrotic neoplastic cells, termed comedonecrosis (yellow arrows). Other features of high-grade DCIS include cellular pleomorphism, marked anisokaryosis, multiple nucleoli, and mitotic figures. Samples stained with Haematoxylin and eosin. Magnification x200. (Antuofermo et al., 2007).*

Low-grade cancers appear less abnormal when analysing cell morphology and tend to have a lower rate of growth and spread, therefore are considered to be easily treatable, whereas high-grade cancer cells are highly abnormal and are associated

with a higher rate of growth and spread (Couture *et al.,* 2018). For both human and canine mammary carcinomas prognosis is generally favourable in patients with early-stage low-grade tumours but prognosis can also depend on other genetic and environmental risk factors (Varallo *et al.,* 2019).

1.4. Incidence and risk factors

1.4.1. Incidence

The incidence of receptor positive human BC has can depend on several factors such as race and ethnicity, with poorer developed countries having a much higher mortality rate (Momenimovahed and Salehiniya, 2019). Non-Caucasian women are 1.4- to 3.1 times more likely to be ER/PR negative (Ci *et al.,* 2002). This also agreed with a study by Bhoo-Pathy *et al*., (2012) which found that Malaysian and Indian women had a higher chance of having hormonal negative receptors and high-grade tumours, therefore a higher mortality rate once developing BC. The incidence of BC is higher in developed countries, ranging from 27 cases per 100,000 in Middle Africa and East Asia to 92 cases per 100,000 people in North America (Ferley *et al.,* 2013). The incidence of BC is expected to rapidly increase in the future due to the ever-increasing population age in developed countries. The highest rates of BC are seen in China, Japan and Indonesia (Yolden *et al.,* 2014; Ghoncheh *et al.,* 2016), potentially due to longer life expectancy. The average global survival rate of BC is increasing, however, Africa has the lowest survival rate of BC because of delays in seeking diagnosis and treatment (Abdulrahman & Rahman, 2012; Cleries *et al.,* 2018).

Due to improved awareness, management, screening and treatment in high-income countries, there is a lower mortality rate in those diagnosed with BC (Carioli *et al.,* 2018; Fan *et al.,* 2015). Incidence varies in countries around the world and although environmental factors can influence the development of BC, the primary risk factors are gender, age, and genetic factors.

1.4.2. Gender

The outcome of BC is associated with hormone signalling in women; therefore, is a rare malignancy found in males, accounting for less than 1% of male cancers (Anderson *et al.,* 2010). As with any other cancers, BC occurs in older adult males who have one or more of the following: hormonal imbalance; family history of BC; exposure to radiation; and the most common risk factor being the presence of the mutated BRCA2 gene (Abdelwahab Yousef AJ, 2017). The total number of BC cases is increasing globally, and this is not due to an increasing female population, but due to a global increase in life expectancy (Lei *et al.,* 2021).

1.4.3. Age

After gender, age is the most common risk factor in the population for developing BC (Thakur *et al.,* 2017). A longer life expectancy results in increased molecular changes such as shorter telomere length and increased deoxyribonucleic acid (DNA) methylation rates, increasing the risk of cancer (Kresovich *et al*., 2019). As age is a leading cause of cancer, it follows that almost 90% of deaths are from women at the age of menopause at 50 + years of age (Desantis *et al.,* 2017). It should also be noted that BC diagnosed in younger pre-menopausal women are commonly larger and appear in more advanced stages, and therefore have a lower survival rate (Assi *et al.,* 2013).

1.4.4. Genetic factors

Inherited genetic factors can predispose people and canines to a higher risk of developing cancer (Vascellari *et al.,* 2016; Yoshikawa *et al.,* 2015). The most common mutation responsible for approximately 40% of hereditary BC cases is the BRCA1/BRCA2 mutations which are inherited via an autosomal dominant method

(Dekanek *et al.,* 2020). By the age of 80 years, the risk of developing BC for those with a BRCA1 mutation is 72% and those carrying a BRCA2 mutation is 69% (Metcalfe *et al.,* 2020).

There is an association between a family history of BC and the chances of developing BC. Even in cases where major indicative mutations like BRCA1/BRCA2 mutations are absent, if patients have 2+ cases of female relatives with cancer under the age of 50 or 3+ cases at any age they could be up to 11 times more likely to develop BC throughout their lifetime (Metcalfe *et al.,* 2009).

In the context of genetic risk factors, basic allelic gene variations also have the potential to predispose women to BC. Allelic variations, investigated in 815 patients by Bauer *et al.,* (2019) were identified in genes associated with DNA damage response pathways such as p53 and MDM2. The variation in the homozygous C-allele of MDM2 has shown to result in the development of BC at an earlier age of approximately 44, compared to other variations found in patients aged 60+. Furthermore, Melvin *et al.,* (2016) investigated the association between family histories of BC using a cohort of 5,359 patients and found no association between family history and mortality rates of BC. This implies that clinical management and patient specific treatment plans, e.g. treating BRCA1 positive ER^+ patients with targeted therapies, greatly increases patient survival.

1.4.5. Obesity

The correlation between obesity and BC has been extensively researched and has shown that a higher BMI can predispose people to malignancies with poorer disease-free survival outcomes (Miller *et al.,* 2018; Bravi *et al.,* 2018; Barone *et al.,* 2020; Zimta *et al.,* 2019; Lehuédé *et al.,* 2019; Lu *et al.,* 2017). These investigations have shown obesity is associated with remodelling of the TME and alterations of hormone signals in the body to promote ER+ cancer in post-menopausal women (McKenzie *et al.,* 2015; Sabol *et al.,* 2020).

Obesity can stimulate the remodelling of white adipose tissue and increase the production of leptin produced by adipose cells (Devericks *et al.,* 2022). The increased production promotes the development of a metabolically activated TME by modification (hypertrophy and hyperplasia) of the white adipocytes. This modification results in a pro-inflammatory environment that can promote BC formation via effects on neoplastic epithelial cells (Ando *et al.,* 2019).

Obesity is correlated to the increased risk of BC development as high levels of insulin in obese patients leads to the stimulation of cancer cell growth via changing tumour glucose metabolism to promote tumourigenesis (Chen *et al.,* 2016). Studies have shown that after BC diagnosis, basic exercise can decrease the risk of mortality (Lee *et al.,* 2018). Similar results have also been found in canines, with overweight dogs developing CMC at an earlier age (Lim *et al.,*2015) and those who were overweight or obese were found to have a shorter survival time following mastectomy (Tesi *et al.,* 2020).

1.5. Advantages of studying CMC in relation to human breast cancer

Dogs are beneficial as a spontaneous model for human cancers as they live in a similar environment to humans and are therefore exposed to similar carcinogens and risk factors; this is not attainable when utilising mouse models for oncology research. The advantages of using CMC as a model for BC is the similarity in terms of incidence, tumour size, lymphovascular invasion, pathologic nodal stage, and histological grading (de Andrés *et al.,* 2022). This means that studying spontaneously occurring cancers in dogs is advantageous to observe differences in treatment modalities utilised for cancer treatment, as data are acquired faster as canines have a shorter lifespan.

Gene expression of primary CMC and BC tumours have shown to have a highly similar gene profiling (Uva *et al.,* 2009). When comparing the transcriptional expression patterns between BC and CMC that had developed radioresistance, it was found there was similar expression in the PI3K, MAPK and WNT pathways (Gray *et al*., 2020). Comparing the gene expression from tumourigenic tissue from CMC showed a similar upregulation of cancer pathways that are seen in BC such as: PI3K/AKT KRAS and MAPK; p16/INK4A; PTEN; BRCA1; and p53 (Klopfleisch *et al.,* 2010; Pinho *et al*., 2012; Uva *et al.,* 2009; Rivera *et al.,* 2009). Furthermore, another study found high similarities for both CMC and BC in important cancer pathways associated with angiogenesis, apoptosis, cell cycle control, DNA damage and anti-apoptosis pathways (Rao *et al.,* 2009). There are also transcriptional similarities in the cancer signalling network, suggesting a close interspecies similarity (Rivera *et al.,* 2008). These similarities are thought to be due to the high homology between the human and canine genomes; however, there appears to be higher complexity in the human genome as there are new variants, short-length insertions and deletions, and some inversion mutations upon parallel DNA sequencing (Wheeler *et al.,* 2008).

A major limitation of this comparative research is the sample size used in CMC studies, the largest study to date by Rivera *et al.,* (2009) used 212 canine mammary tumour cases with 143 controls. To gain a better understanding of the reality of using dogs cancer data in relation to BC, there needs to be larger sample sizes used to attain more robust data about CMC.

1.6. Breast cancer staging

BC in both humans and canines is classified via anatomical size and spread, allowing the staging of the tumours from stage 1 to stage 5 to determine the clinical treatment. Stages are determined by the size of the tumour (T) in cm and the spread of the tumour to the regional lymph nodes, which is graded from N1 to N3 depending on the number of lymph node involvement. Combined with metastasis

(M) with M0 being the absence of metastasis and M1 having the presence of metastasis to other organs (Cassali *et al.,* 2014). The staging of both CMC and BC increases with an increase in tumour size, nodal involvement and metastasis (Table 1.1 and 1.2).

Table 1.1 CMC staging in female canines. *The table shows how tumour size, nodal status and the presence or absence of metastases determines the clinical staging (Anderson, D., 2014).*

Stage	Tumour Size (T)	Nodal Status (N)	Distant metastases (M)
1	< 3 cm	N0	M0
2	3 - 5 cm	N0	M0
3	> 5 cm	N0	M0
4	Any	N1 (positive)	M0
5	Any	Any N	M1

The level of metastasis at stage 5 diagnosis is unknown in dogs and these patients do not receive surgery for the primary tumours because of the advanced progression of the cancer (Table 1.1), however palliative care is provided as the overall survival rate is considerably short (Cassali *et al.,* 2014). The staging of BC and CMC is similar, but human staging has more subcategories that dictate treatment method (Table 1.2).

***Table 1.2 BC staging in humans**. The table shows how the tumours size, nodal status and presence of absence of metastases can determine the clinical stage and sub-staging (Giuliano et al., 2018; Zhu, H. and Doğan, 2021).*

Stage	Substage	Tumour size (T)	Nodal status (N)	Metastases (M)
1	1A	≤ 20 mm	None	M0
	1B	≤ 20 mm	Nodal micro metastases (> 0.2 mm < 2.0 mm)	M0
2	2A	≤ 20 mm	N1	M0
		> 20 mm ≤ 50 mm	None	
	2B	> 20 mm ≤ 50 mm	N1	M0
		> 50 mm	None	
3	3A	≤ 50 mm	N2	M0
		> 50 mm	N1 or N2	
	3B	Extension to the chest wall and/or skin	N0-N2	M0
	3C	Any size	N3	M0
4	4	Any size	Any involvement	M1

Studies have also shown that one quarter of dogs with CMC develop metastasis after surgery removing the primary tumour (Sorenmo *et al.,* 2019). Once metastasis has occurred there are limited benefits from cancer therapies as most patients become terminal or are euthanised once the quality of life diminishes. Due to the detrimental effects of metastasis on both human and canine patients, a greater understanding of the development of metastasis has been a focus of cancer research and treatment development (Edge and Compton, 2010; Giuliano *et al.,* 2017).

1.7. Breast cancer treatment

The principal treatment of non-metastatic BC in both humans and canines is to remove any cancer in the tissue and to prevent recurrence and metastasis (Tran *et al.,* 2016; Cassali *et al.,* 2017). Primary treatment is lumpectomy; removal of the

cancerous tissue from the breast (Hu *et al.,* 2020; Valero *et al.,* 2020) sometimes with post-operative radiotherapy.

1.7.1 Types of breast cancer removal surgery

In canines requiring surgery there are several surgical options available including: single mastectomy which is the removal of one mammary gland containing the tumour tissue and removal of lymph nodes involved; a regional mastectomy, which would remove the mammary glands surrounding a tumour; or removal of the mammary glands in a bilateral or unilateral mastectomy to remove a chain of mammary glands (Papazoglous *et al.,* 2014). In human patients requiring surgery there are more surgical options available as described in Table 1.3.

Table 1.3 Summary of surgical options for the removal of BC. *The table shows the subtypes of surgery and the corresponding anatomical description of the types of surgery available for BC patients (Dorogi et al., 2020; Sun et al., 2021).*

Types of surgery	Subtypes of surgery	Anatomical description
Mastectomy	Radical Mastectomy	The resection of the entire breast, axillary lymph nodes, pectoral muscles.
	Modified Radical Mastectomy	The resection of the entire breast and the axillary lymph nodes.
Breast conservation surgery – forms of lumpectomy	Skin sparing mastectomy	The resection of the entire breast tissue and the nipple areola complex, leaving the skin envelope.
	Areola sparing Mastectomy	The resection of the entire breast tissue, preserving the NAC
	Nipple sparing Mastectomy	The resection of the entire breast tissue, removing the areolar region of the NAC and preserving only the nipple

During the early development of the nipple sparing mastectomy surgery, there were concerns about the process of preserving the nipple areola complex could leave behind potential tumour cells that eventually result in recurrence (Hinton *et al.,* 1984). The most common approach is either a total mastectomy or breast conservation surgery with radiotherapy to ensure the death of any tumour cells

present in the remaining tissue. In recent years, nipple sparing mastectomy surgery has become the most used in mastectomy surgery (Weber *et al.,* 2018), with a current study by Dorogi *et al.,* (2020) showing no long-term difference in cancer recurrence in patients who had received areola sparing mastectomy or nipple sparing mastectomy surgery and had reconstructive surgery.

1.7.2 Endocrine therapy for treatment of breast cancer

In both CMC and BC, effective treatment is surgery followed by radiotherapy and/or chemotherapy to prevent recurrence. However, there is only one large scale study showing the benefit of radiotherapy and chemotherapy treatment in CMC patients (Rossi *et al*., 2018). Whereas these treatment methods are much more developed in human medicine. Systemic therapy is determined by subtype; patients with hormone receptor positive tumours are given endocrine therapy and a minority are also given chemotherapy. The main target in breast cancers is ERα which is over-expressed in 70% of invasive breast cancers, with the closely related PR hormone also being a marker of ERα signalling (Rusidzé *et al.,* 2021). As triple-negative patients lack hormone receptors, these patients receive pre- and post-operative chemotherapy with treatment plans including the platinum DNA cross-linking therapies such as carboplatin (Dieras *et al.,* 2019), with the only adjuvant treatment being capecitabine (Masuda *et al.,* 2017; Denkert *et al.,* 2017).

The use of systemic endocrine therapy to downregulate the ER signalling pathway is the primary systemic therapy utilised for ER +ve or PR +ve BC. The second main method of treatment is targeting ERB2 which is overexpressed in up to 20% of cases and has a poor prognosis with no administration of endocrine therapy. Small molecular anti-tyrosine kinase inhibitors and ERB2 antibodies: trastuzumab (Herceptin); lapatinib (Tyverb); pertuzumab (Perjeta) and trastuzumab emtansin (Kadcyla) are used as treatment for ERB2 +ve patients (Gampenrieder *et al*., 2013). Other chemotherapy drugs include Doxorubicin (Adriamycin) and epirubicin (Pharmorubicin), or a class of drugs known as taxanes; including docetaxel (Taxotere) and paclitaxel (Taxol) (Al Sayed *et al.,* 2019).

1.7.3 Chemotherapy treatment for breast cancer

Chemotherapy can be given as single agent therapy or combined therapy. In human and canine patients' chemotherapy is most effective in fast growing tumours (Sharma *et al.,* 2020). Although the utilisation of chemotherapeutic agents has proven to be effective, there are severe side effects such as vomiting, immune suppression and hair loss (Liu *et al.,* 2021). Metastatic breast cancer is treated depending on the hormonal subtype and grade with the primary focus on prolonging life and improving quality of life with palliative care. Systemic therapy used can be neo-adjuvant or post-operative, or sometimes both. Currently highly metastasised BC and CMC is incurable in most patients, although in human cases of metastatic spread, surgery and radiation are used for palliation of symptoms (Quackenbush *et al.,* 2017).

1.7.3.1 Doxorubicin treatment for breast cancer

Doxorubicin is one of the most common chemotherapy drugs utilised in treatment of canine cancers in veterinary medicine, despite there being discrepancy between studies stating no clinical benefit with Doxorubicin in CMC (Simon *et al.,* 2006) and studies showing increased overall survival (Zambrano-Estrada *et al*., 2018). Radioresistance is associated with the ability of cells to minimise effects of ROS produced by the hydrolysis of water molecules and fix the DNA damage that the ROS create (He *et al.,* 2020). Doxorubicin prevents DNA replication and causes direct and indirect DNA damage. Doxorubicin causes direct breaks in DNA via effect on DNA enzymes, and causes indirect DNA damage as Doxorubicin produces ROS within cells, and these ROS then go on to cause further DNA damage (Sahin *et al.,* 2022; Mastrangelo *et al.,* 2022).The standard scheme of Doxorubicin administration in canines is four cycles of Doxorubicin at a concentration of 30 mg/m^2 being administered intravenously for 20 minutes every 21 days (Zambrano-Estrada *et al.,* 2018), whereas in human medicine treatment of triple-negative breast cancer in humans has a treatment regime of 60 – 75 mg/m2 every 21 days delivered

intravenously for less than 60 minutes (Nicoletto and Ofner, 2022), unless used with other chemotherapeutic agents such as cyclophosphamide where the concentration of Doxorubicin would be used at 30 mg/m^2 to limit toxicity (Hassan *et al.,* 2010). Doxorubicin has a cardiotoxic affect due to a systemic increase in ROS in both canines and humans. A study by showed that increase effusion time to 1 – 6 hours abolished cardiac damage when testing serum CK-MB activity or ECGs (Zambrano-Estrada *et al.,* 2018), which was also found humans (van Dalen *et al.,* 2016).

In veterinary medicine, it is most common practise to give Doxorubicin with cyclophosphamide along with other chemotherapeutics called a "CHOP" protocol as neoadjuvant therapy to shrink locally advanced tumours to allow surgical removal due to the limitation of the concentration of Doxorubicin due to cardiotoxicity (Karayannopoulou and Lafioniatis, 2016). The neoadjuvant chemotherapy using Doxorubicin with prior to surgical removal increases disease free survival to 12 months, compared to 7 months when using Doxorubicin as a monotherapy (Zambrano-Estrada *et al.,* 2018). There are very few studies for optimisation of treatment methods comparing neoadjuvant and adjuvant chemotherapy in CMC as there are conflicting results as to if adjuvant chemotherapy is beneficial to CMC patients; however it should be stated this could be due to the very low patient numbers in these studies which are often less than 30 patients (Karayannopoulou *et al.,* 2001; Simon *et al.,* 2006; Karayannopoulou and Lafioniatis, 2016; Rossi *et al*., 2018).

1.7.3.2 Immunotherapy treatment for breast cancer

A hallmark of cancer is the ability to suppress and avoid the immune system. This is achieved by the tumour cells having the ability to prevent themselves being recognized by immune cells such as T cells. Immuno-oncology research identifies ways of how immune cells kill tumour cells, and ensures that tumour cells cannot block this mechanism. Modern therapies include immune-oncology focused on programmed death ligand 1 (PDL-1). PDL-1 Patients with triple-negative breast cancer are screened and are determined to be PDL-1 positive or negative; where a

combined positive score of >10 % (number of PDL-1 positive immune cells and tumour cells out of the total number of tumour cells) (Jin *et al.,* 2022). PDL-1 phase III clinical trials currently focus on PDL-1 alone, or PDL-1 used in conjugation with other chemotherapeutics such as Paclitaxel PDL-1. One hallmark clinical trial found that to prolong patient survival in patients with triple-negative breast cancer PDL-1 inhibitors must be used in conjugation with chemotherapy to prolong patient survival (Winer *et al.,* 2021) clinical trial number NCT02555657. However, for many of these double-blind randomised control Phase III clinical trials, the overall survival rate is only increased by 2-9 months with each study having a minimum of n=450 for each trial group – clinical trial numbers: NCT02555657, NCT02425891.

1.7.3.3 The use of PARP inhibitors for breast cancer treatment

In addition to the progression in the field of immuno-oncology, the use of PARP inhibitors are currently being explored. PARP inhibitors have been established for a while to be used to induce synthetic lethality in breast cancer patients with BRCA mutations (Cashman *et al.,* 2020). Therefore, are commonly used in triple-negative breast cancer patients who are positive for BRCA mutations. Recent trials such as a Phase III trial PARP inhibitor in patients with BRCA1/2 mutations who were $HER2^-$ investigated the effect of combination therapy of a PARP inhibitor in conjugation with chemotherapy drug of choice by the oncologists (n= 205) compared to chemotherapy monotherapy (n=97). The results showed no significant increase in overall survival but a significant increase in median progression free survival of 2.8 months (Kuemmel *et al*., 2020), trial number NCT02000622. In comparison, the use of PARP inhibitors in CMC is still in its infancy although BRCA2 mutations in canines have been identified for a long time (Thumser-Henner *et al.,* 2022). Progress in this field by veterinary medicine includes identifying the pharmacokinetic profile of a PARP inhibitor in canine patients (n=18) to aid clinical trial information for a human trial using PARP inhibitors in triple-negative human breast cancer trial number NCT00938652. The study found that clinically relevant drug concentrations were not detectable in canine tumour tissues, although toxicity doses could not be determined when canine patients were treated with doses of PARP inhibitor or PARP

inhibitor with chemotherapy; effectively showing that the PARP inhibitor was better tolerated in the canine model (Saba *et al.,* 2016). Despite these findings, as the data provided no benefit to human medicine, the clinical development of the PARP inhibitor was stopped.

1.7.4 Recent developments in breast cancer treatment

The development of veterinary medicine cancer treatments is several years behind human medicine. Treatment of CMC is primarily surgical removal with limited clinical studies using radiotherapy due to the financial cost to the owner. However, in the context of the "One Health Initiative" applicability of human medicine to veterinary medicine seems to have promising prospects (Ramos-Cardona *et al.,* 2022). It has been found that T cell therapy, where T cells are removed from the patient and modified to attack cancer cells and then infused back in to the patient, can be used in veterinary cases of B cell lymphoma (Panjwani *et al.,* 2020). However, the low patient number (n=5) and recovery rate of modified T cells to be infused into canine patients proved problematic, and there is progress being made to optimise culture conditions to increase the number of modified T cells that can be recovered once isolated from canine patients (Gramaldi *et al.,* 2023; Sakai *et al.,* 2022).

There are some novel trials that are incorporating all therapy approaches, such as an ongoing Phase II clinical trial using a PARP inhibitor in conjugation with a PDL-1 inhibitor and radiotherapy in patients (n=32) with negative BRCA mutation status (clinical trial number NCT04837209). Although there is only one clinical arm, therefore no "control" group, it is one of the first of its kind to combine all therapy approaches in triple-negative breast cancer patients.

To summarise, there is a dire need for canine specific treatment options following cancer diagnosis, as the majority follow a generic human treatment plan, with main exclusive veterinary treatment is a Doxorubicin based combination therapy protocol (CHOP) for most cases of veterinary cancer treatment. Although this approach has

show to provide the longest period of overall survival, the response is sub-optimal with recurrent disease and/or metastasis and the absence of further treatment options proving fatal (Chun, 2009). The rate of progress being made in human medicine is promising for the future outcome of human patients with breast cancer; however, due to the critical unmet need of therapy options in veterinary medicine following a cancer diagnosis, exploitation of human therapies could be considered to accelerate the drug/therapy development options for veterinary medicine. The current novel therapies for human medicine are progressing in areas such as immune-oncology combined with chemotherapies, but in the context of triple-negative breast cancer the effect on overall survival rate is considerably small at 2-9 months; therefore, the most current clinical trials are exploring the effectiveness of combination therapies.

1.7.5 Radiotherapy treatment for breast cancer

Radiotherapy treatment can be provided with the intent to cure patients or to provide palliative care in patients with local and metastatic breast cancers. The difference between the types of radiotherapy is the dose and number of treatments given (Wang and Tepper, 2021). Curative radiotherapy to treat local cancer growths following lumpectomy or mastectomy usually involves a complex plan of giving higher total doses in small daily fractions over several weeks, such as daily fraction doses at 1.8 Gy – 2 Gy totalling between 40 – 80 Gy (Koulis *et al.,* 2015) in BC. In studies analysing the effect of radiotherapy on CMC, hypo-fractionated doses are also used in ranges of 3 doses every 2 weeks of 8 Gy totalling 24 Gy; however, radiotherapy is not a common treatment in veterinary medicine due to such high cost, resulting in very few studies analysing the benefits of radiotherapy on CMC (Rossi *et al.,* 2018; Sorenmo *et al.,* 2013). Radiotherapy ensures the death of the tumour and limits the damage to the surrounding non-cancerous tissues, and is commonly used following mastectomy with the aim of ensuring any remaining cancerous cells are killed in BC (Kim *et al.,* 2021). The method of palliative radiotherapy treatment is different as the main goal is to decrease the severity of symptoms as quickly as possible, using more simple plans utilising higher doses of

radiation per treatment for a limited number of treatment sessions, such as giving between 8 Gy to 30 Gy in 1 to 10 sessions depending on the acute toxicity withstood by the patient (Lutz *et al.,* 2014).

Irradiation works on the principle that x-rays cause direct and indirect damage to cells. A small percentage of DNA atoms are hit by x-rays and cause ionisation resulting in the initiation of the intrinsic apoptotic pathway that activates the initiator caspase 9 and the effector caspases 3 and 7 resulting in cell death (Cao *et al.,* 2019). Activation of this pathway can be seen as blebbing of the plasma membrane and the production of apoptotic bodies as the cell is degraded, and this results in cell and tumour shrinkage (Chen *et al.,* 2022). The indirect action of x-rays comes as a result of radiolysis, which is the interactions of the gamma rays with atoms or molecules leading to the production of free radicals. The reaction with water can produce hydroxyl radicals (OH^-), hydrogen atoms (H^+) and superoxide radical anion (O^{2-})(Loh *et al.,* 2020). The only radical that can cause direct DNA damage is the hydroxyl radical OH^-, due to having one electron it can oxidise molecules in a thermodynamically favoured mechanism, either by adding itself to double bonds, or by removing hydrogen from the DNA base pairs. The resulting high levels of ROS causes an imbalance of the redox status within the cell, resulting in oxidative stress (Gao *et al.,* 2023).

For double stranded breaks (DSBs) the main two pathways are non-homologous end joining (NHEJ) and homologous recombination (HR). Human and veterinary patients with a BRCA1/2 mutation can be predisposed to regulation of DDR pathways, increasing their chances of developing breast cancer due to the role of BRCA1/2 in HR (Hakkart *et al*., 2022; Enginler *et al.,* 2014). For single stranded breaks (SSBs) the primary pathway is base excision repair (BER). There is an increase in DNA damage in the form of base pair mismatching in cancer cells due to the extensive cellular stress and a decreased rate of mismatch repair (MMR) has also shown to result in increased radiosensitivity (Meillan *et al.,* 2019).

For MMR, a heterodimer complex of MSH2/MSH6 is recruited and PNAI results in the recruitment of endonucleases, and EXO1 creates a nick in the DNA whilst ligation of correct base pairs is achieved via Ligase I or IV (Figure 1.4).

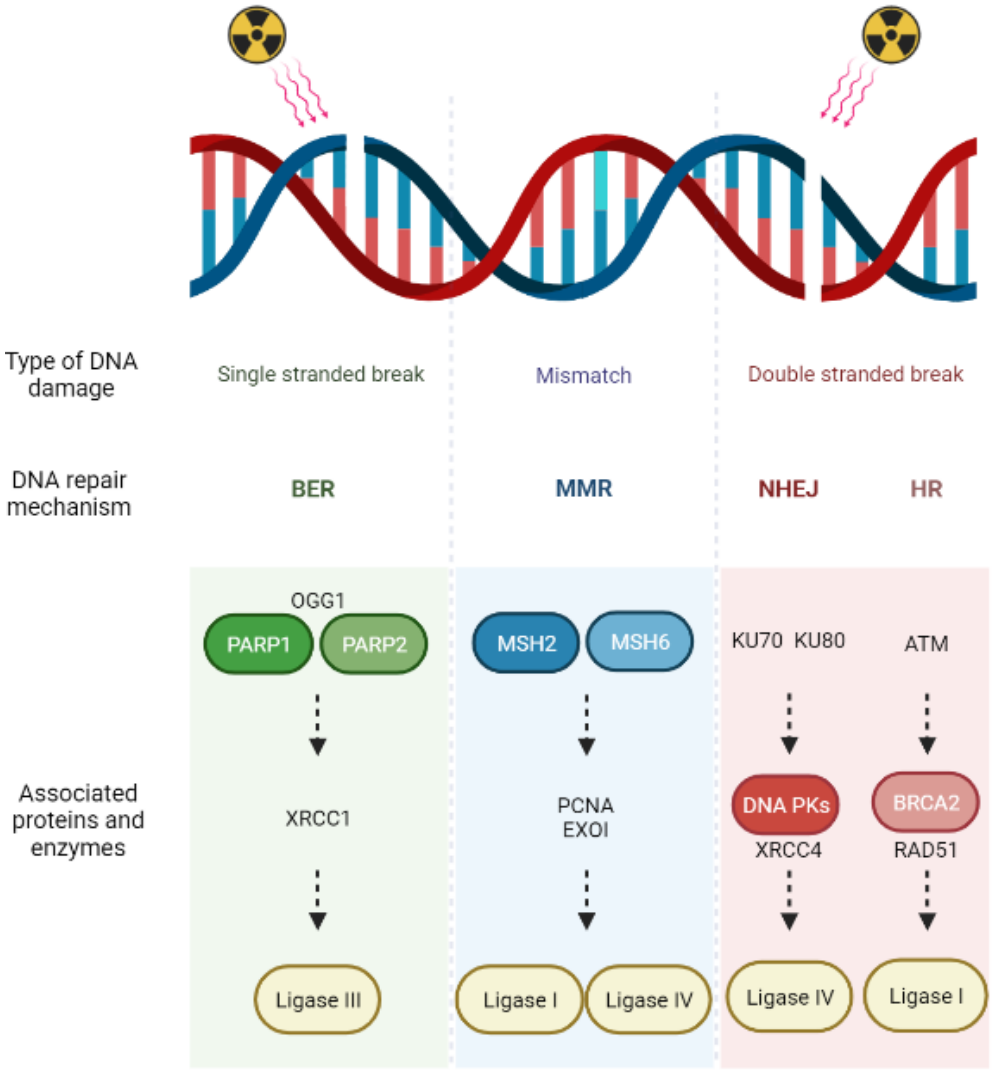


Figure 1.4 Summary of pathways associated with DNA repair. *The single stranded breaks are repaired by BER which is associated with PARP1 and PARP2 proteins resulting in the recruitment of Ligase III to anneal breaks in the DNA. The increase in rate of MMR is repaired in recipient cells via the recruitment of MSH2 and MSH6 which results in the insertion of the correct base pair and annealing by Ligase I and IV. For double stranded break repairs there are two pathways, the most prominent being associated with the ATM complex to achieve homologous recombination with the activation of BRCA2 and RAD51 with the subsequent induction of Ligase I (Adapted from Toss and Cortes, 2013 – Created with BioRender.com).*

HR is the most effective method of DSB repair as it uses the sister chromatid as a template which results in very few mismatches. Due to using the sister chromatid as

a template means HR occurs in the late S phase/ G2 phase of the cell cycle. NHEJ repairs DNA damage by re-ligating the broken ends without a template; therefore, is highly prone to errors resulting in mutations (Yang *et al.,* 2020). As NHEJ does not require sister chromatids to repair the DNA, NHEJ can occur at any point within the cell cycle so is commonly used by cells following irradiation due to its availability (Lieber, MR, 2010). DSBs result in the activation of ATM, a protein kinase that phosphorylates and activates several downstream targets including gH2AX and the tumour-suppressor, p53. In response to DSBs, gH2AX a histone variant, accumulates along regions of DNA with DSBs to recruit proteins associated with the DDR pathway including p53 and BRCA1 (Liu *et al*., 2018). Patients with mutated BRCA1 or p53 are more prone to unregulated cell proliferation and accumulation of DNA damage which can result in a malignant phenotype (Eustace *et al.*, 2022).

1.7.5 Cancer stem cells

Cancer stem cells (CSCs) are a subpopulation within the bulk tumour that can self-renew and initiate tumour growth and recurrence. CSCs can arrest in the G0 phase of the cell cycle which is the most resistant phase of the cell cycle. Markers of the CSC phenotype include increased expression of the WNT and NOTCH pathway which are associated with the self-renewal process (Park *et al.,* 2021). CSCs are also associated with multi-drug resistance, as CSCs express ABC transporters which are associated with chemotherapy resistance (Zhou *et al.,* 2021). Additionally, aldehyde dehydrogenase (ALDH) has increased expression in CSCs and results in the elimination of oxidative stress by removing free radicals induced by irradiation (Poturnajova *et al.,* 2021). CSCs have also shown to have an increased rate of DDR resulting in a protective effect in the context of chemotherapy and radiotherapy (Abad *et al.,* 2020). There are studies indicating that upon acquiring a radioresistant (RR) phenotype, breast cancer cells may revert to a more mesenchymal like phenotype which is associated with an increased expression of markers associated with EMT (Gener *et al.,* 2019).

In a RR cell population, interplay between the CSCs, pro-oncogenic mutations, and upregulation of the DDR pathways results in a highly aggressive and resistant phenotype associated with therapy resistance (Abad *et al.,* 2020). Therefore, markers of radioresistance include a more-mesenchymal phenotype. Increased YAP1 expression is associated with switching to a more CSCs like cell in triple-negative breast cancer cells derived from cancer patients and activates NOTCH and the WNT pathway (Qiao *et al.,* 2021).

1.8. Radioresistance

Radioresistance is the ability of cells to survive a dose of irradiation that would normally be lethal (Todorovic *et al*., 2019). The acquisition of radioresistance limits treatment options available for BC and CMC patients, especially in patients with triple-negative BC due to the ineffectiveness of hormonal therapies (Lv *et al.,* 2021). The spread of radioresistance throughout a tumour has been indicated to be associated with the presence of cancer stem cells (CSCs), these cell types are highly resistant to environmental changes when compared to cancer cells within the bulk tumour (Pustovalova *et al.,* 2021). This means that following the administration of chemotherapy and/or radiotherapy, cancer cells may die, but remaining CSCs result in repopulation of the tumour (Liu *et al.,* 2021).

The emergence of radioresistance is associated with genetic mutations, alterations in DNA damage repair (DDR) pathways, autophagy and cell cycle checkpoints (Assani *et al*., 2019). The most common DDR mutations that are associated with an increased risk of developing mammary carcinoma are BRCA1, BRCA2 and p53 (Metcalfe *et al.,* 2020). Studies have found that BRCA1 mutations can increase chances of being diagnosed with breast cancer before the age of 30 by almost 30% (Hyder *et al.,* 2020), and 5%-8% of those who develop breast cancer under the age of 30 who do not have a BRCA1 or BRCA2 mutation will have a p53 mutation (Schon and TIschowitz, 2018). The mutated p53 is associated with resistance to apoptosis,

alterations to the cell cycle, and promotion of invasion and metastasis which are also key features of triple-negative breast cancer (Berke *et al*., 2022).

Patients with locally advanced cancer that receive radiation therapy often relapse which can lead to metastasis, resulting in a poorer clinical outcome (Nozaki *et al.,* 2020). The exact mechanisms of how cells acquire a radioresistant (RR) phenotype are still yet to be discovered.

1.8.1. Oxidative Stress

The formation of free radicals occurs from the reaction of oxygen with breaks in the DNA strands, meaning cancer cells accumulate more DNA damage under normoxic conditions than hypoxic conditions (Desouky *et al*., 2016). It is estimated that around two thirds of DNA damage induced by radiation is caused by reactive oxygen species (ROS); therefore, the cells ability to remove ROS determines the radiosensitivity of cancer cells (Hall and Giaccia, 2012). ROS removal depends on the activity of antioxidant enzymes. Enzymes that metabolise ROS include catalase and superoxide dismutase (Ambrosone *et al.,* 2005). Superoxide dismutase can be induced with increasing environmental levels of O_2^- and converts O_2^- to H_2O_2 (Rohrdanz E and Kahl, 1998). Catalase is an enzyme that converts H_2O and O_2 and has found to be increased in cancer patient serum following radiotherapy (Tuncer *et al.,* 2022). Increased expression of these enzymes is associated with a poorer outcome in patients (Woolston *et al.,* 2011a; Woolston *et al.,* 2011b).

1.8.2. Hypoxia

Normal oxygenation levels are reported to be ~8.5% or more O_2, and hypoxia (low oxygen) levels are <1% O_2 (Liu *et al.,* 2022). Hypoxia can occur heterogeneously within a developing solid tumour due to abnormal blood vessels resulting in defective microcirculation (Petrova *et al.,* 2018). Hypoxia inducible factor 1- α (HIF1-α) is a transcription factor associated with being an oxygen sensor, in the presence of oxygen HIF1- α is modified by prolyl hydroxylase enzymes (PHDs) to be targeted

for degradation by the proteasome (Wen *et al.,* 2023; Jasiewicz *et al.,* 2022). However, in oxygen starved cancer cells, this modification is blocked by inhibition of the PHDs, and HIF1- α accumulates in the nucleus and binds the hypoxia-response element resulting in the activation of pro-oncogenic processes such as erythropoiesis, angiogenesis, resulting in the increase of oxygen supply to the developing tumour (Li *et al.,* 2019). ROS react with oxygen decreasing oxygen levels in the TME, this results in the stabilisation of HIF1- α which in turn activates transcriptional activity that switches energy production from oxidative phosphorylation to glycolysis; thereby reducing cellular ROS contributing to radiotherapy resistance (Harada *et al.,* 2012). The induction of hypoxia in cancer cells and mechanisms to avoid programmed cell death are also associated with CSC-like properties (Lan *et al.*, 2018). The stabilisation of HIF1- α has shown to activate WNT and Hippo pathways which promote a stem cell phenotype in triple-negative breast cancer (Lee *et al.,* 2017), which is also associated with the increased expression of ABC transporters which contribute to chemotherapy resistance (Samanta *et al.,* 2014).

1.8.3. Cell cycle and DNA damage response

The cell cycle is highly regulated in non-cancerous cells with 4 phases: Gap 1 (G1); Synthetic (S); Gap 2(G2); and the mitotic (M phase). Each phase of the cell cycle has carefully controlled checkpoints via levels of cyclin-dependant kinases and checkpoint kinases. Upon developing a malignant phenotype, cancer cells can manipulate the cell cycle and force progression through phases of the cell cycle (Müllller *et al.,* 2020). RR cells have an increased tolerance to irradiation during the G2/M phase due to the increased rate of DNA damage repair (DRR). The rate of DDR is enhanced via cell cycle arrest between the G2/M phases in RR cells to allow more time for DDR to occur. Therefore, inhibition of the G2/M checkpoint causes early entry into the M phase in RR cells, decreasing the rate of DDR that occurs. Decreasing the time for DDR to occur before mitosis can result in mitotic catastrophe and cell apoptosis (Matheson *et al.,* 2016). In RR mammary carcinomas there are alterations in the G2 phases of the cell cycle, with cancer cells and stem

cell populations having a longer G2 phase, allowing for increased repair of DSBs (double stranded breaks) and SSBs (single stranded breaks) to allow progression through the cell cycle (Tian *et al*., 2011; Anastasov *et al*., 2012).

1.9. Extracellular Vesicles

The first viewing of EVs was probably by Wolf (1967) where they were described as "platelet dust". In 1987 EVs were officially identified as an extracellular vesicle of endosomal origin, secreted from reticulocytes, and were thought to be vesicles to remove waste material from the cell (Johnstone *et al.,* 1987). It was shown in 1996 that EVs secreted by the B lymphocytes induced activation of the T lymphocytes, thereby revealing that EVs affect other cells (Raposo *et al.,* 1996). Nearly a decade later, it was found that EVs are released by both prokaryotes and eukaryotes with their primary function being cell to cell communication. EVs are double membrane vesicles that contain active constituents, such as proteins, lipids and nucleic acids, and that their primary function is to mediate cell communication via paracrine, autocrine and juxtacrine signalling (Ellis *et al*., 2010; Sahoo *et al*., 2011; Higginbotham *et al*., 2011; Al-Nedawi *et al.,* 2009; Whitesdie *et al.,* 2017).

1.9.1. Current advancements in the use of EVs in clinical medicine

Subsequent studies showed that EVs can elicit phenotype, genotype, and morphological changes after the release of EV content after uptake by recipient cells (Ham *et al*., 2018; Terlecki-Zaniewicz *et al.,* 2018; Ruhland *et al.,* 2016). Phenotypical changes seen upon the transfer of EVs derived from CAFs have been shown to induce chemotherapy resistance in recipient ovarian cancer cells (Guo *et al.,* 2019). Other phenotypical changes caused by cancer derived EVs include the induction of EMT. This is identified by a morphological change of cells having an epithelial to a mesenchymal morphology, with a mesenchymal phenotype having elongated morphology with cytoplasmic extensions due to protein remodelling occurring during the transition resulting in cancer cells losing their cell to cell junctions (Xiao *et al.,* 2016). The biological markers of EMT include the decreased expression of E-

cadherin and increased expression of EMT promoting transcription factors such as slug and snail, and mesenchymal markers such as vimentin (Nakamura *et al.,* 2018; Subbalakshima *et al.,* 2022). Genotypic changes occur upon the transfer of mitochondrial DNA which can induce metabolic reprogramming of the recipient cell towards oxidative phosphorylation and increased rates of mtDNA replication which can promote resistance to hormonal therapy (Sansone *et al*., 2017). Additionally, horizontal DNA transfer can be achieved by EVs, as EV content can translocate to the nucleus and be incorporated in to the recipient cells genome (Fischer *et al.,* 2016). The content of the EV reflects the parental cell. This means that cancer cells that have oncogenic content can package the pro-oncogenic content, and then transfer this content to recipient cells. As EV content reflects that of the parental cell, this means hroughout a cell's lifetime, EV content could potentially be used as an indicator of physiological or pathological processes occurring within cells. This has led to a recent surge in investigations of EV content for disease identification and progression to determine if EVs can be used as biomarkers to aid diagnosis and personalise treatment within a clinical setting. The use of EVs in human medicine has progressed in to early experimental stages including the administration of non-engineered EVs (Figure 1.5).

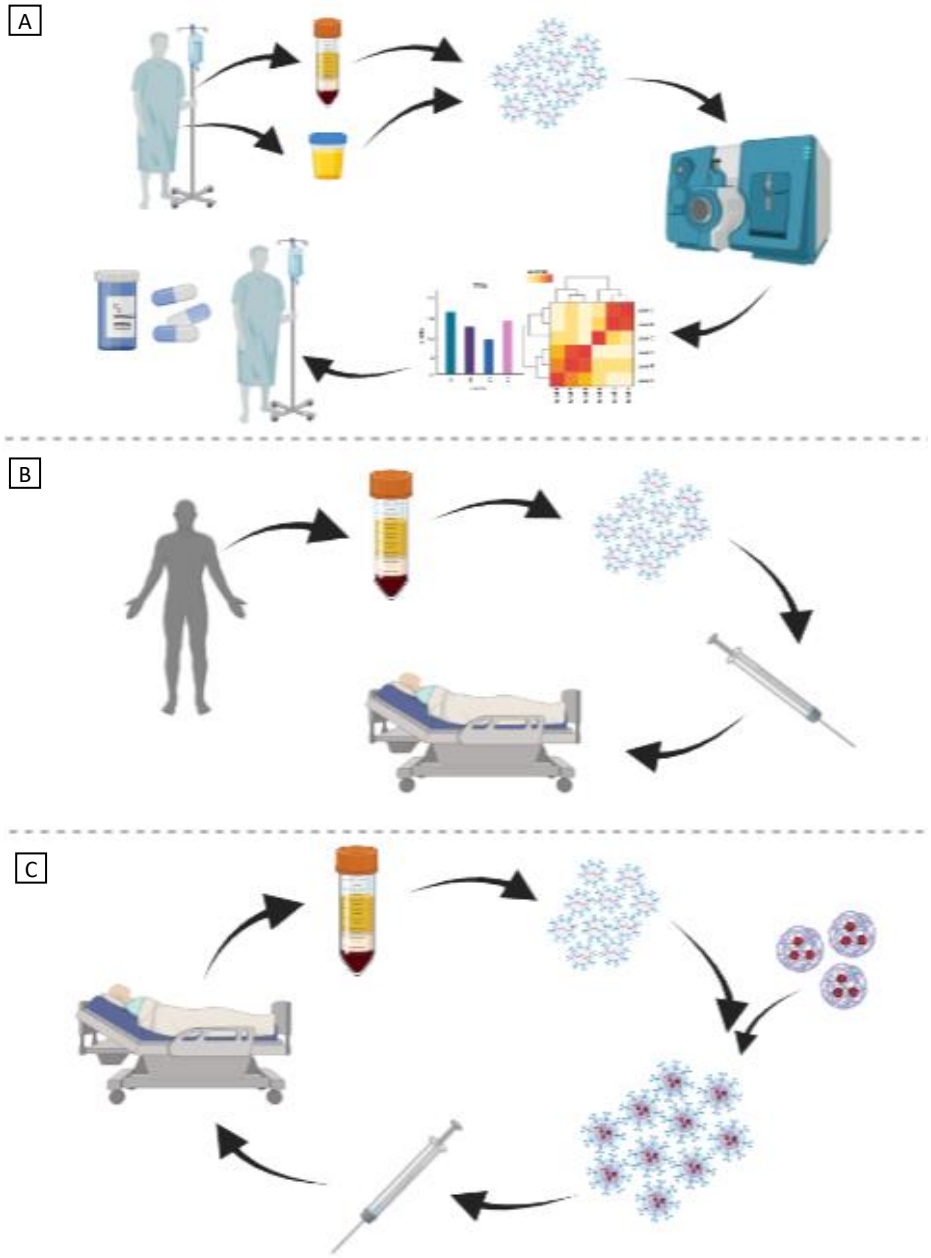


***Figure 1.5 A summary of the uses of EVs in human medicine**. **A)** The patient has EVs taken via serum or urine which are then processed and analysed for biomarkers or barcoding to subcategorise disease state and progression which can then be used to personalise patient treatment. **B)** A healthy donor provides mesenchymal EVs which are then injected in to patients with inflammatory diseases to reverse inflammatory phenotype within tissues. **C)** A patient has EVs isolated from serum and those EVs are then loaded with nanodrugs which are then infused back in to the patient (Created with BioRender.com).*

The profiling of EV content for BC when compared to healthy controls was able to categorise BC samples in to cancer subtype, progression stage and the presence or absence of metastasis (Wang *et al.,* 2018) which could identify the optimal treatment options available to BC patients (Figure 1.5 A). It would be highly beneficial to increase the acquisition rate of the EV profiling data to enable the use of EV samples in a clinical setting, as currently the isolation and analysis of EVs as biomarkers is a rigorous and time-consuming process due to the requirements needed when working with EVs (Théry *et al.,* 2018).

Furthermore, a current use of EVs in experimental therapeutics involves taking EVs derived from mesenchymal cells from healthy donors and administering these to patients with advanced diseases (Figure 1.5 B). An example of this is a Phase IIa trial with one trial arm of n=7 patients who had severe pneumonia (NCT04276987). Patients inhaled mesenchymal EVs with the aim of reversing the severity of pneumonia by inhaling EVs five times a day for 5 days. The results showed the treatment was well tolerated with no side effects and visible improvement of the patients pneumonia within 7 days when analysed by CT scan (Zhu *et al.,* 2022). This demonstrates the reprogramming ability of exosomes in recipient cell, and that EV content can remain active throughout laboratory processing.

1.9.2. Current EV modification techniques

Due to the nature of the formation of EVs resulting in a lipid double membrane, this means the contents of EVs are protected from external environmental factors and degradation. This also applies if EVs are removed from the body and kept in a suitable medium to prevent the lysis of the double membrane vesicles. Studies have found that the EV could be a potential nanodrug delivery system as EV content can be manipulated to directly deliver drugs inside cells (Figure 1.5 C). This is beneficial as EVs are identified as “self” and therefore are not destroyed by circulating macrophages, and unlike synthetic drug delivery systems, easily pass the blood brain barrier and general toxicity can be avoided when EVs can be edited to target tumour cell types (Ye *et al*., 2018). The surface engineering of EVs is achieved via two

methods: genetic engineering and chemical engineering. Genetic engineering of EVs is done by fusing the gene sequence of a guiding protein or polypeptide with a chosen EV membrane protein. This is usually utilised for editing surface peptides and proteins.

Chemical engineering is utilised for editing the EV display of ligands and lipids and is done by chemical reactions, such as changing of transmembrane proteins is done by chemical editing of the surface proteins, known as “click chemistry” which allows for the addition of targeted sequences onto tetraspanins, which are complementary to a specific cell type to promote selective uptake (Choi *et al.,* 2021). Finally, the internal content of EVs can be edited via “EV loading” with hydrophobic or hydrophilic drugs, proteins and ribonucleic acid (RNA), allowing them to become nanocarriers of chemotherapeutic agents (Yong *et al.,* 2019). Incubating relevant cells with chemotherapy drugs *in vitro* results in the incorporation of the chemotherapeutic agent into newly forming EVs within cells. The EVs are then released from cells *in vitro* and can be collected in the cell culture medium, isolated and have surface markers edited to ensure uptake by preferred recipient cells.

These EV editing methods can be simultaneously, as demonstrated by Ye *et al*., (2018) whereby EVs were loaded with the chemotherapeutic drug methotrexate, and surface peptide engineering attached target peptides to allow specific uptake by glioma cells. The results showed successful penetration of the blood brain barrier, glioma tumour cell specific uptake, and prolonged survival in mouse models with glioblastoma.

1.9.3. EV biogenesis and formation

Cells produce a range of spherical double membrane vesicles including: EVs; ectosomes; microvesicles; oncosomes; and apoptotic bodies and these are characterised according to size in diameter: 30-150 nm; 10-300 nm; 100-1000 nm; 500-1000 nm; and 800 nm-1000 nm respectively (Reclusa *et al.,* 2017). Apart from

EVs, these vesicles are formed via processing and packaging from the endoplasmic reticulum and the golgi body and are released by outward budding from the cell membrane (Bebelman *et al*., 2020). Apoptotic bodies are only produced after apoptosis and can be distinguished from microvesicles by their size and their cargo of cell organelles and large nuclear material (Phan *et al*., 2021). Unlike other vesicles, EVs are produced via trafficking throughout the cell and the inward budding of late endosomes The exact mechanism of biogenesis is yet to be discovered but current research has identified the two main pathways: (1) the endosome sorting complex required for transport (ECSRT) dependant; and (2) an ESCRT independent pathway (Wei *et al*., 2020) (Figure 1.6).

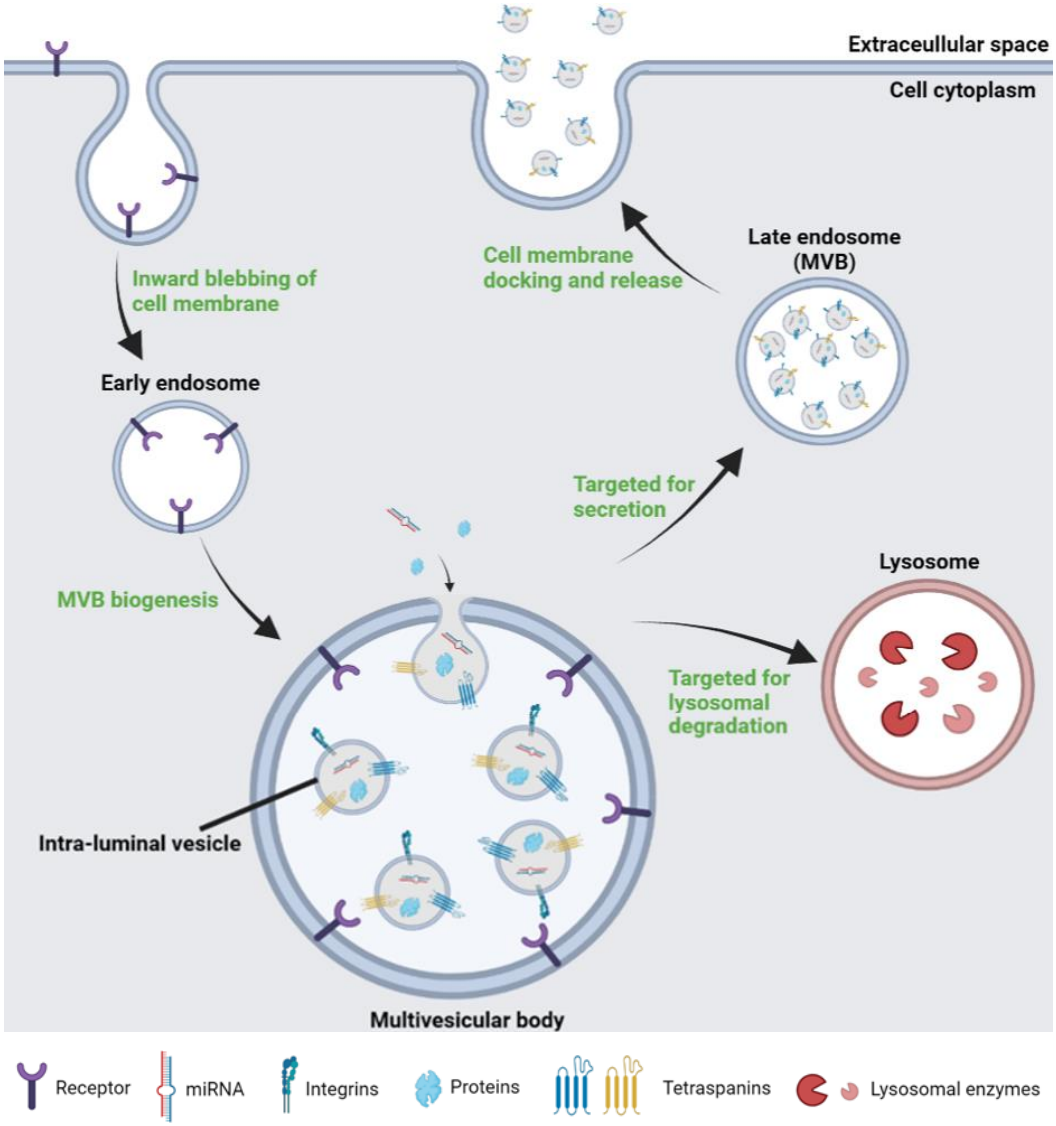


Figure 1.6 An overview of EV formation and degradation/release. *The general life cycle of EV formation, showing the inward budding of the endosome at the cell surface leading to MVB biogenesis. ILV formation involves the inward budding of the MVB surface which is cleaved and released internally to produce ILVs. The MVBs containing ILVs are either directed to the lysosome for degradation, or to the cell membrane for secretion whereby the MVB fuses with the cell membrane and releases the ILVs in to the extracellular space. Once the ILVs are released from the MVBs they are then called EVs. The green text represents biological processes and the black text shows labels (Created in BioRender.com).*

Endosomes travel through the cell and the outer membrane begins to bud inwards whilst being packaged with cellular content, the inwards budding vesicle is then cut and released, leaving a smaller vesicle inside a larger vesicle (Figure 1.6). The outermost vesicle is then termed as a multi-vesicular body (MVB) which contain the

smaller packaged vesicle which are called intra-luminal vesicles (ILVs)(Ghossoub *et al.,* 2014).

1.9.4 Formation, processing and packaging of ILVs within the MVB

The ESCRT dependant pathway accounts for up to 70% of EV production and is associated with five proteins/complexes: Vsp4; ESCRT0; ESCRTI; ESCRTII; and ESCRTIII. The ESCRT dependent pathway requires the recruitment of ESCRT0, ESCRTI, and ESCRTII to the surface of the MVB. The ESCRT complexes recruits ubiquitinated proteins to be packaged into the MVBs (Figure 1.7). These proteins are ubiquinated via E1 enzyme that activates the ubiquitin protein, the activated ubiquitin is then transferred to an E2 enzyme which inserts itself in to an E3 enzyme that contains the protein that is to be targeted for packaging in to the MVBs. The ubiquitin is then added on to the targeted protein. Sequential binding of ESCRTIII and ESCRTIII results in the de-ubiquitination of recruited proteins that are to be packaged in to the ILVs, and the subsequent release ILVs into the MVBs (Soung *et al.,* 2015).

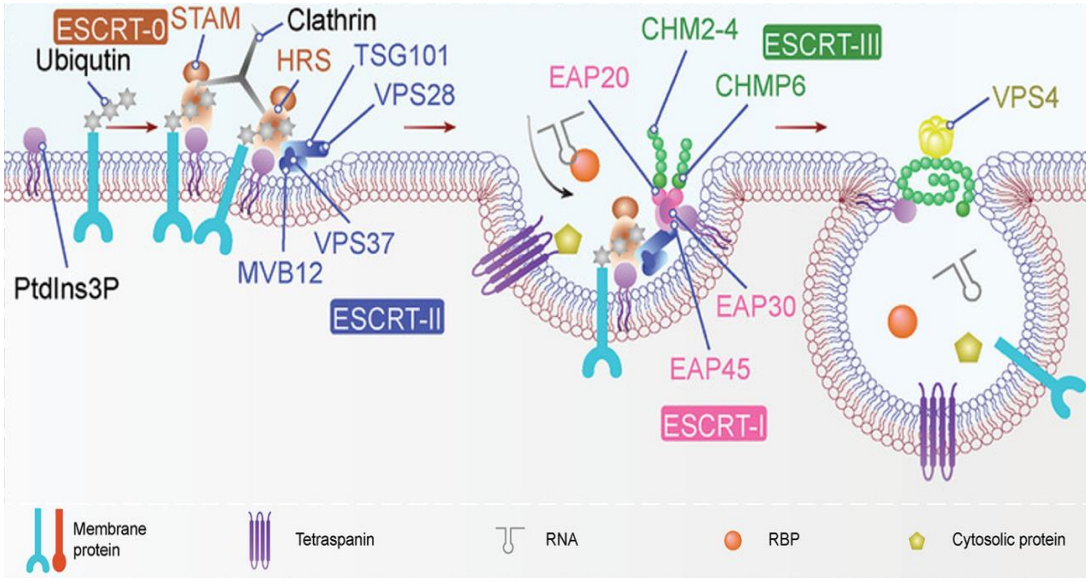


Figure 1.7 The ESCRT dependent pathway *The inward budding of the MVBs is achieved by the recruitment of ESCRT 0, I, II and III and subsequent packaging of ubiquitinated proteins in to the developing ILVs. Several membrane proteins are associated with the membrane of the ILV such as tetraspanins and membrane proteins from the MVB. There are several proteins associated with each ESCRT complex as shown above, including the RNA binding proteins, with VPS4 being associated with the sealing of the membrane to have a fully formed ILV. (Used with permission-Teng and Fussenegger, 2021).*

The ESCRT-independent pathway is associated with the tetraspanin CD63. This alternate pathway is also known as the ceramide/clathrin mediated pathway. An alternative mechanism is associated with the transmembrane protein syntenin involved in the binding of multiple ligands such as syntenin, including chemokines, growth factors, adhesion molecules, and integrins. Cargo dependent syndecan oligomerization and its binding to syntenin (Figure 1.8) result in the recruitment of tetraspanin CD63 and ALIX to the double membrane. This process leads to ILV formation with the recruitment of VPS4 (Villarroya-Beltri *et al.,* 2014).

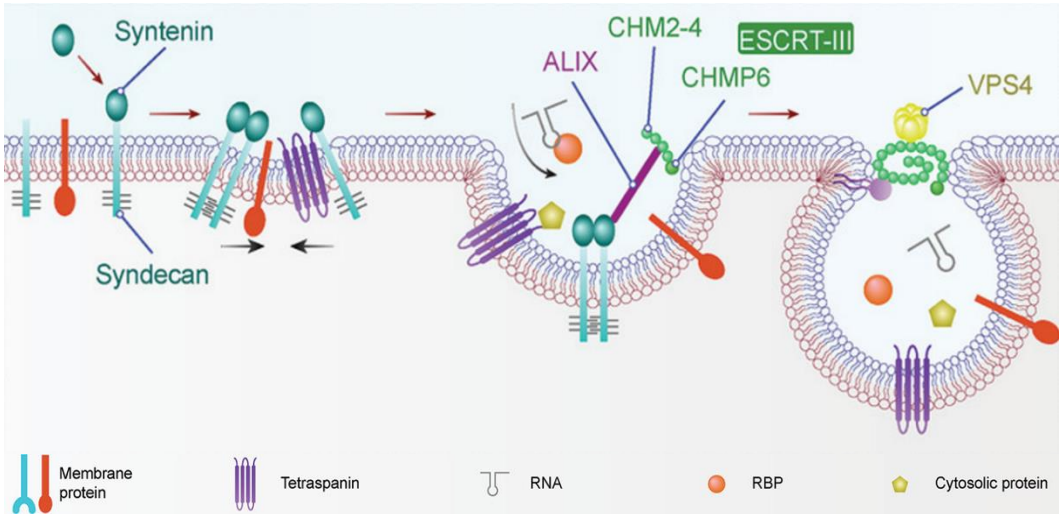


Figure 1.8 The ESCRT independent pathway. *The binding of Syndecan to Syntenin result in the inward budding of the MVB membrane. The membrane of the MVB contains tetraspanins and membrane proteins. ALIX and the ESCRT III are responsible for the processing and packaging of ubiquinated content in to the forming ILVs. The VPS4 protein is then associated with the sealing of packaged ILV protein. (Used with permission-Teng and Fussenegger, 2021).*

Several studies have shown that blocking the ESCRT dependant and independent pathways does not stop EV release entirely. Although it is difficult to categorise the origin of EVs; whether they are derived from recycled EVs that have been taken up by the cells and released or formed via the ESCRT dependant or independent pathway (Sung *et al.,* 2015). There has recently been speculation these pathways are compensatory, and that there is a potential third mechanism of EV formation within cells. These findings indicate that a third pathway associated with lipid clustering

into lipid rafts controls membrane invagination and vesicle formation (Figure 1.9) (Tan *et al.,* 2013; Soung *et al.,* 2015; Kowal *et al.,* 2014).

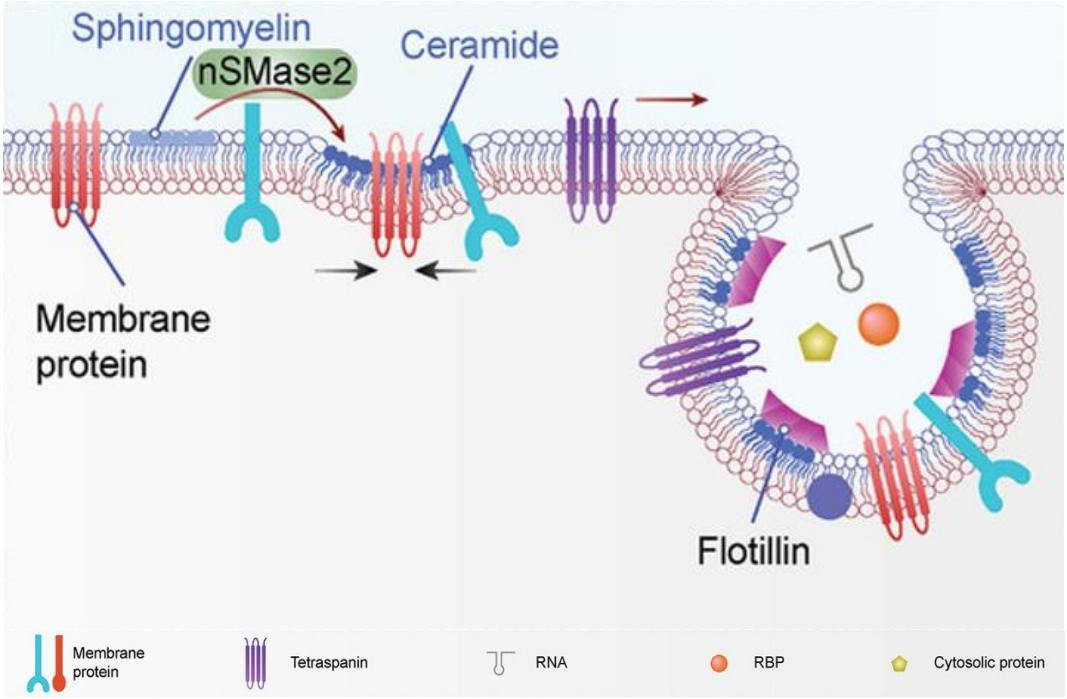


Figure 1.9 Lipid raft dependant ILV formation. *The inward budding of the forming ILVs are initiated via the conversion of sphingomyelin to ceramide via nSMase2. The inwards budding incorporates the tetraspanins on the surface of the developing ILV that is packaged with active content (Used with permission-Teng and Fussenegger, 2021).*

This mechanism of formation is lipid dependant which triggers membrane invagination and budding via the ceramide initiated mechanism, as the hydrolysation of sphingomyelin to ceramide results in the inwards curving of the leaflet of the endosome membrane to begin ILV formation (Stuffers *et al.,* 2009; Trajkovic *et al.,* 2008). The sorting of cargo in this pathway is still yet to be determined, although previous studies have indicated the potential role of tetraspanins as shown in Figure 1.10 (Phuyal *et al.,* 2014; Van Niel *et al.,* 2011).

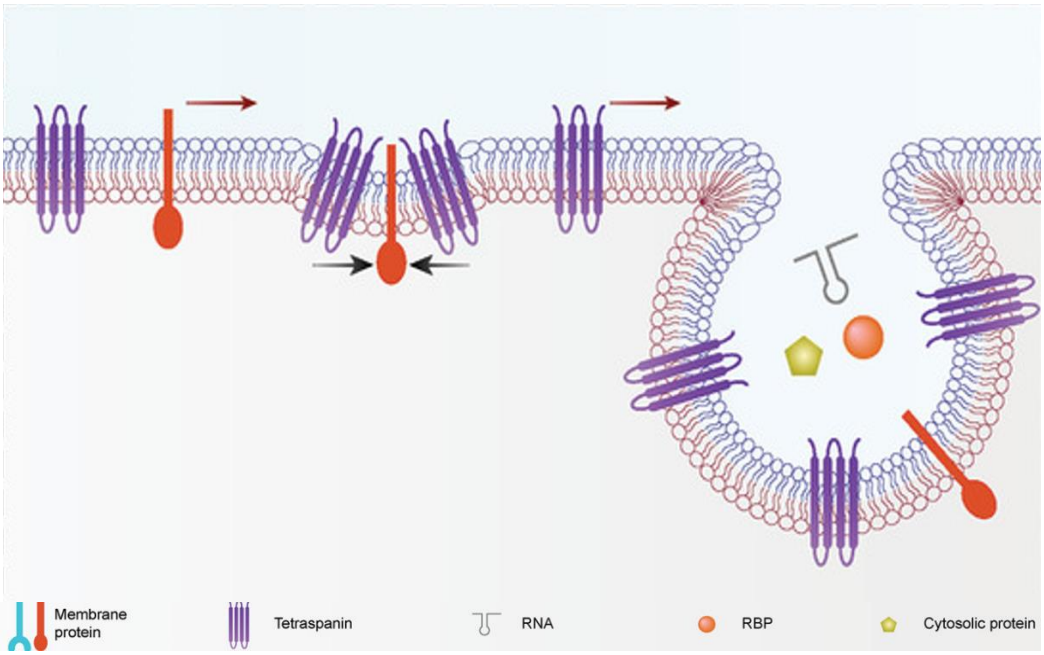


Figure 1.10 ILV formation via the CD63 tetraspanins and Flotillins. *The proposed method of the CD63 and Flotilin induction of the inward budding of the MVB surface and the ILV processing and packaging (Used with permission-Teng, F. and Fussenegger,*

After MVB formation via the ESCRT dependant or independent route, the MVBs can either migrate towards autophagosomes or lysosomes for degradation and the broken-down products can be re-used by the cell. The tagging for degradation of EVs depends upon several things including the current stress state of the cell, as studies have shown that the knockdown of proton pumps and the subsequent alterations in pH decreases the overall number of EVs produced (Parolini *et al.,* 2009). Until recently the mechanism which decides the fate of EVs was unknown. However, a study by Villarroya-Beltri *et al*., (2016) indicated the potential involvement of ISGylation; the addition of the ubiquitin like protein ISG15 to TSG101, which works similarly to ubiquitylation. Ubiquitinated proteins are targeted for degradation via the proteasome, and ISGylated MVBs are targeted for degradation via lysosomes.

1.9.5 Docking of MVBs at the cell membrane and release of EVs

MVBs that are not degraded are transported via the cytoskeleton and microtubules for docking and release from the plasma membrane, this process involves several Rab proteins using GTPase activity. Rab proteins are associated with being the

molecular switches for MVB budding, docking, and membrane fusion. The most widely researched proteins are Rab27a and Rab27b, which are essential for MVB docking at the plasma membrane (Ostrowski *et al.,* 2010). Rab27 was also reported to promote growth, invasion, metastasis, and chemoresistance in a variety of cancer types (Guo *et al.,* 2019). Rab7 is required for the secretion of syntenin- and ALIX-containing MVBs (Guo *et al.,* 2019, Ostrowski *et al.,* 2010). However other proteins have been implicated in the docking of MVBs and the release of EVs such as Rab4, Rab5, Rab35, RalA, cortactin (Sinha *et al.,* 2016). It is currently not clear if the mechanisms that control MVB migration and docking undergo altered regulation as cells transform into a malignant phenotype.

Adhering to the membrane via Rab docking proteins also requires a calcium release to initiate the induction of the final fusion of the MVB to the plasma membrane (Savina *et al.,* 2005). SNARE proteins are membrane bound proteins that work in complimentary pairs to control the release of specific vesicles at the appropriate time (Xu *et al.,* 2022). Distinct SNARE proteins promote the fusion of MVBs with the plasma membrane for the secretion of the different subpopulations of EVs from single cell types. Thus, Inhibition of specific SNARE proteins might only affect the secretion of a particular subpopulation of EVs (Bebelman *et al.,* 2021). After fusion with the membrane, MVBs release ILVs into the extracellular space. Once the vesicles are in the intracellular space they are termed extracellular vesicles “EVs”.

The identification of the distinct population of EVs that are released is still in its infancy, with current research investigating the potential to further categorise the EVs produced by content, membrane stiffness by bending using atomic force microscopy, and size variability (Vorselen *et al.,* 2020; Zhang *et al*., 2018). Recently a study by Lyden *et al.*,(2018) identified two subpopulations; one termed exo-large (90-120 nm) and exo-small (60-80 nm), both being enriched for proteins associated endosomal function, with a primary difference of protein content. The exo-small population had high levels of flotillin 1 and 2, whereas the exo-large population had proteins associated with the Golgi, indicating vesicle formation by potential

membrane budding. The third population were termed exomeres, which were non-membranous nanoparticles ~35 nm in size and extracellular vesicles produced, which were enriched with metabolic enzymes associated with glycolysis. The limitations in the field appear to be linked to equipment available for such analyses on a nanoscale, and reproducibility between labs.

1.9.6. EV uptake

EVs are continuously secreted and taken up by the cells they are derived from and surrounding cells. This constant process of endogenous production and recycling results in a net production of a mixed population of EVs in any cell and the extracellular space.

EV uptake has been extensively researched, with several mechanisms of uptake identified including: direct membrane fusion; clathrin-mediated endocytosis; receptor/ligand binding; caveolin-dependant endocytosis; lipid raft mediated uptake; micropinocytosis; and phagocytosis (Figure 1.11) (Parollini *et al.,* 2009). Macropinocytosis and phagocytosis are associated with EV clearance rather than recipient cell stimulation.

It is not known if the mechanism of uptake of EVs by recipient cells determines the localisation, degradation, or functional use of the EV content. EVs produced endogenously result in specific organotropism but it is unknown if recycled EVs can still undergo modifications once taken up by a cell to also result in organotropism.

Direct fusion with the plasma membrane (Figure 1.11 A) is a mechanism of EV uptake which transfers cargo to recipient cells (Prada and Meldolesi, 2016). Exact details of the mechanism are poorly understood due to the complexity of lipids present on both the plasma membrane of the cell and the lipid bilayer of the EV and these interactions happen on such a small surface area (Nishio *et al.,* 2020). Co-localisation of EVs with Rab53 or Lamp-1 suggested that EVs are internalised and interact with cytoplasmic vesicles (Parolini *et al.,* 2009). There is also a potential role

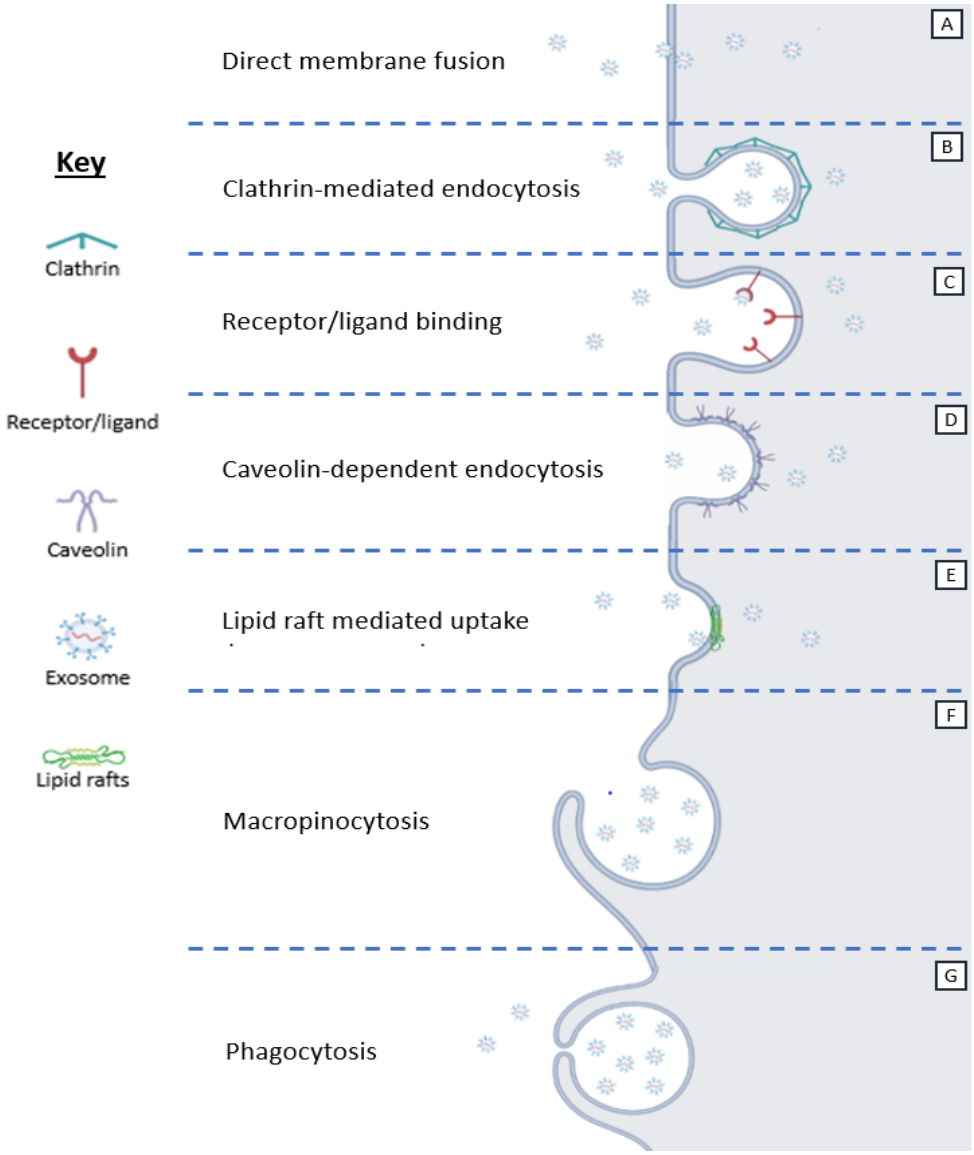


Figure 1.11 Summary of the mechanisms of EV uptake. *These include* ***A)*** *Direct membrane fusion whereby the surface of the EVs fuse with the surface of the cell membrane resulting in cellular uptake. There are several protein-mediated methods of uptake which include* ***B)*** *Clathrin-mediated endocytosis* ***C)*** *Receptor/ligand binding and* ***D)*** *Caveolin-dependant endocytosis. Other methods of EV uptake include* ***E)*** *Lipid raft mediated uptake and* ***F)*** *Micropinocytosis* ***G)*** *Phagocytosis.*

of tetraspanins on the surface of EVs and the surface of recipient cells that may be responsible for the fusion, similar to sperm-oocyte fusion (Rana and Zoller, 2011). Integrins are transmembrane heterodimers that have alpha and beta subunits and are responsible for cell attachment and organotropism (Hoshino *et al.,* 2015) Integrins present on the EV surface may also be responsible for the attachment to recipient cells (Chen *et al*., 2016).Tetraspanins are transmembrane proteins that are found on EVs with CD9, CD63 and CD81 being the signature markers of EVs (Karimi *et al*., 2022; Mizenko *et al.,* 2021). Studies has been shown that when paired with integrins can form a tetraspanins enriched regions that regulate membrane tension during cell adhesion, such complexes have identified to include CD81 with the integrin pattern α4β1, and CD151 with α3β1, with their function being linked to both cell adhesion and cell fusion (Spring *et al.,* 2013; Zevian *et al.,* 2015)

Clathrin-mediated endocytosis (CME) is a mechanism of uptake that involves an interaction between a ligand binding to a receptor on the surface of the cell plasma membrane to initiate internalisation (Figure 1.10, B). The internalisation of materials happens by the formation of clathrin coated vesicles, once internalised the vesicles undergo clathrin uncoating to fuse with the endosome and transfer the cargo within the formerly clathrin coated vesicle (Hu *et al.,* 2015). Studies have shown that inhibition of clathrin pit formation causes EVs to be internalised in a CME independant mechanism, resulting in a reduction of EV internalisation in the recipient cells (Chen *et al.,* 2014; Yang *et al.,* 2015; Lee *et al.,* 2014). This was substantiated by another study showing a mutant phenotype affecting the clathrin coating of the pits in CME also decreased the ability of the cells to take up EVs (Feng *et al.,* 2010).

Receptor/ligand binding is the protein-protein interaction between proteins on the surface of EVs and on the outer membrane of recipient cells which result in endocytosis (Figure 1.11 C). Such protein-protein interactions including selectin binding (CD62) (Van Dongen *et al.,* 2016) or adhesion molecules (Bilen *et al.,* 2017).

The presence of EpCAM-1 and I-CAM on the surface of EVs can mediate endocytosis (Gonda *et al*., 2019).

Caveolin-dependent endocytosis (CDE) is a protein with cholesterol rich domains and is found in the plasma membrane of recipient cells (Figure 1.11 D). The mechanism of CDE is a raft mediated endocytosis that is dependent on caveolin. Caveolae are pit shaped invaginations containing cholesterol in the plasma membrane that are utilised by the cell for endocytosis. This process is thought to be cholesterol and dynamin 2 dependant (Matthaeus *et al.,* 2020; Sandvig *et al.,* 2018), and studies performing cholesterol depletion flattens the caveolae pits (Namba *et al.,* 2013).

Lipid raft mediated uptake is another form of EV uptake (Figure 1.11 E). EVs appear to have the ability to induce the formation of tunnelling nanotubes in recipient cells (Thayanithy *et al.,* 2014). Tunnelling nanotubes are thin actin-based cytoplasmic extensions that can form between cancer cells *in vitro* allowing the transfer of organelles and microvesicles. The formation of these nanotubes in the recipient cell membrane appears at focal points along the cell membrane where there are high levels of lipid rafts. In a study by Thayanithy *et al*., (2014), it was found that a low pH results in an increase in the formation of tunnelling microtubules. The acidic environment of the TME means the increase of tunnelling microtubules could be a mechanism used by cancer cells to increase EV uptake. There is evidence that tunnelling microtubules can be induced as a stress response following irradiation, and the development of microtubules resulted in a protective effect following x-ray irradiation in glioblastoma cell lines (Rustom, A., 2016; Osswald *et al*., 2015). Additionally, Kretschmer *et al.,* (2019) found that stress treatment of the PCa3 prostate cancer cell line had increased microtubule formation when cells were serum starved or kept in hypoxic conditions. Research in to pathways or proteins associated with inducing the formation of tunnelling microtubules are is still in its infancy (Matejka *et al.,* 2019). However, extracellular vesicle recycling showed to increase expression of Rab11 and Rab 8 which are vesicle transporters resulted in

increased tunnelling microtubule formation in a mouse neuronal cell line (Zhu *et al.,* 2018). These findings indicate that the tunnelling microtubules may be a call-for-help response from cells, which could be initiated by exosomes. It would be interesting for further research to investigate the role of tunnelling microtubules on breast cancer therapy resistance.

Phagocytosis (Figure 1.11 G), a process mostly used by immune cells to clear debris, with the smallest particles to be phagocytosed being 85 nm (Rudt and Muller, 1993). There have been several studies showing that EVs can be phagocytosed by cells due to the presence of immune markers and phosphatidylserine on the surface (Sharma *et al.,* 2017). These markers also mediate uptake of EVs via a similar process for nanoparticles called micropinocytosis (Tian *et al*., 2014)(Figure 1.11 F). For example, oncogenic signals induced by mutant KRAS expression promote EV uptake by macropinocytosis in human pancreatic cancer cells (Kamerkar *et al.,* 2017).

1.9.7 EV composition

During the EV biogenesis the packaging of the EV content reflects the parental cell (Skotland *et al.,* 2019). EVs contain protein, nucleic acids and several types of lipids. The primary function of EVs is cell to cell communication, and this is achieved via the exchange of the EV content. Databases, such as Vesiclepedia, Exocarta and EVpedia, are designed to collate information related to the composition of extracellular vesicles derived from several different cell types and species and contain several thousands of protein and mRNA entries (Kalra *et al.,* 2012). EV content can be indicative of disease progression on the molecular level, and transferral of EV content can result in phenotype changes in recipient cells (Zhou *et al.,* 2022). This means that databases can be used to compare EV cargo to potentially predict novel targets in disease pathways.

EV content remains intact due to their highly stable double membrane composed of a lipid head with fatty acid tails in a lipid bilayer formation. The membrane also

contains several tetraspanins on the surface, depending on the cell of origin; however, it is widely agreed that the presence of three tetraspanins in particular, CD9, CD63 and CD81 are general markers of EVs, as these tetraspanins are associated with the formation of EVs within any cell type (Takahashi *et al.,* 2022; Nwokwu *et al.,* 2022; Song *et al.,* 2022). Other proteins are also associated with cell penetration and fusion including integrins for cell ligand binding, MHC I and II. MHC I and II are found prominently on EVs derived from antigen presenting cells (APCs) which typically display MHCs such as B cells, T cells and dendritic cells (Kokima *et al.,* 2017, Raposo *et al.,* 1996). There are studies that have shown that EVs displaying MHCs can result in immune suppression in mouse and human cancer models, although APCs themselves have shown to be more efficient at activating naïve T cells compared to EV isolates (Graner *et al.,* 2009; Clayton *et al.,* 2005; Peinado *et al.,* 2012).

EV content is derived from several sources: the constituents of the cytoplasm in the cell of origin such as: chaperone proteins, enzymes and nuclear material including types of RNA; proteins associated with the ILV formation; and cargo specifically tagged and packaged in to ILVs (Shefer *et al.,* 2022; Hussein *et al.,* 2022). However, research is still ongoing to identify the exact mechanisms of EV packaging that results in the specific EV content which is found in EVs (Figure 1.12).

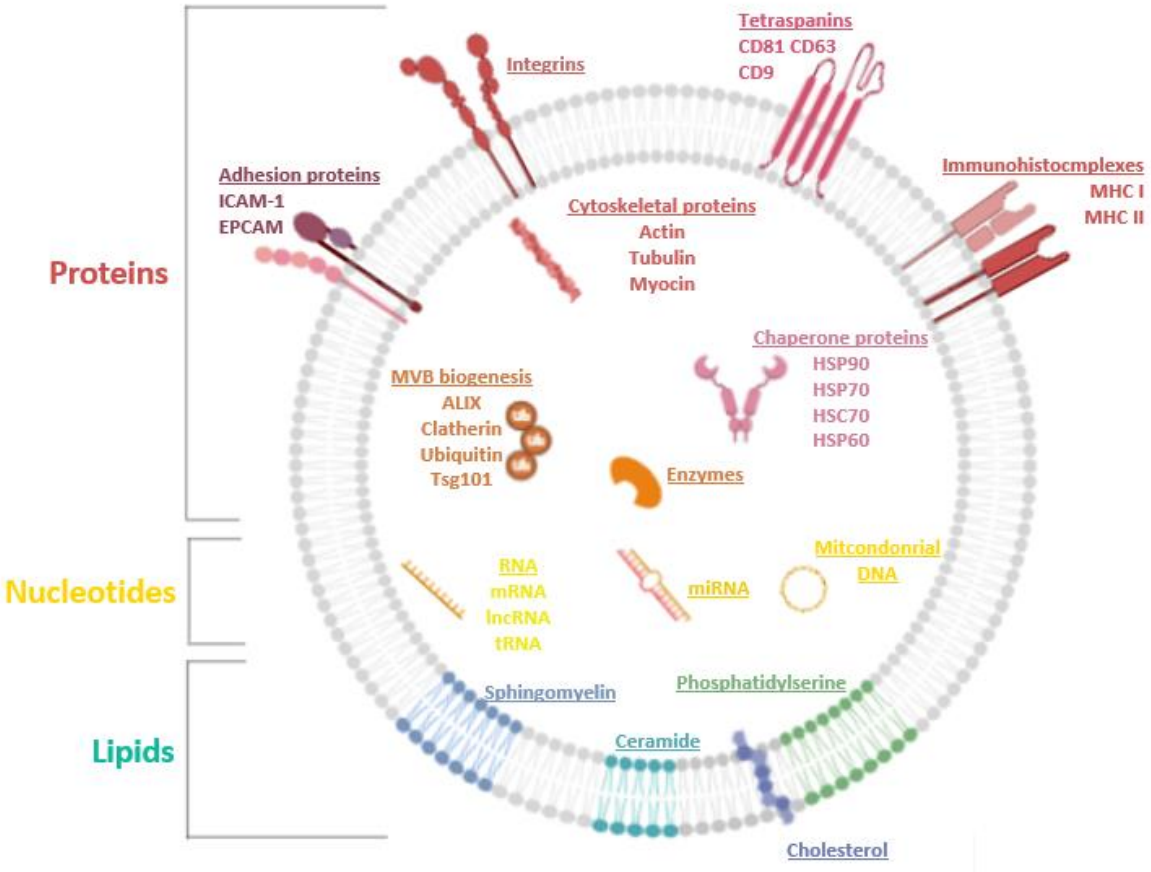


Figure 1.12 Summary of the protein, nucleotide and lipid content of EVs. *EVs are comprised of proteins (red), several types of nucleotides (yellow) which are encapsulated in a double membrane in a lipid bilayer formation which contains different lipids (blue/green) (Created in BioRender.com).*

EV content has been widely analysed, with particular focus on miRNA and proteins as these active constituents have greatly impact the recipient cell phenotype.

1.9.7.1 Protein content of EVs

EVs contain proteins ranging from MVB transport proteins to functional protein cargo packaged from their parental cells. EV protein cargo can be profiled by mass spectrometry and studies have shown EVs can contain between 88 to 500 proteins across cell lines and clinical samples (Rontogianni *et al.,* 2019; Palazzolo *et al.,* 2012; Kruger *et al*., 2015). The Exocarta database is the publicly accessible database containing mass spectrometry profiling data of EVs (http://www.exocarta.org/). This shows that EVs typically contain proteins such as integrins, cellular cytoskeletal

proteins, heat shock proteins (HSPs) and proteins associated with EV formation and release (Chen *et al.,* 2017).

Proteins present in the lipid membrane can include MHCI and MHCII when derived from antigen presenting cells, as well as adhesion proteins such as EpCAM and ICAM-1 which are responsible for attachment to recipient cells (Wang *et al.,* 2021). The presence of integrins and tetraspanins projecting from the lipid membrane are associated with cell adhesion and activation of signalling pathways in recipient cells (Shimaoka *et al.,* 2019). Proteins inside the EV include cytoskeletal proteins such as actin and myosin that are incorporated from the cytoplasm during ILV formation (Chen *et al.,* 2016). Similarly, EV proteins that are present during MVB formation such as ALIX, TSG101, clathrin and ubiquitin, and MVB docking and release pathways such as the Rab protein family are typically found in upon EV mass spectrometry (Fonseka *et al.,* 2019).

Chaperone proteins are named according to their molecular weight in kDa, within EVs there are several Hsps such as Hsp70, Hsc70, Hsp90 and Hsp7 (Chanteloup *et al.,* 2020; Eguchi *et al.,* 2018; Li *et al.,* 2021). Hsp70 is expressed in all cells as a chaperone to assist with protein folding, but has increased expression after the acquisition of a malignant phenotype (Gong *et al.,* 2015). The higher metabolic rate of cancer cells results in an increase in malformed proteins due to incorrect protein folding. These proteins can be rescued by Hsp70 for refolding, which are passed on to Hsp90 to complete folding to the fully native structure (Rutledge *et al.,* 2022). The presence of Hsp60 is associated with the mitochondria, however can be found in higher levels throughout the cell and is thought to be involved in immune cell signalling, and has been found at much higher levels in cancer cells compared to healthy cells (Campanella *et al.,* 2012; Jeppesen *et al.,* 2019; Jones *et al.,* 2018). HSPs can elicit inflammatory and immune effects in recipient cells due to their presence on the surface of EVs (Calderwood *et al.,* 2016).

Other EV proteins include enzymes that are activated once transferred to recipient cells. A study by (Kim *et al.,* 2017) showed the release of lysyl-tRNA synthetase, known to be essential for protein synthesis, from EVs derived from colorectal carcinoma cells. This demonstrates the ability of EVs to transfer active enzymes between cells. In addition, EVs tend to have a rich content of proteolysis enzymes, suggesting that EVs may have the ability to promote cell migration (Lan *et al.,* 2019; Ma *et al.,* 2019). Proteomic analysis and gene ontology showed EVs can promote glycolytic activity in recipient cancer cells, which could promote the ability of cancer cells to adapt to a hypoxic environment (Wang *et al.,* 2020; Hegmans *et al.,* 2004; Zhao *et al.,* 2016).

1.9.7.2 Nucleic Acid content of EVs

The mechanism which results in the inclusion of nuclear components within EVs is still poorly understood. When cell replication of nuclear material goes wrong, cytoplasmic structures containing nuclear material (including chromosomes) are enveloped by a nuclear membrane which known as micronuclei (Yoki *et al.,* 2019). The production of micronuclei is increased with DNA-damaging therapeutics such as radiotherapy, meaning micronuclei could be biomarkers of genomic instability. The envelope enclosing the nuclear material is highly unstable and is eventually broken down, releasing the contents in to the cytoplasm during cell division, allowing the nuclear content to be incorporated in to ILVs inside MVBs (Hatch *et al.,* 2013). Micronuclei are more common in cancer cells due to the high degree of genomic instability. This was shown by Yoki *et al.,* (2019), which showed that cancer cells produce more EVs with high nuclear content compared to non-malignant cells. The build-up of DNA in the cytoplasm in cancer cells could be explained by their deregulated DNA repair pathways (Shen *et al.,* 2015; Ho *et al.,* 2016), resulting in a higher abundance of DNA being incorporated in to developing EVs in the cytoplasm when compared to non-cancerous cells.

It has been proposed that EVs contain DNA in either the form of double stranded DNA or single stranded DNA (Kalluri *et al.,* 2016). The type of DNA accepted to be

found within the EV is mitochondrial DNA (Sansone *et al.,* 2017). However, it is currently disputed if EVs contain nuclear DNA. However, there are several studies showing the presence of single stranded and double stranded DNA in varying integrity such as studies stating that EVs derived from cancer cells have shown to contain higher amounts of DNA compared with non-malignant fibroblast cell lines. (*Kahlert et al.,* 2014; Thakur *et al.,* 2014). The presence of DNA in EVs could depend upon the cell of origin as the mechanisms resulting in DNA packaging during EV synthesis can be cell type specific and highly regulated.

However, some studies have shown that double stranded DNA has been found within EV preparations but also in the supernatant. This highlights a discrepancy and could potentially explain the presence of other DNA types found in EV studies. There are also several studies stating that single stranded DNA found in EVs is from the supernatant isolated alongside tumour cells (Balaj *et al.,* 2011).

Valadi *et al.,* (2007) was the first study to show the presence of RNA and miRNA in EVs. Studies have identified active RNAs within the EV cargo, which can elicit effects on recipient cells. Types of RNA present include: messenger RNA (mRNA); microRNA (miRNA); long coding RNA (lcRNA); non coding RNA (ncRNA). The horizontal transfer of miRNA has been shown to elicit changes in recipient cells following EV uptake.

Coding RNA decides the amino acid sequence of the protein transcribed. Types of RNA include mRNA, which carries the genetic code and can be recognised by the recipient cell to make proteins. Non-coding RNA describes any RNA that is not directly translated or transcribed and is split in to two categories long non-coding RNA, which is 200 nucleotides (nt) long and above, or short non-coding RNA which is less than 200 nt. Non-coding RNAs including: ribosomal RNA (rRNA); transfer RNA (tRNA); small nuclear RNA's (snRNA); all of which have been found within EVs (Baglio *et al.,* 2017; Chen *et al.,* 2016; Herrera *et al.,* 2018; Wang *et al.,* 2020). MicroRNAs (miRNA) are approximately 22 nt and are the most widely studied group of RNAs in

EVs and can mediate post-transcriptional gene silencing by blocking translation of mRNA (Liu *et al.,* 2018). miRNAs are predicted to regulate over 60% of protein-coding genes (Donnarumma *et al.,* 2017) meaning non-coding RNA could be exploited to determine the status of a tumour (Silva *et al.,* 2015). There is also current research to identify if miRNA content of breast cancer can be used as a biomarker of cancer progression and therapy resistance (Hussein *et al.,* 2022; Sueta *et al.,* 2021)

1.9.7.3 Lipid content of EVs

EV membranes are mostly comprised of lipids, with traces of lipids present inside the EV, derived from parental cells that are incorporated into the EV during the formation of ILVs. Theoretically EV lipid composition should be like that of a lipid bilayer, but there is an asymmetric distribution of lipid types in each leaflet of the plasma membrane, with phosphatidylcholine and sphingolipids mostly in the outer leaflet and the other lipid classes are mainly located in the inner leaflet (Van meer *et al.,* 2008). Interestingly, these studies show a two to three times enrichment from cells to EVs of cholesterol, sphingomyelin, glycosphingolipids, and phosphatidylserine, which also indicates that EV membranes contain lipid raft like domains (Skotland *et al.,* 2019; van meer *et al*., 2008; Hessvik *et al.,* 2016).

Biogenesis and release of EVs could be cell type dependant based on the lipid content. In the oligodendroglial precursor cell line, Oli-neu, it was found that inhibition of an enzyme, SMase, that creates ceramide from sphingomyelin, caused a decrease in the production of EVs (Trajokovic *et al.,* 2008). This effect was also reported in a human embryonic kidney cell line (Kosaka *et al.,* 2010) and T cells (Mittelbrunn *et al.,* 2011). However, this effect was not seen in all cell lines tested in the literature to date such as the human melanoma cell line and prostate cancer cell line PC-3 (van Niel *et al.,* 2011; Phuyal *et al.,* 2014). Furthermore, vesicles formed via different formation pathways within a cell might utilise different pathways, like those shown for syntenin-containing EVs from the BC cell line MCF-7 (Ghossoub *et al.,* 2014).

1.10. Role of EVs in cancer

After decades of research, it has been found that upon the acquisition of a malignant phenotype, the EVs begin to nurture the survival and development of cancer (Feng *et al.,* 2019). EVs have been identified as key players throughout the timeline of cancer development; from the initial modification of the tumour microenvironment achieved by tumour cells, to the initiation of metastasis to the spread to distal sites (Fong *et al.,* 2015; Fang *et al*., 2015; Zhang *et al.,* 2017). A hallmark paper by Hoshino *et al.,* (2015) identified specific integrin patterns on EVs can predict the secondary site of metastasis. Integrin patterns contain an alpha (α) and a beta (β) subunit and are found in different combinations. The study by Hoshino *et al.,* (2015) found that integrin patterns α6β4 and α6β1 result in metastasis to the lung, and the integrin pattern of αvβ5 results in metastasis to the liver regardless of the tumour type of origin. This was also confirmed in a follow-up study where β4 was found to induce metastasis to the lung in breast cancer (Grigoyeva *et al.,* 2023). It was found that delivery of the EV content induces an inflammatory phenotype and appears to educate the surrounding cells to promote the growth and proliferation of incoming cancer cells, by providing nutrients and hindering immune cell invasion to the pre-metastatic niche (Rooman *et al.,* 2017).

1.10.1. Role of EVs in the tumour microenvironment

For the stabilisation and growth of developing tumours, it is necessary for several types of crosstalk within the tumour microenvironment, with EVs being identified as imperative communicators between cells (Webber *et al.,* 2013). EVs influence recipient cells within TME to favour oncogenic development via the initiation of angiogenesis, invasiveness and progression (Maji *et al.,* 2013; Shimada *et al.,* 2016; Teng *et al.,* 2017; Wang *et al.,* 2014).

In hypoxic conditions Hsu *et al*., (2017) found that lung cancer-derived EVs from hypoxic conditions had increased levels of miR-23a which could upregulate PHD1 and 2. This increase caused an accumulation of HIF1-α in endothelial cells which resulted in the induction of angiogenesis and promoted vascular permeability. This study alongside others have demonstrated the ability of EVs derived from cancerous cells in a hypoxic environment to induce HIF1-α and activate AKT and ERK to result in angiogenesis (Liu *et al.,* 2011; Hannafon *et al.,* 2015).

1.10.1.1 The role of EVs in the nurturing of developing cancer cells

EVs derived from CAFs prevent mitochondrial oxidative phosphorylation by increasing the levels of glycolysis and glutamine-dependent reductive carboxylation in cancer cells. The CAF EVs also supply amino acids that are deficient in recipient cancer cells in a manner like micropinocytosis to nurture developing tumour cells within the TME (Sung *et al.,* 2020). Previously, studies have shown that KRAS proteins (proteins that relay signals from the cell membrane to the cell nucleus) are required for cells to utilise micropinocytosis to absorb extracellular proteins (Commisso *et al.,* 2013). However, EVs can shuttle amino acids to recipient cells like micropinocytosis independently of KRAS signalling, and the protein content of these EVs undergo proteolysis and are used in the glutamine pathway to create carbon sources in starved cancer cells (Zhao *et al.,* 2016), therefore, EVs can shuttle nutrients required for cancer cell carbon metabolism during tumour growth, nutrient deprivation and cell stress. Moreover, it has been shown that the transfer of EVs from cancer cells can cause the switch from normal fibroblasts, which have anti-tumour properties, to pro-tumourigenic fibroblasts (Goulet *et al.,* 2018).

Similarly, EVs derived from cancer cells stimulate phenotypic changes in immune cells present in the TME, such as macrophages, as the uptake of EVs from cancer cells can result in a phenotype change from M1 to M2, via the transferral of EV miRNA content (Su *et al.,* 2016; Chen *et al.,* 2017; Ying *et al.,* 2016).

1.10.1.2 The role of EVs in tumour-protective immune suppression

Cancer progression partially involves systemic immune suppression, for example in a non-cancerous environment dendritic cells process antigens and maintain the immune system by the activation of toll-like receptors, whereas Fabbri *et al.,* (2012) has found that in a cancerous environment miRNA content of EVs derived from cancer cells can bind as ligands and inhibit toll-like receptors on dendritic cells, meaning EVs can inhibit the innate immune response. EVs derived from antigen presenting cells, such as dendritic cells, also have MHC I and II on their surface. Gauvreau *et al.,* (2009) found that MHC II are presented on EVs derived from APCs and are packaged into EVs in a ubiquitin-independent manner. EVs derived from antigen presenting cells, such as macrophages and dendritic cells, can modulate NK cells, CD8+ and CD4+ T cells to favour tumour development (Seo, N. 2018). Furthermore, the transfer of EVs have been shown to play a role in the alteration of cells towards a tumour promoting phenotype, in cancer cells within the bulk tumour and for components of the TME such as immune cells and CAFs (Guo *et al.,* 2019).

Under normal circumstances, T cells can recognise and attack tumour cells. Following the remodelling of the tumour microenvironment, PD-1 can bind to PD-L1 and results in an inhibitory signal, inhibiting T cell activation and proliferation whilst stimulating T cell apoptosis. It was found by Chen *et al.,* (2018) that EVs derived from cancer cells also carry PD-L1 which can result in an overall suppression of the immune system, and that PD-L1 on EVs has the same structure as it does on the surface of tumour cells and can effectively bind to PD-1 on T cells (Chen *et al.,* 2018).

1.10.2. The role of EVs in the formation of pre-metastatic niches and distal metastasis

EVs increase the invasive and metastatic capabilities of primary cancer cells, with cancer metastasis commonly resulting in a high occurrence of mortality in comparison to primary tumours (Song *et al.,* 2020). For primary tumours to spread throughout the body, there must be initial interactions between the migrating tumour cells and the distal secondary site for the tumour cells to prime the pre-metastatic niche for invasion. Upon invasion of the secondary site, developing cancer calls have many environmental factors to overcome including: the immune system; decreasing local oxygen status; and lack of blood supply to supply nutrients to developing tumours (Elia and Haigis, 2021).

EVs migrate to distal sites and possess the ability to prime the pre-metastatic niche to be suitable for incoming cancer cells (Hoshino *et al.,* 2012). This modulation is achieved by altering distal sites to have a nurturing environment for migrating cancer cells such as local immune suppression and reprogramming non-malignant cells to decrease glucose uptake allowing for an increase in nutrient availability for incoming tumour cells (Fong *et al.,* 2015). Once incoming tumour cells arrive at the secondary site EV transfer can promote suppression of endothelial junction proteins to promote vascular leakiness which helps evasion of the immune system and modulation of stroma to promote tumour propagation (Jiang *et al.,* 2017; Rooman *et al.,* 2017; Alipoor *et al.,* 2018).

In the context of BC, the secondary sites are the brain, lungs and bone (Wong *et al.,* 2020). Studies have identified the process specific organ metastasis of EVs includes: integrin patterns; miRNA content in EVs produced from the primary cell; and potential ligands on the surface of EVs (Hoshino *et al*., 2015; Lima *et al.,* 2021; Tominaga *et al*., 2015; Korpal *et al.,* 2011). In a study investigating the metastasis of

prostate cancer cells, it was found EVs derived from prostate cancer cells had specific integrin combinations of integrin α2 and integrin α6 were responsible for metastasis to the bone marrow (Ricci *et al.,* 2013). Integrin combinations have also been implicated in the uptake of EVs as knockdown of β_4 and β_5 decreased uptake and metastasis of cells (Hoshino *et al.,* 2015). A similar study showed specific integrin expression on EVs derived from BC cells determined migration to either the liver ($\alpha_v\beta_5$) or lung ($\alpha_6\beta_4$ and $\alpha_6\beta_1$).

Although it has been shown that integrin patterns can determine organotropism, it is unknown how much of an influence the miRNA content of EVs can elicit, as there are studies *in vivo* showing the association of specific miRNA with organotropism showing metastasis to the distal sites of the brain, lung and bone (Zhang *et al.,* 2015; Wu *et al.,* 2020; Hashimoto *et al.,* 2018). The interplay between the miRNA content and integrin patterns determining metastasis is currently unknown, but the current research shows both appear as vital players in the metastasis of cancer, making EVs a focus of cancer development.

1.10.3. The role of EVs in the acquisition of radioresistance

EVs have been shown to play a pivotal role in the development and spread of cancer (Hoshino *et al.,* 2015, but their role in the development of radioresistance is not as widely researched and is therefore poorly understood. It is known that EVs transferred from RR cancer cells can reprogram non-radioresistant (nonRR) recipient cells to become more tolerant to environmental changes that favour the development of radioresistance (Mutschelknaus *et al.,* 2016). Due to the content of EVs reflecting the biological status of the parental cells, this means circulating miRNA content of EVs could be used as a biomarker of radiotoxicity (Dinh *et al.,* 2016).

The exact mechanisms of how EV transfer can affect radiosensitivity in recipient cells are not yet known, but the current literature has indicated changes associated with DDR, stem cell phenotype and a change in metabolism to adapt to hypoxic conditions (Hang *et al.,* 2021; Chen *et al.,* 2021). A study by Mrowczynski *et al.,* (2018) showed that stromal cells increase activation of the STAT1 pathway in recipient cancer cells to induce radiotherapy resistance. In glioblastoma there was an increase in oncogenic cargo and a decrease in tumour-suppressive cargo in EVs released from radioresistant cancer cells, highlighting the potential role of EVs in promoting aggressive and cancer treatment resistant phenotypes (Quezada *et al.,* 2018).

Recent studies have shown that the transfer of EV cargo could be contributing factors to the development of radioresistance via EV transfer to nonRR recipient cells resulting in increased DDR and induction of stem cell phenotypes. Boelens *et al.,* (2014) showed that EV transfer from stromal cells to BC cells can induce a protective effect to both irradiation and chemotherapy by activation of NOTCH3 and RIG-1 via RNA transfer. Previous studies have also shown in colon cancer cells that enhanced resistance is due to the acquisition of a more stem cell phenotype via induction of TGF-B signalling (Chen *et al.,* 2020; Liu *et al.,* 2020). This ability to revert cells to a stem cell phenotype is associated with increased resistance towards cancer therapies (Biddle *et al*., 2016). Additionally, irradiation has found to induce senescence in cancer cells following irradiation (Elbakrawy *et al.,* 2020). Senescence is the state of permanent growth arrest, preventing cellular proliferation; therefore, avoiding apoptosis induction that can follow during cell proliferation checkpoints (Jaber *et al.,* 2023). Following irradiation, prostate cancer cell line would enter cellular senescence due to DNA damage and would increase EV biogenesis and release in a p53 dependant manner after irradiation at 4 Gy (Lehnmann *et al.,* 2007; Lehnmann *et al.,* 2008)

1.10.4. Hypoxia and EVs

The theory that EV transmission could activate hypoxia was explored by Takeuchi *et al.,* (2015) who found EV proteome profiles related to oxygenation status of tumours and potentially activate hypoxia-dependant signalling pathways in recipient cells. Expression of HIF1-α increases to allow cancer cells to adapt to hypoxic conditions creating hypoxia tolerance (Li *et al.,* 2017). This also agrees with Kucharzewska *et al.,* (2014) who found that EV protein and miRNA content reflects hypoxic status. Furthermore, it has been found that cells have an increased resistance to radiotherapy in a hypoxic environment (Thomas *et al.,* 2013), potentially due to increased cellular communication as there is an increase in the production of EVs under hypoxic conditions (Eldh *et al.,* 2010).

Hypoxic status also affects mitochondria within cells, and mitochondria are also a target of radiotherapy treatment as irradiation results in mitochondrial dysfunction and an increase in the number of mitochondria within the cell (Kam and Banati, 2013). Radiation can induce point mutations in mitochondria, leading to mitochondrial fission which can activate mitophagy (Murphy *et al.,* 2005; Kobashiwaga *et al.,* 2011; Yamamori *et al.,* 2015). Mitochondrial DNA has been found within EVs and has been implicated in signalling associated with the radio-induced bystander effects (RIBE) on recipient cells. Upon receiving irradiation, surrounding cells experience increased DNA damage via induction of chromosomal instability, with studies showing that the mitochondria depleted cell line (Rho0 cells) do not elicit RIBE side effects or phenotypes such as increased rates of DNA damage or increased inflammation. Whereas EVs from CAF cells (with mtDNA present) resulted in the increased induction of DNA damage implying the role of mitochondria in RIBE (Ariyoshi *et al.,* 2019).

1.10.5. Radiation induced bystander effects

Targeted irradiation results in high-dose irradiation focused on a small area of tumour cells. The acute damage to nearby cells is much less than the targeted region, but similar biological changes are seen in the non-targeted cells such as: chromosome aberration; induction of mutations; DNA damage; micronucleus formation (MN); cell death (mitotic and apoptotic); and induction of oncogenic transformation (Hu *et al.,* 2021; Le *et al.,* 2017; Farias *et al.,* 2018). The EVs released from RR cancer cells appear to have more oncogenic content including growth factors with angiogenic potential and RNA that can promote migration and metastasis in recipient cells (Jelonek *et al.,* 2015; Singh *et al.,* 2014; Fong *et al.,* 2015) with recent studies showing EVs from RR cells are associated with radiation related communication (Mrowczynski *et al.,* 2018).

It has been found that irradiated cells have an increased rate of DDR for both the ATM and ATR related pathways, with a study showing the activation of such pathways after DNase treatment, indicating RNA transfer as a potential activation method (Mutchellaskus *et al.,* 2016). EVs are responsible for the RIBE in neighbouring cells *in vitro*, demonstrating the ability of EVs to confer phenotypical changes in recipient cells after radiation (Jella *et al.,* 2014; Song *et al.,* 2016). Similar observations were seen *in vivo* whereby EVs from irradiated mice were isolated and injected into mice whereby damaging effects of ionising radiation were seen such as increase DNA damage and production of growth cytokines associated with the stress response indicating an increase of inflammation in recipient mice (Szatmari *et al.,* 2019; Cai *et al.,* 2017).

Ariyoshi *et al.,* (2019) showed the horizontal transfer of EVs elicits RIBE in recipient cells, potentially by the transfer of EV RNA. The potential role of tetraspanins, such as CD81, have been identified as a mechanism of increased EV uptake following

radiation, as cells that had received ionising radiation had increased rates of CD29 and CD81 co-localisation on the cell which increased uptake of EVs (Du *et al.,* 2020) and inhibition of CD29 via antigen binding resulted in a significant decrease of EV uptake and radiosensitisation of RR cancer cells. (Hazawa *et al.,* 2014).

EVs from RR cells have altered content which can induce RIBE in recipient cells, it is currently unknown which exact mechanisms EVs can promote the survival of recipient nonRR cells following irradiation in BC. There are studies indicating potential mechanisms by which recipient cells can become more resistant. Such mechanisms include being reverted to a mesenchymal and stem cell-like phenotype (Konge *et al.,* 2018; Yadav *et al*., 2019); however, the exact signalling pathway and proteins involved are still yet unknown.

The current literature has shown the pivotal role of EVs in the development, spread and recurrence of BC. EVs are essential for cell to cell communication meaning their role in the development of radioresistance should be fully explored. EVs derived from chemotherapy resistance cells have shown to induce chemotherapy resistance in recipient cells. Furthermore, cells that receive one dose of irradiation have altered EV content, increased EV production and uptake. In BC and CMC studies there are gaps in knowledge when analysing the effect of EVs derived from radioresistant (RR) cells on the acquisition of radioresistance. Additionally, there are even fewer studies investigating potential novel therapeutic targets and biomarkers of radioresistance based on proteomic content that could be applicable to human and veterinary medicine.

1.11. The rationale of the study: Hypothesis, aims and objectives

The development of radioresistance in BC and CMC patients can often result in treatment failure due to limiting the treatment options and the development of metastases (Meehan *et al.,* 2020). EVs are double lipid membrane nanovesicles that have the role of cell to cell communication in healthy cells (Bischoff *et al.,* 2022). The content of EVs reflects the parental cell from which it is derived and contains active protein, RNA and lipids with can elicit effects in recipient cells. Cancer cells also release EVs, and the content has been identified as pro-oncogenic, having the ability to promote growth and development as well as determining the secondary site of metastasis (Tortolici *et al.,* 2021; Hoshino *et al.,* 2015). It has been found that EVs can aid the development of chemoresistance by transferring ABC pumps which help the efflux of chemotherapeutic agents out of the cell (Aberuyi *et al.,* 2021). There are fewer studies analysing the role of EVs in the development of radioresistance in BC and even fewer in CMC. There are studies showing that number of EVs produced by cells and taken up by recipient cells are significantly increased after single dose irradiation, and that this can induce an alteration of EV content to become pro-oncogenic (Tortolici *et al.,* 2021). However, there are very few studies investigating the effect of EVs on the acquisition of radioresistance. Therefore, the hypothesis of this project was that EVs derived from RR cells can result in the acquisition of radioresistance in recipient cells. To investigate this hypothesis, the aims of this project were:

1) To isolate EVs from the nonRR REM134 (canine) and MDA-MB-231 (human) cell lines and the RR REM134 (canine) and RR MDA-MB-231 (human) cell lines.

2) Investigate the effect of EVs derived from RR cells on the phenotypes associated with resistance in recipient cells and breast cancer CSCs compared to EVs derived from nonRR cells.

3) Identify potential novel therapeutic targets or biomarkers of radioresistance by comparing the proteomic content of EVs derived from nonRR and RR cells.

The objectives of this PhD are:

1) Characterise the panel of nonRR and RR cell lines in terms of morphology, markers of EMT, cell cycle analysis.

2) Optimise the isolation, visualisation and quantification of EVs by Exo-easy isolation kit or ultra-centrifugation, transmission electron microscopy and nanosight tracking analysis.

3) Determine the effect of EVs derived from RR cells on recipient cell viability, migration rate, chemosensitivity and radiosensitivity. Investigating the role of EVs derived from RR cells on the breast cancer stem cell (CSC) population by analysing the effect on tumoursphere formation, chemosensitivity and radiosensitivity.

4) To isolate EVs derived from nonRR and RR cells and analyse proteomic content by mass spectrometry. The identified proteins will be used in Ingenuity pathway analysis (IPA) to map pathways associated with radioresistance to discover novel therapeutic targets and to analyse the data for potential biomarkers of radioresistance.

Chapter 2: Materials and Methods

2.1.General materials and methods

PBS was provided by Roslin Institute (Roslin, Midlothian, UK). Centrifuges used include the 5415R benchtop centrifuge which was used for all centrifugations for 1 mL to 2 mL Eppendorf tubes (Loughborough, UK). Falcon tubes (Greiner, Gloucesteshire, UK) that were 15 mL or 50 mL were centrifuged in a 5810R tabletop centrifuge with the swing bucket rotor A-4-62. Centrifuges used throughout this project were the ones described above unless stated otherwise.

2.2.Tissue culture of cell lines

REM134 canine mammary carcinoma cell line and MDA-MB-231 human breast cancer cell and their isogenic radio-resistant (REM134 RR, and MDA-MB-231 RR) were used. The REM134 cell line was first characterised by Else *et al.,* (1982) at the University of Edinburgh from a spontaneous primary carcinoma. The classification of the REM134 cell line is unknown, but the receptor status is reported to be ER^- PR^- $HER2^+$ and has WT p53 (Gray *et al.,* 2020). The MDA-MB-231 cell line were derived from an adenocarcinoma via pleural effusion in a 51-year-old woman with metastasis with a receptor status of ER^- PR^- $HER2^-$ and has mutated p53 (Cailleau *et al.,* 1978).

All cell lines were gifted from Dr. Mark Gray (University of Edinburgh) who developed radioresistant cells from parental cell lines by irradiating at 2 Gy, followed by weekly irradiation increasing by 0.5 Gy for 12 weeks (Gray *et al*., 2020). Upon receiving these cells, they were irradiated every two weeks until radioresistant to 15 Gy.

2.2.1. Maintenance of cell lines

Cells were grown as monolayer cultures in T80 tissue culture flasks (unless stated otherwise) in Dulbecco's Modified Eagle's Medium (DMEM), with REM134 cells in DMEM + 4.5 g/L D-Glucose, L-Glutamine – Pyruvate, and MDA-MB-231 cells grown in DMEM + 1 g/L D-Glucose, L-Glutamine + Pyruvate (ThermoFisher Scientific, Paisley, UK). Each media was supplemented with 10% Foetal Bovine Serum (FBS) with 1% Penicillin/Streptomycin (ThermoFisher Scientific, Paisley, UK). Cells were maintained in a humid environment at 37 ^{o}C and 5% CO_2 in a Hera incubator (HERA cell 150i, Thermo Scientific, USA).

2.2.2. Passaging of Adherent cells

Once cells reached 70-80% confluency, media was aspirated and cells were washed in phosphate-buffered saline (PBS), and cells were trypsinised in 1 mL 0.25% Trypsin-EDTA (Gibco) and incubated at 37^{o}C for 3-5 minutes. Once cells began to detach, 7 mL of DMEM supplemented media was added to neutralise the trypsin. Cells were diluted to desired concentration and transferred into a new flask (T25, T80 or T180) and incubated at 37^{o}C with 5% CO_2 until further use. Due to the small volume of trypsin used and cells being diluted in a comparably large volume of medium which neutralises the trypsin, cells were not centrifuged at every passage to remove excess trypsin, but were centrifuged to remove trypsin before performing assays due to smaller volumes of medium being used; therefore removing trypsin before assays.

2.2.3. Counting cells

Cells were trypsinised with 0.25% trypsin and centrifuged at 500 *x g* for 5 minutes and resuspended in 5 mL of EV-depleted media. To count cells 10 µL of trypan blue dye (Gibco) was added to 10 µL of resuspended cells to distinguish between dead and alive cells, and 10 µL of this mix was applied to a Neubauer counting chamber (SLS). Three corner sections were counted excluding dead cells (stained with trypan blue) and averaged. The resulting number of cells/mL were calculated as follows: average x 2 x

10^4. Alternatively, cells were mixed in a 1:1 ratio with trypan blue and 10 µL added to a slide and cells were counted by a cell counter (Countess II, Invitrogen).

2.2.4. Isolation of breast CSCs

Breast CSCs were isolated by protocols used by Pang *et al.,* (2011), whereby cells are seeded in to ultra-low attachment plates to promote non-adherent cell culture (Corning, USA) in harsh DMEM/F12 medium which has optimal conditions for CSCs, resulting in the cell death of non-CSC populations. Cells were seeded in 2 mL per well DMEM/F12 medium containing 20 nM progesterone, 100 µM putrescine, 20 µg/mL insulin, 25 µg/mL transferrin and 30 nM sodium selenite (Sigma Biochemicals, Uk). Growth factors including human bFGF and EGF (10 ng/mL) (Peprotech, USA), were added in to the 2 mL medium per well and replenished every other day.

2.2.5. Freezing and thawing cells

Cells were counted, then centrifuged at 500 *x g* for 5 minutes, media was removed and the remaining pellet was diluted to $3x10^6$ cells/mL in FBS (ThermoFisher Scientific, Paisley, UK) supplemented with 10% Dimethyl sulfoxide (DMSO). An amount of 0.5 mL of cells were aliquoted into 2 mL cryovial tubes (Starlab) which were then place in dry ice and transferred to a Cryo Freezing container (NALGENE) before freezing at -70^{o}C overnight before being frozen at -150^{o}C.

To revive cells, the cryovials were taken from the -150 ^{o}C and kept in dry ice until taken to the lab the cells were then thawed at 37^{o}C and 5 mL of pre-warmed appropriate DMEM was added slowly in a 15 mL falcon tube to prevent osmotic shock. Once mixed with media, to remove the freezing media containing DMSO, the cells were centrifuged at 500 *x g* at room temperature for 5 minutes to wash the cells. After centrifugation, the media was removed and the pellet resuspended in 10 mL of the appropriate DMEM. The resuspended cells were then added to a T80 flask and incubated at 37^{o}C and 5% CO_2.

2.2.6. Maintenance of radioresistant phenotype

Radioresistant cell lines REM134 RR and MDA-MB-231 RR were gifted from Dr. Mark Gray (Gray *et al.,* 2019), and were established by irradiation at an initial dose of 2 Gy and were irradiated weekly with increasing doses of 0.5 Gy for 12 weeks. Cells were grown in T80 tissue culture flasks in appropriate supplemented media until 80% confluent, cells were then trypsinised as per section 2.1.2, then transferred to a 50 mL falcon tube. Cells were then irradiated at a single dose of 15 Gy using a gamma irradiator (Gammacell 1000 Elite) and further diluted in media to avoid overcrowding of cancer cells in the flask if necessary. Cells in this project were irradiated every 4-6 weeks to ensure a radioresistant phenotype, cells were irradiated in suspension in falcon tubes due to pragmatic availability of the irradiators at Roslin Institute. Following irradiation, cells were not trypsinised for at least 72 hours to minimise cellular stress and death. Although immortalised breast cancer cell lines were used in this project, the cancer cells were passaged for no more than 90 times before discarding and taking more from the master stock.

2.2.7. Preparation of EV depleted media

FBS (ThermoFisher Scientific, Paisley, UK) was aliquoted in to 50 mL ultracentrifuge tubes (Beckman) and then ultra-centrifuged in a SW32 Ti fixed rotor at 120,000 *x g* for 18 hours at 4°C as per published recommendations to remove ~95% of the EVs present in FBS (Thery *et al.,* 2006; Shelke *et al.,* 2014). The EV fraction was then removed and the remaining FBS was frozen at -20^{o}C until further use. FBS with the EV fraction removed was then referred to as EV depleted FBS. Samples of EV depleted FBS was analysed alongside initial batches of EVs isolated from cancer cells when establishing EV analysis by NTA to confirm EV depletion (data not shown). EV depleted FBS was then added to the appropriate DMEM with 1% Penicillin/Streptomycin (ThermoFisher Scientific, Paisley, UK), and filtered through 0.2 µm filter units to ensure sterilisation before use.

2.2.8. EV isolation via QIAGEN Exo-easy kit

The EVs isolation kit from QIAGEN works by precipitating and then capturing EVs to a membrane which are then removed from the spin column with a final elution step. This was chosen to trial initial EV isolation due to being less labour intensive than UC, with literature stating it can achieve isolation of vesicles in the 30 -150 nm size range (Kim *et al.,* 2020). Cells were grown in T180 flasks until 70% confluent and the media removed. Cells were then washed twice with PBS and fresh EV depleted FBS was added and after 24 hours the medium was transferred in to a 50 mL falcon tube. Conditioned media was centrifuged at 500 *x g* for 5 minutes to remove cell debris and then filtered with a 0.22 µm filter to remove larger particles. The remaining medium was transferred to the exo-easy™ spin column from the Exo-easy maxi kit (QIAGEN) and the protocol was performed according to the manufacturer's instructions. In summary, all media was added in a 1:1 ratio with the XBP buffer so a total of 16 mL was then centrifuged at 500 *x g* for 1 minute at room temperature. The flow through was discarded and 10 mL of the XWP buffer was added and centrifuged at 5000 *x g* at room temperature for 5 minutes to remove the residual buffer from the column. The spin column was then transferred to a new tube and the bound EVs were eluted with 400 µL of XE buffer. EVs were stored at 4°C if to be used immediately, otherwise were stored at -80°C and typically used within 2 months.

2.2.9. EV isolation via ultracentrifugation

Cells were grown in T80 flasks until 70% confluent and cells were rinsed twice with 5 mL of PBS and fresh EV depleted medium was added. After 24 hours the medium was removed and added to a 15 mL or 50 mL falcon and centrifuged at 500 *x g* for 10 minutes. The medium was then filtered through a 0.22 µm filter (Millex) and transferred to 12 mL ultracentrifugation tubes (Beckman). Samples were ultra-centrifuged at 120 000 *x g* (SW41 swing bucket rotor) at 4^{o}C for 90 minutes. The supernatant was removed and EVs were resuspended in 900 µL PBS and stored at -70^{o}C until further use.

2.2.10. Transmission electron microscopy

EV samples, obtained from either the Exo-easy isolation kit or ultracentrifugation, were mixed with 2% paraformaldehyde at a 1:1 ratio and stored at 4°C until processing. Processing was carried out at Kings Building TEM facilities at University of Edinburgh by Steve Mitchell: 5 µL of the sample was added to formvar-coated grids and incubated at room temperature for 20 minutes. Grids were washed with 100 µL of PBS and 50 µL of 1% glutaraldehyde for 5 minutes at room temperature. Grids were then incubated with 100 µL of dH_2O for 2 minutes at room temperature to perform a wash step, and this water wash was repeated eight times. After washing, to contrast and embed slides, 50 µL of 1% uranyl-oxalate solution (pH7) was added to the grid for 5 minutes with 50 µL of methyl cellulose-UA added for 10 minutes on ice. The excess fluid was removed by blotting with filter paper and the grids were air dried for 5 to 10 minutes and samples were viewed on a JEOL JEM-1400 Plus TEM operating at 80 kV. Representative images were collected on a GATAN OneView camera.

2.2.11. Nanosight tracking analysis

Nanosight tracking analysis measures the size and distribution of particles present by the principle of Brownian motion which measures how particles move through a solution using a laser. The nanosight is fixed on to the stage of a microscope with a 20 x magnification that is attached to a CCD camera. The laser flare observed known as the “thumbprint” region is observed and to avoid background glare, nanoveiscles focused by the beam were captured at two screen widths away from the background light from the flare region. One millilitre of sample was loaded on to the nanosight and particle concentration was determined and diluted in the range of $4x10^8$ - $12x10^8$ particles/mL. The nanosight (LM10) was washed between samples with filtered PBS, which had been filtered through a 0.22 µM filter to remove salt crystals. Parameters were set at 15,000 particle detection for 60 seconds for capture settings and the smallest vesicle size set at 30 nm, with analysis performed by Nanosight software version 2.3. A minimum of three technical repeats were ran when trialling EV isolation methods.

2.2.12. Lysis and quantification of EV protein content

EVs were lysed with urea lysis buffer (7 M Urea (Sigma Aldrich, USA), 0.1 M DTT, 0.01% Triton X-100, 25 mM NaCl, 20 mM HEPES pH 7.6 (Sigma-Aldrich, USA)) by adding 3:1 volume of urea buffer to the EV sample and mixing thoroughly. The samples were incubated for 30 minutes on ice and then centrifuged at 13,000 *x g* for 5 minutes at 4 ^{o}C. Supernatants were transferred to 1.5 mL Eppendorf tubes and stored at -70 ^{o}C. Protein concentration of samples was determined by Bradford assay. BSA standards at 0.1 mg/mL, 0.25 mg/mL, 0.5 mg/mL, 1 mg/mL, 2 mg/mL, 5 mg/mL and 10 mg/mL were used as controls. One microlitre of BSA standards were added to designated wells of a 96 well plate in duplicate, and 1 µL of protein samples were loaded in triplicate. 200 µL of Bradford reagent (Bio-Rad Laboratories, Watford, UK) was added to each well and mixed by pipetting. The plate was incubated at room temperature for 2 minutes. Absorbance 595 nm was determined using the Victor3 plate reader (Perkin Elmer) and the relative protein concentration of the samples was determined by comparing them to the BSA standards.

2.2.13. Fluorescent staining of EVs

Stains used include Vybrant™ DiI which stains lipids and emit fluoresces at 565 nm. Hoescht dye was used to stain nuclear material and fluoresces at 486 nm. EV samples previously stored at – 70^{o}C were thawed at room temperature. Samples were mixed by vortexing for 10 seconds and diluted to 100 µg/mL to ensure there would be excess EVs. Fifty microlitres of EV sample (or PBS alone as a control) was transferred to a 1.5 mL Eppendorf tube. The lipid dye, Vybrant™ DiI dye (Novex life technologies) was added at a dilution of 1 in 200 as advised by manufacturer instructions, meaning 0.25 µL DiI was added to 50 µL of EV sample containing a total of 100 µg/mL of EV particles and incubated for 45 minutes at 37^{o}C. EVs were then washed through EV spin columns (Life technologies) to remove excess dye which can result in clumping and appear to be the same size as microvesicles upon viewing. The removal of excess dye also decreases the background when viewing under the microscope. The columns were used according to the manufacturer's instructions whereby the columns were

hydrated with 650 µL filtered PBS and incubated at room temperature for 15 minutes. The columns were then centrifuged at 750 *x g* at room temperature for 2 minutes at room temperature to remove excess PBS and the EV sample was added to the gel column and centrifuged again for 750 *x g* at room temperature for 2 minutes at room temperature and the eluted EV sample was immediately used for the experiment. For this experiment, 50 µL of filtered PBS was used as a negative control.

2.2.14. Live imaging of EV uptake by recipient cells

Cells were imaged on a live cell microscope with heat pad and CO_2 chamber (LSM880 Zeiss confocal microscope). Twenty-four hours prior to imaging 275,000 cells were seeded into 1.5 mL of EV-depleted medium and added to two 2 cm^2 well coverglass chamber slides (Thermo Fisher Scientific). Before imaging cells were washed twice with 2 mL of appropriate pre-warmed EV-depleted medium to remove any dead cells. 1 µL of Hoescht stain (Thermo Fisher Scientific) was added to 2 mL of EV depleted DMEM (1:2000 dilution) directly on top of the cells and incubated with cells for 2 minutes at 37^{o}C. To remove potential background dye, cells were washed twice with 1.5 mL of DMEM medium that was pre-warmed to 37^{o}C. The EV sample was then added to the cells and images/videos were captured immediately at x 63 magnification with an 8 cycle z-stack for a total of 10 minutes per sample. All images analysed were done with the help and guidance of the Bioimaging facility at Roslin Institute, particularly with the help of Robert Fleming and Graeme Robertson.

2.2.15. Analysis of EV uptake via flow cytometry.

Following visualisation of EV uptake on the LSM880 confocal microscope, cells were washed twice with ice cold filtered PBS and resuspended in 400 µL ice cold PBS. To identify and remove any dead cells from the analyses, 0.02 µL of Sytoxred dead cell marker was added directly to the sample. A Fortessa X-20 flow cytometer (BD Biosciences, USA) was used at a low flow rate. As a control for flow cytometry, unstained cells from each cell line were used for gating and the event count was set to 10,000. Flojo version 10.1r3 was used to analyse flow data via plotting an axis of forward scatter (*y-axis*) vs side scatter (*x-axis*) and then the single cells were gated.

SSC-A vs R670-30A (side scatter vs sytox red stain) was then plotted to gate the live cells. A graph of DiI vs Hoescht was plotted and median fluorescence intensity (MFI) was transferred in to a table for analysis of EVs from non-RR cells or RR cells alongside cells treated with PBS as a control as an indicator of background dye present.

2.3. Protein methods

2.3.1. Harvesting and lysis of cell pellets

Cells were grown in appropriate media until 70-80% confluent, and media was removed. Cells were washed once with 5 mL of PBS and 1 mL of ice-cold PBS was added, and cells were scraped on ice with a disposable cell scraper (Becton Dickinson) and transferred to a 1.5 mL tube. Cells were centrifuged at 1500 *x g* for 3 minutes at 4^{o}C and the supernatant was removed and the remaining pellet snap frozen in dry ice. The pellet was resuspended in 2 x the pellet volume of urea lysis buffer (7 M urea, 25 mM NaCl, 20 mM HEPES pH 7.6, buffered with NaOH, 0.1 M Dithiothreitol, 0.05% Triton X-100) then incubated on ice for 30 minutes. The sample was centrifuged for 13,000 *x g* for 3 minutes at 4^{o}C and the lysate transferred to a new Eppendorf, snap frozen and stored at -70^{o}C.

2.3.2. Quantification of protein concentration

BSA standards at 0.1 mg/mL, 0.25 mg/mL, 0.5 mg/mL, 1 mg/mL, 2 mg/mL, 5 mg/mL and 10 mg/mL were used as controls. One microlitre of protein sample was mixed with 9 µL of dH_20 to produce a 1 in 10 dilution. One microlitre of BSA standards were added to designated wells of a 96 well plate in duplicate, and 1 µL of 1 in 10 diluted protein samples were loaded in triplicate. Two-hundred microlitres of Bradford reagent (Bio-rad) was added to each well and mixed by pipetting. The plate was incubated at room temperature for 2 minutes. Relative absorbance was determined by reading the absorbance at 595 nm using the Victor3 multilabel plate reader (Perkin Elmer) and the relative protein concentration of the samples was determined by comparing them to the BSA standards.

2.3.3. SDS PAGE

Bio-Rad Protean II minigel system was used to carry out sodium dodecyl sulphate - polyacrylamide gel electrophoresis (SDS PAGE) (see below). The resolving gel (12% acrylamide, 380 mM Tris (pH 8.8) that was adjusted to pH 8.8 with 12 M HCL, 0.1% SDS, 0.1% Ammonium persulphate, 0.08% TEMED was poured between the plates and a layer of isopropanol was added on top to remove potential air bubbles. Once the resolving gel had set, the isopropanol was removed and stacking gel was added and the appropriate combs were inserted until the stacking gel (5% acrylamide, 1.26 M Tris (pH 6.8) which was adjusted to pH 6.8 with 12 M HCL, 0.1% SDS, 0.1% Ammonium persulphate, 0.01% TEMED had set. The cassette was submerged in to 1 x running buffer (25 mM Tris, 0.1% SDS pellets, 190 mM Glycine with 1 L deionised H_2O).

The desired total amount of protein to add for each sample was calculated from the Bradford assay (2.2.3) to obtain this amount the appropriate volume of 4 x SDS sample buffer (1 M Tris-Cl/SDS, pH 6.8 M, 80% Glycerol, 20% SDS, 0.1 M EDTA, 1% bromophenol blue was added. Samples were then denatured by boiling in a heat block at 95^{o}C for 5 minutes, and then an appropriate volume was loaded on to the polyacrylamide gel. Gels were resolved at 200 V for 1 hour until the bottom marker of the ladder had migrated to the bottom of the glass plates. The stacking gel was removed and the separated proteins were then transferred to a nitrocellulose membrane. The transfer cassette was assembled in the following order: sponge, 2 pieces of cartridge paper, gel, 0.22 µm pore Hybond-C™ nitrocellulose membrane (Amersham, Pharmacia Biotech, UK), 2 pieces of cartridge paper, sponge.

2.3.4. Western blotting

All components were saturated in transfer buffer 1 x (25 mM Tris base and 190 mM glycine, 20% methanol in a total volume of 1 L dH_2O). The transfer cassette was inserted into an appropriate tank filled with transfer buffer and resolved at 100 V for 1 hour, or overnight at 20 V at 4^{o}C. Efficient transfer was assessed by the transfer of pre-stained protein markers. Membranes were stained with ink (0.3% india ink diluted

in PBS) for 10 minutes at RT on an orbital shaker to detect the presence of protein bands, washed in PBS-Tween (0.1%) for 5 minutes and blocked in 5% milk (PBS, 10% Tween, 5% semi-skimmed milk (Sigma-Aldrich, USA) for 1.5 hours at room temperature, or overnight at 4^{o}C.

Membranes were used to detect specific proteins by incubating with the indicated primary antibody at specified dilutions outlined in section 2.3.5, overnight in a humidified chamber at 4^{o}C, or at room temperature for 90 minutes. Three 15 minute wash steps in PBS-Tween were performed, and the horse raddish peroxidase (HRP)-conjugated secondary antibody (LI-COR) was applied at 1:1000 dilution in 10 mL 5% milk for an hour. Then washed a further 3 times in PBS-Tween for 15 minutes.

2.3.5. Antibodies

Western blots for markers of EMT were chosen to be the epithelial marker E-cadherin, and mesenchymal markers including β-catenin, slug and snail, and vimentin. Upon the acquisition of a mesenchymal phenotype, it would be expected that E-cadherin expression decreases, and β-catenin, vimentin and slug and snail expression would increase (Subbalakshmi *et al.,* 2022). Primary antibodies were added at the stated dilutions which resulted in the western blot bands produced (Table 2.1).

Table 2.1 The table of primary antibodies used with the expected molecular weight in kDa and the working dilution factor. *Each antibody used has the corresponding company and catalogue number recorded.*

Antibody	Expected size (kDa)	Dilution	Company	Catalogue number
β-actin	42	1:5000	Abcam	ab6276
β-catenin	92	1:500	Cell signalling	9587
E-cadherin	120	1:5000	BD laboratories	610182
Slug & snail	29	1:500	Abcam	ab180714
Vimentin	57	1:5000	Abcam	ab8069

Secondary antibodies were added at the appropriate concentration (Table 2.2) and incubated for an hour at room temperature before imaging on the LICOR Odyssey phosphorimager system (LI-COR Biosciences, USA).

Table 2.2 Table of secondary antibodies with their working dilution along with the company and catalogue number. *Secondary antibodies listed include those used on the LICOR system, all antibodies listed were sourced from LICOR.*

Antibody	Dilution	Conjugate	Wavelength (nm) used on LICOR	Catalogue number
Donkey anti-goat	1:15000	IRDye 680RD	700	925-68074
Donkey anti-mouse	1:15000	IRDye 800CW	800	925-32212
Donkey anti-rabbit	1:15000	IRDye 680RD	700	926-68073

2.3.6. Fluorescent detection of protein via the LICOR Odyssey

Membranes were washed for 5 minutes at room temperature with PBS-Tween to remove excess. Membranes were then placed in to the LICOR Odyssey phosphorimager system (LI-COR Biosciences, Nebraska, USA) and the appropriate area was highlighted to select the area in which the membrane was placed. The 700 nm and 800 nm channels were selected at an intensity of 5.0 and the resolution adjusted to 42 µm for smaller membranes, if a membrane with 15 wells was used, the resolution was adjusted to 42 µm, whereas the auto-selected resolution was chosen for gels that were ran with 10 wells. After checking the above settings were chosen, the image was acquired and membranes were placed back in to PBS-Tween.

Images were acquired and analysed in Image Studio version 5.0 (LI-COR Biosciences, Nebraska, USA). where, for the sake of clarity, all control bands such as actin were changed to a green colour and proteins of interest were changed to a red colour.

2.4. Cell cycle analysis

Cells were grown to 80% confluency to ensure enough cells were present, counted and $1x10^6$ cells were pelleted (as per section 2.2.1). The cells were then resuspended in 70% ethanol. To ensure a single cell suspension, the mixture was constantly vortexed and ethanol was gradually added in a dropwise fashion. These samples were stored at -20°C. In preparation for cell cycle analysis, the samples were thawed, then the cells were pelleted at 500 *x g* at 4°C for 5 minutes, the ethanol supernatant was removed and washed twice in 5ml PBS. After the second wash, were pelleted for a third time at 850 *x g* at 4°C for 5 minutes and the PBS removed, and 50 µL of 100 µg/mL RNase A (Qiagen) added and incubated at 37°C for 2 hours. Then 200 µL of 50 µg/mL Propidium Iodide (Sigma-Aldrich, USA) was added and incubated at room temperature for 45 minutes prior to flow cytometry on the Fortessa x20 flow cytometer (BD Biosciences, USA). Cells were analysed by plotting forward scatter vs side scatter to identify the single cells, the pulse area (*y-axis*) vs the pulse width (*x-axis*) was plotted and the debris cells were excluded via the gating of the correct cells, and the propidium iodide stain (*y-axis*) vs the forward scatter (*x-axis*) was plotted to create a PI histogram of the cell cycle by counting 10,000 events per sample. The higher the MFI correlated to the G2/M phase and the lower MFI was associated with the G1/G0 phase of the cell cycle. These analyses were all performed in the flow department with the assistance of Dr Anna Raper at Roslin Institute. Data was analsyed using FlowJo software to produce cell cycle histograms.This was achieved with the assistance of Dr. Anna Raper to attain all flow data.

2.5. Migration assay

Migration assays were performed using ibidi inserts (Ibiditreat) according to the manufacturer's instructions whereby cells were counted (2.1.3) and diluted to the appropriate concentration depending on the cell line. Seventy microlitres of diluted cells were placed within each well of the insert. Cells were seeded at varying concentrations to achieve cell confluency in ~ 24 hours, with MDA-MB-231 at $4.5x10^5$,

MDA-MB-232 RR at $4.75x10^5$, REM134 at $3.45x10^5$ and REM134 RR at $3.75x10^5$ and incubated at 37°C in 5% CO_2 in a humidified incubator until confluent. Once the cells were confluent, the insert was removed to produce a 500 µm +/- 50 µm gap and 1 mL of EV-depleted media was pipetted in to the well, and the size of the gap was measured at indicated time points by taking microscope images (Zeiss Axiovert 40 CFL) at 5 x magnification until the closure of the gap. Migration distance was recorded at stated time points with measurements by Axiovision software version 4.7.2. The relative width migration was calculated as follows: 100 (A-B)/A where A is the width measured at 0 hr and B is the width of the cell wound after. For experiments where effect of EVs on recipient cells was analysed, $2x10^4$ cells were seeded in 1 mL of EV depleted media per well in a 12 well plate and PBS, and 50 µg/mL of nonRR or RR EVs were added at and incubated for 24 hours. The concentration of EVs to be dose titrated was determined by the application of 50 – 200 µg/mL in literature studying breast cancers (Kang *et al.,* 2019; Kia *et al.,* 2019; Wang *et al*., 2019). Cells were then seeded and the assay performed as described above. Data were then normalised to the cells treated with PBS control.

2.6. Colony formation assays with EV dose titrations

The colony forming ability of individual cells was assayed by seeding single cells (for cell lines MDA-MB-231 and MDA-MB-231 RR, $5x10^1$ cells/well of a 6 well plate and for REM134 and REM134 RR, $1x10^3$ cells/well of a 6 well plate) in 3 mL EV-depleted medium. Immediately after seeding cells were treated with a dose of either 50 µg/mL or 100 µg/mL of isolated EVs were added (the largest volume of PBS containing EVs was also the volume of PBS added to the cells treated with PBS control and this was used throughout all assays involving treatment with EVs. The plates were rocked to mix. All samples were repeated in triplicate. Plates were incubated in a humid environment at 37°C and 5% CO_2 in a Hera incubator. Colonies were visible 10-14 days after seeding. The growth medium was removed, and colonies were washed with PBS. Colonies were then fixed by adding 5 mL of 100% methanol (Fisher) and incubated for 5 minutes at room temperature. Methanol was removed and colonies were allowed

to air dry. Colonies were stained with Giemsa stain (Sigma-Aldrich, USA) 1:20 with dH_2O for 20 minutes and then washed twice with water. Colonies were air dried at room temperature for 24 hours and all wells counted by hand with a digital counter, each colony was marked to try to ensure accuracy.

2.7. Colony formation assays after irradiation

All cell lines were seeded at $1x10^4$ cells per well in a 24 well plate in 1 mL of the appropriate EV-depleted DMEM supplemented with EV-depleted FBS and PS. Each cell type were treated with 50 µg/mL of the corresponding non-radioresistant and radioresistant EVs added, and PBS added to the controls. The EVs were then incubated with the cells for 24 hours and cells were trypsinised with 160 µL of 0.25% trypsin. The cells were incubated at 37°C until the cells detached from the bottom of the well and were then resuspended in 1 mL of EV-depleted DMEM. Cells were counted and seeded at the necessary concentrations in 3 mL of EV-free DMEM; REM134 and REM134 RR at $1x10^4$ cells/well; MDA-MB-231 and MDA-MB-231 RR at 50 cells/well. Cells were seeded in 6 well plates in triplicate and irradiated immediately at 0 Gy, 2.5 Gy and 5 Gy in a GSR D1 gamma irradiator. Following irradiation cells were incubated at 37°C with 5% CO_2 for 10 days and colonies were stained and counted as outlined above. Colonies were counted and all biological and technical repeats were averaged, and the standard error of the mean shown by error bars.

2.8. Chemosensitivity assays

Doxorubicin was used at clinically relevant doses of 0.1 – 0.01 µM (Creasy *et al*., 1976; Pritchard *et al.,* 2012). Cells were trypsinised as described above and $5x10^2$ MDA-MB-231 and MDA-MB-231 RR cells were added in 50 µL to a 96 well plate in triplicate, and $1 x10^3$ REM134 and REM134 RR cells. For cancer stem cells, $1x10^3$ cells for each cell line was added in 50 µL of CSC media. For both cell lines and cancer stem cells, the cells were left to attach for 24 hours and 50 µg/mL of EVs were added in 25 µL, and incubated for 12 hours. A dose titration of Doxorubicin was prepared from a stock

concentration that was dissolved in DMSO to result in a final concentration of 3.7 mM (Pfizer, UK), which resulted in the strongest concentration of DMSO being 0.03% incubated with cells. The Doxorubicin stock was diluted in the appropriate medium to result in final concentrations of 0 µM, 0.01 µM, 0.01 µM and 1 µM in 25 µL. On day 5 the cell viability assay was performed as stated below in section 2.10. Cell chemosensitivity was determined by normalising the percentage cell viability to the control for all cell lines and EVs types added. Bar charts were created displaying the average of the three technical repeats +/- the percentage standard error of the mean.

2.9. Tumoursphere formation assay

All cell lines were seeded at $1x10^4$ cells per well in a 24 well plate in 1 mL of the appropriate EV-depleted DMEM supplemented with EV-depleted FBS and PenStrep. Each cell type was treated with 50 µg/mL of the corresponding non-radioresistant and radioresistant EVs added, and PBS added to the controls. The EVs were then incubated with the cells for 24 hours and cells were trypsinised with 160 µL of 0.25% trypsin. The cells were incubated at 37^{o}C until the cells detached from the bottom of the well and single cell suspension confirmed by observing by light microscopy. Cells were then resuspended in 1 mL of EV-depleted DMEM. Cells were seeded in 6 well plates in 2 mL of N2 media (DMEM/F12, 20 nM progesterone, 100 µM putrescine, 30 nM sodium selenite, 25 µg/mL transferrin, 20 µg/mL insulin) which results in death of non-CSC cells due to harsh environmental conditions that only CSCs can thrive (Lee *et al.,* 2016; Rugamba *et al.,* 2021). Human epidermal growth factor (10 ng/mL) and human basic fibroblast growth factor (10 ng/mL) (Peprotech, USA) was added on alternate days until completion of the assay. Cells were seeded at varying densities depending on the cell line and were allowed to grow between 5-17 days. To ensure only tumourspheres were counted and not several cells clumped together, only tumourspheres over 50 µm were counted, as cell aggregates can be in the size range of 1 – 50 µm (Lee *et al.,* 2016). REM134 and REM134 RR cells were seeded at $6x10^3$ cells per well, and grew incredibly quickly; therefore, to prevent tumoursphere overpopulation within the wells the assay was finished after 5 days. MDA-MB-231 and MDA-MB-231 RR cells

were seeded at $3x10^3$ cells and tumourspheres were counted on day 17 due to much slower tumoursphere growth.

Tumourspheres over 50 µm in diameter were counted using a Zeiss Axiovert 40 CFL microscope with images taken at 5 x and 10 x magnification and size measurements were recorded by Axiovision software version 4.7.2. To count the number of tumourspheres present, 5 random fields of vision on the 5 x magnification were counted and an average or median was calculated depending on the normality of the data. Tumourspheres were counted in random fields of vision until 75 total were counted.

2.10. Cell viability

MDA-MB-231 and MDA-MB-231 RR cell lines were seeded at $5x10^2$ cells in 50 µL EV-free medium. REM134 and REM134 RR were seeded at $1x10^3$ cells in 50 µL EV-free medium. EVs samples were diluted in EV-free media to result in final concentrations of 10 µg/mL, 20 µg/mL, 30 µg/mL, 50 µg/mL and 75 µg/mL (control lanes of 0 µg/mL had PBS added as a vehicle control) in 50 µL total. Cells were seeded for 24 hours and treated with 50 µL of appropriate EV concentration was added on to cells. After 5 days from seeding the cells, Cell Titer-Glo® reagent (Promega, UK) was added in a 1:1 ratio according to the manufacturer's instructions whereby the powder and liquid reagents were thoroughly mixed and 100 µL was added to each well containing 100 µL of media containing cells and were shaken on a plate shaker for 10 minutes and luminescence values were recorded at 560 nm wavelength by using a Victor3 multilabel plate reader (Perkin Elmer, UK). Each individual plate was blank corrected to the well containing medium alone, three biological repeats were averaged, and this was performed three times to result in three technical repeats. The technical repeats were averaged and standard deviation calculated. The percentage cell survival was then calculated and the corresponding %stdev calculated and plotted.

2.11. Analysis of EV content for mass spectrometry

2.11.1. Preparation of EV samples

Cells at 70-80% confluency had EV depleted media added and incubated at 37°C for 24 hours, the medium was collected and centrifuged at 3184 *x g* for 10 minutes to remove debris on a 5810 R Eppendorf benchtop centrifuge. The supernatant was removed and filtered through a 0.22 µm filter. The filtered supernatant was removed and added to clean Beckman ultracentrifuge tubes and centrifuged at 120 000 *x g* for 70 minutes at 4°C in a SW41 swing bucket rotor in a Beckman Optima XL-100K ultracentrifuge (Beckman Coulter, Uk). To perform a wash step, the supernatant was discarded, and the ultracentrifuge tube filled with filtered PBS and ultracentrifuged again at 120 000 *x g* for 70 minutes at 10°C. PBS was poured out the tube and excess PBS was removed with a pipette. To resuspend the EV pellet a 100 µL of fresh filtered PBS was added and the tube was vortexed for 20 seconds and the contents of the tube was transferred to a low protein binding tube and stored at – 20°C until quantification.

2.11.2. Quantification of EVs samples by micro bicichoninic acid assay

Quantification of EV samples was perfomed by the department of Proteomics and Metabolomics at Roslin Institute. To determine EV protein concentration to be used for mass spectrometry, a micro bicichoninic acid assay was used (Thermo Scientific, UK) to quantify protein content. Protein standards were prepared using PBS to result in final concentrations of 200 µg/mL, 40 µg/mL, 20 µg/mL, 15 µg/mL, 10 µg/mL, 7.5 µg/mL, 5 µg/mL, 2.5 µg/mL. A 96 well plate was used to pipette 150 µL sample (if not enough sample volume, then PBS was added to result in a final volume of 150 µL and dilution factor noted). Then 150 µL of working reagent solution was added followed by the plate being rotated on a plate shaker at RT for 30 seconds. The plate was covered and incubated for 2 hours at 37 °C to allow the colourmetric result to develop, and absorbance was read at at 562 nm by a Synergy HT plate reader (BioTek Instruments, USA). Results were blank corrected and final protein concentration determined by measuring against the standard curve.

2.11.3. EV protein digestion

Protein solubilisation and digestion was performed by the Proteomics and Metabolomics core facility at Roslin Institute. Protein digestion was achieved by suspension strapping where 20 µg of protein was taken for each sample and lysis buffer (10% SDS, 100 mM Triethylammonium bicarbonate, pH 7.5) added to make a final volume of 23 µL. Samples were then vortexed and sonicated for 15 minutes at room temperature. Ten mM DTT was added to a final concentration of 1% and incubated at 56^{o}C for 1 hour. To alkylate the disulfides, 750 mM iodoacetamide buffer at a final concentration of 2.5% was added and was incubated at room temperature in the dark for 35 minutes. Protein samples had 12% phosphoric acid (pH <1) added, and were trapped via the addition of binding/wash buffer (100 mM (Triethylamonium bicarbonate) TEAB (final) in 90% methanol, pH 7.5) at 6 times the volume of the sample which was then transferred into an S-trap micro spin column (ProtiFi, USA). The sample was centrifuged at 4000 *x g* at room temperature for 30 seconds three times to trap the proteins, with the spin columns being rotated 180^{o} between each centrifugation step. The supernatant was then discarded. To clean the protein collected, a wash step of adding 150 µL of binding/wash buffer was added and centrifuged at 4000 *x g* at room temperature for 30 seconds and this wash step was repeated four times with the trap column being rotated 180^{o} after each centrifugation step. The S-trap column was centrifuged at 4000 *x g* at room temperature for 1 minute to remove all binding/wash buffer and the supernatant was kept. The S-trap column was transferred in to a clean 1.5 mL Eppendorf for digestion. For the digestion of proteins, 20 µL of digestion buffer (50 mM TEAB with 1 µg trypsin per 10 µg sample) was added to the S-trap column and the cap placed back on to the column. The column was then incubated for 2 hours at 47^{o}C in a waterbath.

2.11.4. Elution of EV peptides

Protein elution was performed by the Proteomics and Metabolomics core facility at Roslin Institute. Elution of the digested proteins (peptides) was achieved by adding 200 µL of 50 mM triethylammonium bicarbonate and centrifuging the spin column for 2 minutes at 4000 g. Two-hundred microlitres of 0.1% formic acid was added and

then centrifuged again for 2 minutes at 4000 g, then 200 µL of 0.1% formic acid in 30% methyl cyanide was added to the spin column and centrifuged for a final step at 4000 *x g* for 2 minutes. The eluted peptides were dried in a speed vacuum (Model SPD1010, ThermoFisher Scientific, UK) at room temperature. Sample was added to make a final volume of 20 µL with 0.4% formic acid in 4% methyl cyanide and then stored at -20°C to be analysed via mass spectrometry.

2.11.5. Protein digestion, dimethyl labelling and liquid chromatography tandem mass spectrometry

Protein mass spectrometry was performed by the Proteomics and Metabolomics core facility at Roslin Institute. Purified peptides were separated over a 90 minute gradient on an Aurora-25 cm column (IonOpticks Australia) using an UltiMate RSLCnano LC System (Dionex) coupled to a timsTOF fleX mass spectrometer via a CaptiveSpray ionisation source. The gradient was delivered at a flow rate of 200 nL/min and washout was performed at 500 nL/min. The column temperature was set at 50°C. For data dependent acquisition-parallel accumulation serial fragmentation, the full scans were recorded from 100 to 1700 m/z spanning from 1.45 to 0.65 Vs/cm^2 in the mobility (1/K0) dimension. Up to 10 PASEF MS/MS frames were performed on ion-mobility separated precursors, excluding singly charged ions which are fully segregated in the mobility dimension, with a threshold and target intensity of 1750 and 14,500 counts, respectively. Raw mass spectral data was processed by Dr. Dominic Kurthain at the Protein and Metabolomics Department at Roslin Institute. Proteins were identified using PEAKS Studio X-Pro Software (Bioinformatics LTD). Search was performed against Uniprot Human and Dog sequence database with mass spectrometry stage 1 precursor tolerance of 20 ppm, mass spectrometry stage 2 tolerance of 0.06 Da. Fully-tryptic digestion allowing one missed cleavages, fixed modification of cystine [+57.02] and oxidation of methionine and deamination of asparagine and glutamine were also specified. Quantitative label free quantification analysis was performed with default parameters and ID transfer option enabled.

2.12 Analysis of global protein changes in EVs

Mass spectrometry analyses produced excel files with expression "intensity" values for each protein identified. These data were taken and uploaded in to RStudio v 1.4 to plot heatmaps to assess global protein expression in EV content. The EV data from the non-radioresistant cell lines had the median expression value calculated across the replicates, the expression of protein in the non-radioresistant datasets was then compared to the median from their triplicate. The median expression value of each triplicate from EVs from RR cancer cells were then normalised to the median expression values from the corresponding non-radioresistant dataset. The value produced was then $\log_2$ transformed to reduce extreme variation seen in the datasets. Data were then clustered according to their Entrez numbers. The heatmaps were generated in Rstudio by Dr Mortiz Haneklaus.

2.12.1 Analysis of EV protein content via Ingenuity Pathway Analysis

Protein content derived from Mass Spectrometry was sorted into a SPIDER waterfall excel documents. The excel files with identified proteins were calculated to be a ratio calculated as treatment vs control whereby the EV content derived from RR cells was taken as the treatment group compared to the nonRR derived EVs being used as the "control". Therefore, normalising the expression intensity from the RR cell EVs to the nonRR EVs to allow the correct formatting to be uploaded in to IPA. Data were processed as "expression ratios" to proceed with core analyses. For the normalised data derived from the MDA-MB-231 RR cells, the data was filtered for core analysis by specifically filtering for triple-negative breast cancer and "stem cells". Similarly, for the normalised data derived from the REM134 RR cells was filtered for "mammals" instead of "human" as no canine option was available. The entire selection of breast cancer was selected along with "stem cells". The filtered datasets were then analysed for associated "disease and functions", this collates the data found and associates identified molecules with a disease or function.

To identify potential pathways associated with the radioresistant phenotype in the normalised REM134 RR and MDA-MB-231 RR datasets the disease type "radioresistance of tumour cells" was imported from the IPA database and mapped. For both datasets (mapped separately), data were overlaid on to the IPA database, and z-score was set to +/- 2 ($p<0.01$) for expression and the disease of "cancer" was selected. The top 15 enriched proteins were mapped on to the radioresistance pathway to build a network of predicted molecules in pathways that may cause radioresistance. For analysis of potential biomarkers from the filtered datasets, the data was further filtered for "breast cancer" and "stem cells", for molecules in all biofluids, then for "disease progression", "prognosis", "diagnosis", and "response to therapy". The biomarkers identified were then processed through a comparative biomarker analysis to compare potential biomarkers identified within both datasets.

2.13 Statistical Analyses

2.13.1 Analyses of data to determine statistical significance

Data were analysed in Minitab 19. Anderson-Darling tests were performed to determine the normality distribution of the data, $p<0.05$ was not normal. This was used to certify if non-parametric or parametric tests were to be used to determine statistical significance. Where appropriate, two tailed two sample t-tests were used for normally distributed parametric data whereby equal variances were assumed. Where data were not normally distributed and could not be log transformed to result in normally distribued data, a Wilcoxon signed-rank test was used. P-values were used as follows: 0.05 = *; 0.01 = **; 0.001 = ***; 0.00001 = ****.

2.13.2 Analyses of protein data in IPA

The filtered datasets uploaded into IPA were analysed for enrichment of canonical pathways. The p-value used was B-H p-value and the z-score cut off (significant expression) was set to 1.3 (equivalent of $p<0.05$), data was shown for z-scores of 2

(p<0.01) and 4 (p<0.0001). The enrichment of canonical pathways shows both higher and lower expression of protein pathways compared to proteins from the nonRR REM134 and MDA-MB-231 cancer cells.

Chapter 3: Characterisation of non-radioresistant and radioresistant cancer cells and optimisation of EV isolation

3.1 Introduction

Radioresistance is the ability of cancer cells to survive what should be a lethal dose of ionising radiation, resulting in the recurrence and advancement of cancer and decreasing the effectiveness of radiotherapy treatments (Cabrera-Licona *et al.,* 2021). It has been shown that around 33.8% of patients with node positive breast cancer relapse within 10 years of receiving radiotherapy treatment (McGale *et al.,* 2014). Despite being a major cause of treatment failure, relatively few studies have specifically investigated the mechanisms responsible for radioresistance. Cancer cell radioresistance is a common feature in a plethora of cancer types in both animals and humans, with several studies indicating that EVs may have a potential role in blocking both chemotherapy and radiotherapy resistance (Chen *et al.,* 2021; Weinman *et al*., 2021). There are studies that have characterised the phenotype of established radioresistant (RR) cell types (Mutschelknaus *et al.,* 2016, Gray *et al.,* 2019); however, although EVs have shown to have a prominent role in the manipulation of the TME to promote the development of the tumour and transferring chemotherapy resistance to recipient cells, there are very few studies investigating the role of EVs in the acquisition of radiotherapy resistance.

The hypothesis of this project was that EVs derived from RR cells can result in the acquisition of radioresistance in recipient cells. This chapter aims to characterise the REM134 RR and MDA-MB-231 RR cell lines and the nonRR REM134 and MDA-MB-231 cell lines by observing cell morphology, expression of markers of epithelial-to-mesenchymal transition (EMT) and alterations in the cell cycle and to successfully isolate EVs and confirm the size range by NTA and TEM. This could identify the

presence of a radioresistant phenotype and to successfully isolate EVs means they can be used in assays to confirm if EVs derived from radioresistant cells can confer a radioresistant phenotype.

The data in this chapter shows that RR cells have a more mesenchymal phenotype, and an increased percentage of cells in the G2 phase of the cell cycle when compared to their nonRR counterparts. The data also showed that the RR cells have a faster rate of migration when compared to the nonRR cell lines. These characteristics identified in the RR cell lines used in this study are consistent with previous work in which these radioresistant cell lines were established (Gray *et al.,* 2019). After characterising the cell lines, EV isolation and visualisation was optimised in accordance with minimal information for studies of EVs (MISEV) guidelines which was last reviewed in 2014 and more recently reviewed in 2018. The MISEV guidelines state how much detail should be included when reporting methods to encourage transparency and the normalisation of methods used when isolating, visualising, and determining EV concentration. As a result of the MISEV guidelines, protocols and suggested requirements were published by leaders in the field of EVs in 2014 and 2018 (Lotvall *et al.,* 2014; Thery *et al.,* 2018). The most recent MISEV guidelines advise the identification of EVs should include two separate identification methods including one image based, one close up and one wide field image, and a second non-image based method. Therefore, TEM was chosen in this project for close up and wide field images, and to confirm size distribution and EV concentration NTA was chosen for this project as the non-image based method. In this project optimisation of EV isolation was initially attempted by removing tissue culture media from cells and trying to isolate EVs by using commercially available kits. Subsequently, a protocol was developed to use the kits plus additional ultracentrifugation (UC) steps, and finally the method chosent to isolate EVs was to use UC alone. EVs were then visualised and quantified by transmission electron microscopy (TEM) and nanosight tracking analysis (NTA), respectively.

3.2 Results

3.2.1 Radioresistant cells have a more spindle-like morphology than non-radioresistant cancer cells

The panel of cell lines used include the nonRR canine cell line (REM134) and its corresponding RR cell line (REM134 RR) and the nonRR human triple-negative breast cancer cell line (MDA-MB-231) and its RR cell line (MDA-MB-231 RR). Phase contrast imaging was used to compare the morphology of cells nonRR cell lines (REM134 and MDA-MB-231) and the RR cell lines (REM134 RR and MDA-MB-231 RR). The RR cell lines were initially derived by Dr. Mark Gray (Gray *et al.,* 2019), by treating cells with increasing doses of irradiation and propagating surviving cells. All RR cells (REM134 RR and MDA-MB-231 RR) used in this project were shown to be resistant up to 15 Gy. To compare the morphology of the nonRR cell compared to the RR cell lines, cell morphology was observed via phase contrast microscopy. The nonRR REM134 cell type appeared to have rounded morphology (Figure 3.1 A), compared to the REM134 RR cells where most cells had a spindle-like projections (Figure 3.1 B). There was less variation between the MDA-MB-231 and the MDA-MB-231 RR cell lines (Figure 3.1 C, D) which both had a spindle-like morphology with cytoplasmic extensions.

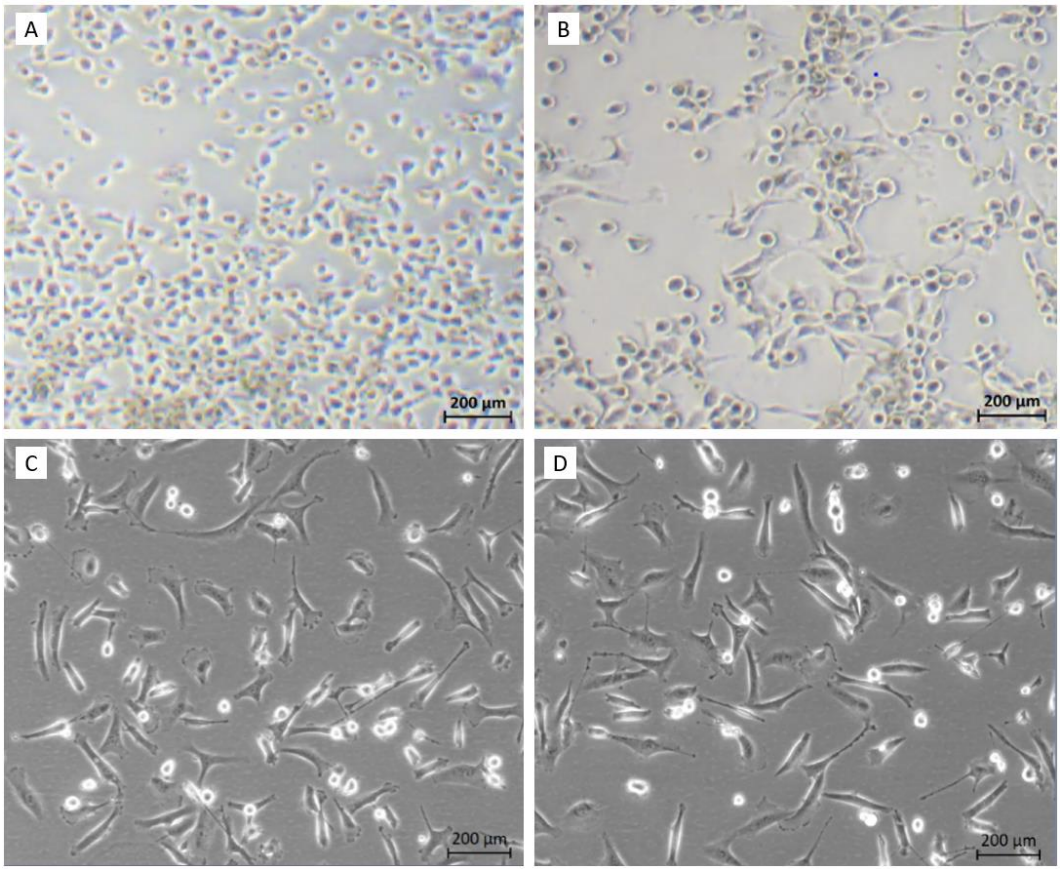


Figure 3.1 The REM134 RR cell line has a more mesenchymal phenotype than REM134 cells. *Phase contrast images were captured at 10 x magnification showing the morphology of all cell lines* ***A)*** *REM134* ***B)*** *REM134 RR* ***C)*** *MDA-MB-231* ***D)*** *MDA-MB-231 RR.*

Breast cancer CSCs were derived from the stable cell lines by enriching for breast CSCs using DMEM/F12 medium that creates a harsh environment for non-CSC breast cancer cells, resulting in the death of non-CSC populations. The protocol used in this project has previously been verified for use with cancer cells (Lee *et al.,* 2016; Pang *et al.,* 2011). The medium is supplemented with relevant growth factors to ensure growth of breast CSCs in culture (as outlined in Chapter 2; section 2.10). The breast CSCs were seeded in to an adherent flask and images were captured to analyse cellular morphology when cells were observed by phase contrast microscopy (Figure 3.2).

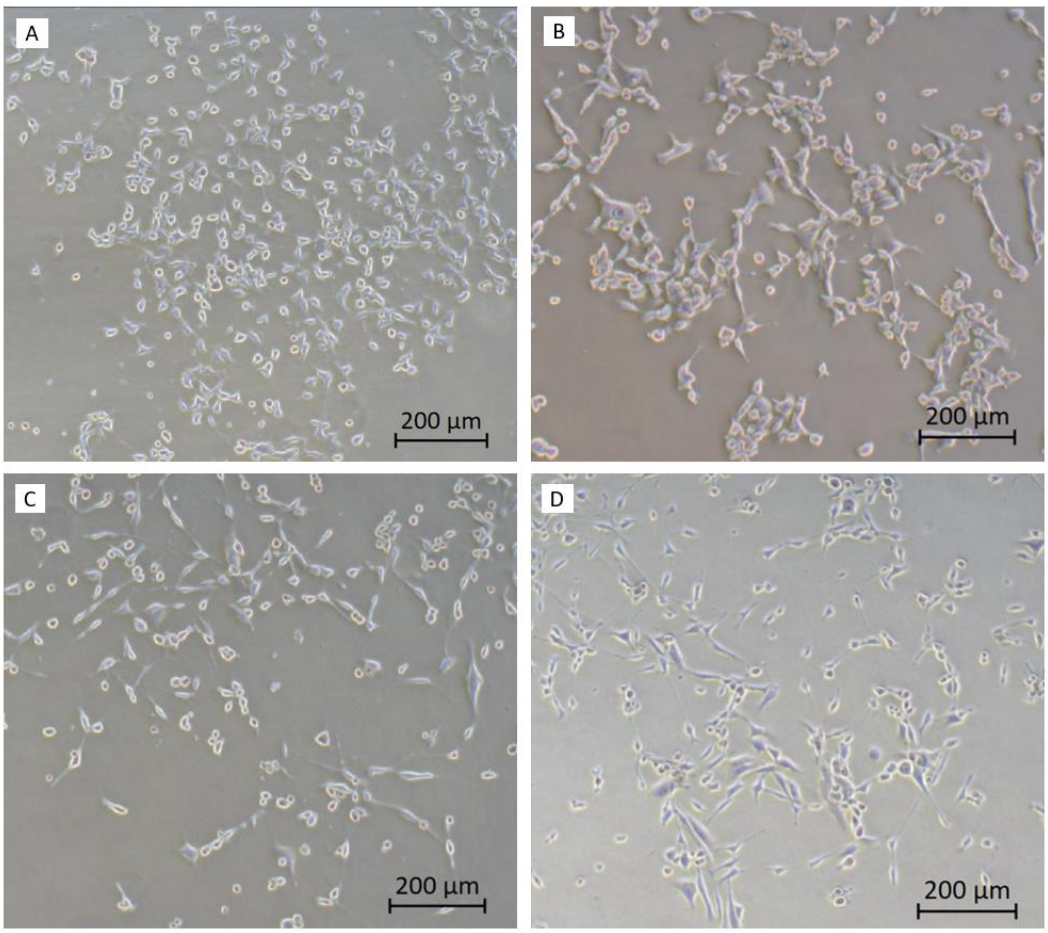


Figure 3.2 Adherent breast CSCs derived from RR cell lines have a more mesenchymal stem type. *Phase contrast images at 10 x magnification showing the morphology of all breast CSC cells* ***A)*** *REM134* ***B)*** *REM134 RR* ***C)*** *MDA-MB-231* ***D)*** *MDA-MB-231 RR.*

The REM134 CSCs (Figure 3.2 A) had a rounder morphology and REM134 RR CSCs (Figure 3.2 B) had a more elongated shape with cytoplasmic projections. There were also morphological differences between the MDA-MB-231 and MDA-MB-231 RR CSCs (Figure 3.2 C, D), with the MDA-MB-231 RR CSCs being larger in size with more cytoplasmic extensions.

3.2.2 Radioresistant REM134 RR and MDA-MB-231 RR breast cancer cells have a more mesenchymal phenotype

EMT is the transition of cells from an epithelial cell type which is associated with the loss of cell-to-cell junctions that hold the cells in place, towards a mesenchymal cell type which is associated with a more flexible and motile cell, that can release

metalloproteinases to break through the basement membrane (Akrida *et al.,* 2022). Cell lines were analysed for epithelial markers, such as cell-to-cell junction marker E-cadherin, and mesenchymal markers including β-catenin, slug and snail, and vimentin. Upon the acquisition of a mesenchymal phenotype, it would be expected that E-cadherin expression would decrease, and β-catenin, vimentin and slug and snail expression would increase (Subbalakshmi *et al.,* 2022).

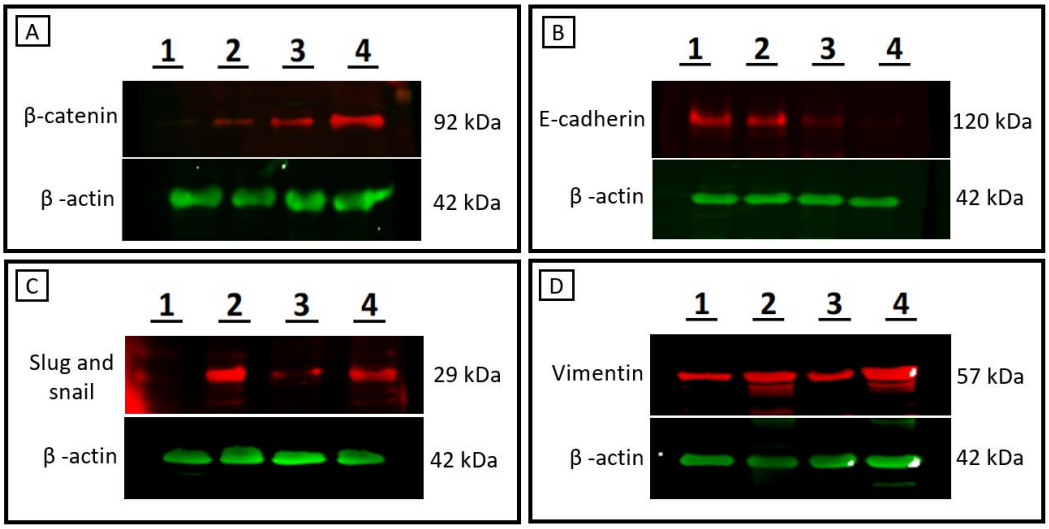


Figure 3.3 Western blots of markers of EMT show that the RR cell lines have an increased expression of mesenchymal markers*. Lanes were loaded with 20 µg of cell lysate in the following order 1) REM134 2) REM134 RR 3) MDA-MB-231 4) MDA-MB-231 RR. Markers of EMT* ***A)*** *β-catenin (dilution 1:500)* ***B)*** *E-cadherin (dilution 1:5000)* ***C)*** *slug and snail (dilution 1:500)* ***D)*** *vimentin (dilution 1:5000) were used along with β-actin (dilution 1:5000) as a loading control. Expression was visualised by the LICOR system.*

Western blots showed that that there was an increased expression of β-catenin (Figure 3.3 A) in the RR cell lines (lanes 2 and 4 compared to lane 1 and 3). There was no obvious difference in the amount of E-cadherin in the RR cell lines compared to nonRR cell lines (Figure 3.3 B), with very little expression seen between MDA-MB-231 and MDA-MB-231 RR (Figure 3.3 B, lanes 3 and 4). There was also an increase in the level of transcription factor slug and snail in the RR cell lines (Figure 3.3 C) compared to the nonRR cell lines. Similarly, there was an increased expression of vimentin in the RR cell lines compared to the corresponding nonRR cell lines (Figure 3.3 D). This data implies that there is increased expression of mesenchymal markers in the REM134 RR and MDA-MB-231 RR cell compared to their nonRR counterparts.

3.2.3 Radioresistant cell lines have a faster migration rate than non-radioresistant cell lines

In cancer cells, the presence of a mesenchymal phenotype is characteristic of cells undergoing an EMT. This is a more invasive phenotype associated with poorer prognosis in patients (Yu *et al.,* 2021). Since the RR cells had a more mesenchymal phenotype when compared to the nonRR cell lines, migration rates were compared between nonRR and RR cell lines by performing a wound healing assay. This assay works on the principle of making a wound (cell free area) in a confluent monolayer of cells and tracking the migration of the cells at the edge of the wound over a time course to determine the rate of at which the wound closes.

These results showed that the MDA-MB-231 cells migrate faster than the REM134 cells: the nonRR MDA-MB-231 cell line closed the wound in 28 hours compared to 48 hours for the nonRR REM134 cell line; and the MDA-MB-231 RR cell line closed the wound at 12 hours compared to the REM134 RR cell line, which closed at 24 hours. The REM134 RR had a significantly faster migration rate, (Figure 3.4 B; $p<0.01$) at 12 hours with 25% higher migration rate when compared to the REM134 cancer cell line (Figure 3.4 A). The MDA-MB-231 RR cell line migrated significantly faster (Figure 3.4 B; $p<0.001$) at 8 hours with a 54% faster migration rate when compared to the MDA-MB-231 cell line at 8 hours (Figure 3.4 B).

.

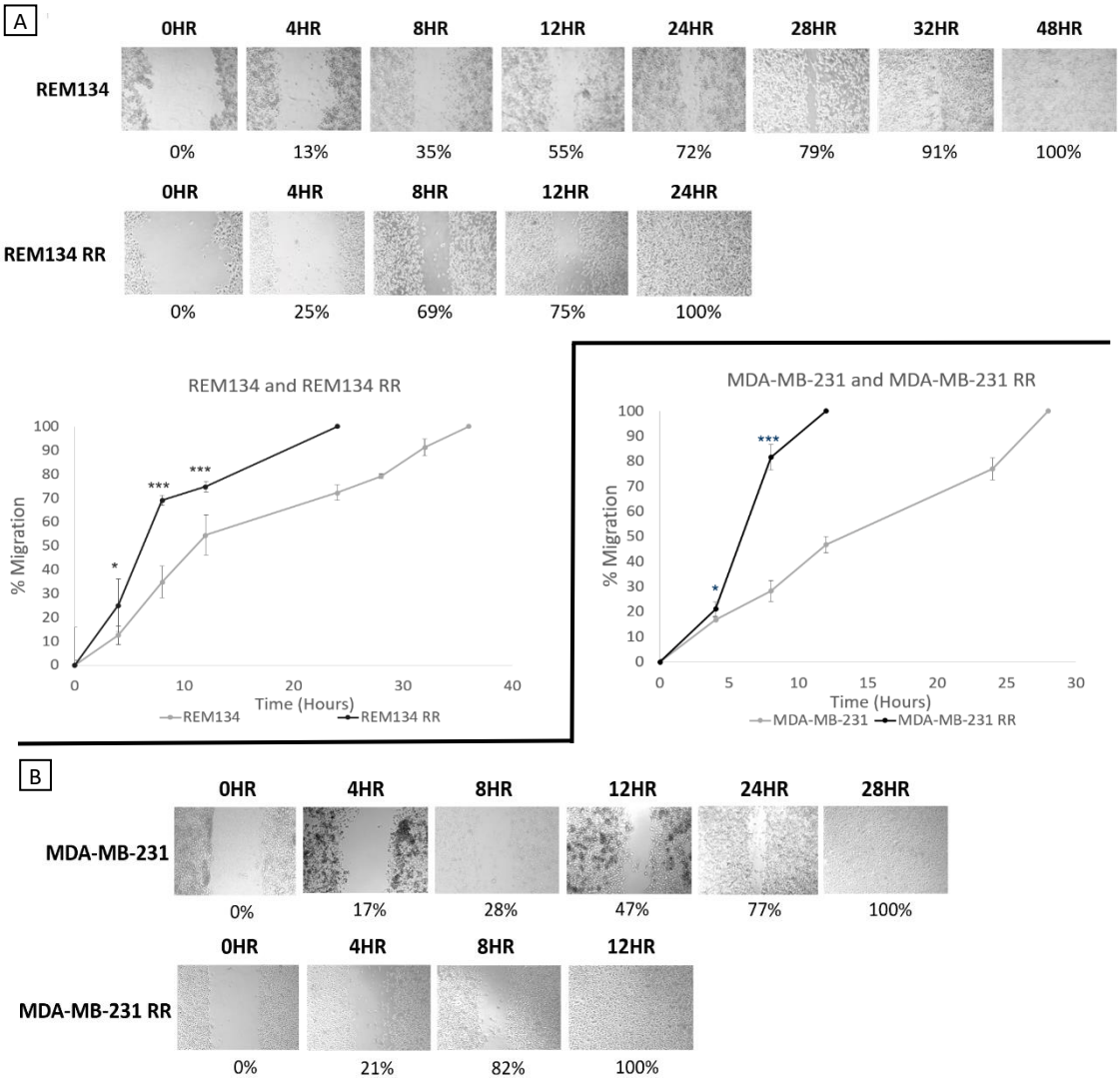


Figure 3.4 RR cell types have a faster migration rate compared to the nonRR cell lines. ***A)*** *REM134,REM134 RR, MDA-MB-231 and MDA-MB-231 RR cancer cells were seeded into an ibidi insert plate and incubated for ~24 hours until confluent, a wound was made in the cell monolayer and measured to determine rate of migration. Pictures were taken at the stated time points. n=3 technical replicates. Averages were taken for each time point, and % migration was calculated (100 (A-B)/A where A is the width measured at 0 hr and B is the width of the cell wound after). Error bars show +/- %SD. Statistical significance was determine by a two tailed t-test * p ≤ 0.05, ** p ≤ 0.01; *** p ≤ 0.001.*

The results showed that the RR cancer cell lines migrated significantly faster than the nonRR cancer cell lines, meaning that breast cancer cells that acquire radioresistance have a more aggressive phenotype compared to nonRR cancer cells.

3.2.4 Radioresistant cell lines have a higher percentage of cells in the G2 phase

After characterisation of cell morphology and expression of markers of EMT and migration, cell lines were characterised according to their cell cycle profile with the aim to establish if there were differences in distributions of the cell cycle between the nonRR (REM134 and MDA-MB-231) and RR (REM134 RR and MDA-MB-231 RR) cancer cells. To analyse the percentage of cells in each phase of the cell cycle, flow cytometry was utilised. Forward scatter (size of the cell) versus side scatter (granularity of the cell) was plotted to show the size distribution and cell content in a cell population. As cells progress through the cell cycle, their DNA content and cell size alter. Therefore, cells were gated appropriately to remove debris and doublets and histograms of the selected cells were plotted to show the distribution of cells in the cell cycle (Figure 3.5).

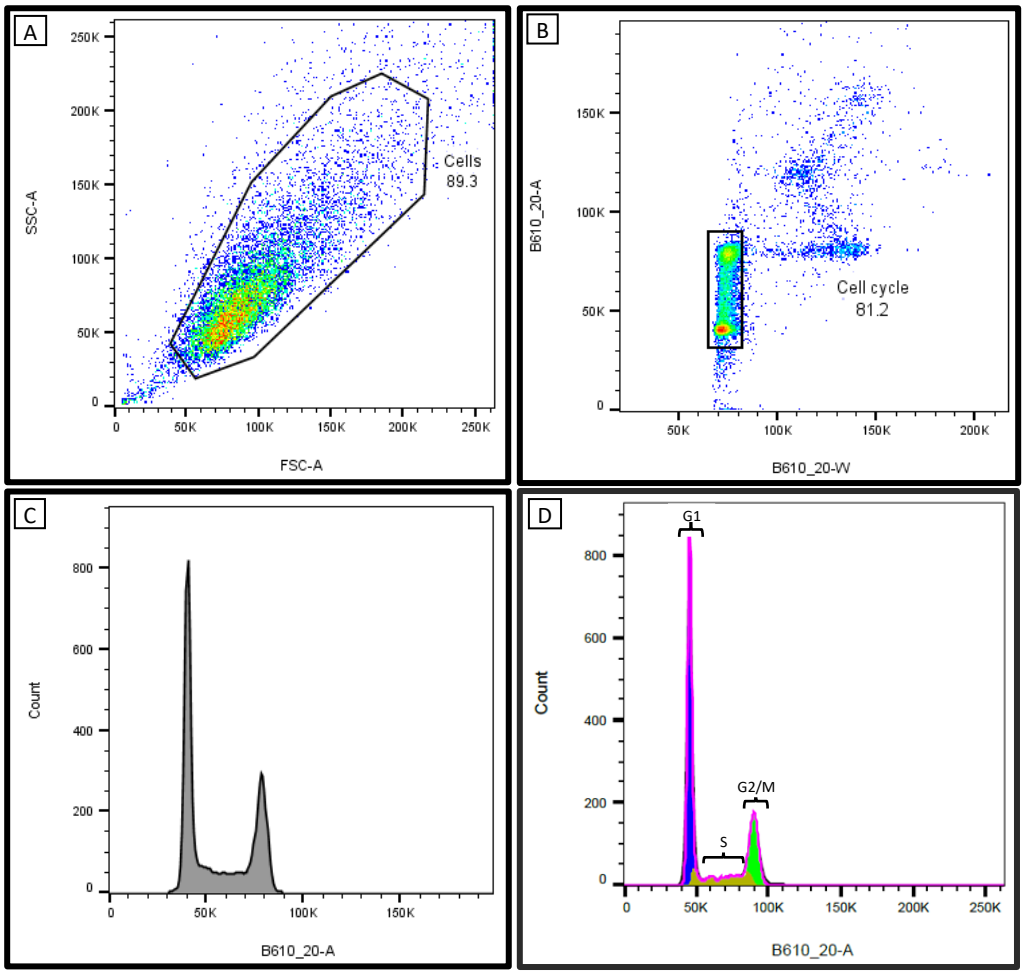


Figure 3.5 Workflow for cell cycle analysis. *Cells were stained with propidium iodide (B610_20-A). To remove debris, forward scatter vs side scatter were plotted and cells gated (A). To remove doublets and unstained cells, propidium iodide width by area was plotted and single cells showing the typical cell cycle layout were gated (B). Single cells were plotted as propidium iodide area vs cell count to plot a cell cycle histogram (C). In FlowJo, the cell cycle analysis was performed using the Watson pragmatic model chosen to identify separate parts of the cell cycle (D).*

These data were quantified by plotting cell cycle histograms for all cell lines as shown below (Figure 3.6), this allowed a direct comparison of the distribution of cells throughout the cell cycle which could then be quantified in to percentages.

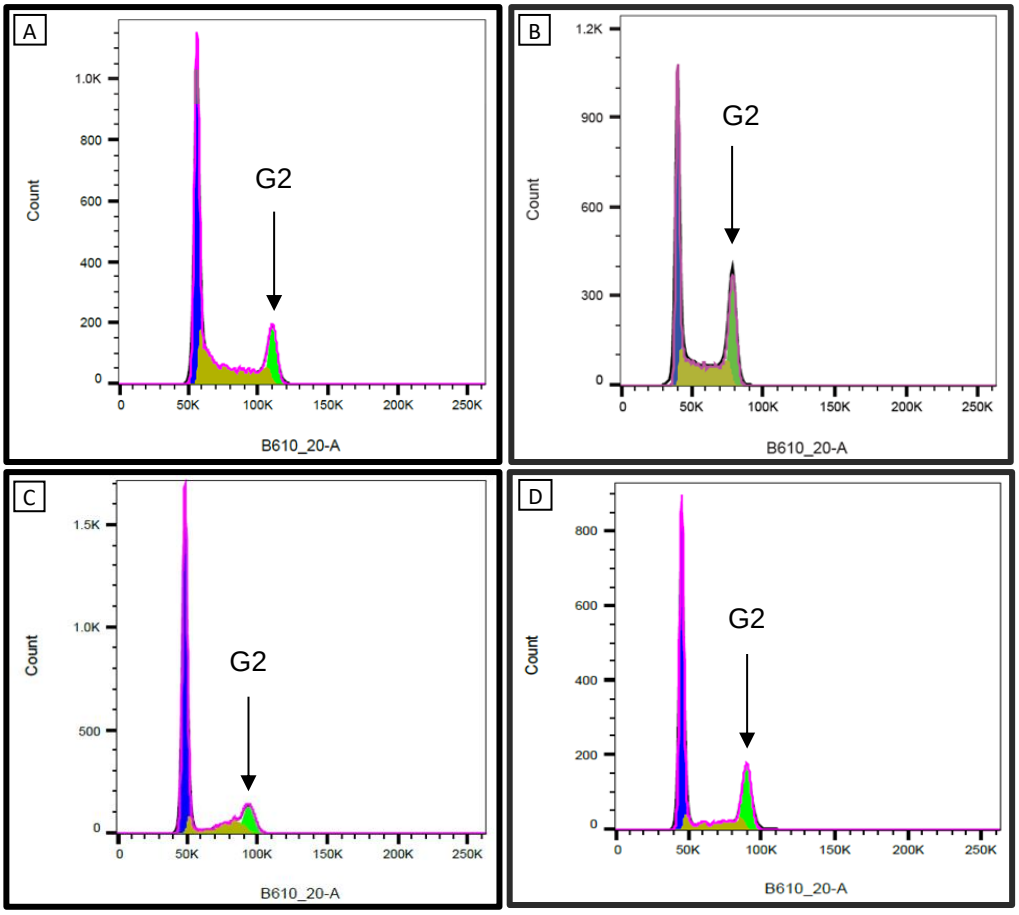


Figure 3.6 RR cell lines have a higher percentage of cells in the G2 phase of the cell cycle. *B610-20 laser was used to measure propidium iodide stain. Cell cycle analysis using propidium iodide to stain 1x10^6 cells were analysed to create the standard depiction of the cell cycle showing the G1 phase (purple), S phase (yellow) and G2/M phase (green) of the cell cycle for all cell lines A) REM134 B) REM134 RR C) MDA-MB-231 D) MDA-MB-231 RR.*

The cell cycle analysis showed that both nonRR cell lines (Figure 3.6 A, C) had a smaller percentage of cells in the G2 phase of the cell cycle compared to their RR counterparts (Figure 3.6 B, D). In FlowJo, the phases of the cell cycle were quantified and exact percentages were shown in Table 3.1 below.

Table 3.1 REM134 RR and MDA-MB-231 RR cell lines have almost double the percentage of cells in the G2 phase of the cell cycle. *Data shown were calculated in FlowJo after 1x10^6 cells were stained with propidium iodide stain and histograms of cell cycle analysis plotted. Data shows average of technical repeats n=2* ± %SD.

Phase of cell cycle	Cell line			
	REM134	**REM134 RR**	**MDA-MB-231**	**MDA-MB-231 RR**
G0/G1	64.2% ± 1.2	47% ± 1.4	68.6% ± 0.2	62.1% ± 0.3
S	13.9% ± 6.9	18.7% ± 0.1	17.4% ± 1.2	8.8% ± 0.2
G2/M	18.0% ± 0.1	31.8% ± 4.0	12.8% ± 0.6	33.2% ± 9.4

Histogram data were converted into percentages which showed there were almost double the percentage of cells of REM134 RR in the G2 phase of the cell cycle (31.8%) compared to REM134 (18.0%). This was also seen between human nonRR and RR breast cancer cells, with 12.8% of MDA-MB-231 in the G2 phase of the cell cycle and 33.2% of MDA-MB-231 RR cancer cells in the G2 phase. This means that the RR cell lines could have a higher rate of DDR (DNA damage repair) which can result in an increased cancer cell survival rate following irradiation.

3.2.5 Optimisation of EV isolation, quantification and visualisation

After characterisation of the panel of cell lines, methods of EV isolation were trialled and optimised with the aim to isolate EVs from all cell lines: REM134, REM134 RR, MDA-MB-231 and MDA-MB-231 RR to use in functional assays. The use of these EVs in functional assay could determine if the radioresistant phenotype could be transferred via EVs in breast cancer. The gold standard method of EV isolation is ultra-centrifugation (UC) (Chen *et al.,* 2022), where samples are spun at exceptionally high speeds compared to general centrifugation. However, this requires several cycles of centrifugation and the process is laborious. The recent explosion of interest in EVs in the field of human medicine has led to the development of other EV isolation methods, such as commercial kits that claim to isolate pure EVs in one fifth of the time required for UC. One of these kits includes the Exo-easy maxi kit, which isolates EVs by a spin column and collects EVs in the membrane which are then eluted with a buffer (Macias *et al.,* 2019). Due to the time efficiency proposed by the Exo-easy maxi kit, this method was initially trialled in

experiments and subsequently quantified the EV yield using nanosight tracking analysis (NTA). NTA works on the principle of Brownian motion; whereby suspended nanoparticles have a laser passed through allowing the calculation of approximate nm sizes based on nanoparticle movement (Monakhova *et al.,* 2021). The methods trialled for EV isolation are shown below (Figure 3.7).

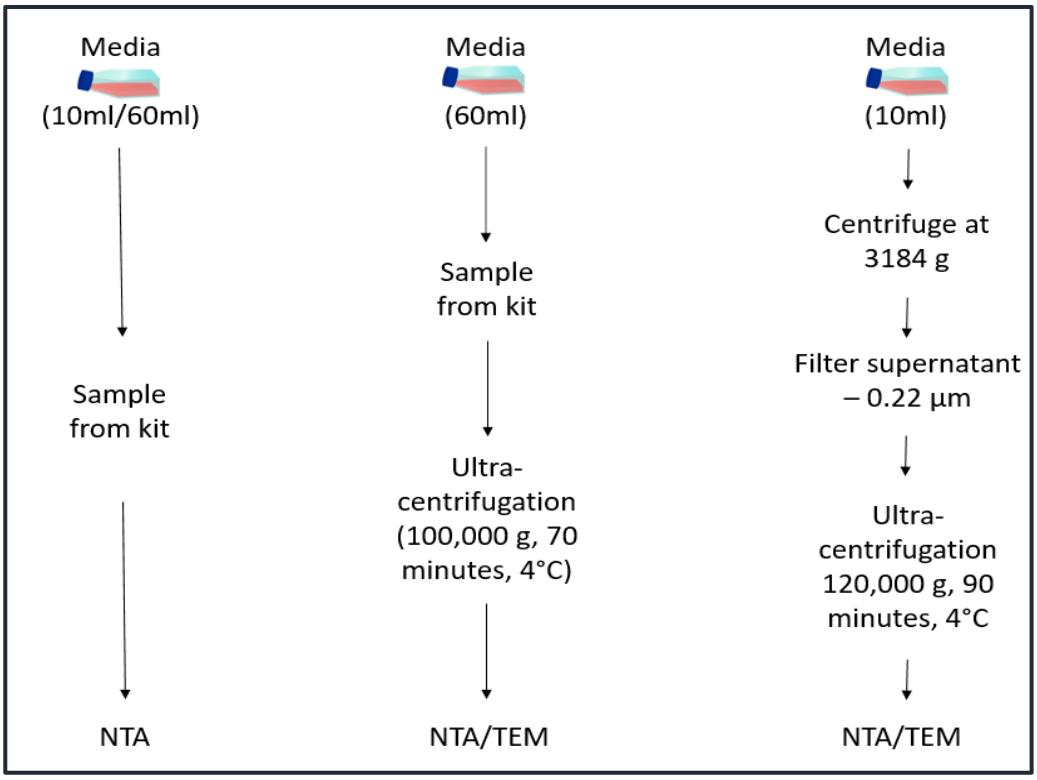


Figure 3.7 Workflow utilised to isolate, visualise and quantify EVs*. Isolation methods began with trialling the Exo-easy isolation kit, with UC alone being used to isolate EVs. NTA and TEM was used for visualisation. REM134 cells were used for the trialling of all methods.*

Initial EV samples isolated by the Exo-easy isolation kit were analysed via NTA (Figure 3.7). EV samples should be within the range of 30 – 200 nm on NTA equipment (Lichen *et al*., 2019). However, the size range varied greatly between repeats; from 0 nm (background particles), to ~298 nm indicating that the Exo-easy isolation kit did not result in the isolation of the correct vesicle size (Figure 3.8 A).

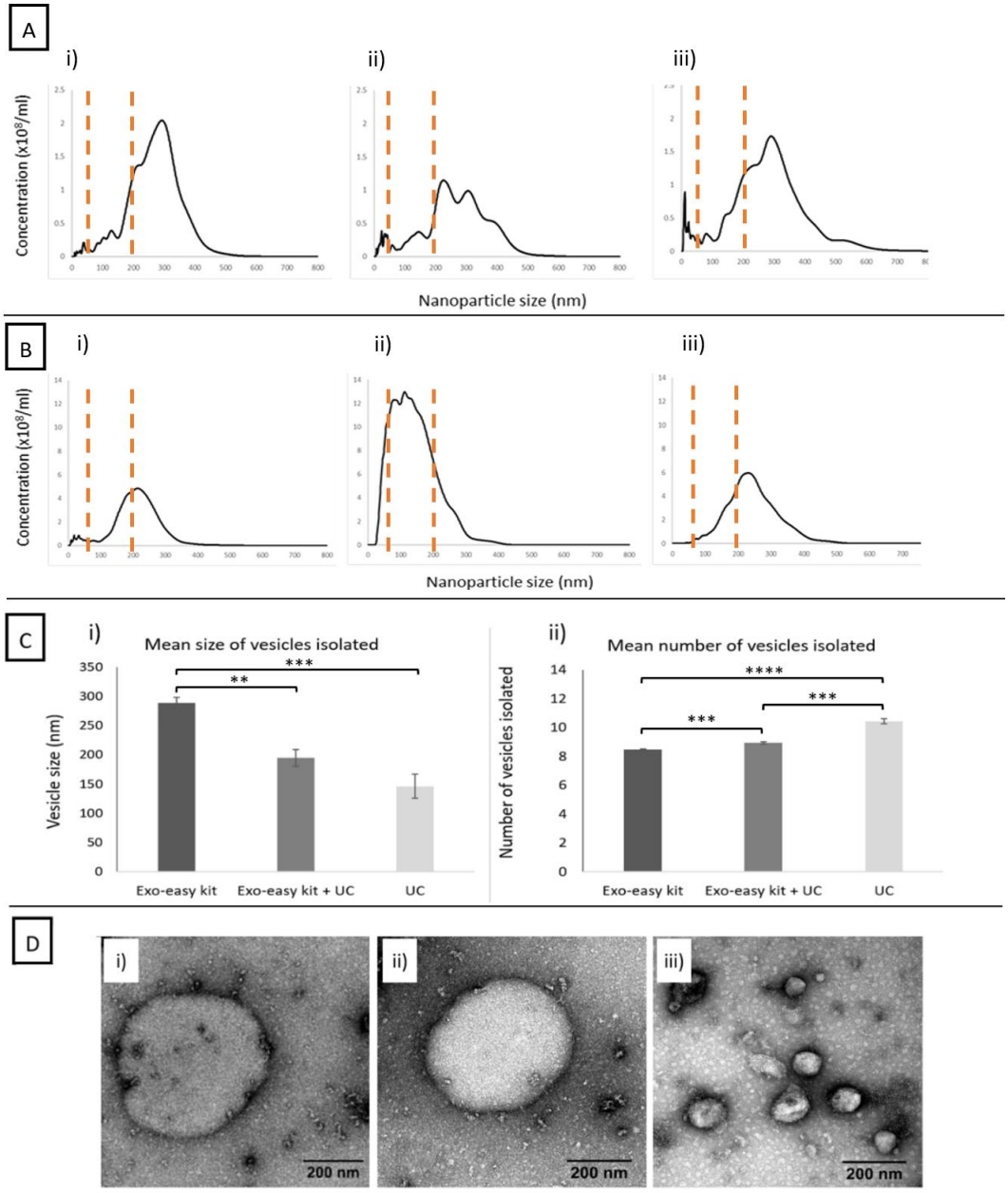


Figure 3.8 Size distribution of vesicles after using the Exo-easy isolation kit with and without UC*. The expected size range of EVs are shown by red dotted lines between 50 nm to 200 nm* ***A)*** *EVs from the Exo-easy kit using 10 mL of medium. Technical repeats REM134 cells n=3.* ***B)*** *EVs isolated from the Exo-easy kit from 60 ml of medium and an additional UC step at 100,000 x g for 70 minutes. Technical repeats from REM134 cancer cells n=3.* ***C) i)*** *Data showing mean vesicle size +/- SEM* ***ii)*** *Data showing vesicle concentration. Raw data were LOG10 transformed and plotted. Technical repeats n=3 for data obtained by using Exo-easy kit and Exo-easy kit and UC. n=4 for UC data. Statistical significance was analysed by a two tailed students' t-test. Error bars indicate ±SD ** p ≤ 0.01; *** p ≤ 0.001, **** p ≤ 0.00001* ***D)*** *Representative images of vesicles observed by TEM* ***i)*** *Typical vesicles isolated from the Exo-easy kit* ***ii)*** *Typical vesicles isolated from the Exo-easy kit and a UC step* ***iii)*** *Typical vesicles isolated from UC at 120,000 x g for 90 minutes.*

The corresponding table for the NTA showed the concentration of particles were in the range of 2.46 x10^8 particles/mL to 3.66 x10^8 particles/mL from the three repeats (Table 3.2). The mean size was in the range of 273 nm to 305 nm, whereas the mean size range for EVs should be in the range of 100-120 nm (Logozzi *et al.,* 2020), indicating that several other types of microvesicles were being isolated by the Exo-easy isolation kit. Therefore, an ultra-centrifugation (UC) step was added to concentrate EV samples and to increase the final concentration of EVs. A final UC step at 100,000 *x g* was used to isolate EVs from 60 mL of media collected from two T175 flasks to increase the total number of EVs isolated. It was observed that the UC step removed most of the background particles present in the samples, due to no or very few particles present in the 0 nm to 30 nm range (Figure 3.8 B i, ii, iii). The size of EV isolated was significantly increased ($p<0.001$) when using UC compared to the Exo-easy kit (Figure 3.8 C i), and the number of particles visualised by NTA significantly increased when using UC compared to the Exo-easy kit (Figure 3.8 C ii; $p<0.00001$) and Exo-easy kit with a UC step ($p<0.001$). There was a decrease in the mean size of particles from 273 – 305 nm to 151 – 205 nm (Table 3.2) and the concentration also increased following the addition of the UC step, from a concentration of 3.66 x 10^8 when using the Exo-easy isolation kit, to 1.11 x10^9 EVs/mL when using an additional UC step.

Table 3.2 Raw NTA data showed that UC resulted in a higher concentration of vesicles at a lower size range compared to the other methods trialled. *The data shows the mode (nm) and mean (nm) size of vesicles isolated by the Exo-easy kit n=3, the Exo-easy kit and a UC step n=3 and UC alone n=1 per cell line.*

Method of vesicle isolation	Repeat	Mode (nm)	Mean (nm)	StDev (nm)	Concentration (particles/mL)
Exo-easy kit	i	282	288	120	3.66x10^8
	ii	351	305	92	2.67x10^8
	iii	274	273	126	2.46x10^8
Exo-easy kit and UC step	i	195	199	94	6.37x10^8
	ii	151	168	67	1.11x10^9
	iii	205	217	80	8.9x10^8
UC at 120,000 *x g* for 90 minutes	REM134	94	110	28	1.08x10^{10}
	REM134 RR	101	126	46	1.33x10^{10}
	MDA-MB-231	151	178	96	2.39x10^{10}
	MDA-MB-231 RR	167	171	86	6.00x10^{10}

However, the mean size of the vesicles isolated (199 – 217 nm) is still larger than what is typically seen for EVs (100-120 nm)(Logozzi *et al.,* 2020). Higher concentrations were obtained after using the Exo-easy kit with an additional UC step; therefore, UC was chosen as the method of isolation. An initial centrifugation step at 3184 *x g* is used to remove any cells and cellular debris, followed by filtration through a 0.22 µm filter to remove further microparticles and aggregates, followed by an UC step at 120,000 *x g* for 90 minutes (outlined in Figure 3.7). This resulted in a further increase in vesicle concentration from $x10^8$ when using the Exo-easy kit and a UC step to $x10^{10}$ vesicles, and further decrease in the mean sizes (Table 3.2).

TEM allows the visualisation of nanoparticles via observing diffraction patterns obtained after passing an electron beam through samples (Rauch *et al.,* 2005). Due to the electron beam having shorter wavelengths than light, this allows resolution of ~1 nm which is a lower resolution than scanning electron microscopy and atomic force microscopy (Brydson *et al.,*2015). The decrease in vesicle size observed by NTA data (Figure 3.8 C; Table 3.2) was confirmed by TEM including a wide field image and close up images of the EVs advised by MISEV guidelines (Figure 3.8 D; Figure 3.9).

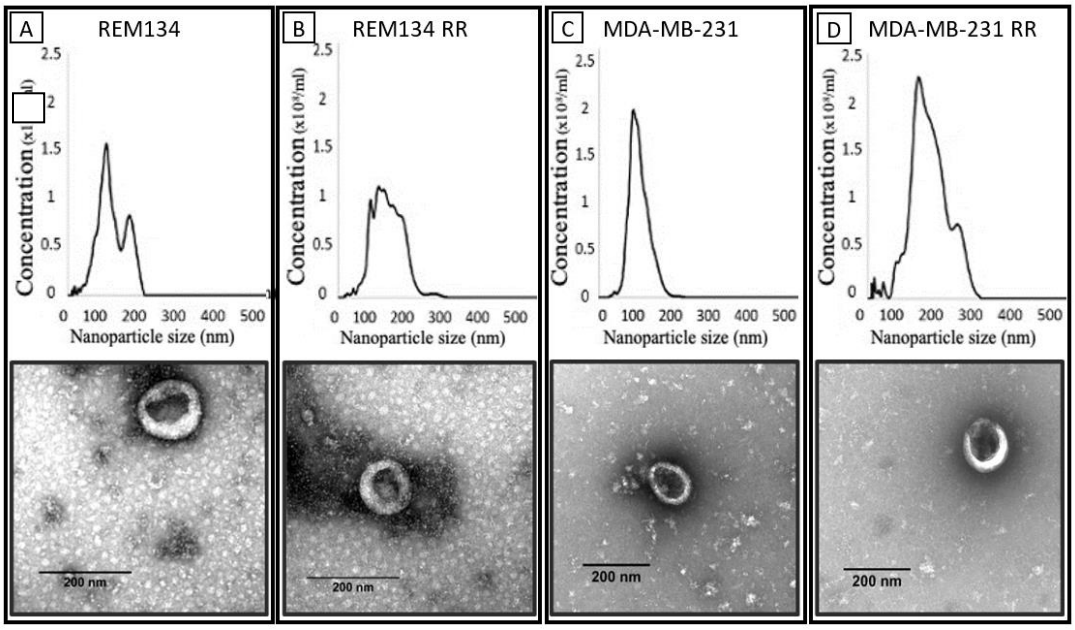


Figure 3.9 Isolation of EVs from all cell lines. *Figure showing the NTA data in the upper panel and corresponding TEM images of EVs isolated by UC from the following cell lines* ***A)*** *REM134* ***B)*** *REM134 RR* ***C)*** *MDA-MB-231* ***D)*** *MDA-MB-231 RR.*

The TEM and NTA images from the optimised EV isolation protocol data shown in Table 3.2 are shown in Figure 3.9. Visualisation of EVs via TEM from UC showed that vesicles seen were in the range of 30 – 150 nm, and the observed the characteristic collapsing of the EV can be seen that is associated with the fixation and dehydration step involved in the processing of EVs for TEM for all cell lines (Figure 3.9) (Brydson *et al.,* 2015).

To summarise, it was found the use of UC alone isolated EVs more efficiently than the commercially available kit, allowing the isolation of EVs from 10 mL of media compared to using 60 mL of media when using the Exo-easy isolation kit and an additional UC step (Figure 3.8). This was shown by the characteristic NTA and TEM images associated with EVs (Figure 3.9) from all cell lines.

3.3 Discussion

The acquisition of radioresistance in breast cancer results in confounding problems in terms of treatment options and mortality. To verify the hypothesis of this project, the role of EVs in the acquisition of radioresistance in breast cancer was investigated. Initial investigations required characterisation of the panel of RR and nonRR cell lines used. It was found the RR cell lines had a more mesenchymal phenotype and were potentially more migratory. Previous studies have shown that characteristics of RR cells include a mesenchymal phenotype, a higher migration rate and an increase in the percentage of cells in the G2 phase of the cell cycle (Gray *et al*., 2019; Mutschelknaus *et al.,* 2017; Peng *et al.,* 2020). Previous work by Gray *et al.,* (2019) showed that RR cells have a higher migration rate compared to their nonRR counterparts potentially due to increased activation of PI3K/AKT pathway. Although RR cells characteristics were identified, further experiments are needed to expand on this work and identify if EVs are a direct mediator of radioresistance in recipient cells, and if so, identify potential mechanisms driving this process. Cell line characteristics were identified to determine if they are consistent with the

documented characteristics that are associated with an RR phenotype in the literature.

Cell morphology was characterised by phase contrast microscopy, where it was found that the radioresistant cell lines had cytoplasmic extensions and a more spindle like phenotype with this being more apparent when comparing the REM134 and REM134 RR cell lines (Figure 3.1 A, B). The acquisition of radioresistance is associated with the induction of EMT which results in a more spindle-like morphology (Wiechec *et al.,* 2022). The REM134 cell line appeared to lack the spindle-like projections seen in the REM134 RR cell line, this difference may be more noticeable than when comparing morphology between the MDA-MB-231 and MDA-MB-231 RR cell lines, as the MDA-MB-231 cell line already has an evident spindle-like morphology. In addition to the EMT markers employed in this project, it may have been useful to have investigated expression of N-cadherin between nonRR REM134 and MDA-MB-231 and RR REM134 RR and MDA-MB-231 RR cancer cells. Although E-cadherin and N-cadherin are both markers of cell to cell junctions present in an epithelial cell type, N-cadherin expression is associated with the release of metalloproteinases that lead to invasive properties in breast cancer (Leal-Orta e*t al.,* 2021). The REM134 RR cell line had cytoplasmic projections and had a faster rate of migration (Figure 3.4) and increased expression of mesenchymal markers β-catenin, vimentin and slug and snail when compared to the REM134 nonRR cancer cells (Figure 3.3). Hence, it would be expected for the expression of E-cadherin to be decreased in the REM134 RR cancer cells, but there appeared to be no obvious difference in E-cadherin expression between the REM134 and REM134 RR cancer cells (Figure 3.3, lanes 1 and 2). Due to this discrepancy it would have been useful to use more than one cell to cell junction marker to ensure consistency between results and rule out experimental error. Therefore, it would be beneficial to confirm EMT status by identifying expression of tight junction proteins such as claudins and gap junction proteins such as connexin 43 (Geoffroy *et al.,* 2020; Kjenseth *et al.,* 2012).

CSCs are a subset of the tumour population that are highly resistant to environmental changes and cancer therapies. After performing literature searches this study is the first to derived CSCs from radioresistant breast cancer cells, CSCs have not been derived from established radioresistant cell lines. Characterisation of breast CSC morphology showed the CSCs derived from the MDA-MB-231 RR and the REM134 RR cell lines had a more mesenchymal phenotype with a spindle like formation and cytoplasmic extensions when compared to the breast CSCs derived from the nonRR cell lines. It was interesting to see that REM134 RR CSCs had more cells with spindle-like morphology when compared to the nonRR REM134 CSCs (Figure 3.2 A, B), this contrasts with the MDA-MB-231 nonCSCs, as both the nonRR and RR had a spindle-like appearance (Figure 3.2 C,D). Breast cancer stem cells have a more mesenchymal phenotype when compared to non-CSCs (Strietz *et al.,* 2021), which has recently been termed "epithelial-mesenchymal plasticity" whereby CSC populations retain some epithelial features such as cytokeratin content but have a mesenchymal phenotype and have increased rates of migration (Yang *et al.,* 2020). The breast CSC isolation protocol used in this project was established and verified by Pang *et al*., (2011), but it would have been useful to perform validation experiments to confirm a CSC population such as flow cytometry or western blotting for stem cells markers such as pluripotency markers Oct4 and Nanog (Xin *et al.,* 2022), alongside confirming a breast cancer population by detecting for hormone receptors such as ER, PR and HER2. The REM134 and REM134 RR cell lines would have ER^- PR^- $HER2^+$ and the MDA-MB-231 and MDA-MB-231 RR breast cancer cell line would have ER^- PR^- $HER2^-$, as it has previously been demonstrated that there is no change in hormone receptor status in these cell lines upon the acquisition of an RR phenotype (Gray *et al.,* 2019).

The epithelial features identified in the breast CSCs aligned with western blot analysis of markers of EMT (Figure 3.3) which showed that the RR cell lines appeared to have increased expression of mesenchymal markers. This agrees with the literature stating that RR cells lose an epithelial phenotype and acquire a mesenchymal phenotype, shown by the decreased expression of cell to cell junction protein E-cadherin and the increased expression of mesenchymal marker vimentin

(Aschenbrenner *et al.,* 2021; Bi *et al*., 2020). Studies have shown that an increase in the β-catenin signalling axis and been associated with radioresistance (Osuka *et al.,* 2021), as β-catenin is associated with the WNT signalling pathway which is associated with cancer cell proliferation, and migration via the acquisition of a mesenchymal phenotype (Meng *et al.,* 2020; Li *et al.,* 2018). Western blots indicated there was an increased expression of the transcription factor slug and snail in REM134 RR and MDA-MB-231 RR cells (Figure 3.3 C). The expression of slug and snail transcription factors is associated with the acquisition of malignant phenotypes by inducing EMT (Nakamura *et al*., 2018) and the regulation of ATP binding cassette (ABC) transporters which play a key role in therapy resistance (Jiang *et al*., 2017). These findings taken together indicate that the RR cell lines have a more mesenchymal phenotype. Additionally, when investigating rates of migration between the nonRR cancer cells and the RR cancer cells it was found that the RR cancer cells had a faster rate of migration (Figure 3.4). This is a characteristic seen in other RR cancer cells that is associated with a mesenchymal phenotype and potentially due to the activation of the AKT pathway (Gray *et al.,* 2019, Mutschelknaus *et al*., 2016).

In addition to the decreased expression of markers of epithelial cell lines, and increased expression of markers associated with a mesenchymal phenotype upon acquiring a radioresistant phenotype, other cellular changes occur such as changes within the cell cycle. In a non-cancerous state, cells progress through the cell cycle of G1, S phase, G2 phase and M phase, with the progression in to G2/M phase being tightly controlled by ATM (Mladenov *et al.,* 2019). The G2 checkpoint has the role of preventing the premature progression through the cell cycle to the M phase, which results in premature mitosis of cells which can result in apoptosis if the cells have acquired too many DSBs. By delaying entry to the M phase, cells can decrease the apoptosis events that occur. Upon receiving irradiation, the G2 phase delay allows activation of BRCA1 to promote DNA damage repair by both HR and single-strand annealing in very late S phase/early G2 phase in RR cells (Batenburg *et al.,* 2019), meaning an increase in the percentage of cells in the G2 phase of the cell cycle is associated as a characteristic of radioresistant breast cancer cells (Peng *et al.,* 2020).

This delay allows activation of DNA damage repair, via the activation of BRCA1 to promote DNA damage repair by both HR and single-strand annealing in very late S phase/early G2 phase in RR cancer cells (Batenburg *et al.,* 2019; Xu *et al.,* 2021; Yang *et al.,* 2021). The RR cells were irradiated at 15 Gy every 4-6 weeks to ensure a selection pressure to select for radioresistance in the surviving cell population as previously done by Gray *et al.,* (2019) and it was found RR cells had almost twice the percentage of cells in the G2 phase of the cell cycle when compared to their nonRR counterparts (Figure 3.6; Table 3.1).

These findings agree with characteristics of RR cancer cells published in literature to date. Although characterisation of RR cancer cells has been studied, there are very few studies investigating the specifics of how the RR cancer cells acquire radioresistance. EVs have also shown to play a major role in the nurturing, growth and spread of cancer, as well as conferring chemotherapy resistance to naïve cancer cells. Consequently, to observe the effect of EVs on recipient cells, this required isolation of EVs from the REM134, REM134RR, MDA-MB-231 and MDA-MB-231 RR cancer cells.

All methods of EV isolation rely on the removal of other microvesicles to obtain a sample of pure EVs. Optimisation of EV isolation in this project showed that UC was the most consistent and efficient method of EV isolation when compared to the use of the Exo-easy kit in terms of consistent results and EV size (Figure 3.8 C). The NTA analyses showed larger size microvesicles that had the morphology of ectosomes when analysed by TEM that do not have the cup shaped morphology in TEM analysis (Figure 3.8 D i, ii) (Surman *et al.,* 2020). Other studies have also found that much larger vesicles may be isolated when analysing their samples by NTA, and proteomic analyses found primarily proteins associated with vesicle formation by the Golgi apparatus which is not typical for EVs (Surman *et al.,* 2017; Veerman *et al*., 2021; Stranska *et al.,* 2018).

After trialling the Exo-easy kit with highly variable results, a final UC step was used to isolate smaller vesicles that are associated with the size of EVs, and although this decreased the size of EVs obtained (Figure 3.8 C) there were still microvesicles not typical with EVs present in the isolated samples (Figure 3.8 D ii). EV isolation was successfully optimised as well as visualisation, and quantification by UC, TEM and NTA (Figure 3.9) in accordance with the MISEV guidelines to fulfil the objective of isolating EVs to use in functional experiments. It was noted that the REM134 RR and MDA-MB-231 RR cancer cells released more EVs than their nonRR counterparts – REM134 and MDA-MB-231 (Figure 3.9) which was also found by Mutschelknaus *et al.,* (2016) when comparing EV release by radiotherapy resistant head and neck squamous cell carcinoma cell lines. EV release has found to be increase EV release in normal astrocytes and malignant glioblastoma cell lines following irradiation at 2.3 Gy (Arscott *et al.,* 2013) and cancer cells under stress conditions such as hypoxia and changes from optimal extracellular pH have increased EV release (Boussadia *et al*., 2018). The mechanism by which radioresistance can result in increased EV release is yet to be fully researched, with only one primary study showing that irradiation of human umbilical cord vein cell lines have increased activation of the WNT pathway and transcription of EV biogenesis markers Rab-27a, Rab-27b, Alix, and CD63 following irradiation (Bagheri *et al*., 2018). The radioresistant REM134 RR and MDA-MB-231 RR cancer cells could have increased EV release due to cellular stress factors from irradiation such as increased ROS and activation of the WNT pathway, which could also be associated with the more mesenchymal phenotype observed in Western blots (Figure 3.3). Further research could focus on comparing the expression of CSC markers such as NOTCH, OCT4 and NANOG between the nonRR (REM134 and MDA-MB-231) and RR (REM134 RR and MDA-MB-231 RR) along with EV biogenesis markers to validate the potential mechanisms by which EV release occurs in human and canine mammary carcinomas.

To summarise, it was found that the RR cancer cells have a more mesenchymal phenotype when compared to their nonRR counterparts after analyses of phase contrast microscopy images and western blots of mesenchymal markers β -catenin, slug and snail and vimentin. The REM134 RR and MDA-MB-231 RR cancer cells also

had a higher percentage of cells in the G2 phase of the cell cycle which is associated with an increased rate of DDR when compared to the nonRR cancer cells. These characteristics found in the RR cancer cells agree with published studies characteristics of in RR breast cancer cells (Lee *et al*.,2022; Zhao *et al.,* 2018). As EVs have shown to be a potential facilitator of a pro-tumourigenic TME, and promote cancer cell growth, proliferation and migration, methods of EV isolation were trialled from the panel of cell lines to allow the use EVs in functional assays to investigate effects of EVs derived from RR cells on recipient cells in the context of radioresistance. Therefore, it was decided to isolate vesicles by using UC, as this method showed promising repeatability and a higher nanovesicle yield in the correct size range for EVs when compared to the Exo-easy isolation kit.

Chapter 4: EVs derived from RR cancer cells can transfer radioresistance to recipient non-CSC and CSCs

4.1 Introduction

Radiation resistance is a significant challenge in the treatment of recurrent, advanced and metastatic breast cancer in humans and canines. Therapy resistance begins with a small percentage of cells that establish a resistant phenotype. The underlying molecular mechanism driving propagation of the RR phenotype throughout the tumour cell population has not yet been fully elucidated. EVs are secreted from nearly all cell lines and can alter phenotype and proteome of recipient cells. The discovery of EVs has led to increased research focused on the role of these microvesicles in several disease morbidities including cancer initiation, development and progression; however, the role of EVs in the acquisition of radioresistance has yet to be explored. Given that in veterinary medicine, the emergence of radioresistance in bitches with CMC causes 50% of deaths highlights a significant clinical need for better diagnosis and treatment (Siegel *et al.,* 2019). The effect of EV transfer from therapy resistant cells to non-therapy resistant cancer cells is not fully understood, although the transfer of EVs between cells has been shown to induce phenotype changes in recipient cells. Therefore, the hypothesis of this project was that EVs derived from RR cells can result in the acquisition of radioresistance in recipient cells. This chapter aimed to investigate the effect of EVs derived from REM134 RR and MDA-MB-231 RR cancer cells on recipient cancer cells by analysing the effect on cell viability, therapy resistance and the effect on CSC population *In vitro*.

To determine the effects of EVs on recipient cells, EVs derived from both nonRR and RR cell lines were added to both cell lines (see Figure 4.1 for the experimental set-up).

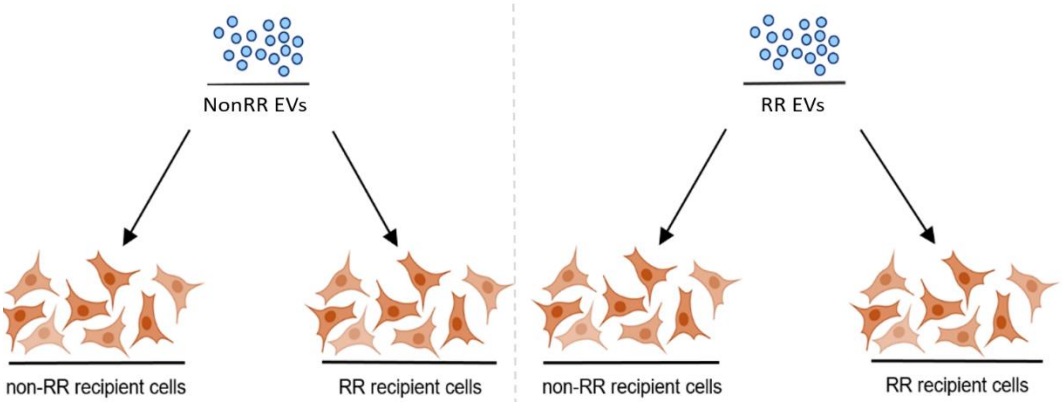


Figure 4.1 Workflow used to determine the effects of EVs on recipient cells*. Medium was removed from cells and EVs were isolated from all cell lines by UC. For all assays canine EVs from REM134 and REM134 RR cells were added to nonRR and RR REM134 canine cancer cells and human EVs from MDA-MB-231 and MDA-MB-231 RR cancer cells being added to nonRR and RR MDA-MB-231 human cancer cells.*

Initial experiments confirmed that the EVs isolated were biologically active after processing and storage. One of the pitfalls of working with EVs which contain active protein and RNA cargo is that incorrect processing and storage can lead to inactivation of EV content (Bahr *et al.,* 2020). The aim of this chapter was to investigate the effect of EVs derived from REM134 RR and MDA-MB-231 RR breast cancer cells on recipient cell viability (section 4.2.1), migration (section 4.2.3) and cancer therapies (Section 4.2.4 and section 4.2.5). Studies have shown that EVs derived from cancer cells can induce a malignant phenotype in non-cancerous cells (Mutschelknaus *et al.,* 2017; Mutschelknaus *et al.,* 2016). Likewise, EVs derived from chemotherapy resistant cancer cells can confer a chemotherapy resistant phenotype in naïve cancer cells (Zhao *et al.,* 2021). If EVs derived from RR cells can induce a RR phenotype in recipient cancer cells, this could contribute to the understanding of the development of radioresistance throughout a tumour population following radiotherapy and the importance of further research in the context of cancer radioresistance. For chemotherapy based assays used in this project, drug concentrations were chosen to reflect potential concentrations that reach cancer cells in the TME *in vivo* after patient administration and biological sink effects (Foldi *et al.,* 2021; Bharti *et al.,* 2021).

4.2 Results

4.2.1 EVs derived from RR cells increase cell viability of all recipient cells

To determine if the EVs isolated were active, a cell viability assay was performed whereby the indicated cells were seeded in 96 well plates and treated with the indicated dose of EVs 24 hours later. Cell viability was determined 72 hours post-treatment with a CellTiter-Glo® assay which measures ATP production, where cells alone and cells treated with PBS were used as controls. It was found that EVs derived from the REM134 RR and MDA-MB-231 RR were able to significantly increase cell viability in both nonRR and RR cell lines (Figure 4.2). Data showed that the addition of EVs derived from RR cells significantly increased the cell viability of nonRR cells from 100% to 200% with the addition of 75 µg/mL of isolated EVs. Similarly, the addition of EVs derived from RR cells on to the RR cell lines increases the cell viability from 100% to 150% in both RR cell lines (Figure 4.2).

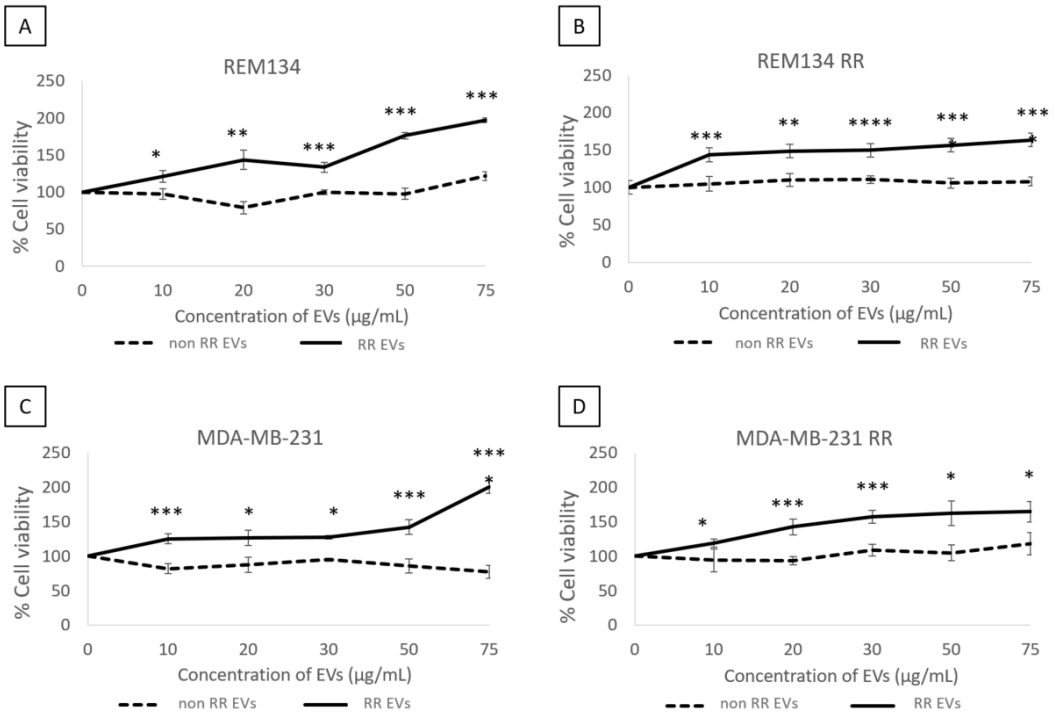


Figure 4.2 EVs derived from REM134 RR and MDA-MB-231 RR cells increase the cell viability of recipient cells*. Cells* ***A)*** *REM134* ***B)*** *REM134 RR* ***C)*** *MDA-MB-231* ***D)*** *MDA-MB-231 RR were seeded on day 1, and EVs were added 24 hours after seeding at 10, 20, 30, 50 and 75 µg/mL. Percentage cell viability was analysed after 5 days by the following calculation (treatment/control) x 100. Cells were treated with PBS as a control (0 µg/mL). Data were averaged and normalised to cells treated with PBS control. Data shown are n=3 technical repeats mean cell viability ± %SD and significance was analysed by a two tailed students' t-test. * p ≤ 0.05, ** p ≤ 0.01; *** p ≤ 0.001, **** p ≤ 0.00001*

To determine if the increase in cell viability observed was not only due to an increase in metabolic activity (production of ATP), a colony formation assay was performed. Colony formation measures the ability of live cells to grow and proliferate by their ability to form a colony, whereas cell viability measures alive cells by quantifying ATP production. The colony formation assay results showed that EVs derived from REM134 RR and MDA-MB-231 RR cancer cell lines could also significantly increase the fold change formation of colonies (Figure 4.3).

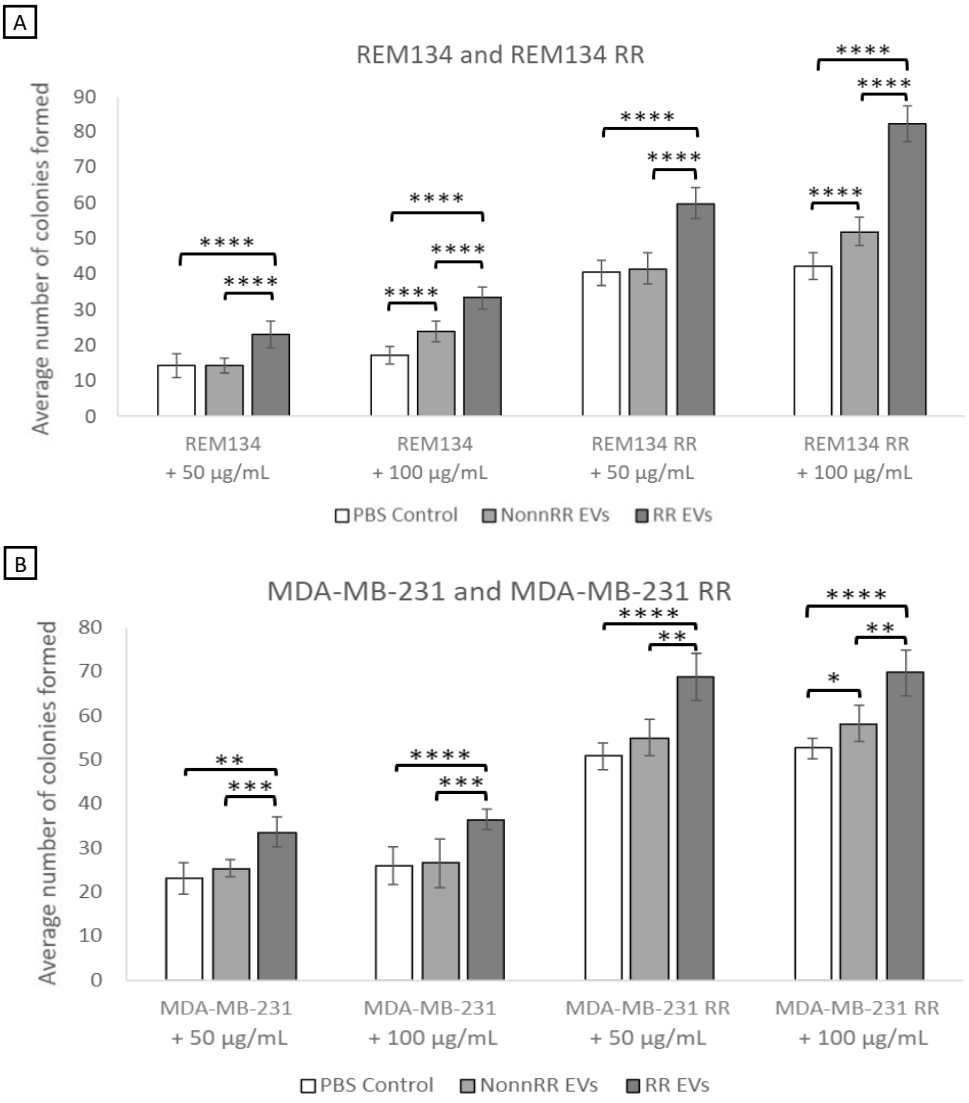


Figure 4.3 EVs from REM134 RR and MDA-MB-231 RR cells significantly increase colony forming ability. *Cells were treated with PBS as a control or 50 µg/mL and 100 µg/mL of EVs derived from nonRR and RR cancer cells. Effects of EVs was determined by a colony formation assay* ***A)*** *REM134 and REM134 RR* ***B)*** *MDA-MB-231 and MDA-MB-231 RR. Data shows mean colony formation ±SD technical replicates n=3, statistical significance was analysed by a two tailed students' t-test. * p≤0.05, ** p≤0.01; *** p≤0.001, **** p≤0.00001*

Preliminary data indicated that EVs derived from REM134 RR cancer cells could significantly increase colony forming ability ($p<0.0001$) when incubated with both REM134 and REM134 RR cancer cells (Figure 4.3 A). Data also showed that EVs derived from MDA-MB-231 RR cancer cells could further increase colony forming ability in MDA-MB-231 RR cancer cells ($p<0.00001$) when compared to MDA-MB-231 RR cell treated with PBS as a control (Figure 4.3 B). To quantity the effect of EVs from nonRR (REM134 and MDA-MB-231) and RR (REM134 RR and MDA-MB-231 RR) cancer cells, the colony formation data were transformed to show the fold change increase following incubation with EVs (Figure 4.4).

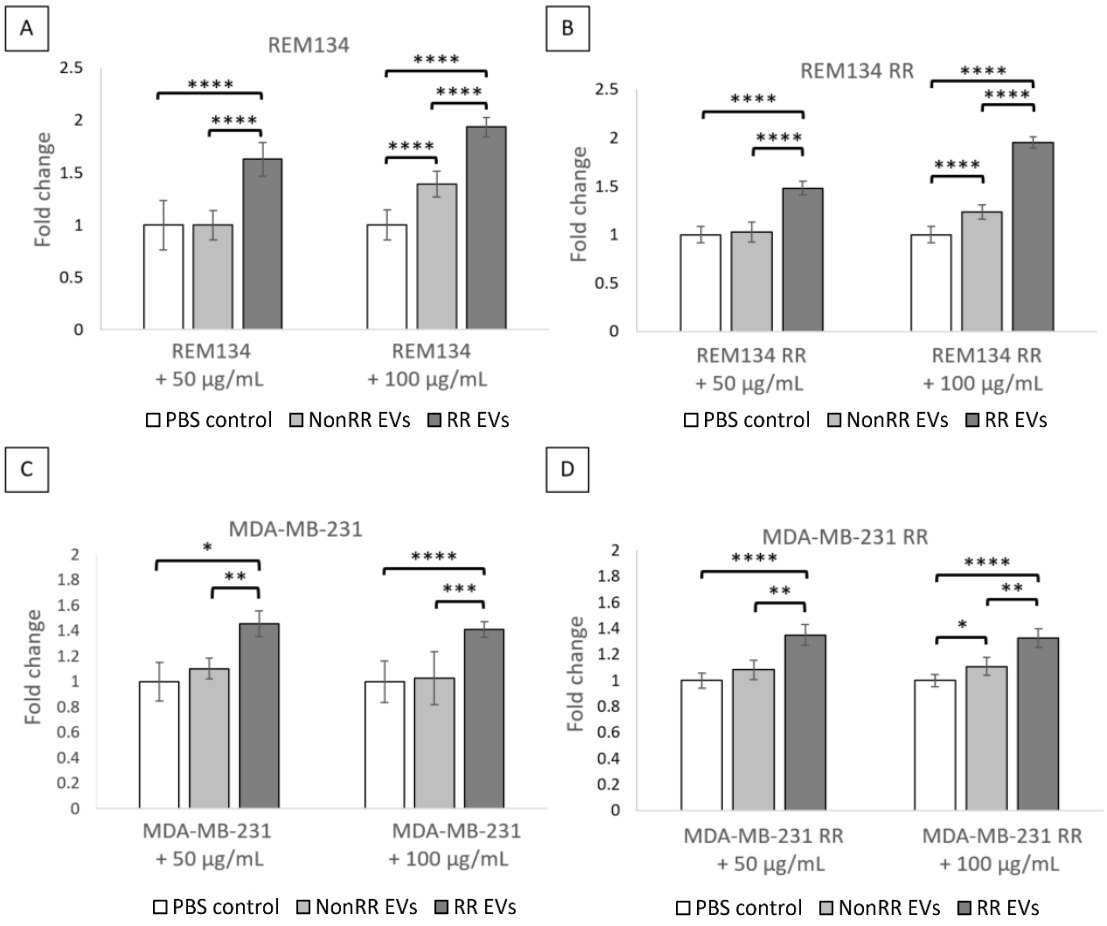


Figure 4.4 EVs from REM134 RR and MDA-MB-231 RR cells significantly increase colony forming ability. *Cells were treated with PBS as a control or 50 µg/mL and 100 µg/mL of EVs derived from nonRR and RR cancer cells.* ***A)*** *REM134* ***B)*** *REM134 RR* ***C)*** *MDA-MB-231* ***D)*** *MDA-MB-231 RR. All data were normalised to the corresponding cancer cells treated with PBS as a control, meaning PBS is taken as 1-fold. Data shows mean colony formation ±SD technical replicates n=3. Statistical significance was analysed by a two tailed students' t-test. * p≤0.05, ** p≤0.01; *** p≤0.001, **** p≤0.00001*

EVs derived from RR cells significantly increased the number of colonies formed for the REM134 (Figure 4.4 A) and the REM134 RR (Figure 4.4 B) cell lines when compared to the addition of PBS to cells and the addition of EVs from nonRR cells ($p \leq 0.00001$). There was also a significant 1.5 fold increase in colonies formed in the MDA-MB-231 cancer cell line ($p < 0.05$) when treated with 50 µg/mL of EVs from RR cells when compared to cells treated with PBS as a control, and a significant 1.5 fold increase ($p \leq 0.00001$) when treated with 100 µg/mL of EVs when compared to cells treated with PBS as a control (Figure 4.4 C).

Data showed that analyses of the MDA-MB-231 RR (Figure 4.4 D) cancer cell line had a significant 1.4 fold increase in colonies formed ($p \leq 0.00001$) when treated with 50 µg/mL and 100 µg/mL of EVs derived from RR cancer cells when compared to cells treated with PBS as a control. This dose was chosen as this is within the range used in literature when studying the effects of EVs derived from breast cancer cells (Kang *et al.,* 2019; Kia *et al.,* 2019; Wang *et al*., 2019). The colony formation assay showed cell treatment with both 50 µg/mL and 100 µg/mL of EVs equally increased colony formation; therefore, a concentration of 50 µg/mL was used in further experiments to conserve EV samples.

4.2.2 EVs derived from RR cells have a greater rate of uptake

After identifying that EVs derived from RR cancer cells can increase cell viability and colony forming ability (shown in section 4.2.1), this project aimed to identify if this could be attributed to selective uptake of EVs derived from RR cancer cells compared to EVs from nonRR cancer cells. Hazawa *et al.,* (2014) identified that there was selective uptake of EVs derived from irradiated cells, but this was only tested in cancer cells that received 8 Gy of irradiation. To identify if EVs derived from RR cancer cells are selectively taken up by both non-RR and RR cancer cells, an EV uptake assay was developed whereby cancer cells were stained with Hoechst stain to stain the nucleus and EVs were stained with DiI stain at a 1 in 200 dilution as recommended by manufacturer's instructions to stain outer membrane of EVs. Trial

runs were performed and optimised in collaboration with Dr. Anna Raper and Robert Flemming at the Roslin Bioimaging facility to optimise staining by minimising background signal of Hoescht and DiI concentrations. This was done by microscopy and flow cytometry to confirm cell numbers needed and optimal dye concentrations to be used (outlined in section 2.2.13). Cells were incubated with EVs for 45 minutes and cell uptake was calculated by flow cytometry analysis and quantification in FlowJo (Figure 4.5).

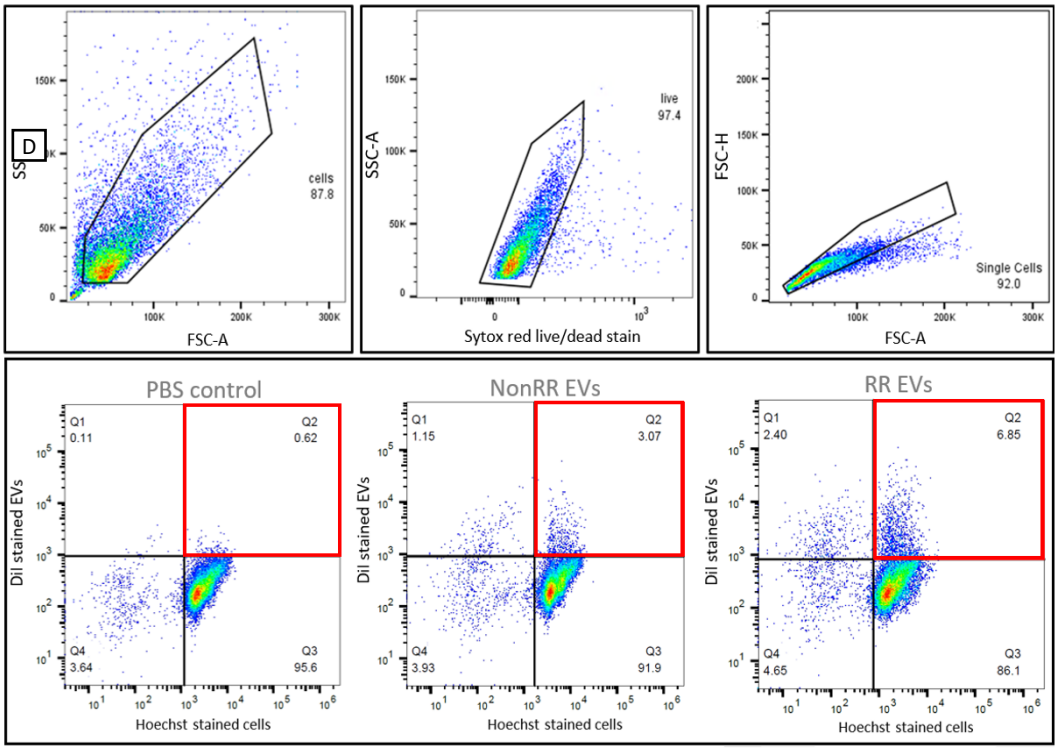


Figure 4.5 Flow cytometry workflow to quantify EV uptake. *Before running on the Fortessa X20 PBS was added to ensure a final volume of 500 µL* ***A)*** *Ten thousand events that were counted as cells were gated to remove background debris* ***B)*** *Dead cells were removed from the analyses by the addition of Sytox red which stains dead cells, allowing the gating of live cells* ***C)*** *Out of live cells, single cells were gated to prevent doublets from being analysed* ***D)*** *Hoechst stained cells plotted against DiI used to stain EVs to determine uptake of EVs by measuring the median fluorescence intensity (Q2-quadrant highlighted red). Representative images show REM134 cells incubated with PBS added as a control, 100 µg/mL NonRR REM134 EVs, and the addition of 100 µg/mL REM134 RR EVs. Analyses were performed in FlowJo software.*

The Q2 value (uptake of EVs) for each cell line depicts the median fluorescence intensity. Analyses showed very little background signal for samples with PBS stained with DiI. To ensure direct uptake and to account for residual DiI stain on the outer membrane, several wash steps were performed as outlined in Chapter 2.3.8

and median fluorescence intensity (MFI) data normalised to cells treated with PBS control. The MFI values from the Q2 quadrants (Figure 4.5 D) was analysed to observe any potential differences in uptake of EVs derived from nonRR cancer cells and RR cancer cells (Figure 4.6).

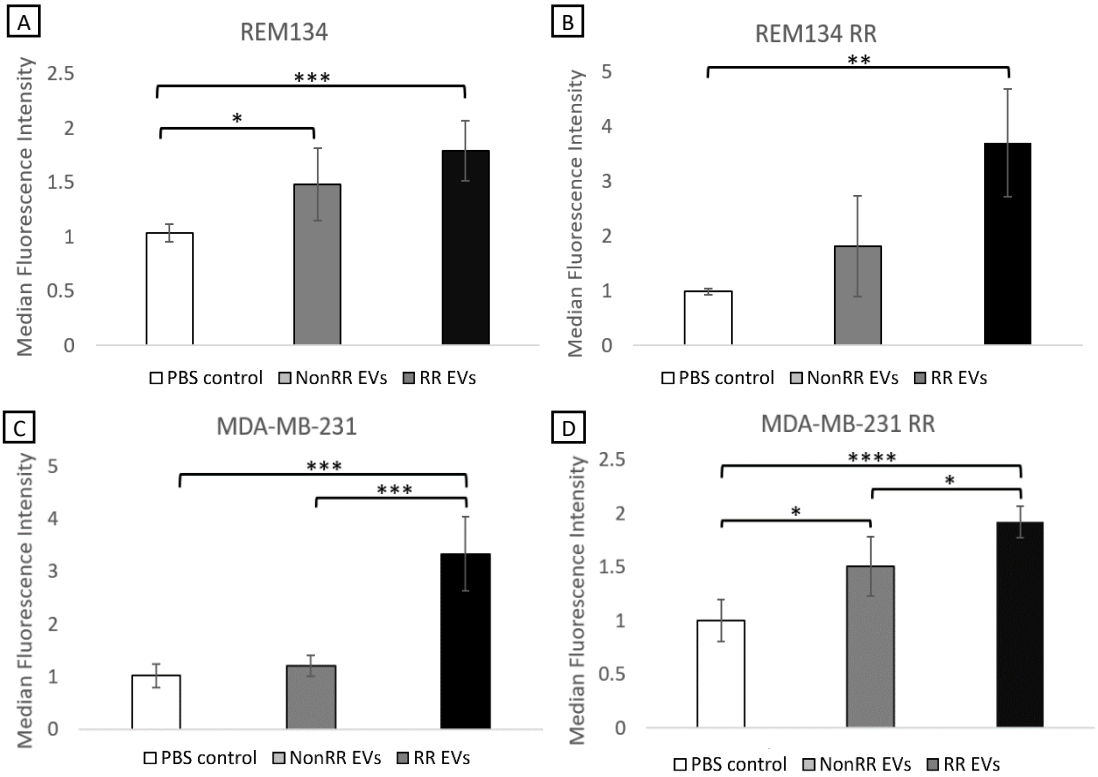


Figure 4.6 EVs derived from REM134 RR and MDA-MB-231 RR cells are more readily taken up by both nonRR and RR cancer cells*. Cells were stained with Hoechst stain and EVs were stained with DiI to quantify EV uptake per live single cell. EVs were incubated with cells at 37°C for 45 minutes before analysis by flow cytometry.* ***A)*** *REM134* ***B)*** *REM134 RR* ***C)*** *MDA-MB-231* ***D)*** *MDA-MB-231 RR. Data shows median uptake of EVs (DiI), technical replicates n=5 were averaged normalised to cells treated with PBS as a control to remove background signal. Error bars indicate ±SE of the median, statistical significance was analysed by a two tailed students' t-test. * p ≤ 0.05, ** p ≤ 0.01; *** p ≤ 0.001, **** p ≤ 0.00001.*

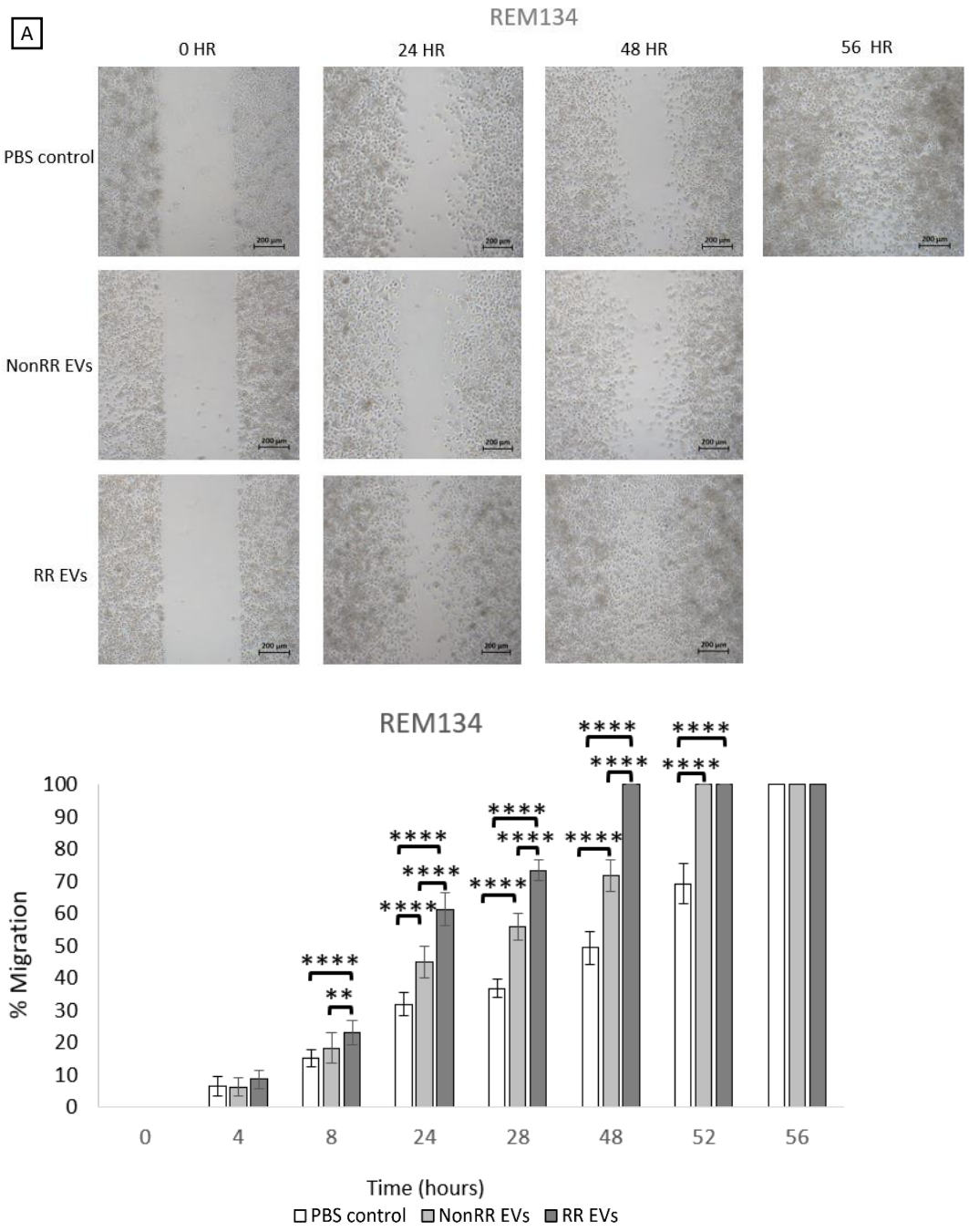
Data showed there was a higher rate of uptake of EVs derived from RR cell lines when compared to cells treated with PBS as a controls in all cell lines used (Figure 4.6), with variability seen between the significance of uptake when comparing EVs derived from cells treated with PBS as a control and nonRR cancer cells. There was also variability in significance between uptake of EVs derived from nonRR cancer cells and RR cancer cells. When comparing between human and canine cell lines, there was a two-fold increase ($p<0.0001$) between the uptake of EVs derived from RR cells between the REM134 cell line compared to cells treated with PBS as a

control (Figure 4.6 A), compared to almost four-fold increase ($p<0.0001$) in uptake in REM134 RR cells (Figure 4.6 B). However, there was a greater uptake of EVs in the nonRR human cancer cell line (Figure 4.6 C) than the MDA-MB-231 RR cell line (Figure 4.6 D), with there being a two-fold increase in uptake of EVs compared to cells treated with PBS as a control in the MDA-MB-231 RR cell line (Figure 4.6 D), and there was almost a four-fold increase ($p<0.01$) in EV uptake when compared to the cells treated with PBS as a control for the MDA-MB-231 cell line (Figure 4.6 C).

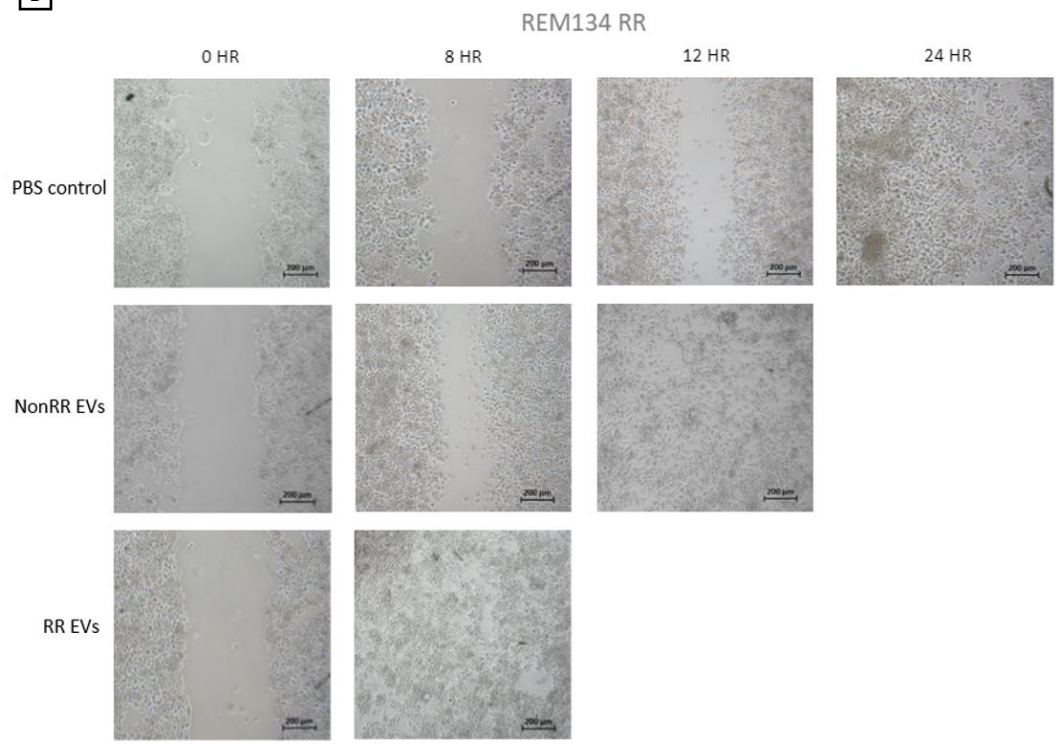
4.2.3 EVs derived from RR cells can increase the rate of migration of recipient breast cancer cells

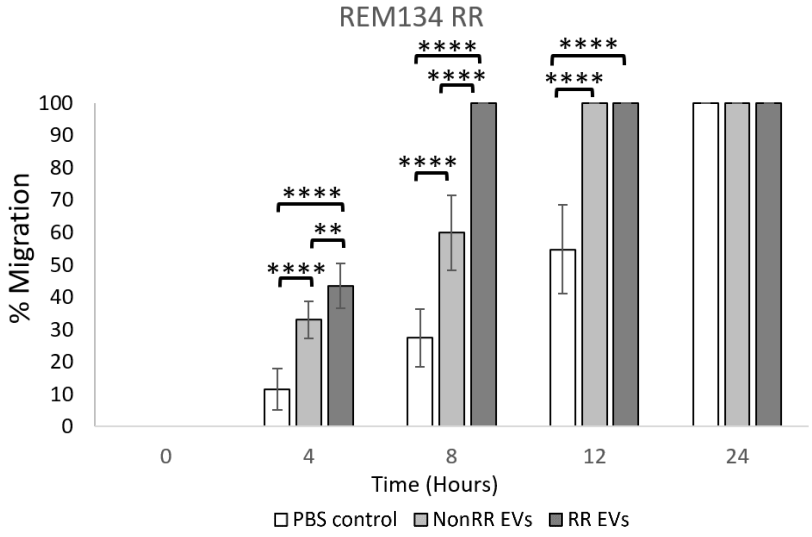
This project found that EVs derived from RR cancer cells could increase the cell viability and colony formation of nonRR and RR recipient cells. The few studies analysing the effect of EVs on migration such as Mutschelknaus *et al.,* (2017) found that EVs derived from RR cancer cells can increase the migration rate of nonRR recipient cells. This experiment aimed to compare effects on breast cancer cell migration rates by EVs from nonRR (REM134 and MDA-MB-231) cells and RR (REM134 RR and MDA-MB-231 RR) cells on both cell types – nonRR and RR cancer cells which appears to have been overlooked in the literature. Wound healing assays work on the principle of creating a measurable wound in a layer of confluent cells and measuring the rate of closure of the wound to assess the rate of breast cancer cell migration of the cells.

Cells were pre-treated with PBS as a control, EVs derived from nonRR cell lines, or EVs derived from RR cell lines (EV concentration of 50 µg/mL) for 24 hours, with canine EVs being added on to canine cancer cells and human EVs being added to human cancer cells. Cells were then seeded in the ibidi system and grown until confluent (approximately 24 hours) before making the wound by removing the ibidi insert. The results showed that EVs derived from RR cells could significantly increase the rate of migration of all recipient breast cancer cells (Figure 4.7).

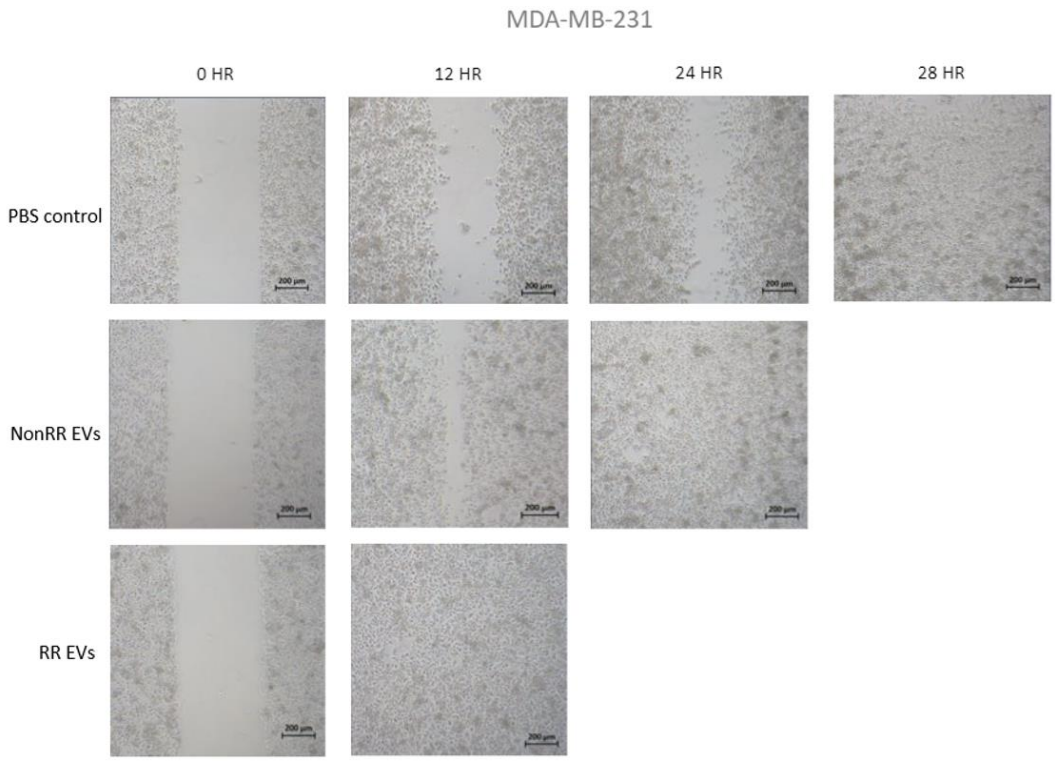

A
REM134
0 HR
24 HR
48 HR
56 HR
PBS control
NonRR EVs
RR EVs
REM134
% Migration
Time (hours)
PBS control
NonRR EVs
RR EVs

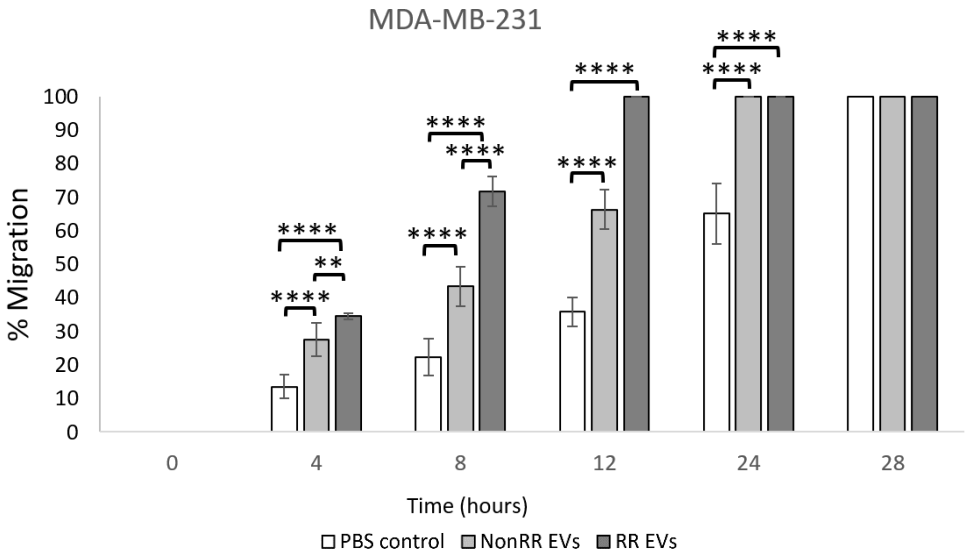
B


REM134 RR
0 HR
8 HR
12 HR
24 HR
PBS control
NonRR EVs
RR EVs


REM134 RR
% Migration
100
90
80
70
60
50
40
30
20
10
0
****
**
****
****
****
****
****
0
4
8
12
24
Time (Hours)
PBS control
NonRR EVs
RR EVs

C


MDA-MB-231
0 HR
12 HR
24 HR
28 HR
PBS control
NonRR EVs
RR EVs


MDA-MB-231
% Migration
100
90
80
70
60
50
40
30
20
10
0
****
**
0
4
8
12
24
28
Time (hours)
PBS control
NonRR EVs
RR EVs

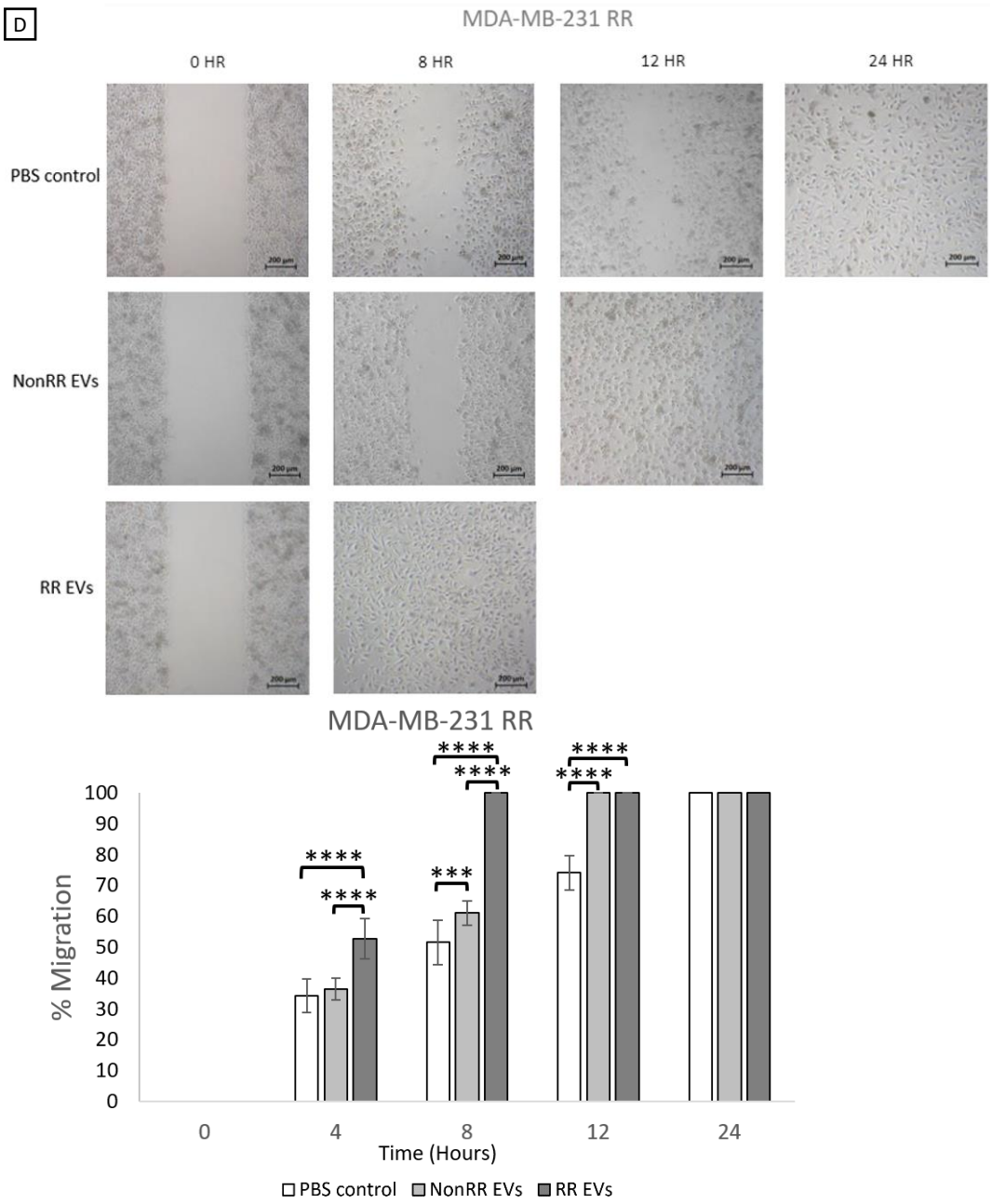


Figure 4.7 EVs derived from REM134 RR and MDA-MB-231 RR cancer cells increase the migration rate of all recipient cells. *Cells* ***A)*** *REM134* ***B)*** *REM134 RR* ***C)*** *MDA-MB-231* ***D)*** *MDA-MB-231 RR were incubated with 50 µg/mL of EVs. Canine EVs were added to canine cancer cells and human EVs were added to human cancer cells, in a 6 well plate for 24 hours and then seeded in 1 mL of EV-depleted media in the ibidi wells. After reaching confluency, the insert was removed. n=3 technical repeats. Percent migration was calculated (100 (A-B)/A where A is the width measured at 0 hr and B is the width of the cell wound after). Data shows % Migration ± %SD. statistical significance was analysed by a two tailed students' t-test. ** p ≤ 0.01; *** p ≤ 0.001, **** p ≤ 0.00001*

When comparing the migration rate of untreated cells, REM134 RR cells incubated with PBS alone (vehicle control) had a higher migration rate, with the wound closing within 24 hours (Figure 4.7 B), compared to REM134 cells incubated with PBS alone, closing the wound within 56 hours (Figure 4.7 A). When comparing the human cell lines: the MDA-MB-231 RR cell line closed of the wound at 24 hours (Figure 4.7 D), compared to the MDA-MB-231 cell line, which closed the wound at 28 hours (Figure 4.7 C). This shows that the RR cell lines both had a higher migration rate when compared to their nonRR counterparts.

It was found that EVs from nonRR cancer cells could significantly increase migration ($p<0.00001$) when compared to cells treated with PBS for all time points apart from REM134 at 4 hour and 8 hour time point, and MDA-MB-231 RR at the 4 hour time point. All results considered, it appeared EVs from nonRR cells could increase the rate of migration in nonRR and RR cell lines.

REM134 RR cells treated with EVs derived from RR cells had a closure of the wound at 8 hours, compared to 12 hours when treated with EVs derived from nonRR cells, and 24 hours for cells treated with PBS (Figure 4.7 B). All cells that were treated with EVs derived from RR cell lines had an increased rate of migration compared to cells treated with PBS and EVs from nonRR cells. The closure of the wound for REM134 occurred at 48 hours when treated with EVs derived from RR cells, 52 hours when treated with EVs when treated with EVs derived from nonRR cells, and at 56 hours for the cells treated with PBS (Figure 4.7 A). The same trend was seen in the MDA-MB-231 cell line. Treatment of 4.5×10^5 cells with EVs derived from RR cell lines resulting in wound closure at 12 hours, compared to 24 hours for EVs derived from nonRR cells, and 28 hours for cells treated with PBS (Figure 4.7 C). The addition of EVs derived from RR cancer cells to MDA-MB-231 RR cells resulted in closure of the wound at 8 hours, and EVs derived from nonRR cell type resulted in wound closure

at 12 hours. This means that EVs derived from RR cells can increase the migration rate of all recipient cells.

To summarise, it was found the RR cells migrate faster than the nonRR cells when comparing untreated (cells treated with PBS as a control). The addition of EVs derived from nonRR cells could increase the migration rate of all recipient cells when compared to cells treated with PBS, and the addition of the EVs from RR cancer cells could further increased the rate of migration in recipient cells when compared to treatment with EVs from nonRR cells. Therefore, it appears that EVs derived from REM134 RR and MDA-MB-231 RR can increase migration rates in all recipient cells, and an increase in migration rate can be associated with the acquisition of a radioresistant phenotype (Mutchkelnaus *et al*., 2016).

4.2.4 EVs derived from RR cells can increase the chemoresistance of all naïve recipient cells and increase radioresistance of recipient cells

Chemotherapy is a primary treatment for breast cancer patients, with Doxorubicin being one of the most common chemotherapeutics used in human and veterinary medicine (Nicoletto and Ofner, 2022; Turna *et al.,* 2022). Doxorubicin is typically infused intravenously and due to pharmacokinetics drops from 5 – 1 µM within two hours of administration but at intra-tumoural concentrations of 0.1 – 0.01 µM for several days (Creasy *et al.,* 1976; Pritchard *et al.,* 2012). Therefore, Doxorubicin concentrations for chemosensitivity assay were chosen to include these clinically relevant doses of 0.1 - 1 µM. This project aimed to determine the role, if any, of EVs derived from RR cancer cells on the survivability of recipient cells following chemotherapy treatment with Doxorubicin. This was achieved by using a Cell titre glo assay which quantifies ATP to assess cell viability. Cells were seeded cells in 96 well plates and incubated with EVs for 24 hours, Doxorubicin was added 12 hours after the addition of EVs, and cell viability read 72 hours post-Doxorubicin treatment (Figure 4.8).

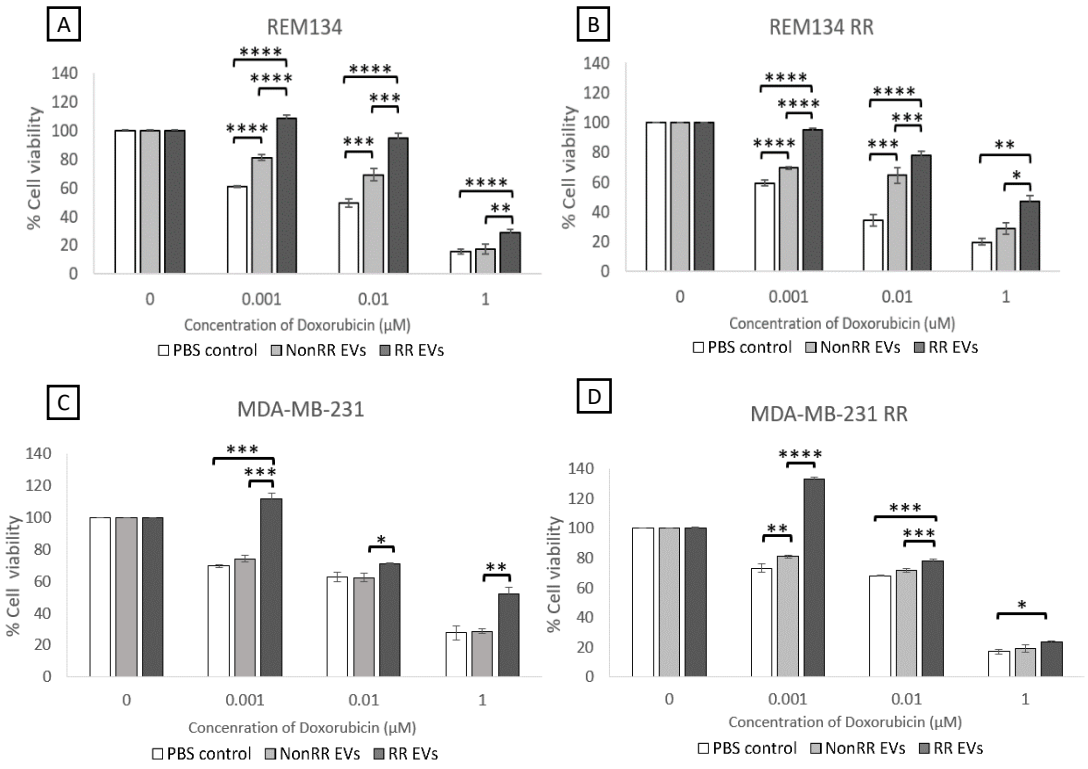


Figure 4.8 EVs derived from REM134 RR and MDA-MB-231 RR cells increased chemoresistance in recipient cells. *Cells were incubated with 50 µg/mL of EVs for 24 hours, with canine EVs added to canine cell lines, and human EVs added to the human cell lines. Cells were treated with Doxorubicin at 0, 0.001, 0.01 and 1 µM with cells treated with PBS as a control. Cell viability was assessed 72 hours after Doxorubicin treatment.* ***A)*** *REM134* ***B)*** *REM134 RR* ***C)*** *MDA-MB-231* ***D)*** *MDA-MB-231 RR. n=3 technical repeats. Percentage viability was calculated by the following calculation (treatment/control) x 100. Data shows mean cell viability ±SD. Statistical significance was analysed by a two tailed students' t-test *p≤ 0.05 ** p ≤ 0.01; *** p ≤ 0.001, **** p ≤ 0.00001*

When comparing the cell viability of untreated cells (Cells treated with PBS as a control) between the nonRR and RR cell lines, it was noted the cell viability decreased with increasing concentrations of Doxorubicin. This could mean the RR cell lines do not have an inherent resistance to chemotherapy when not treated with EVs.

There was a significant increase in cell viability ($p<0.001$ – $p<0.00001$) between the cells treated with PBS and treatment with EVs derived from REM134 cells in the REM134 (Figure 4.8 A) and the REM134 RR (Figure 4.8 B) cell lines. EVs from RR cell

lines significantly increased the percentage viability in both nonRR and RR recipient cell lines when compared to cells treated with PBS as a control (Figure 4.8). There was a highly significant increase in recipient cell viability seen at doses of 0.001, 0.01 µM Doxorubicin when REM134 and REM134 RR cells were treated with EVs derived from REM134 RR cells compared to cells treated with PBS ($p<0.0001$) (Figure 4.8 A, B).

There was also a significant increase in cell viability ($p<0.05$ – $p<0.00001$) seen in the MDA-MB-231 and MDA-MB-231 RR cell lines (Figure 4.8 C, D) when they were treated with EVs derived from MDA-MB-231 RR cell lines when compared to EVs derived from the nonRR cell line.

These results show that with no EV treatment, chemotherapy treatment resulted in a decrease in cell viability, but the addition of EVs from REM134 RR and MDA-MB-231 RR cancer cells could significantly increase cell viability after treatment with Doxorubicin when compared to PBS treated and treatment with EVs derived from nonRR cells.

4.2.5 EVs derived from RR breast cancer cells can increase radioresistance of naïve and radioresistant recipient cancer cells

The effects of EVs derived from RR cells on recipient cells were analysed in the context of radiotherapy. The hypothesis of this project was that EVs derived from RR breast cancer cells can confer a radioresistant phenotype to recipient nonRR breast cancer cells; therefore, the aim of this experiment was to identify if nonRR breast cancer cells can survive doses of irradiation that would normally be lethal to breast cancer cells after being incubated with EVs from RR breast cancer cells. Fractionated radiotherapy is used in curative cancer treatment whereby small doses from 2 – 4 Gy are given over three weeks to a cumulative total of 30-40 Gy (Kim *et al.,* 2021). Therefore, a colony formation assay was designed whereby breast cancer cells were treated with PBS or EVs (50 µg/mL) and cells were seeded at very low densities to

result in single cell populations and cells were immediately irradiated at clinically relevant doses of 2.5 Gy, 5 Gy or sham irradiated at 0 Gy as a control. Cells were left for 10 days, and colonies were counted to determine how many colonies could grow from the seeded cells that received irradiation.

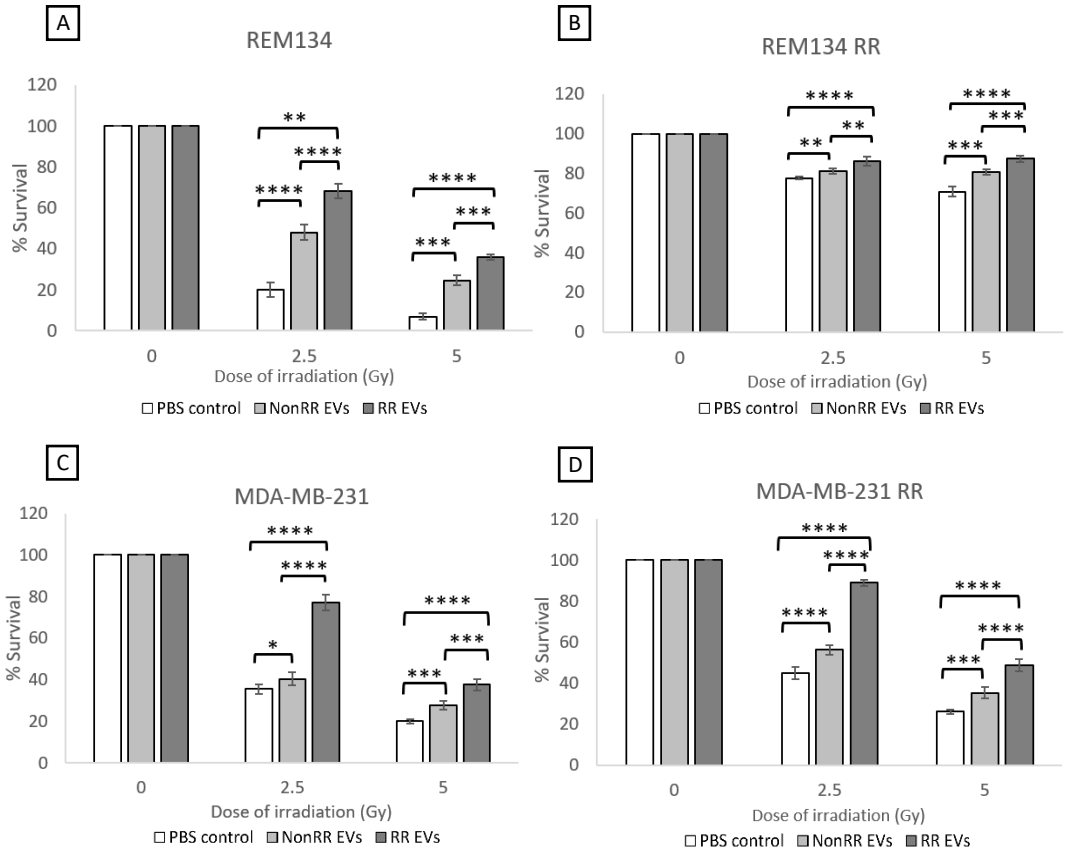


Figure 4.9 EVs derived from REM134 RR and MDA-MB-231 RR cells can increase recipient cell survival following irradiation. *Cells were seeded in a colony formation assay* ***A)*** *REM134* ***B)*** *REM134 RR* ***C)*** *MDA-MB-231* ***D)*** *MDA-MB-231 RR incubated with 50 µg/mL of EVs derived from corresponding nonRR or RR cell lines and cells treated with PBS as a control for 24 hours and irradiated at stated doses of Gy. n=3 technical repeats. Percentage viability was calculated by the following calculation (treatment/control) x 100. Data shown is % Survival ± %SD. Statistical significance was analysed by a two tailed students' t-test* p ≤ 0.05, ** p ≤ 0.01; *** p ≤ 0.001, **** p ≤ 0.00001*

EVs derived from RR breast cancer cells could significantly increase the survival in REM134 (20% at 2.5 Gy, 10% at 5 Gy) and REM134 RR breast cancer cells (80% at 2.5 Gy, and 70% at 5 Gy) when compared to cells treated with PBS as a control (no EVs added)(Figure 4.9 A, B). It was noted the MDA-MB-231 breast cancer cell line had a higher basal percentage survival compared to the REM134 cell line, with there being ~35% survival in the MDA-MB-231 cell line when PBS was added as a control and

cells were treated with 2.5 Gy, compared to ~20% in the REM134 cell line. The untreated MDA-MB-231 cells (Figure 4.9 C) had a lower percentage survival (~35% at 2.5 Gy, 20% at 5 Gy) when compared to the MDA-MB-231 RR cancer cell line (45% at 2.5 Gy, 30% at 5 Gy) (Figure 4.9 D).

Cells treated with EVs from nonRR cells resulted in significant percentage cell survival ($p<0.05$-$p<0.00001$) when added on to all cell lines. There was a further increase in percentage survival in all cell lines when EVs from RR cell lines were added, especially in the REM134 RR cell line when treated with EVs derived from RR cells to ~90% survival at 2.5 Gy and 5 Gy (Figure 4.9 B). There was also a significant increase in percentage survival ($p<0.0001$) from ~10% in cells treated with PBS, to ~40% survival at 5 Gy in the REM134 cell line following treatment with EVs derived from RR cells (Figure 4.9 A).

There was also a stark increase in colony formation in the MDA-MB-231 and MDA-MB-231 RR cell lines following the addition of EVs derived from RR cell lines ($p<0.00001$) at all doses of Gy (Figure 4.9 C, D). The addition of EVs derived from MDA-MB-231 RR cells significantly increased colony formation in the MDA-MB-231 cell line compared to cells treated with PBS as a control at 2.5 Gy and 5 Gy (Figure 4.9 C; $p<0.00001$). The EVs derived from MDA-MB-231 RR cells could also significantly increase colony formation following 2.5 Gy and 5 Gy (Figure 4.9 D; $p<0.00001$).

Likewise, at the dose of 5 Gy, the MDA-MB-231 cell line (Figure 4.9 C) had ~20% survival compared to ~5% survival in the REM134 cell line (Figure 4.9 A). This indicates the established RR cell lines were radioresistant due to having a higher percentage survival when compared to their nonRR counterparts when treated with cells treated with PBS as a control, and the transfer of EVs from RR cell lines can induce radioresistance in recipient cells.

4.2.6 EVs derived from RR cells can increase chemotherapy resistance in recipient breast cancer stem cells

The CSC population is a subset of the bulk tumour with an inherent resistance to adverse environmental changes and cancer therapies. After identifying that EVs from RR breast cancer cells appear to confer a radioresistant phenotype, the aim of this project was to determine if this could be due to effects on the breast CSC population. To determine the effect of EVs on the proliferation and response to chemotherapy of breast CSC populations, a cell viability assay was performed whereby breast CSCs were pre-incubated with corresponding EVs derived from nonRR or RR cells for 24 hours.

For chemosensitivity assays, breast CSCs were seeded as single-cells at 500 cells per well in a 96 well plate, incubated for 24 hours at 37°C then treated with EVs. Doxorubicin was added 12 hours later and cells were incubated for a further 72 hours then cell viability was calculated with the use of the CellTiter-Glo® 2.0 assay to determine cell viability after treatment. EVs derived from RR cells can increase the resistance of all recipient CSCs following treatment with chemotherapy and the addition of nonRR EVs significantly increased cell viability in the MDA-MB-231 CSCs at all doses of Doxorubicin (Figure 4.9 C). However, the addition of nonRR EVs did not significantly increase the cell viability for all doses of Doxorubicin in the breast CSCs when compared to cells treated with PBS. It was also found that addition of EVs from RR cells could significantly increase recipient cell viability ($p<0.001$-$p<0.00001$) when compared to cells treated with PBS. Similarly, the addition of EVs from RR cells

could significantly increase recipient cell viability ($p<0.05$-$p<0.00001$) when compared to the addition of EVs derived from nonRR cells (Figure 4.9).

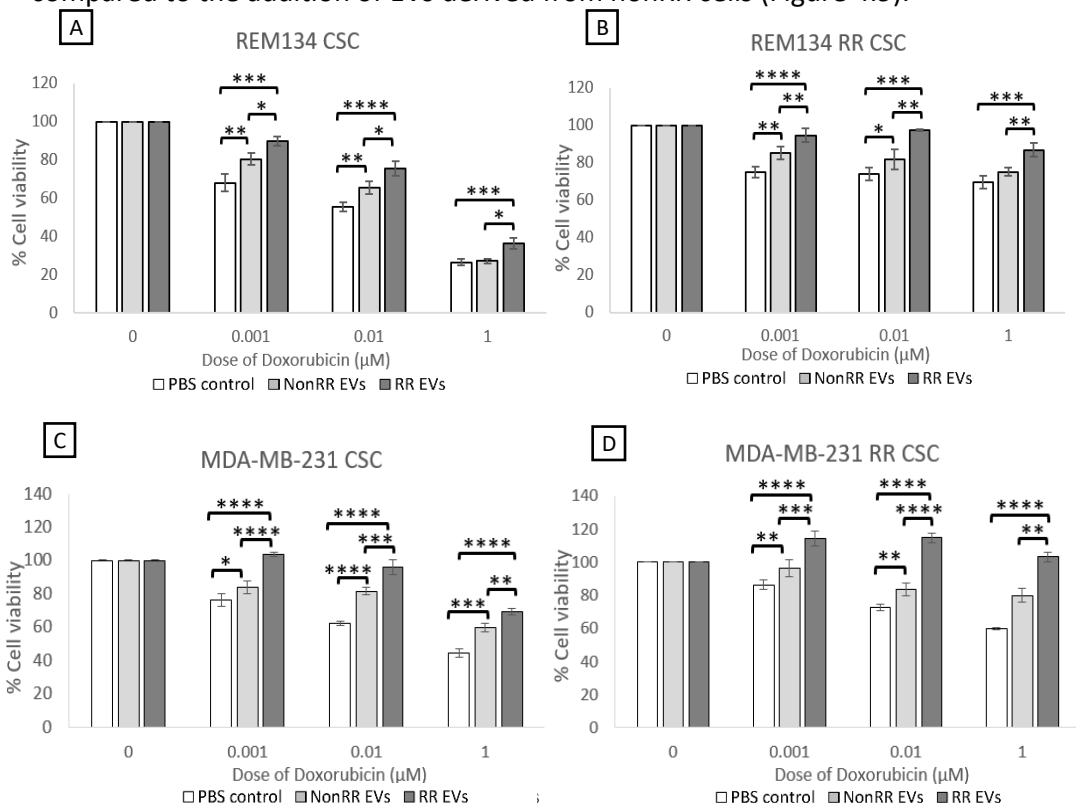


Figure 4.10 EVs derived from REM134 RR and MDA-MB-231 RR breast cancer cells increase the cell viability of chemotherapy naïve breast CSCs. *CSCs were derived from the following cells **A)** REM134 CSCs **B)** REM134 RR **C)** MDA-MB-231 **D)** MDA-MB-231 RR and incubated with EVs from corresponding nonRR or RR cancer cells for 24 hours before being treated with the stated doses of Doxorubicin. Cells were treated with PBS as a control. Chemosensitivity was determined after 5 days. n=3 technical repeats. Percentage viability was calculated by the following calculation (treatment/control) x 100. Data shows % cell viability ± %SD Statistical significance was analysed by a two tailed students' t-test. * $p \leq 0.05$, ** $p \leq 0.01$; *** $p \leq 0.001$, **** $p \leq 0.00001$*

It was noted that observing the baseline level of resistance in the CSCs (cells treated with PBS as a control) that the REM134 RR CSC population were resistant to Doxorubicin chemotherapy treatment with a cell viability of ~70% in the cells treated with a dose of 1 µM Doxorubicin (Figure 4.10 B) compared to the REM134 CSC population which had ~20% cell viability at 1 µM Doxorubicin, compared to cells treated with PBS as a control (Figure 4.10 A). Likewise, MDA-MB-231 RR CSCs had a cell viability of ~60% at 1 µM Doxorubicin (Figure 4.10 D) compared to ~40% viability in the MDA-MB-231 CSCs at 1 µM Doxorubicin (Figure 4.10 C).

All cell lines used in these experiments were chemotherapy resistant naïve cells, this considered, it appears chemotherapy resistance can be transferred to both human and canine breast cancer cells via EVs from their corresponding RR cancer cells.

4.2.7 EVs derived from RR cells can increase radiotherapy resistance in recipient breast cancer stem cells

After discovering that EVs derived from RR cells can increase recipient cell chemoresistance, experiments were designed to analyse the effect of EVs from REM134 RR and MDA-MB-231 RR cells on recipient cell radioresistance. EVs were incubated with breast CSCs for 24 hours, and then cells were seeded as single cells at a low density and then immediately irradiated at 0, 2.5 or 5 Gy (Figure 4.11).

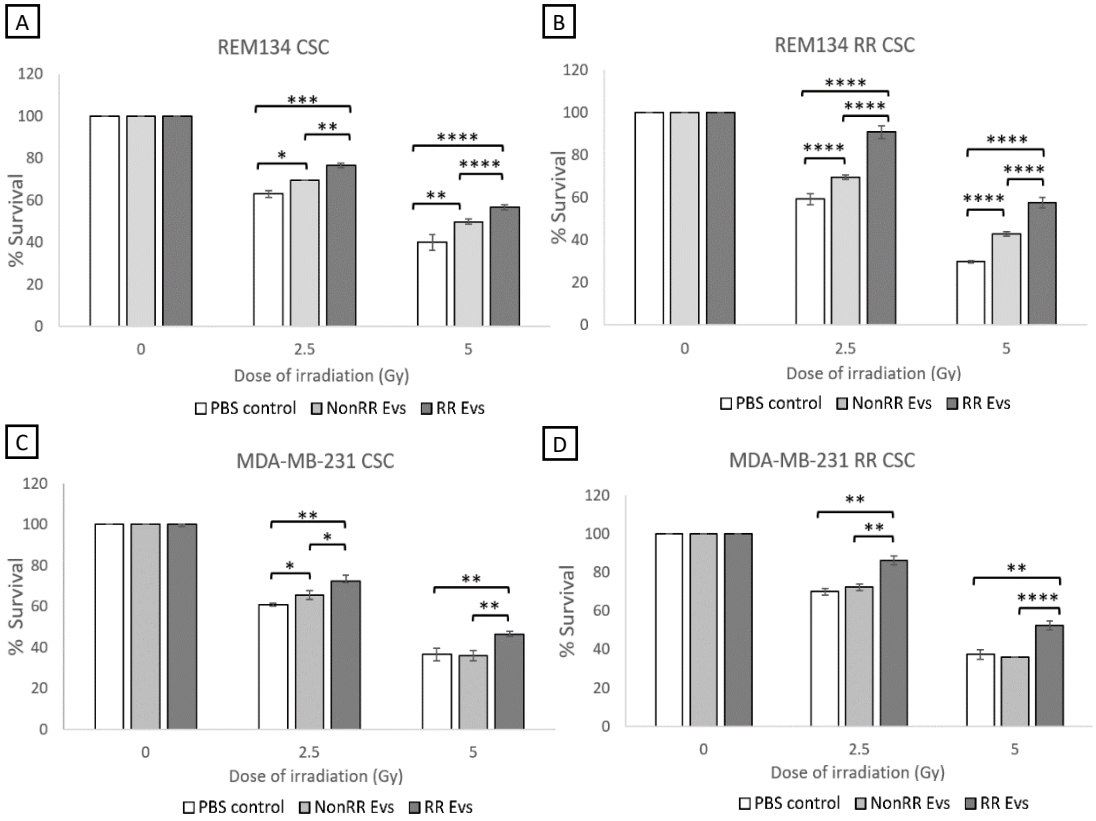


Figure 4.11 EVs derived from MDA-MB-231 RR and REM134 RR cells increase the breast CSC survival following irradiation. *The colony forming ability of breast CSCs from* ***A)*** *REM134* ***B)*** *REM134 RR* ***C)*** *MDA-MB-231* ***D)*** *MDA-MB-231 RR. Breast CSCs were pre-incubated with 50 µg/mL of EVs derived from corresponding nonRR or RR cell lines and cells treated with PBS as a control for 24 hours. n=3 technical repeats. Means were normalised to cells sham irradiated at 0 Gy. Percentage viability was calculated by the following calculation (treatment/control) x 100. Data shown is % Survival ± %SD of the mean. Statistical significance was analysed by a two tailed students' t-test * p ≤ 0.05, ** p ≤ 0.01; *** p ≤ 0.001, **** p ≤ 0.00001.*

When comparing the untreated cells, the percentage survival for all breast CSCs was higher than non-CSC populations in breast CSCs treated with PBS control, with between 60-70% at 2.5 Gy and 40-45% at 5 Gy. The addition of EVs from nonRR cells resulted in a significant increase in survival in the REM134 CSCs ($p<0.05$ – $p<0.01$) when compared to cells treated with PBS (Figure 4.11 A), and the REM134 RR CSCs ($p<0.00001$) when compared to cells treated with PBS (Figure 4.11 B). However, the addition of EVs derived from nonRR cells only resulted in a significant increase in survival in the MDA-MB-231 CSCs ($p<0.05$) when compared to cells treated with PBS (Figure 4.11 C), but the addition of EVs derived from nonRR cells did not result in a significant increase in cell survival in any other MDA-MB-231 CSC or MDA-MB-231 RR CSC results (Figure 4.11 D).

It was found that EVs from the RR cell line resulted in a significant increase in all recipient cells survival following irradiation. In the REM134 and the REM134 RR CSCs (Figure 4.11 A, B), treatment with EVs derived from RR cells was significantly increased when compared to cells treated with PBS as a control ($p<0.00001$). In the REM134 RR CSCs addition of EVs derived from RR cells resulted in almost double the number of breast CSCs surviving irradiation at 5 Gy (from ~30% survival to ~60% survival) when compared to cells treated with PBS as a control (Figure 4.11 B).

The same effect was seen in the MDA-MB-231 and MDA-MB-231 RR CSCs, with treatment of EVs from RR cells being significantly increased when compared to cells treated with PBS as a control ($p<0.01$) at both 2.5 Gy and 5 Gy (Figure 4.11 C, D). Likewise, in MDA-MB-231 CSCs the treatment with EVs from RR cells was significantly increased when compared to treatment with EVs from nonRR cells at both 2.5 Gy ($p<0.05$) and 5 Gy ($p<0.001$; Figure 4.11 C). Similarly, treatment of the MDA-MB-231 RR breast CSCs with EVs from MDA-MB-231 RR cells could significantly increase colony formation following irradiation when compared to treatment with Evs from nonRR cells at both 2.5 Gy ($p<0.001$) and 5 Gy ($p<0.00001$; Figure 4.11 D).

To summarise, it was found that untreated breast CSCs had a similar baseline percentage survival, and EVs derived from RR breast cancer cells lines could significantly increase the chemoresistance and radioresistance of all recipient breast CSCs when compared to breast CSCs treated with PBS control and breast CSCs treated with EVs derived from nonRR cells.

4.2.8 EVs derived from RR cells can increase the size and number of tumourspheres formed

CSCs are present as a subpopulation in tumours that can self-renew and are highly tolerant to environmental changes and cancer therapies when compared to cancer cells within the same population (Pustovalova *et al.,* 2021). Following cancer treatment, CSCs remain and can result in cancer relapse due to growth and proliferation leading to a new cancer cell population (Liu *et al.,* 2021). To determine the effect of EVs from RR cells on CSC populations, a tumoursphere formation assay was performed to observe any effects on the size and number of tumourspheres formed. Adherent breast CSCs were pre-incubated with 50 µg/mL of EVs isolated from nonRR or RR cell lines for 24 hours. Breast CSCs were then seeded in N2 medium in low-attachment plates and growth factors added to stimulate the growth of 3D tumourspheres. The media used is nutrient deficient and does not sustain the growth of non-CSCs, resulting in enrichment of a breast CSC population as previously validated by Pang *et al.,* (2011). It was found that EVs derived from RR cells could increase the number of tumourspheres formed when compared to both cells treated with PBS as a control and EVs isolated from nonRR cells (Figure 4.12).

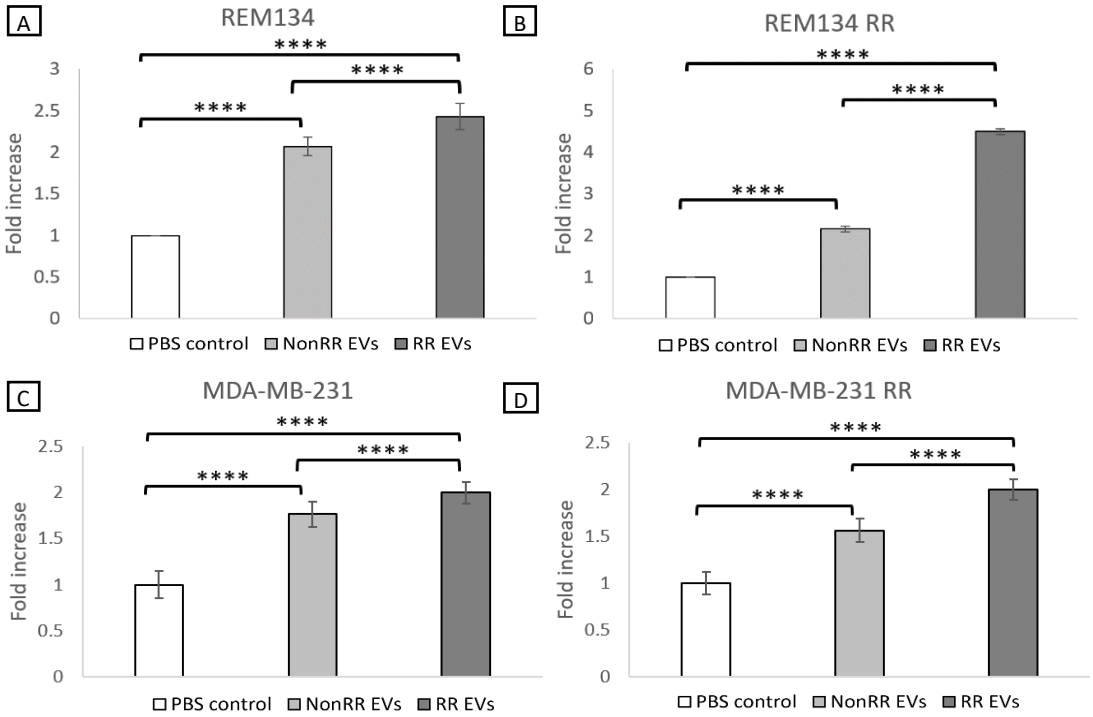
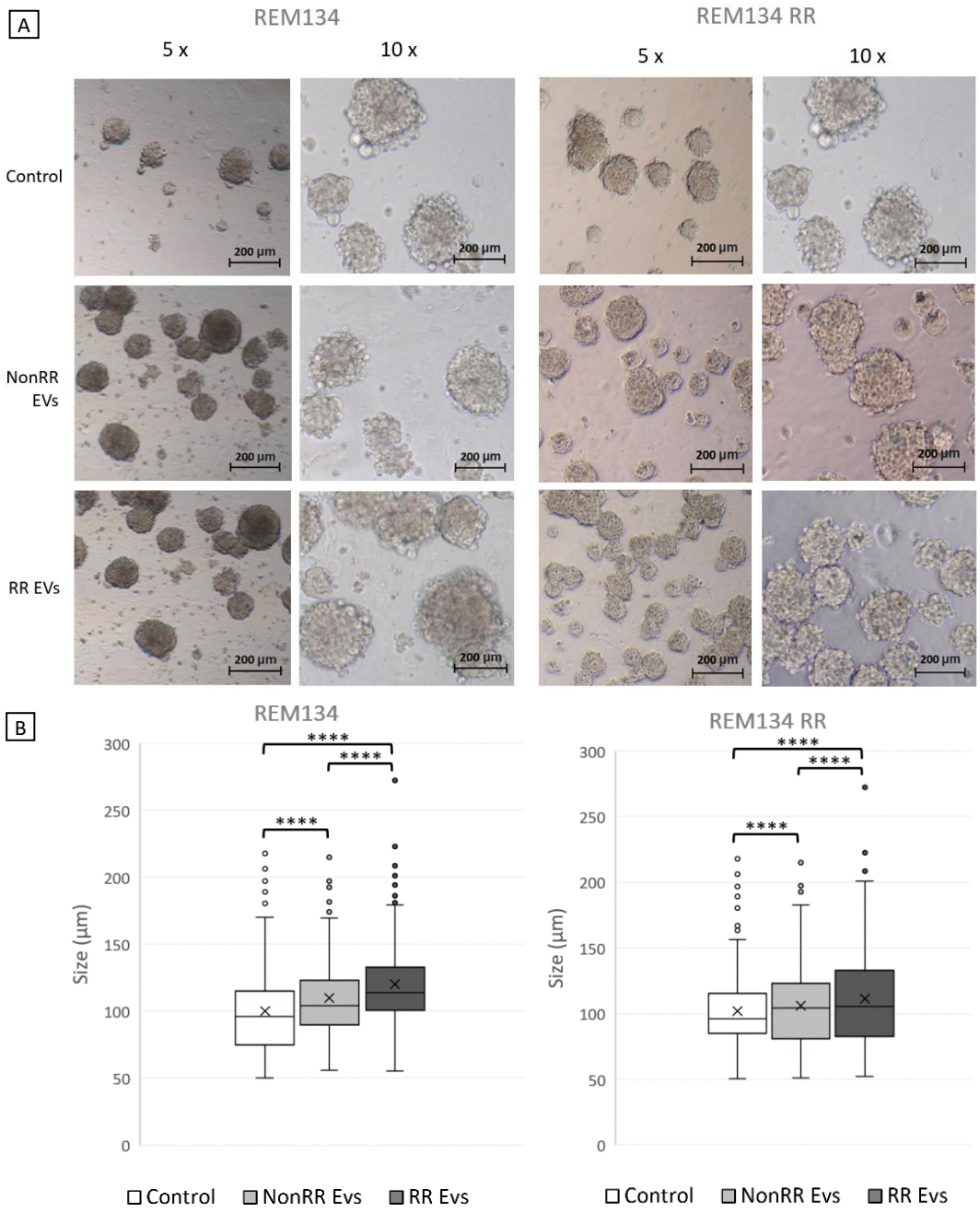


Figure 4.12 EVs derived from nonRR and RR cell line can increase the number of tumourspheres formed*. Breast CSCs derived from **A)** REM134 **B)** REM134 RR were grown for 7 days and counted, whereas **C)** MDA-MB-231 and **D)** MDA-MB-231 RR tumourspheres were grown for 17 days. Breast CSCs were pre-incubated with 50 µg/mL of EVs derived from nonRR or RR cell lines and cells treated with PBS as a control for 24 hours. n=3 technical repeats. Data were normalised to cells treated with PBS as a control. Data shows fold increase ±SD. Data normality was analysed via an Anderson-Darling normality test, statistical significance was analysed by a two tailed students' t-test.. **** $p \leq 0.00001$*

For all breast CSCs, the number of tumourspheres formed after addition of EVs derived from RR cells significantly increased ($p<0.00001$) when compared to cells treated with PBS as a control (Figure 4.12). Similarly, the number of tumourspheres formed after treatment with EVs from nonRR cells significantly increased ($p<0.00001$) when compared to cells treated with PBS as a control. There was a similar result seen with the addition of EVs derived from the nonRR cell lines in the REM134 and the REM134 RR CSCs, with a significant two-fold increase ($p<0.0001$) for both breast CSC populations (Figure 4.12 A, B). However, with the addition of EVs derived from the REM134 RR cell line, there was a fold increase of 2.5 ($p<0.00001$) seen in the REM134 tumoursphere population (Figure 4.12 A), compared to a fold

increase of 4.5 ($p<0.00001$) in the REM134 RR tumoursphere population when compared to cells treated with PBS control (Figure 4.12 B).

A very similar result was seen between the MDA-MB-231 and the MDA-MB-231 RR fold increase in tumoursphere population whereby the addition of EVs from nonRR cells resulted in a significant ~1.75 fold increase ($p<0.00001$) in the formation of MDA-MB-231 tumourspheres (Figure 4.12 C), and a significant 1.5 fold increase ($p<0.00001$) in the formation of MDA-MB-231 RR tumourspheres (Figure 4.12 D). Microscopy images of tumourspheres were taken (Figure 4.13 A) and measured (Figure 4.13 B). The untreated REM134 tumourspheres were smaller than the untreated REM134 RR tumourspheres. In the REM134 tumourspheres, the addition of the EVs derived from nonRR and RR cancer cells resulted in a significant increase ($p<0.00001$) in tumoursphere size when compared to the cells treated with PBS as a control. Likewise, REM134 RR tumoursphere formation assays showed that EVs derived from nonRR and RR cancer cells could significantly increase tumoursphere size ($p<0.00001$) when compared to cells treated with PBS as a control (Figure 4.13 B).



4.13 EVs derived from nonRR and RR REM134 and REM134 RR cancer cells significantly increased the size of the tumourspheres formed. *REM134 and REM134 RR breast CSCs were pre-incubated with 50 µg/mL of EVs derived from nonRR or RR cell lines and cells treated with PBS as a control for 24 hours. REM134 and REM134 RR spheres were grown in low-adherent plates for 5 days. n=3 technical repeats.* ***A)*** *Light microscopy images were taken of tumourspheres and microscopy images captured with a 5 x and 10 x objective. Scale bar shows 200 µm.* ***B)*** *Tumourspheres were measured in zen (blue edition) software. Size data were normalised to cells treated with PBS as a control. Data normality was analysed by an Anderson-Darling normality test and a Wilcoxon signed rank test was performed to determine statistical significance. Data shows median size of tumourspheres ±SD. **** $p \leq 0.00001$.*

It was noted that MDA-MB-231 RR tumourspheres appeared larger when comparing CSCs treated with PBS as a control (~90 µm) when compared to the MDA-MB-231 tumourspheres in the cells treated with PBS as a control (~60 µm). Results showed that EVs from nonRR cells could significantly increase tumoursphere size for all cell lines ($p<0.00001$) when compared to cells treated with PBS as a control (no EVs). The largest size increase was seen in the MDA-MB-231 cells, with a significant increase ($p<0.00001$) from ~ 60 µm to 100 µm (Figure 4.14 B). A similar result was seen when EVs from MDA-MB-231 RR cancer cells were added, with there being a significant increase ($p<0.00001$) when compared to cells treated with PBS as a control, and when compared to effect of EVs derived from nonRR cells (Figure 4.14 B). It was found the biggest increase in size was seen in the MDA-MB-231 tumourspheres when treated with EVs derived from RR cells, with a significant increase of a median of ~60 µm in the cells treated with PBS as a control, to ~130 µm ($p<0.00001$) when treated with EVs from RR cells (Figure 4.14 B). This means that EV content from nonRR and RR cancer cells can significantly increase the size of forming tumourspheres.

Individual tumourspheres appeared larger for all breast CSCs after treatment with EVs derived from RR cells. It was also noted that the MDA-MB-231 RR tumourspheres were not consistently spherical and had an irregular shape when compared to MDA-MB-231 tumourspheres (Figure 4.14 A).

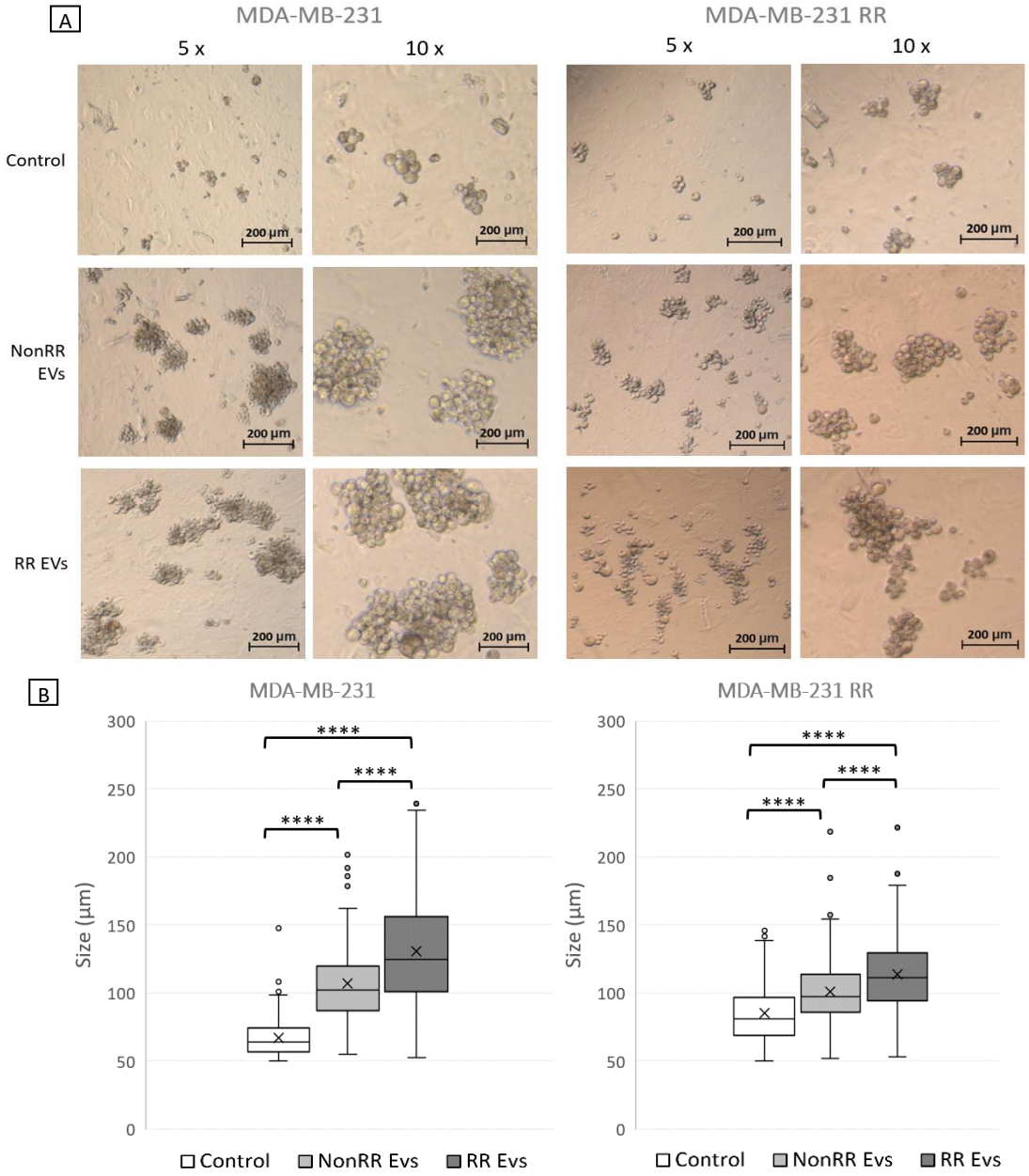


Figure 4.14 EVs derived from nonRR and RR MDA-MB-231 cancer cells significantly increased the size of the tumourspheres formed. *MDA-MB-231 and MDA-MB-231 RR breast CSCs were pre-incubated with 50 µg/mL of EVs derived from nonRR or RR cell lines and cells treated with PBS as a control for 24 hours. MDA-MB-231 and MDA-MB-231 RR spheres were grown in low-adherent plates for 17 days. n=3 technical repeats. A) Light microscopy images were taken of tumourspheres and microscopy images captured with a 5 x and 10 x objective. Scale bar shows 200 µm. B) Tumourspheres were measured in zen (blue edition) software. Size data were normalised to cells treated with PBS as a control. Data normality was analysed by an Anderson-Darling normality test and a Wilcoxon signed rank test was performed to determine statistical significance. Data shows median size of tumourpshere ±SD. **** $p \leq 0.00001$.*

These data indicate that EVs derived from REM134 RR and MDA-MB-231 RR cancer cells can increase size and number of tumourspheres formed by CSCs, which may contribute to the acquisition of a radioresistant phenotype.

4.3 Discussion

The development of radioresistance in human and veterinary medicine can lead to relapse and metastasis and eventually treatment failure (Liu *et al.,* 2020). There are studies showing the effects of EVs derived from cancer cells on their non-malignant counterparts (Zoon *et al.,* 2022); however, there are very few studies investigating the role of EVs derived from established RR cells on recipient cells (Abranmowicz *et al*., 2019). The hypothesis of this project is that EVs derived from RR breast cancer cells can confer a radioresistant phenotype to recipient breast cancer cells. The aims of this chapter were to determine if EVs from RR breast cancer cells could induce cellular changes associated with a radioresistant phenotype. The data showed that EVs derived from RR cells could increase the cell viability, colony forming ability, cell migration potential, chemoresistance and radioresistance in recipient cells including both non-CSC and breast CSC cell populations. Additionally, EVs derived from nonRR and RR cells were able to increase the size and number of tumourspheres formed.

Data showed that EVs from RR cancer cells can increase recipient cell viability and colony formation and are more readily taken up by recipient cells when compared to EVs derived from nonRR cells. However, data from the EV uptake assay showed that EVs derived from RR cell lines are more readily taken up by all recipient cells when compared to EVs derived from nonRR cancer cells (Figure 4.11). One potential explanation for this could be that cells that have received irradiation produce more EVs (Arscott *et al.,*2013), and irradiated cells take up EVs more readily (Mutschelknaus *et al.,* 2016). Therefore, this could explain the higher rate of RR cell uptake of EVs derived from RR cancer cells. However, in the nonRR cell lines, there was also an increase in uptake of EVs derived from RR cancer cell lines. Only a few

other studies have shown that EVs derived from cells that have been irradiated once have a higher rate of uptake by nonRR cells (Arscott *et al*., 2013). It has been proposed that in irradiated cells CD29/CD81 co-localise to increase the uptake of EVs in irradiated cells. Therefore, the nonRR cells may be taking up all EVs, but as the RR cells have an increased uptake, potentially with additional selective uptake, this may explain why the RR cell lines had an increased rate of EV uptake. It would be interesting to pursue this further, because if there is selective uptake of EVs only derived from RR cancer cells, the mechanisms or molecules involved could be novel anti-radioresistance targets. It would be useful to stain EVs from nonRR cancer cells with one colour fluorophore, and then EVs from RR cancer cells a different colour. Then add an anti-CD29 or anti-CD81 antibody to block the predicted interaction between CD29 and CD81 to confirm if the uptake of EVs from RR breast cancer cells is decreased. The assay performed could be similar to the one used in this project, but use a 96 well plate format to increase the number of repeats to create a clearer final dataset. In addition, the use of extra controls would prove beneficial to validate the results found in this project such as unstained EVs to detect background EV fluorescence. Further studies could also confirm uptake due to surface membrane interactions by "shaving" EVs with trypsin or commercial kits (Bhatta *et al.,* 2021). The uptake of EVs from nonRR and RR cancer cells could be quantified and compared to see if there is selective uptake of EVs derived from RR cancer cells.

Studies have shown that RR cells can migrate faster than nonRR cells (Gray *et al.,* 2019), with this potentially being attributed to the activation of the AKT pathway (Mutchkelnaus *et al.,* 2017) and it has been found that EVs from cells that received one dose of irradiation could increase migration in recipient cells (Arscott *et al.,* 2013). The cells used in this project were established RR cell lines, meaning their EV content may be altered upon acquiring an RR phenotype, and the transfer and uptake of these altered EVs resulted in the significant increase in the migration rate in recipient cells. The transfer of EVs is also associated with the acquisition of chemotherapy resistance, where cells can survive doses of chemotherapy that would be considered lethal. In a study by Zhao *et al.,* (2021) a human laryngeal

cisplatin resistant cell line was established by exposing cells to increasing doses over 8 months. It was found that EVs derived from the cisplatin chemotherapy resistant cells could transfer ABCs to chemotherapy naïve cells, increased their ability to actively pump out cisplatin resulting in a higher resistance. Similarly, the cell lines are resistant to irradiation by being gradually exposed to increasing doses until they could survive doses of irradiation that would be considered lethal. These cells had never been previously exposed to chemotherapy but could survive doses of Doxorubicin that proved lethal to their nonRR counterparts. However, the ability of cells to develop a radioresistant phenotype is in part due to their ability to minimise effects of ROS produced by the hydrolysis of water molecules and fix the DNA damage that the ROS create (He *et al.,* 2020). Doxorubicin works primarily as an intercalating agent between G bases of DNA, prevent the unzipping of DNA and thus preventing DNA replication (Sahin *et al*., 2022). Secondly, Doxorubicin causes the topoisomerase II enzyme to induce DSBs by trapping topoisomerase II on to DNA, inducing protein-linked DNA breaks (Mastrangelo *et al.,* 2022). Finally, Doxorubicin can result in the production of ROS, which then causes DNA damage in a similar manner to irradiation (He *et al.,* 2020). A potential explanation for the ability of the EVs derived from RR cancer cells to increase chemoresistance in recipient cells could be associated with their ability to effect DDR in recipient cells, as chemotherapeutics are DNA damaging molecules. Studies have shown EVs derived from RR head and neck cancer cells can increase the rate of DNA damage repair in recipient cells, resulting in an increased radioresistance (Mutschelknaus *et al*., 2017). It has also been found that EVs derived from RR cancer cells can induce a stem-cell like phenotype in recipient cells that may also confer a resistant phenotype (Kabakov *et al.,* 2021). The associated characteristics of CSCs are the ability of self-renewal, intense proliferation, and cancer therapy resistance (Zheng *et al.,* 2021). An increase in these stem-cell like characteristics induced by the uptake of EVs from the RR cancer cells could induce chemoresistance in recipient cells (Zhao *et al.,* 2018). It should be noted that the Doxorubicin used in the chemosensitivity assays was reconstituted in DMSO which can be toxic to cells; however, concentrations of 0.6-0.15% and below have found to have no toxic effects to mammary carcinoma cell lines such as MDA-MB-231 and MCF-7 (Nguyen *et al.,* 2020). As stated in the

methods section (2.8), the highest concentration of DMSO that would have been used with the cell lines in this assay would have been 0.03%. Therefore, the toxicity effect would have been minimal as studies have shown that 1% or less of DMSO results in no observable cellular toxicity in MDA-MB-231 breast cancer cells (Dubois *et al.,* 2017). However, this has not been tested in the REM134 cancer cell lines in literature; therefore, it would be useful to have treated cells with the relevant percentage of DMSO as a control along with cells treated with PBS.

The cancer therapy resistant phenotype seen in cells treated with EVs derived from RR cancer cells may also be promoted by the increase in the size and number of tumourspheres. Data showed that EVs derived from nonRR and RR cells could significantly increase the size and number of tumourspheres formed for all cell lines, indicating that the content of EVs derived from RR cancer cells stimulates breast CSC proliferation and growth. It was also found that REM134 RR tumourspheres had a smaller size range when compared to the REM134 tumourspheres (Figure 4.13), and there was a significantly higher abundance of the REM134 RR tumourspheres with a 6 fold increase compared to 2 fold increase in the REM134 tumourspheres compared to cells treated with PBS as a control (Figure 4.13). This effect on the breast CSC population may also explain the increase in therapy resistance observed, because if the number of breast CSCs within the cell population increases following the addition of EVs derived from RR cancer cells, then the cell population will have a higher resistant to therapy. There are a few potential pathways that may be activated to increase the size of the breast CSC population, with several studies associating proliferation of the breast CSC population with AKT activation (Steinbilcher *et al.,* 2018). Activation of the AKT pathway was found to be a potential marker of a radioresistant phenotype in the same cell lines used in this project (Gray *et al.,* 2020), but activation of this pathway was also associated with an increased rate of migration by increasing markers of EMT and activation of the WNT pathway which promotes a more stem-like phenotype in the MDA-MB-231 cancer cell line (Zhu e*t al.,* 2021; Wan *et al.*, 2021). Thus meaning that activation of the AKT pathway in the REM134 RR and MDA-MB-231 RR cancer cells could enhance radioresistance by also inducing a stem-cell like phenotype.

Interestingly, a study established an RR CSC population by exposing cells to fractionated irradiation for 82 days, the CSC population activated AKT and decreased Cyclin D1 and CDK4 and the use of AKT inhibitors resulted in decreased radioresistance of the CSC population (Shimura *et al.*, 2018). It would be beneficial to repeat the experiment for tumoursphere formation assays in conjunction with AKT inhibitors to see the increase in CSC proliferation can be abrogated.

These data show that EVs derived from RR cell lines appear to confer a radioresistant phenotype to recipient cells, potentially via increasing the size of the breast CSC pool via increased uptake of EVs derived from RR cells. This is a critical finding as the development of radioresistance in cancer patients often proves to be fatal. The discoveries from this project points the focus on radioresistance prevention towards EVs; therefore, future research should focus on the content of EVs derived from RR cells (both protein and miRNA cargo). This would untangle the complicated cellular pathways that could be manipulated in recipient cells for them to acquire radioresistance. To date there have been very few studies that have analysed pathway changes that occur upon the acquisition of a RR phenotype in breast cancer, with these studies identifying activation of the PI3K/AKT pathway (Gray *et al.,* 2019), increased rate of DDR (Yan *et al.,* 2007) and activation of AKT/GSK3β (Shimura *et al.,* 2010).

It is important to note the similarities and differences between the human and canine datasets, overall EVs derived from the REM134 RR cells and the MDA-MB-231 RR cells could increase the recipient cell migration, cell viability following chemotherapy treatment with Doxorubicin and colony formation following radiotherapy. The REM134 RR and MDA-MB-231 RR cells had enhanced migration compared to their nonRR REM134 and MDA-MB-231 counterparts, which is to be expected as upon the acquisition of a radioresistant phenotype in breast cancer cell lines results in a more epithelial phenotype which leads to an increased rate of migration (Yadav *et al.,* 2019). It was noted that upon the acquisition of a

radioresistant phenotype that there was only a 4 hour difference between closure of the wound between MDA-MB-231 and MDA-MB-231 RR cancer cells (Figure 4.7 C, D). This difference was much less profound when comparing to the CMC REM134 cancer cell line closing the wound at 24 hours (Figure 4.7 A) compared to REM134 RR cancer cells which resulted in closing of the wound at 56 hours (Figure 4.7 B). However, this was also found by Gray *et al*., (2019) who compared migration rate of MDA-MB-231, MCF-7, and ZR-751 breast cancer cells and their corresponding RR counterparts and found that MDA-MB-231 and MDA-MB-231 RR had the smallest difference (albeit significant) between migration rates when compared to other human breast cancer cell lines. It was hypothesised this could potentially be due to the receptor status of the cell lines used, as the REM134 breast cancer cell line is ER^- PR^- $HER2^+$ and the MDA-MB-231 breast cancer cell line is ER^- PR^- $HER2^-$ and there is a correlation between increasing number of negative hormone receptors and rate of migration (Gray *et al.,* 2020). In addition, it would have been informative to confirm the retention of the RR phenotype in the REM134 RR and MDA-MB-231 RR cancer cells used in this project. In a previous study, MCF-7 RR breast cancer cells were developed using the same irradiation time course as the REM134 RR and MDA-MB-231 RR breast cancer cells used in this project. REM134 RR and MCF-7 RR cells were passaged 24 times for a duration of 6 months before being irradiated at 2,4 and 6 Gy and data showed they had maintained their radioresistant phenotype (Gray *et al.,* 2020).

The cells in this project were passaged in EV-depleted medium which can affect cellular growth and proliferation (Kornilov *et al.,* 2018). It would have been useful to use flow cytometry or western blotting to detect for increased expression of proteins associated with a radioresistant phenotype such as ATM signalling to confirm such a phenotype in cells that appear to have acquired a RR phenotype following incubation with EVs from REM134 RR or MDA-MB-231 RR cancer cells (Mutchellaskus *et al.,* 2016).

To summarise, EVs derived from REM134 RR and MDA-MB-231 RR cancer cells appear to be able to induce a radioresistant phenotype in recipient cells. Unexpectedly, EVs derived from the REM134 RR and MDA-MB-231 RR cancer cells could also induce a chemoresistant phenotype in chemotherapy sensitive naïve breast cancer cells. This could potentially be due to promoting a CSC phenotype and/or the ability of EVs from RR breast cancer cells to promote the growth and proliferation of the breast CSC population in both nonRR breast CSCs and RR CSCs (Figure 4.13 and 4.14).

Chapter 5: Comparative analysis of the protein cargo of EVs derived from nonRR and RR cancer cell lines

5.1 Introduction

Data from this project indicated radioresistance can be transferred by EVs to recipient cells in Chapter 4. Studies have shown that EV content includes RNA and protein content (Jenjaroenpun *et al.,* 2013; Khan *et al.,* 2011). Specifically, mRNA and miRNA content of EVs can influence protein expression and gene expression of recipient cells, respectively (Mittelbrunn *et al.,* 2001). EVs contain active protein and to date there are very few studies analysing the proteomic changes in EV cargo upon the acquisition of a radioresistant phenotype. A key study from Mutschelknaus *et al*., (2017) used head and neck carcinoma cells that were RR to irradiation doses of 6 Gy. EVs were isolated from nonRR and RR cells and performed mass spectrometry on the EV protein content to determine differences in protein levels. Data analyses indicated there was significantly higher expression of the PI3K/AKT pathway in EVs derived from RR cells, and treatment of recipient cells with an AKT inhibitor inhibited the increased migration rate associated with exposing unirradiated recipient cells to EVs derived from RR cells. This shows that the protein cargo of EVs can activate signalling pathways in recipient cells and elicit protein expression changes.

The aims of this chapter were to use proteomic data to identify enriched pathways/networks associated with radioresistance that may reveal potential novel therapeutic targets, then analyse these data to identify prospective biomarkers of radioresistance in breast cancer. Protein mass spectrometry works by identifying proteins by comparing identifying peptides from a theoretical sequence database and comparing what is detected in the sample and identifying the closest match. Proteomic analyses of EVs from cancer cells can contain anywhere between 100 proteins (Brown *et al.,* 2020) to 3660 proteins (Gao *et al*., 2021). This can also depend on the method of isolation used as summarised by Risha *et al.,* (2020)

showing that by using commercial kits can result in as low as 5 proteins being identified, and 983 being identified by using UC. In this project, UC was used for the isolation of the EVs from MDA-MB-231 and REM134 nonRR and RR cell lines, the protein content of these EVs was quantified and identified by mass spectrometry. Bioinformatic profiling of the EV cargo was performed with the aim to identify specific networks that drive radioresistance, which could in turn reveal novel drug targets or potential biomarkers of radioresistance. Such findings could provide building blocks for future research to develop alternate therapies for cancer patients with suspected radioresistance. Here, protein content of EVs was identified by liquid chromatography-tandem mass spectrometry (LC-MC/MC) to analyse and quantify the difference between EV content from nonRR REM134 and MDA-MB-231 cells and RR cancer cells REM134 RR and MDA-MB-231 RR. The identified proteins were then analysed in IPA to identify overlapping proteins between human and canine cancer cells that are associated a phenotype of radioresistance, and potential pathways and biomarkers associated with radioresistance in breast cancer.

5.2 Results

5.2.1 EVs derived from REM134 RR and MDA-MB-231 RR cell lines have higher expression of pro-oncogenic content and decreased expression of tumour and CSC suppressors when compared to their corresponding nonRR cancer cell lines

This project hypothesis was that EVs derived from REM134 RR and MDA-MB-231 RR breast cancer cells can confer a radioresistant phenotype to recipient breast cancer cells, with data from Chapter 4 showing the working hypothesis could be accepted. The aim of this Chapter was to determine potential pathways and biomarkers associated with a RR phenotype by analysing EV protein content. This experiment aimed to assess global protein changes that may occur in EVs when breast cancer cells become radioresistant. EVs from cell lines used in this project: REM134, REM134 RR, MDA-MB-231 and MDA-MB-231 RR were trypsin digested then analysed by LC-MC/MC to identify protein expression levels. Heatmaps were plotted of increased and decreased expression and clustered by their Entrez protein identifiers (IDs). There were 792 proteins identified in the canine dataset (REM134

and REM134 RR), and 902 identified in the human dataset (MDA-MB-231 and MDA-MB-231 RR). To compare global protein expression levels in EVs from nonRR and RR cancer cells, proteins were clustered by their Entrez protein number (Figure 5.1).

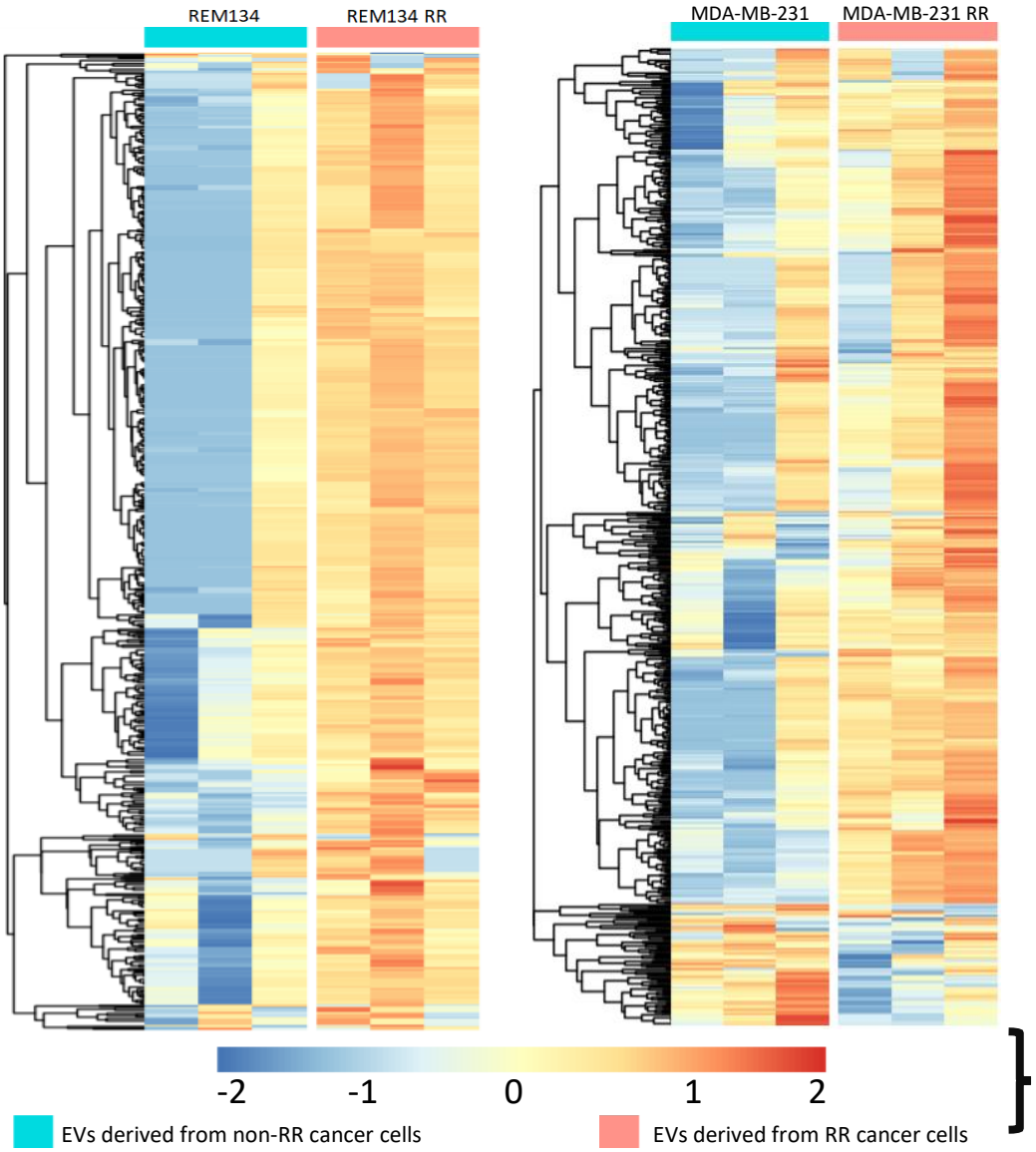


Figure 5.1 Preliminary heatmap analyses showed that EVs from the REM134 RR and MDA-MB-231 RR cancer cells had more upregulated proteins than their nonRR counterparts. *Clusters were determined by the Entrez protein ID in R studio. The median value of protein expression in the nonRR dataset was calculated, then each technical replicate compared to the median value of all nonRR. EV protein expression from RR cancer cells were normalised to the median value of all nonRR triplicates. If the median value of expression was zero in the EVs from non-radioresistant dataset, and the median value of the expression in the dataset from EVs from radioresistant cells was over 1000, they were included in the analyses; however, if the median was zero in the non-radioresistant dataset, and less than 1000 increased expression in the radioresistant dataset, these data were excluded as would not be statistically significant. Dark blue shows decreased expression, and red shows increased expression. Z-score is the significance value for expression, The final z-score was shown to be in the range of -2 to +2. The black bracket (lower right) shows a potential difference in protein expression levels between the human datasets.*

In general, the global protein expression patterns showed higher expression in the EVs from the REM134 RR and MDA-MB-231 RR cancer cells when compared to the corresponding EVs derived from REM134 and MDA-MB-231 cancer cells (Figure 5.1). However, there appeared to be a potential downregulation of a cluster of proteins in the human dataset (highlighted by the black bracket). To identify overlapping molecules associated with radioresistance, IPA software analyses was used to filter through the total number of proteins from each dataset (792 from the canine dataset, and 902 in the human dataset). A filter for "cancer" was applied to the canine dataset, and a filter for "triple-negative breast cancer" was used for the human dataset to ensure irrelevant molecules were not carried forward for downstream analyses. The generic term of "cancer" was applied to the canine dataset as IPA generates protein data by comparing to datasets uploaded in to IPA and extensive filters can result in IPA not being able to identify novel pathways that may not have been previously identified by IPA. Venn diagrams were plotted to show the protein distribution when comparing the canine and human datasets (Figure 5.2).

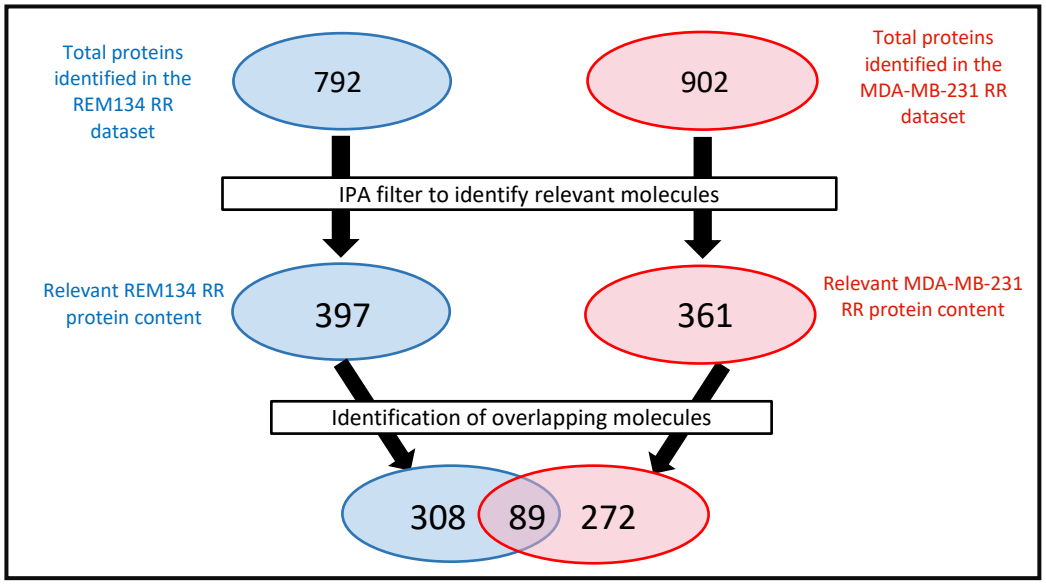


Figure 5.2 The quantity of overlapping proteins associated with radioresistance was determined by IPA core analyses. *The proteomic data was filtered by an IPA core analysis to remove irrelevant molecules not associated with cancer, venn diagrams were plotted to quantify the number of proteins associated with a radioresistant phenotype, by comparing normalised protein content found in EVs derived from REM134 RR and MDA-MB-231 RR cancer cells.*

In total there were 397 proteins associated with radioresistance in the REM134 RR content, and 361 molecules in the MDA-MB-231 RR dataset. There was found to be 89 overlapping molecules that were shared between the REM134 RR and MDA-MB-231 RR that were found to be associated with radioresistance (Figure 5.2).

The identified proteins were derived from established protocols to isolate EVs and this was confirmed by NTA (as per section 3.2.5). Proteins identified were subject to an IPA subcellular location analysis which scans uploaded protein datasets and compares those to the IPA database. IPA then provides the subcellular location where identified proteins are found. The subcellular distribution of proteins identified from the canine and human datasets is similar to the distribution of EV protein content found in literature, which states most proteins identified should be derived from the cytoplasm, followed by nuclear material (Harris *et al.,* 2015). The findings were consistent between the canine dataset and human dataset with 170 proteins located in the cytoplasm from the canine dataset and 153 for the human dataset (Table 5.1).

Table 5.1 The content found in EVs were mostly located in the cell cytoplasm. *The cellular location of all proteins utilised for further analyses were mapped and counted.*

Cellular location	Canine dataset	Human dataset
Cytoplasm	170	153
Nucleus	95	91
Plasma membrane	89	86
Extracellular space	38	28
Other	5	3

After confirming the protein content had the typical cell location distribution of EVs, the next aim was to identify any overlapping molecules identified from the REM134 RR and MDA-MB-231 RR EVs. Molecule overlap analysis in IPA does not state if protein expression was increased or decreased, but can identify matching molecules. Analyses found there were 89 overlapping molecules associated with the radioresistant phenotype (Table 5.2).

Table 5.2 The overlapping molecules in the EVs derived from the RR cell lines. *Table showing the overlapping protein molecules including; enzymes, transporters, growth factors, phosphatases, transcription regulators and "other".*

Symbol	Gene Name	Type(s)
AARS1	alanyl-tRNA synthetase 1	enzyme
ABCB7	ATP binding cassette subfamily B member 7	transporter
ABR	ABR activator of RhoGEF and GTPase	other
ACAA1	acetyl-CoA acyltransferase 1	enzyme
ACACA	acetyl-CoA carboxylase alpha	enzyme
ACACB	acetyl-CoA carboxylase beta	enzyme
ACAT2	acetyl-CoA acetyltransferase 2	enzyme
ACLY	ATP citrate lyase	enzyme
ACTB	actin beta	other
ACTN4	actinin alpha 4	transcription regulator
ACY1	aminoacylase 1	peptidase
ACYP1	acylphosphatase 1	enzyme
ACYP2	acylphosphatase 2	enzyme
ADH5	alcohol dehydrogenase 5 (class III), chi polypeptide	enzyme
ADSL	adenylosuccinate lyase	enzyme
AGA	aspartylglucosaminidase	enzyme
AK4	adenylate kinase 4	kinase
AKT1	AKT serine/threonine kinase 1	kinase
ALDH2	aldehyde dehydrogenase 2 family member	enzyme
SLC25A5	solute carrier family 25 member 5	transporter
STS	steroid sulfatase	enzyme
ACAN	Aggrecan	other
APOC1	apolipoprotein C1	transporter
BMP2	bone morphogenetic protein 2	growth factor
BPGM	bisphosphoglycerate mutase	phosphatase
COL12A1	collagen type XII alpha 1 chain	other
COL1A1	collagen type I alpha 1 chain	other
ACTL6A	actin like 6A	other
APTX	Aprataxin	phosphatase
ASCL1	achaete-scute family bHLH transcription factor 1	transcription regulator
BTF3	basic transcription factor 3	transcription regulator
CCNC	cyclin C	other
CCNH	cyclin H	transcription regulator
CDKN1C	cyclin dependent kinase inhibitor 1C	other
CEBPG	CCAAT enhancer binding protein gamma	transcription regulator
CLK3	CDC like kinase 3	kinase
NR0B1	nuclear receptor subfamily 0 group B member 1	ligand-dependent nuclear receptor
PTTG1IP	PTTG1 interacting protein	other

Symbol	Gene Name	Type(s)
ALDOA	aldolase, fructose-bisphosphate A	enzyme
ALS2	alsin Rho guanine nucleotide exchange factor ALS2	other
AMD1	Adenosylmethionine decarboxylase 1	enzyme
AOX1	aldehyde oxidase 1	enzyme
AP1G1	adaptor related protein complex 1 subunit gamma 1	other
RUNX2	RUNX family transcription factor 2	transcription regulator
SETX	senataxin	enzyme
TEAD1	TEA domain transcription factor 1	transcription regulator
TWIST1	twist family bHLH transcription factor 1	transcription regulator
VPS13B	vacuolar protein sorting 13 homolog B	transporter

The 89 overlapping molecules identified in the EVs derived from RR cells including AKT1 which is associated with migration and invasion (Hasbal-Celikok *et al.,* 2021) and TWIST1 is associated with EMT and the induction of stem-like phenotypes in cancer cells (Cui *et al.,* 2021; Fattahi *et al.,* 2021). TEAD1 transcription regulator is associated with the promotion of EMT (Tome-Garcia *et al.,* 2018) and was identified in both EVs derived from RR cancer cells. Metastasis is associated with EMT, and COL1A1 and COL1A2 are associated with breast cancer metastasis were in EVs from the human and canine RR cancer cells. In addition to molecules associated with EMT, cell cycle regulator molecules CCNC,CCNH and CDKN1C were also overlapping molecules in the EVs derived from the RR cancer cells. Furthermore, APOC1 is associated with cellular proliferation and cell cycle progression and ABCB7 which is an ABC transporter associated with chemotherapy resistance (Kim *et al*., 2021).

Following analyses of increased and decreased fold expression in the EV content in RR cancer cells, molecules associated with tumour and CSC suppression had lower expression compared to EV content from nonRR REM134 and MDA-MB-231 cancer cells. Data indicated there were higher protein expression of molecules associated with cell cycle regulation, tumour progression, promotion of EMT and DDR compared to EV content from nonRR REM134 and MDA-MB-231 cancer cells. This

means that the EVs isolated from RR cells most likely can enhance pro-oncogenic features in recipient cells.

5.2.1.1 Analysis of protein expression in EVs derived from REM134 RR cells.

The aim of this analysis was to identify proteins with increased and decreased expression in the REM134 RR EVs. For IPA analyses used from here onwards, the expression data for EV content from RR cancer cells were normalised to the expression in EVs from nonRR cells (RR EV expression/nonRR EV expression). Therefore, IPA calculates the expression fold change of proteins in EVs from breast cancer REM134 RR and MDA-MB-231 RR cells. To identify which protein molecules had the highest and lowest expression fold change, expression fold changes were ranked according to the highest increased and lowest decreased expression fold change. The first analysis showed the molecules with the highest expression fold change in the EVs from REM134 RR cancer cells (Table 5.3).

Table 5.3 Molecules with the highest fold change in the EVs from REM134 RR cells were associated with EMT and DNA damage repair. *The expression fold change was determined by comparing expression to the EVs derived from the nonRR REM134 cell line. The molecules identified were then ranked from the highest expression fold change.*

Expr Fold Change	Symbol	Gene Name	Type(s)
255	GFPT1	glutamine-fructose-6-phosphate transaminase 1	enzyme
53	MECP2	methyl-CpG binding protein 2	transcription regulator
53	TWIST1	twist family bHLH transcription factor 1	transcription regulator
48	GJA3	gap junction protein alpha 3	transporter
48	GJA5	gap junction protein alpha 5	transporter
41	GCH1	GTP cyclohydrolase 1	enzyme
41	GCHFR	GTP cyclohydrolase I feedback regulator	other
39	ACTG2	actin gamma 2, smooth muscle	other
38	ZFP36L1	ZFP36 ring finger protein like 1	transcription regulator
36	APTX	aprataxin	phosphatase
36	ABO	ABO, alpha 1-3-N-acetylgalactosaminyltransferase and alpha 1-3-galactosyltransferase	enzyme
32	ALDH3A2	aldehyde dehydrogenase 3 family member A2	enzyme
32	FAXDC2	fatty acid hydroxylase domain containing 2	other
30	LIG3	DNA ligase 3	enzyme

Identified molecules with higher protein expression from the REM134 RR EVs had an incredibly high fold change when compared to their nonRR counterparts, with the metabolic reprograming enzyme GFPT1 having an expression fold change of 255, and the EMT promoting transcription factor TWIST1 (Cui *et al.,* 2021) had an increased expression fold change of 53 (Table 5.2). Other enzymes that had high expression fold change were APTX phosphatase (36) and LIG3 (30) which are both associated with DDR (Horton *et al.,*2018; Bian *et al.,* 2021). These data show that EVs from REM134 RR cancer cells have higher expression of molecules associated with EMT and DDR repair compared to nonRR REM134 cancer cells, meaning they may have the ability to confer a pro-oncogenic phenotype to recipient cells. Molecules were then ranked from the lowest to the highest expression, and the 15 molecules with the lowest expression compared to nonRR REM134 cancer cells were analysed (Table 5.4).

Table 5.4 Proteins with decreased expression fold change from the REM134 RR cells included tumour suppressors and stem-cell inhibitors. *The expression fold change was determined by comparing expression to the EVs derived from the nonRR REM134 cell line. The molecules identified were then ranked from the lowest expression fold change to the highest, at the top 15 molecules identified.*

Expr Fold Change	Symbol	Gene Name	Type(s)
-4	PIGR	polymeric immunoglobulin receptor	transporter
-4	PIK3C2A	phosphatidylinositol-4-phosphate 3-kinase catalytic subunit type 2 alpha	kinase
-4	PIK3C2B	phosphatidylinositol-4-phosphate 3-kinase catalytic subunit type 2 beta	kinase
-4	PRCP	prolylcarboxypeptidase	peptidase
-2	HSF2	heat shock transcription factor 2	transcription regulator
-2	FOXA3	forkhead box A3	transcription regulator
-2	DUSP3	dual specificity phosphatase 3	phosphatase
-2	MMP7	matrix metallopeptidase 7	peptidase
-2	POMGNT1	protein O-linked mannose N-acetylglucosaminyltransferase 1 (beta 1,2-)	enzyme
-1	ALOX5AP	arachidonate 5-lipoxygenase activating protein	enzyme
-1	NT5E	5'-nucleotidase ecto	phosphatase
-1	NTF3	neurotrophin 3	growth factor
-1	MARCKSL1	MARCKS like 1	other
-1	DLST	dihydrolipoamide S-succinyltransferase	enzyme
-1	NAB1	NGFI-A binding protein 1	transcription regulator

PIGR has increased protein expression in cancer cells but can have lower expression in cells that acquire therapy resistance (Chen *et al.,* 2022). PIGR had the lowest expression in EVs from the REM134 RR cancer cells when compared to nonRR REM134 cancer cells (Table 5.3). The FOXA3 decreases stem cell-like features in cancer cells (Li *et al.,* 2021) and had the 6th lowest protein expression with an expression fold change of -2, and the MARCKSL1 protein is a tumour suppressor (Kim *et al.,* 2016) that also had lower expression compared to the nonRR REM134 cancer cells.

The data analyses of the EV protein expression data from REM134 RR indicates that overall there is higher expression of DDR repair proteins and those associated with EMT, and that decreased proteins were inhibitors of CSC features and tumour suppressing abilities.

5.2.1.2 Analysis of protein expression in EVs derived from MDA-MB-231 RR cells.

After identifying molecules with highest and lowest expression in EVs derived from REM134 RR cancer cells compared to nonRR REM134 cancer cells, the molecules with the highest expression from MDA-MB-231 RR EVs compared to the nonRR MDA-MB-231 cancer cells were analysed and it was noted that regulators of the cell cycle had higher expression (Table 5.5).

Table 5.5 Proteins with increased expression fold change in the EVs derived from MDA-MB-231 RR cells were associated with the cell cycle and altered mitochondria. *The expression fold change was determined by comparing expression to the EVs derived from the nonRR MDA-MB-231 cell line. The molecules identified were then ranked from the molecules with the highest expression fold change to the lowest with the top 15 molecules shown.*

Expr Fold Change	Symbol	Entrez Gene Name	Type(s)
55	CHRNB4	cholinergic receptor nicotinic beta 4 subunit	transmembrane receptor
54	BNIP2	BCL2 interacting protein 2	other
45	CTNNA1	catenin alpha 1	other
45	CDK9	cyclin dependent kinase 9	kinase
30	ADCY7	adenylate cyclase 7	enzyme
27	COX7A2	cytochrome c oxidase subunit 7A2	enzyme
22	DDOST	dolichyl-diphosphooligosaccharide--protein glycosyltransferase non-catalytic subunit	enzyme
22	CD48	CD48 molecule	other
21	ATP2C1	ATPase secretory pathway Ca2+ transporting 1	transporter
20	ABCA2	ATP binding cassette subfamily A member 2	transporter
19	CD34	CD34 molecule	other
18	ALK	ALK receptor tyrosine kinase	kinase
17	ABR	ABR activator of RhoGEF and GTPase	other
16	ACTN1	actinin alpha 1	transcription regulator
15	CRYBG1	crystallin beta-gamma domain containing 1	other

The transmembrane receptor CHRNB4 had the highest expression fold change of 55, notably other proteins identified were CDK9 with an expression fold change of 45 which is associated with the cell cycle (Mandal *et al.,* 2021). The enzyme COX7A2 also had increased expression fold change of 27 and is associated with chemoresistance in cancer patients (Zhang *et al.,* 2016). The 9th highest was ATP2C1 with an increased expression fold change of 21, and ABCA2, an ABC transporter that promotes drug resistance (Aberuyi *et al.,* 2021) had the 10th highest expression with a fold change of 20.

To investigate decreased proteins that may reveal attenuated pathways in recipient cells after uptake of EVs from human breast cancer RR cells, expression fold change

was ranked from most decreased and the 15 molecules with the lowest expression fold change were analysed (Table 5.6).

Table 5.6 Proteins with decreased expression fold change in EVs from MDA-MB-231 RR cells were associated with tumour suppression and increased cancer resistance. *The expression fold change was determined by comparing expression to the EVs derived from the nonRR MDA-MB-231 cell line. The molecules identified were then ranked from the lowest expression fold change to the highest.*

Expr Fold Change	Symbol	Entrez Gene Name	Type(s)
-36	BAG1	BAG cochaperone 1	other
-20	ATRX	ATRX chromatin remodeler	transcription regulator
-12	CETN2	centrin 2	enzyme
-8	ACVR1B	activin A receptor type 1B	kinase
-7	KYAT1	kynurenine aminotransferase 1	enzyme
-7	CRK	CRK proto-oncogene, adaptor protein	other
-6	ANXA4	annexin A4	other
-5	NAT1	N-acetyltransferase 1	enzyme
-5	HCCS	holocytochrome c synthase	enzyme
-4	CLIC1	chloride intracellular channel 1	ion channel
-4	PDLIM1	PDZ and LIM domain 1	transcription regulator
-4	SPG7	SPG7 matrix AAA peptidase subunit, paraplegin	peptidase
-4	CTH	cystathionine gamma-lyase	enzyme
-4	APP	amyloid beta precursor protein	other
-4	COX11	cytochrome c oxidase copper chaperone COX11	enzyme

The largest decrease in expression fold change was BAG1 with an expression fold change of -36, ATRX had the second most decreased fold change at -20 and can downregulate DDR (Qin *et al.,* 2022). Notably, the 6th most decreased expression fold change (-5) was the NAT1 enzyme that has shown to inhibit proliferation in cancers by downregulating AKT (Cai *et al.,* 2021). There was also a decreased expression fold change of -4 for PDLIM1 which is known to suppress EMT in cancer cells and inhibit metastasis (Chen *et al.,* 2016; Huang *et al.,* 2020).

This data shows that REM134 RR and MDA-MB-231 RR EV content has increased expression of proteins associated with pro-oncogenic phenotypes such as migration,

proliferation and DDR. Likewise, the proteins that have decreased expression were associated with pathways have tumour suppressive effects.

5.2.2 Functional analyses indicated enrichment of protein content associated with a more aggressive phenotype of cell growth, proliferation and migration and in the EVs derived from RR cells.

The aim of this analysis was to identify biological functions that were enriched in EVs upon the acquisition of a radioresistant phenotype. EV protein molecule content from the REM134 RR and MDA-MB-231 RR cancer cells were processed through a "Disease and functions" analysis in IPA. This function groups of molecule associated with diseases and the correlating biological functions and ranks these by statistical significance. Filters were applied to pre-selected for the disease of "cancer", therefore analyses show functions in the context of cancer in EVs derived from REM134 RR (Figure 5.3 A), and MDA-MB-231 RR (Figure 5.3 B). EV content analyses from REM134 RR and MDA-MB-231 RR cancer cells indicated a highly significant increase in expression of pathways associated with a more aggressive phenotype in cancer cells.

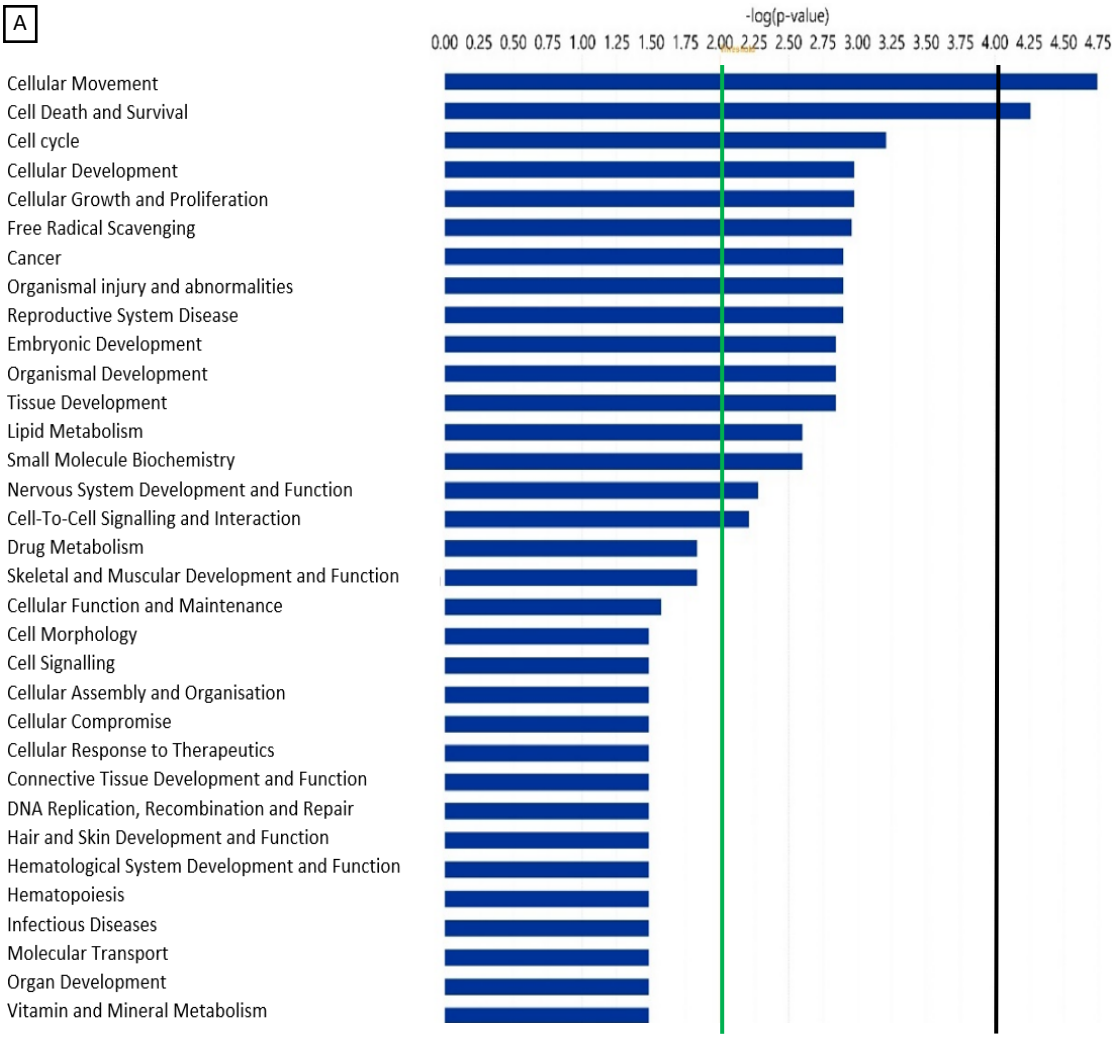


Figure 5.3 continued overleaf…

Figure 5.3 continued…

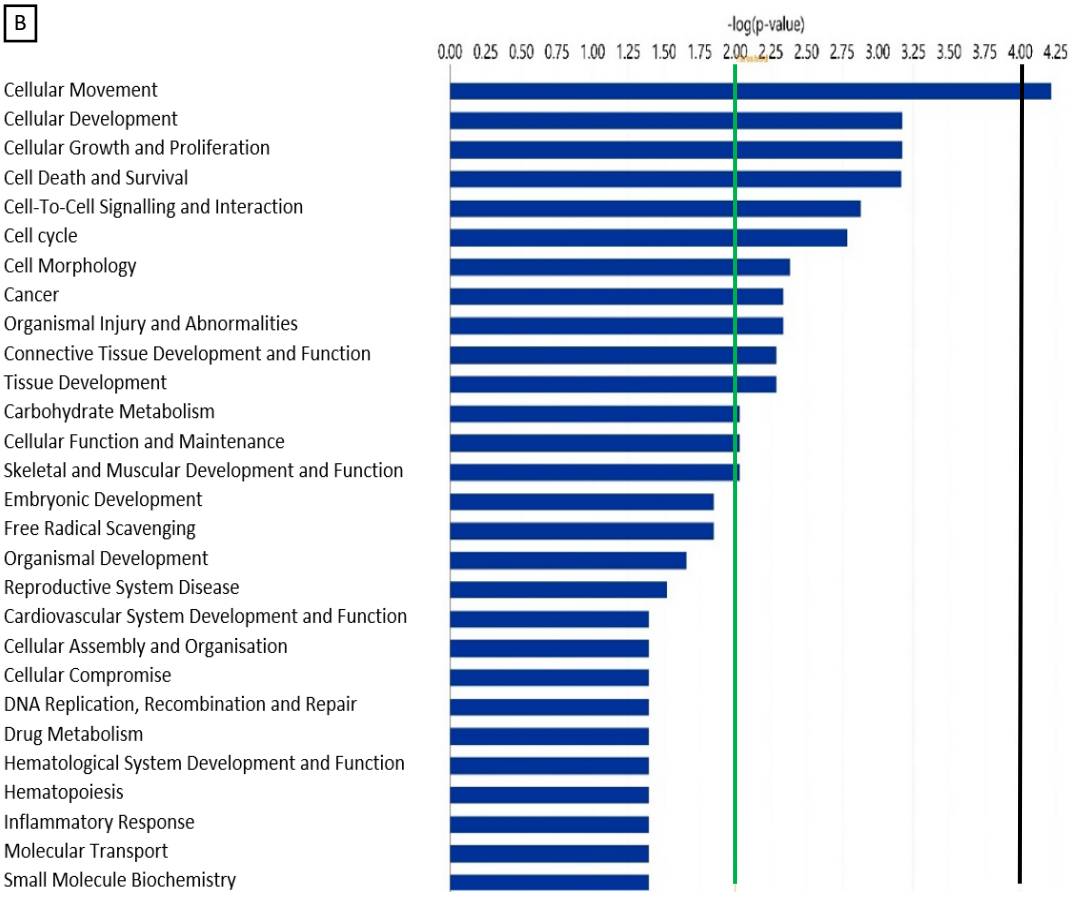


Figure 5.3 Functional expression analysis showed EVs derived from RR cells contained proteins associated with a more aggressive cell phenotype A) *shows expression analysis of RR/nonRR REM134 EV content* ***B)*** *shows expression analysis of RR/nonRR MDA-MB-231 EV content. The p-value used B-H p-value to determine significance. A z-score cut off was set at 1.3 (p=0.05), which are all shown on the charts above. The green line is indicative of a z-score of 2 (p=0.01) and the black line is indicative of a z-score of 4 (p=0.001).*

Cell movement, death and survival and expression of molecules associated with regulation of the cell cycle were highly expressed ($p<0.001$) in EVs derived from REM134 RR cells (Figure 5.3 A). Similarly, cellular movement was the most highly expressed function in EVs derived from MDA-MB-231 RR cells (Figure 5.3 B). The content of both RR cell lines was significantly enriched with phenotypes associated with cancer cell aggressiveness, and it was also noted how there were increased functions associated with cell metabolism such as lipid and carbohydrate metabolism. There was also a significant enrichment of “embryonic development” and “DNA damage and repair” function in the EV content of both REM134 RR and MDA-MB-231 RR. By IPA definition the embryonic development function is

associated with increased stem cell generation. EV protein content from REM134 RR and MDA-MB-231 RR cancer cells were normalised to nonRR EVs, this means that EVs derived from REM134 RR and MDA-MB-231 RR cells have significantly increased expression of proteins associated with a more CSC and aggressive phenotype in cancer cells. These findings also highlighted the general function of the content of the EVs derived from REM134 RR and MDA-MB-23 RR cell lines have different content to that from the content of EVs derived from nonRR cells.

All findings considered, bioinformatic analyses indicated that EVs derived from human and canine RR breast cancer cells have increased expression of proteins associated with cell growth, motility, metabolism and DNA replication and damage repair.

5.2.3 Analysis of canonical pathway activation indicated similarities in increased and decreased protein expression between the EVs derived from REM134 RR and MDA-MB-23 RR cell lines.

As there were similarities between disease and function groups in EVs derived from REM134 RR and MDA-MB-231 RR cell lines, this analysis aimed to investigate the specific canonical pathways that could potentially be associated with an RR phenotype by analysing protein content from EVs derived from the REM134 RR and MDA-MB-231 RR cell lines. Proteomic data was processed through IPA analysis to produce a canonical pathway analysis according to z-score which determines statistical significance specifically for expression values. The canonical pathway analysis takes the protein data and calculates the number of proteins and fold expression within a given network. These pathways were ranked according to expression intensity with a z-score cut off value of +/-1.3 (the equivalent of a p-value

of p=0.05 or less). These pathways were ranked from highest expression to lowest for the REM134 RR and MDA-MB-231 RR cells (Figure 5.4).

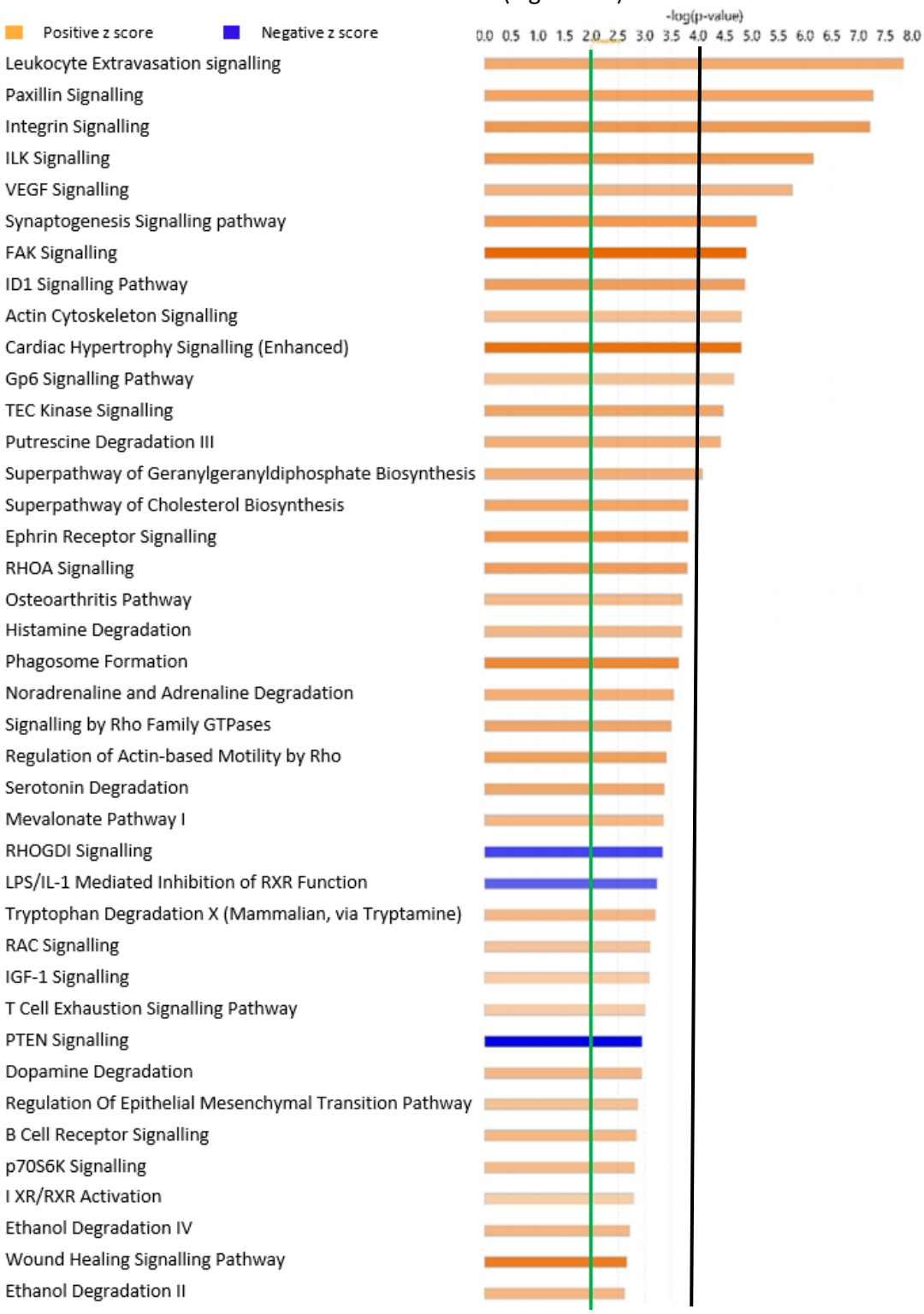


Figure 5.4 continued overleaf…

Figure 5.4 continued…

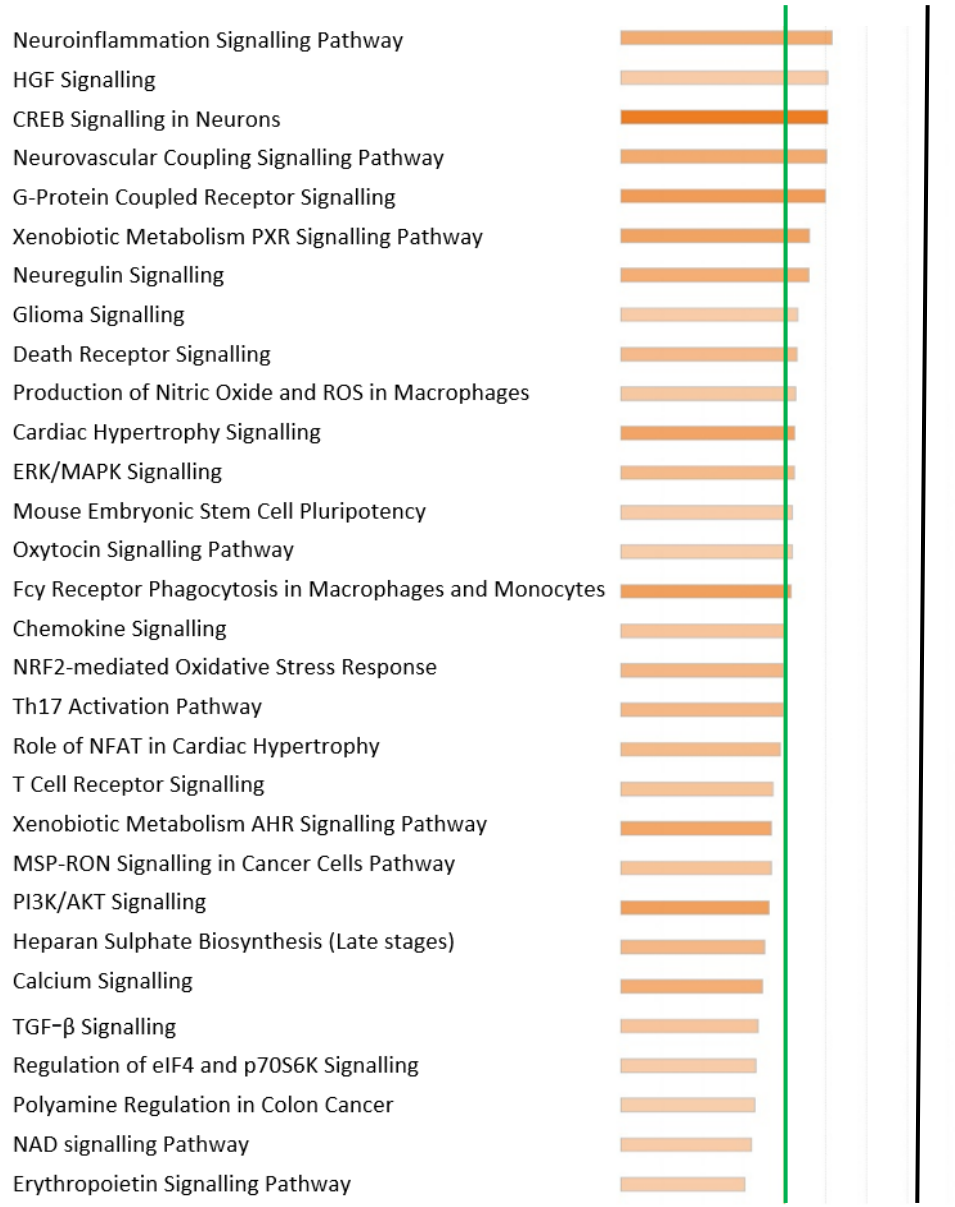


Figure 5.4 Canonical pathways potentially activated by EVs derived from REM134 RR cell line. *The ratio data inputted to IPA as the "RR EVs content/nonRR EV content" were subject to canonical pathway analysis. Pathways are ranked from the highest level of expression to the lowest. The z-score cut off was set to +/- 2 to ensure statistical significance, orange shows the z-score with darker orange being a higher z-score. The p-value used was a B-H p-value to determine significant pathway enrichment with -log10 P-value of greater than 1.3 considered significant (equivalent of p<0.05 shown by the green line; p <0.01 shown by black line; to the right of the black line shows p<0.001.*

Most of the pathways were enriched in the EV content derived from REM134 RR cells, apart from the significant decreased expression of Rho GDP-dissociation inhibitor (RHOGDI) signalling. Downregulation of RHOGDI is associated with

cytoskeletal remodelling; therefore, associated with processes such as vesicle trafficking, proliferation, cell cycle and migration (Lu *et al.,* 2016). Additionally, LPS/IL-1 mediated inhibition of RXR function and PTEN signalling were highly expressed. The most highly expressed canonical pathways were FAK signalling, cardiac hypertrophy, phagosome formation and would healing signalling pathway and CREB signalling in neurons. Many of the significantly increased canonical pathways were known cancer signalling pathways such as TGF-B signalling, ERK/MAPK pathway, and stem cell pluripotency pathways. It was also noted that wound signalling was significantly increased, indicating the content of exosomes from REM134 RR cancer cells contain proteins associated with increased rate of migration. The same analyses were then performed for the EVs content derived from the MDA-MB-231 RR cells (Figure 5.5).



Figure 5.5 continued overleaf...

Figure 5.5 continued…

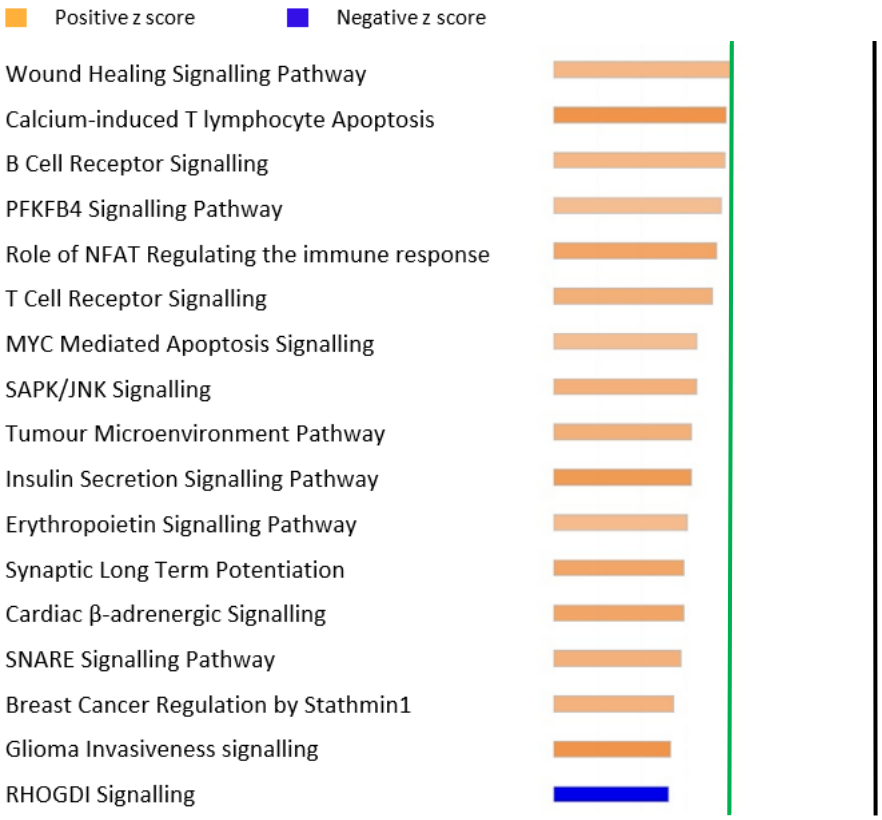


Figure 5.5 EVs derived from MDA-MB-231 RR cells potentially activate canonical pathways associated with increased cell migration, survivability, proliferation and DNA damage repair. *The ratio data inputted to IPA as the "RR EVs content/nonRR EV content" were subject to canonical pathway analysis. Pathways are ranked from the highest level of expression to the lowest. The z-score cut off was set to +/- 2 to ensure statistical significance, orange shows the z-score with darker orange being a higher z-score. The p-value used was a B-H p-value to determine significant pathway enrichment with -log10 P-value of greater than 1.3 considered significant (equivalent of p<0.05 shown by the green line; p <0.01 shown by black line; to the right of the black line shows p<0.001.*

Interestingly, the canonical pathway analyses of EV content from the MDA-MB-231 RR cancer cells (Figure 5.5) indicated increased expression for pathways that also appeared the bioinformatic analyses for EVs derived from REM134 RR (Figure 5.4). Data analyses of EVs from the MDA-MB-231 RR breast cancer cell line indicated the integrin signalling pathway had the highest z-score of 9.0. The RHOGDI signalling pathway was decreased in both the MDA-MB-231 RR EVs and the EVs from the REM134 RR cells. The ratio of expression seen for the MDA-MB-231 RR indicated that oxidative phosphorylation was one of the most highly increased pathways with a z-score of 5.5, as was Synaptogenesis signalling pathway and the calcium transport

I pathway. It was also noted that SNARE signalling had significantly increased expression ($p<0.05$) in the MDA-MB-231 RR cancer cell line, which is associated with the fusion of docking vesicles to the cell membrane before release (Xu *et al.,* 2022).

To observe pathway enrichment in EVs from REM134 RR and MDA-MB-231 RR cells compared to their corresponding nonRR REM134 and MDA-MB-231 cancer cells, a comparison analysis was performed. The comparison analysis in IPA compares statistically increased and decreased pathway expression from both REM134 RR and MDA-MB-231 RR datasets (Figure 5.6).

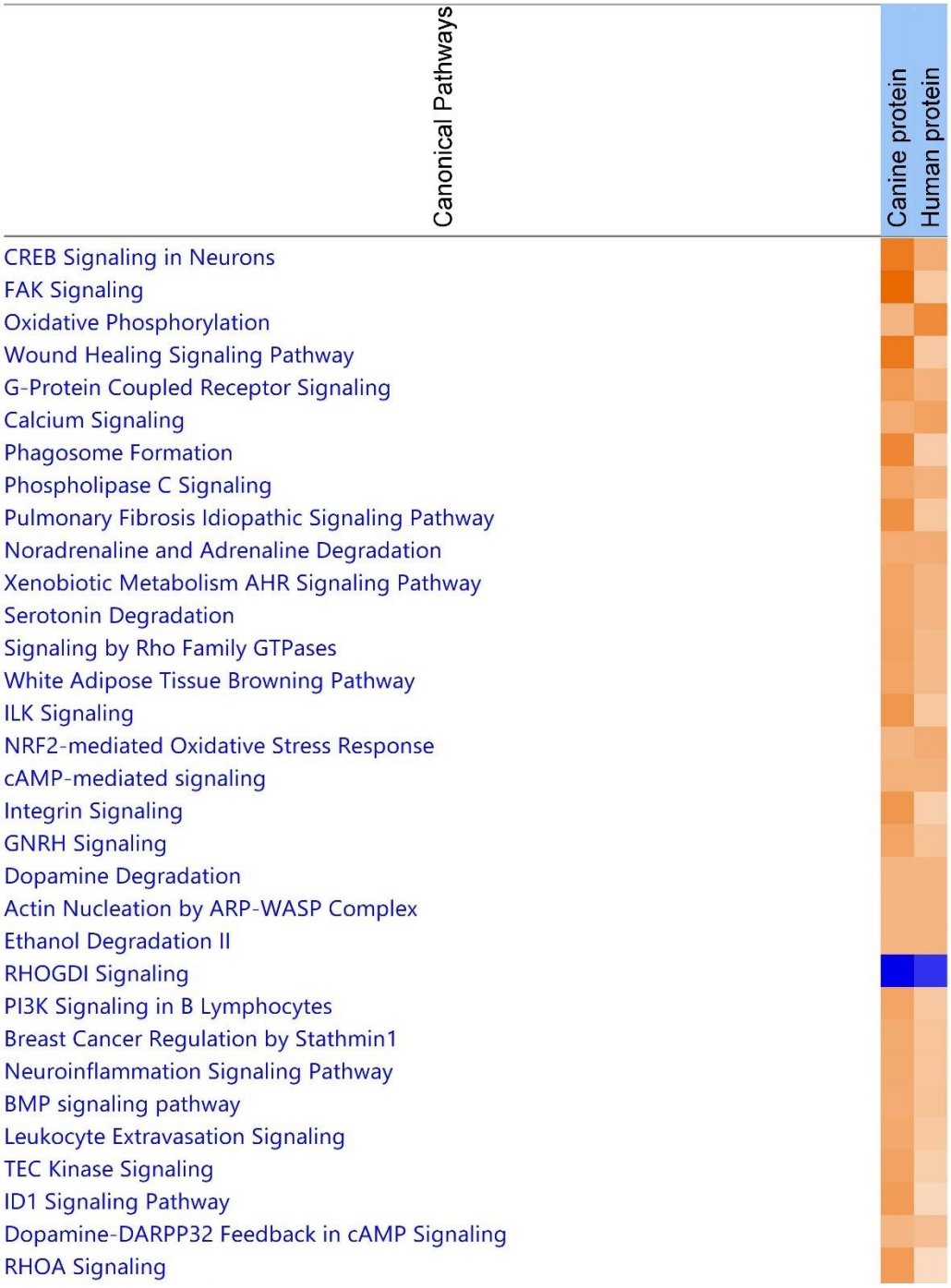


Figure 5.6 continued overleaf…

Figure 5.6 continued…

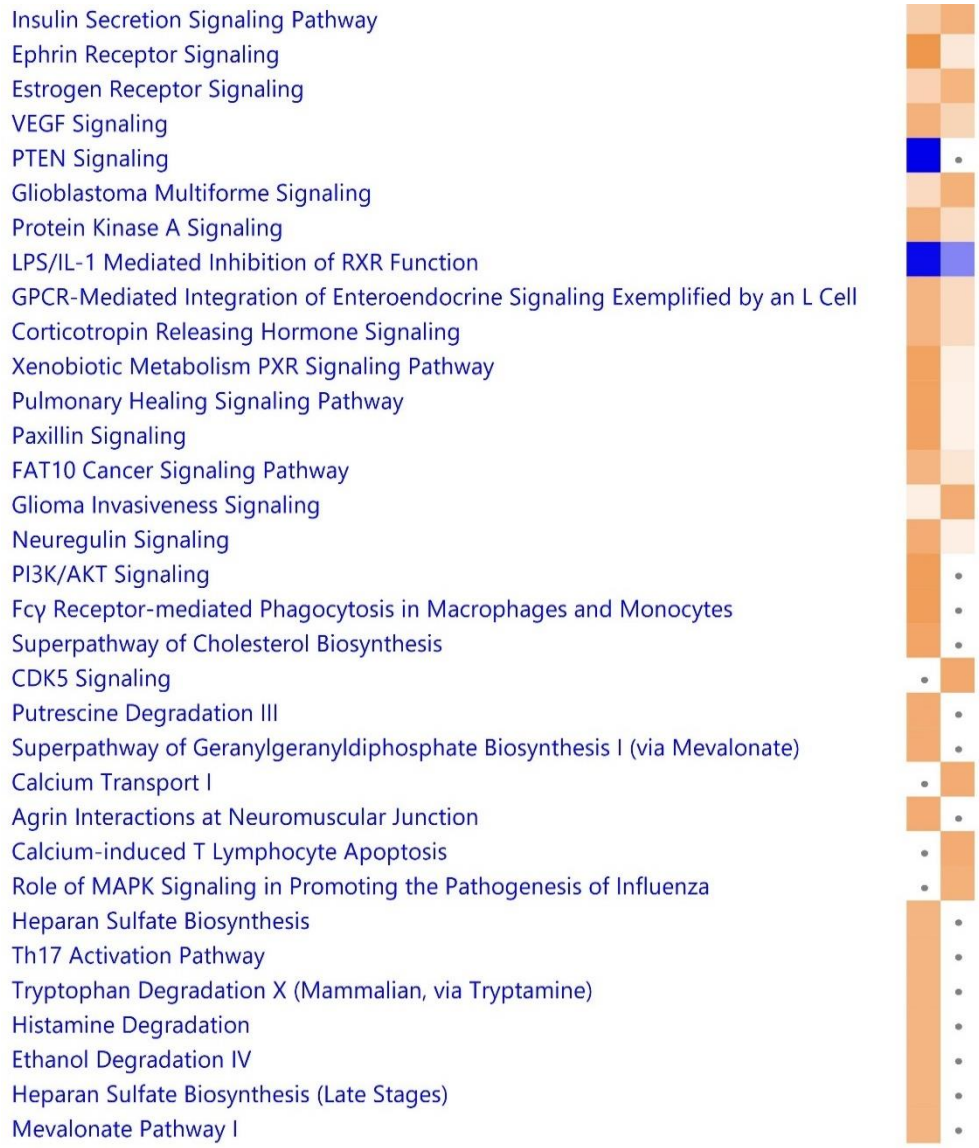


Figure 5.6 Canonical pathway enrichment was similar when comparing the EV protein content derived from the REM134 RR and the MDA-MB-231 RR cell lines. *The ratio data inputted to IPA as the "RR EVs content/nonRR EV content" were subject to canonical pathway analysis. Pathways are ranked from the highest level of expression to the lowest. The z-score cut off was set to +/- 2 to ensure statistical significance, orange shows the z-score with darker orange being a higher z-score The orange colour intensity shows the level of enrichment, with a lighter shade meaning weaker enrichment, and a darker shade showing a stronger enrichment. The p-value used was a B-H p-value to determine significant pathway enrichment with -log10 P-value of greater than 2 considered significant (equivalent of p<0.01). The significant expression and statistically significant data is shown above, with data ranked with highest expression to lowest. Proteins that were not present in the corresponding data set are marked by a dot.*

Canonical pathway analysis showed which pathways had increased and decreased expression depending on the molecules identified in the EV content. The proteins identified in the EV samples were associated with high expression of the CREB signalling pathway in EVs derived from both human and canine RR cell lines. The only mutual pathway with decreased expression was RHODGI signalling (Figure 5.6). Upon closer analysis, most of the canonical pathways had increased expression in the EVs from the REM134 RR and the MDA-MB-231 RR cancer cells. Canonical pathways found towards the top of the chart are associated with cellular proliferation, migration and survival (Armandari *et al*., 2021; Dawson *et al.,* 2021; Boreel *et al.,* 2021).

Most pathways had increased expression; however, comparison of canonical pathways with decreased expression (using the RXR function) indicated they were mainly associated with suppression of cellular proliferation. This data indicates that EVs derived from the RR cancer cell lines may have the ability to stimulate pathways that may enable the proliferation and survival of recipient cancer cells which could lead to the acquisition of radioresistance.

5.2.4 Potential novel targets of radioresistance could be cell cycle regulators and cell proliferation/migration proteins.

The aim of this chapter was to determine potential biological networks associated with radioresistance by the analysis of EV protein expression from REM134 RR and MDA-MB-231 RR cancer cells. EV content can reflect the parental cell from which they are derived (Skotland *et al.,* 2019). This was achieved by normalising expression content of "RR/nonRR" to result in normalised expression data for EV protein content in REM134 RR and MDA-MB-231 RR cancer cell lines. Therefore, further analyses were performed to identify potential targets or biomarkers of radioresistance. Data were linked to published proteomic data in IPA that had associations with radioresistance in tumour cells. Basic networks were built for the REM134 RR and MDA-MB-231 RR cell lines to identify any interconnecting networks/pathways that were associated with radioresistance by overlaying the top

15 enriched networks from EVs on to current proteomic data associated with radioresistance in the IPA database (Figure 5.7).

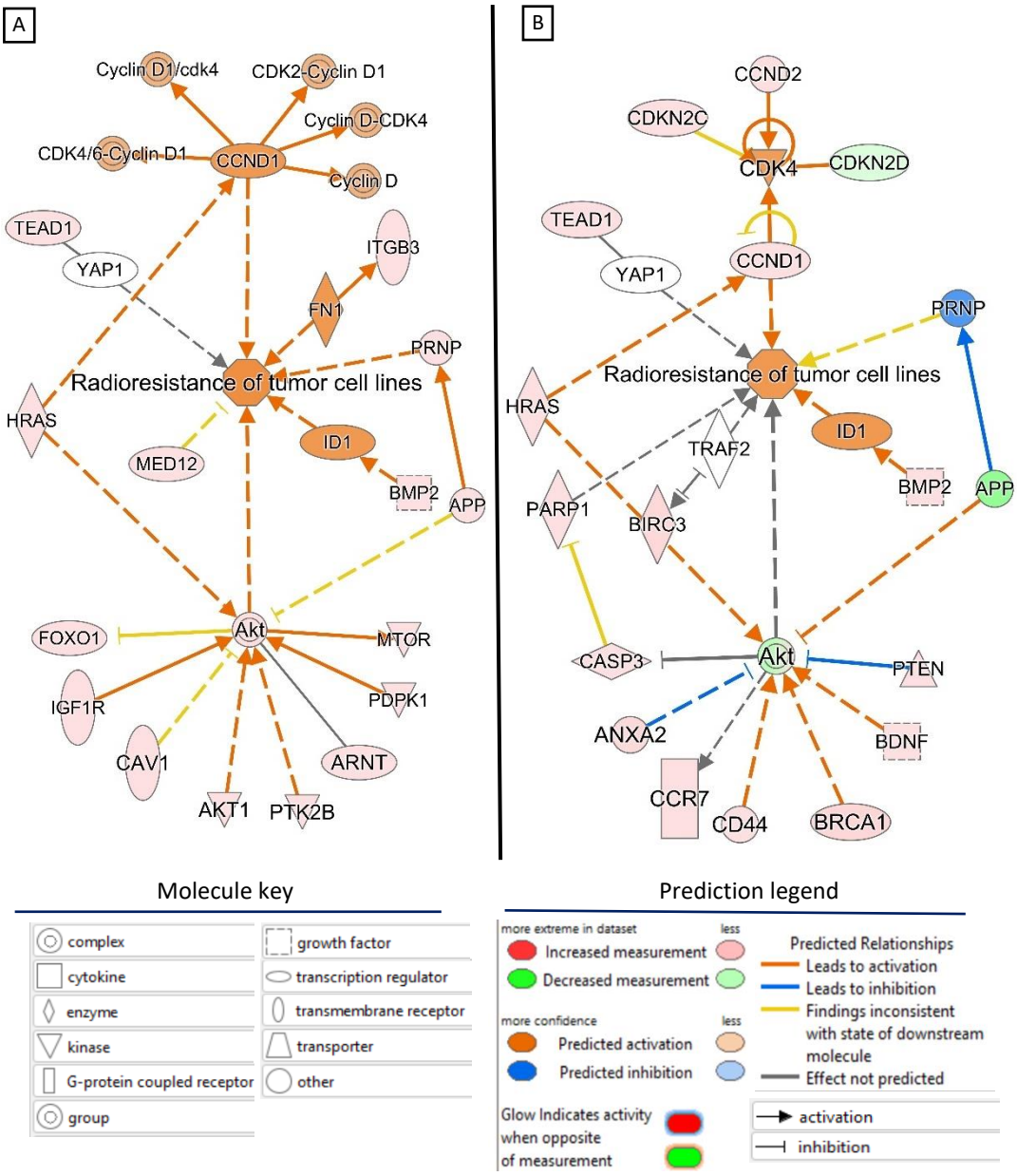


Figure 5.7 Networks associated with radioresistance were similar between the EV cargo derived from REM134 RR and MDA-MB-231 RR cell lines. *To input data to IPA the EV protein content from RR cells was normalised to the nonRR content for both cell lines. The radioresistant phenotype in the IPA database was used as the central "disease" and protein in each dataset were overlaid to create a network for both REM134 RR* ***(A)*** *and MDA-MB-231 RR* ***(B)*** *EV content. The prediction legend shows the upregulation or downregulation of proteins found to be within the network.*

Analyses of the canonical pathways from EVs derived from the REM134 RR and MDA-MB-231 RR cell lines indicated highly similar increased expression of specific

pathways as shown in Chapter 5.2.3. The networks derived from REM134 RR and MDA-MB-231 RR EVs that were associated with radioresistance were also highly similar (Figure 5.7 A, B). All identified pathways had increased expression (orange) in the network associated with the RR phenotype. The identified pathways shown in the network were the CCND1 pathway, AKT Pathway; linked by HRAS. The CCND1 pathway is associated with cyclin D1, and CDK4/CDK6. The network plotted based on the expression of EVs from REM134 RR (Figure 5.7 A) indicated the AKT pathway to be associated with FOXO1, IGF1R, CAV1, AKT1, PTK2B, ARNT, PDPK1 and MTOR. Whereas in the network plotted from the MDA-MB-231 RR EVs (Figure 5.7 B) indicated the AKT pathway was associated with CASP3, ANXA2, CCR7, CD44, BRCA1, BDNF and PTEN. Surprisingly, there were prion proteins found to be associated with the dataset. The APP pathway was activated with in turn activated PRNP to promote a RR phenotype in the REM134 RR network, but in the MDA-MB-231 RR network the decreased expression of APP leads to the inhibition of PRNP, and this downstream effect on the acquisition of radioresistance was “Inconsistent”. ID1 also had increased expression by BMP2; FN1 enzyme had increased expression by the ITGB3 receptor; YAP1 transcription factor that was shown to have neither increased or decreased expression, but there increased expression of the transcription factor TEAD1 signalling associated with the radioresistant phenotype.

The network derived from the MDA-MB-231 RR cell line had a stark similarity to the REM134 RR network after filtering for the most enriched pathways associated with radioresistance. The identification of such pathways could provide a deeper understanding of the mechanisms involved in the acquisition of radioresistance. The network plotted from proteomic data from EVs derived from the MDA-MB-231 RR cell had increased (orange) and decreased (green) connections compared to the nonRR MDA-MB-231 cancer cells (Figure 5.7). This network also pointed to CCND1, which was linked to AKT by the HRAS enzyme which was also seen in the REM134 RR network (Figure 5.7). The AKT pathway had connections with BDNF and PTEN, both of which had increased expression. This network had a separate connection specifically for CDK4, which was associated with CDKN2C, CCND2, and CDKN2D; which had decreased expression compared to the nonRR REM134 cancer cells.

Similarly to the REM134 RR network, this network also indicated associations with ID1 transcription regulator expression were increased by BMP2 growth factor, and YAP1 being associated to TEAD1 being increased. In contrast to the REM134 RR network, the prion moleucles here (APP and PRNP) had decreased expression, and the presence of a TRAF2 enzyme that was connected to a BIRC3 enzyme had increased expresssion.

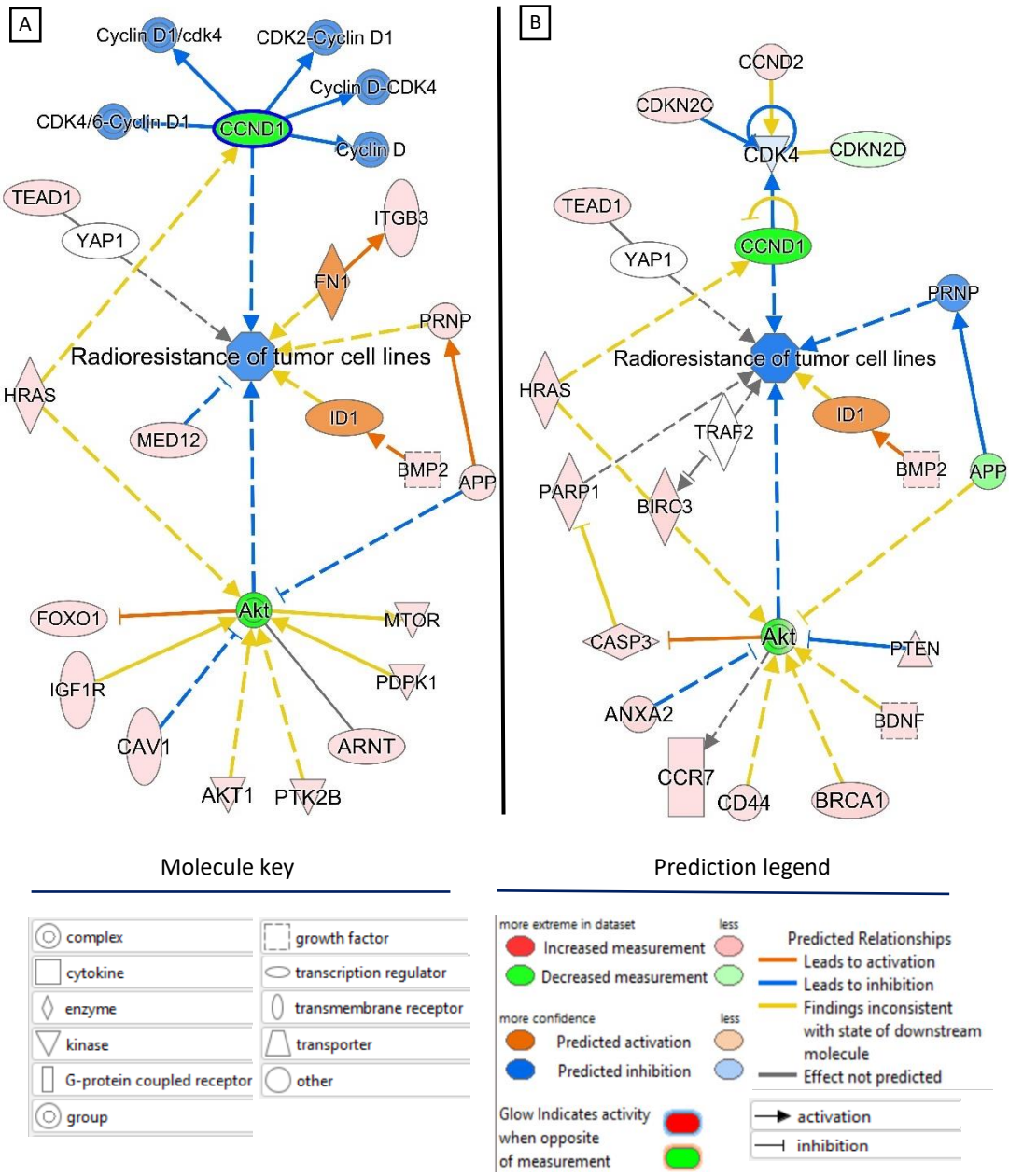


Figure 5.8 Decreasing expression of CCND1 and AKT could potentially inhibit radioresistance. *In IPA the map pathway tool was used to theoretically decrease expression (green) of CCND1 and AKT which showed predicted inhibition (blue) of the phenotype of radioresistance.*

It should be noted that for REM134 RR content that the downregulation of CCND1 alone did not result in the predicted inhibition of radioresistance. It was necessary to also downregulate AKT for the inhibition of radioresistance to occur. The same effect was seen for the content of both REM134 RR (Figure 5.8 A) and MDA-MB-231 RR (Figure 5.8 B). In addition, the HRAS protein that results in activation of CCND1 and AKT could also be a potential therapeutic target in conjunction with the downregulation of CCND1 and AKT (Figure 5.8).

The findings taken from the mapped networks associated with radioresistance indicated the role of cell cycle proteins, HRAS enzyme and AKT complex. Furthermore, out of the molecules identified in the networks shown (Figure 5.8) the only way to theoretically "inhibit" radioresistance was by downregulation of CCND1 and AKT in both REM134 RR and MDA-MB-231 RR networks. It was also noted that downregulation of HRAS could potentially result in a synergistic effect. Interestingly, prion proteins were identfied in both radioresistance networks; PRNP is a prion precusor protein that was indicated to be assiocated with APP, which are both associated with radioresistance.

To summarise, the data anlyses of protein content from EVs inidcated that EVs from REM134 RR and MDA-MB-231 RR were enriched for proteins associated with promotion of CSCs and enhanced pro-oncogenic phenotype. Additional analyses outlined networks associated with radioresistance in REM134 RR and MDA-MB-231 RR EVs. These networks were highly similar, with key molecules being cyclin proteins, AKT, prion proteins and the Hippo pahtway (TEAD and YAP1). Futher studies should focus on validating these networks in functional assay in *in vitro* models and clincial cases in patients with suspected radioresistant breast cancer.

5.2.5 CCNH, COL1A1, CSTB, AKT1, ALK and APOC1 could be potential biomarkers of radioresistance

The aim of this analysis was to identify potential biomarkers of radioresistance based on EV protein content. The data input to IPA can only be as an expression ratio, all data shown was input as the ratio of “RR EV expression/nonRR EV protein expression”, therefore all data is normalised to the nonRR REM134 and MDA-MB-231 EV protein content.The analysis “biomarker tool” in IPA, as before, the “all mammals” option was selected along with cell lines as stem cells and all cancer types that are available. This is because biomarkers are identified by comparing to pathway datasets uploaded in to IPA and extensive filters can result in IPA not being able to identify novel pathways and biomarkers. All of the biofluid options (blood, urine etc) were selected along with the biomarker applications of; ”response to therapy”; “unspecified application” alongside “not a known biomarker”. Single biomaker analyses were performed on the original data that was inputted in to IPA, to filter proteins specifc to triple-negative breast cancer, and identified potential 38 biomarkers (Figure 5.9 A). A single biomarker analysis was also performed for the normalised content derived from the REM134 RR cells, which resulted in the identification of 43 biomarker proteins (Figure 5.9 A). A comparison biomarker analysis was then performed to identify proteins signatures that had significant protein expression between both the normalised REM134 RR and MDA-MB-231 RR content. The comparison biomarker analyses indicated that there were six overlapping biomarkers that could potentially be used as biomarkers of radioresistance (Figure 5.9).

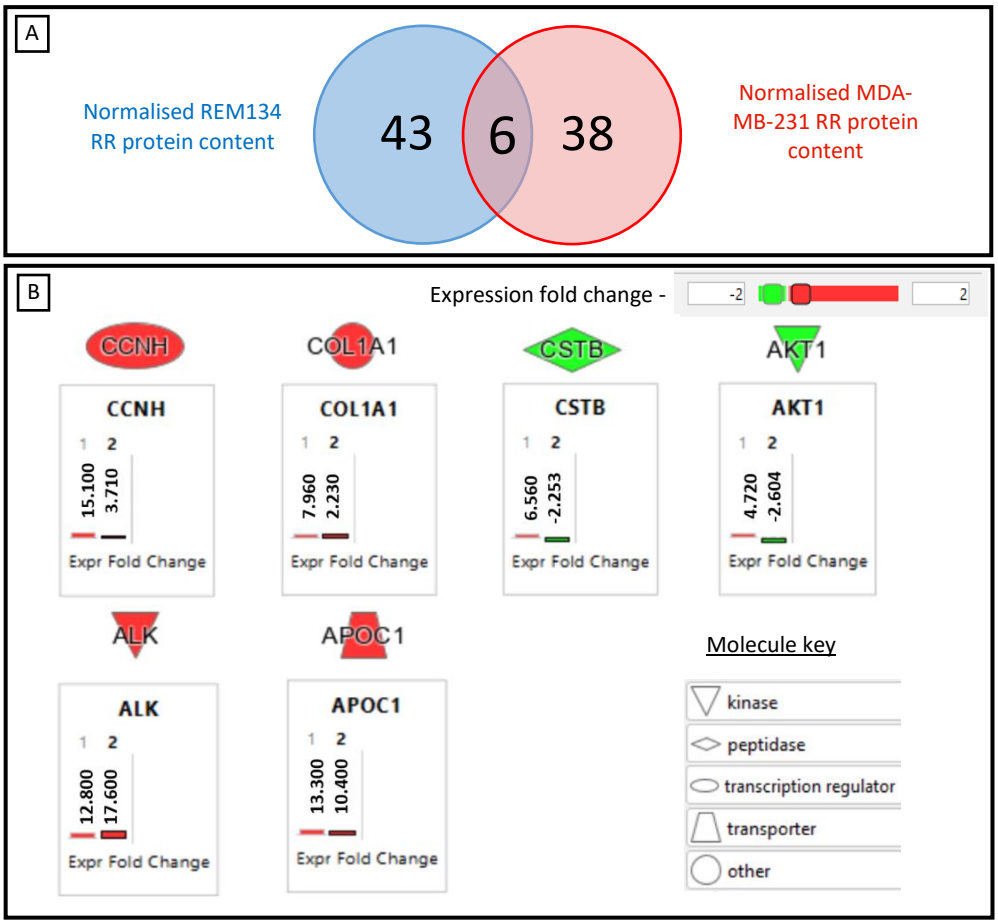


Figure 5.9. CCNH, COL1A1, CSTB, AKT1, ALK and APOC1 were identified as potential biomarkers following IPA analyses. *Biomarkers were filtered for "disease progression", "prognosis", "diagnosis" and "response to therapy" with expression fold change set to cut offs of +/- 2. There were 43 biomarkers identified from the normalised REM134 RR dataset compared to 38 found in the normalised MDA-MB-231 RR dataset. The 6 overlapping biomarkers were plotted with REM134 RR expression fold change shown by column "1" and MDA-MB-231 RR expression fold change shown by column "2" under each biomarker identified.*

To deterine potential biomarkers of radioresistance in human and canine breast cancer, the content of the REM134 RR and MDA-MB-231 RR breast cancer cell lines were normalised to their corresponding nonRR (REM134 and MDA-MB-231). The biomarker function in IPA was applied to identify overlapping molecules that were expressed. This analyses indicated six biomarkers were shared between the REM134 RR and MDA-MB-231 RR datasets (Figure 5.9). The highest expression fold change was seen in anaplastic lymphoma kinase (ALK), a kinase receptor on the cell surface that transmits signals from the cell surface (Tsukahara, 2022), with a 12.800-fold increase for content from REM134 RR EVs compared to 17.600-fold increase in the

EVs derived from MDA-MB-231 RR. There was an increased fold expression in both EV content from REM134 RR and MDA-MB-231 RR EVs of apolipoprotein C1 (APOC1), which is a cellular transporter of lipids that can stablilise the lipoprotein structure in cells (Xiao *et al*., 2021). Cyclin H (CCNH) is a cyclin transcription regulator and is associated with cell cycle control (Barkovskava *et al*., 2021), and had a 15.100-fold increase in expression in the normalised RR EV content and a 3.710-fold increase in the normalised MDA-MB-231 RR EV content. Collagen type 1 alpha 1 chain (COL1A1) which makes collagen (Manoor, 2021) had decreased expression in both the MDA-MB-231 RR and REM134 RR content.

Interestingly, biomarkers were found that had gulation in one cell line and downregulation in the other. In the REM134 RR EV cargo, cystatin B (CSTB) had an increased expression of 6.560-fold and a significant 2.253-fold decreased expression in the MDA-MB-231 RR EVs. CSTB expression prevents the enzyme cathespin leaking from the lysosome causing proteolysis within the cell (Xu *et al.,* 2021). Likewise, a serine/threonine protein kinase 1 (AKT1) which promotes cell growth and survial (Zhang *et al.,* 2021) had a 5-fold increased expression in the REM134 RR EVs, and had -3 fold decreased expression in MDA-MB-231 RR EV content. This could potentially be species and or cell line difference, as AKT1 can be decreased in the MDA-MB-231 cell line whilst having increased AKT2 (Leal-Orta *et al.,* 2021) which could result in the half activated and half deactivated AKT in the network plots of radioresistance (Figure 5.8). The prescence of AKT1 and the involvement of cell cycle control correlates with the earlier findings of proteins associated with the radioresistance network (Figure 5.7). That were also identified as potential biomarkers of radioresistance (Figure 5.9 B).

Following network analyses that showed high homology between human and canine radioresistance netowrks (as per Chapter 5.2.4). This chapter aimed to identify biomarkers of radioresistance by comparing biomarkers between species.These data analyses highlighted six potential biomarkers of radioresistance found within EVs derived from RR breast cancer cells; CCNH, COL1A1, CSTB, AKT1, ALK and APOC1.

However, these biomarker would have to be validated in *in vitro* studies or in EV samples from human and veterinary patients with suspected breast cancer radioresistance.

5.3 Discussion

Radiotherapy works by focusing irradiation to the site of the tumour, causing radiolysis of water molecules that produce ROS; $O_2^{-\cdot}$, H^+, OH^- ions which then go on to react with DNA and cause DSBs and SSBs (Tolouee *et al.,* 2022). The DNA damage that occurs cannot be repaired causing the cancer cell to undergo apoptosis. However, cancer cells can acquire radioresistance, which means they can survive doses of irradiation that should be lethal (Todorovic *et al.,* 2019). The development of radioresistance can lead to recurrence and metastasis and the molecular mechanisms by which this occurs is still unclear in both human and veterinary medicine (Nozaki *et al.,* 2020). Therefore, the hypothesis of this project was that EVs from radioresistant breast cancer cells can induce a radioresistant phenotype in recipient cells. Data in Chapter 4 showed that EVs derived from REM134 RR and MDA-MB-231 RR could increase recipient cell viability, colony forming ability and therapy resistance in non-CSC and breast CSC populations. Therefore, the aim of this chapter was to analyse EV protein content to identify pathways that may be associated with the acquisition of a radioresistant phenotype and potential biomarkers of radioresistance in breast cancer.

5.3.1 EVs derived from REM134 RR and MDA-MB-231 RR breast cancer cells have increased expression of pro-survival and CSC proteins and decreased expression of tumour suppressor proteins

There are very few studies specifically examining effects of EVs isolated from nonRR and RR cells (Tutanov *et al.,* 2020). To identify potential novel targets and biomarkers of radioresistance a discovery approach called the “shotgun” method was utilised. This is where all proteins identified by mass spectrometry are analysed and filtered by

bioinformatics; allowing pathways and networks to be identified. Here, LC-MC/MC was used, this method uses two mass spectrometry detectors which allows for the detection of lower molecular weight compounds. EVs from all cell lines were isolated, digested and proteins identified by LC-MC/MC and then analysed via IPA software to identify differences and/or similarities between the protein cargo of EVs derived from nonRR and RR cell lines. Following the filtering of mapped proteins, most of these proteins originated from the cytoplasm of the cell (Table 5.1). EV formation happens in the cytoplasm of the cell, and although there are specific contents that are tagged with ubiquitin to be packaged in to developing EVs, a large proportion of the surrounding cytoplasm is incorporated in forming EVs; therefore, it is typical to have most molecules located in the cytoplasm when analysing EV mass spectrometry data (Harris *et al.,* 2015). The presence of nuclear material in EVs has found to be a common feature in cancer cells, as micronuclei present in the nucleus are prone to collapsing due to membrane instability. This results in the content being released in to the cytoplasm where ILVs are being processed and packaged with the MVBs, meaning that nuclear material is incorporated in to the EVs (Yokoi *et al.,* 2019). Proteomic data was compared between proteins found in EVs derived from REM134 RR cancer cells and MDA-MB-231 RR cancer cells which revealed 89 overlapping proteins (Table 5.2). It was noted that the VPS13B transporter was present, which is associated with tethering to early endosomes to facilitate processing and packaging of lipids in to developing MVBs; however, is not directly associated with the ESCRT dependant or independent pathway (Koike *et al.,* 2019). There was senataxin (SETX) present in EVs derived from MDA-MB-231 RR and REM1E34 RR cancer cells (Table 5.2) which is a DDR enzyme that is recruited to DSBs to contribute to the repair of DNA breaks (Cohen *et al*., 2018). In addition to this, there were several molecules identified including cell cycle regulators, such as CCNC, CCNH, CDKN1C, meaning cell cycle regulation is a factor shared between EVs derived from REM134 RR and MDA-MB-231 RR cancer cells. Additionally, molecular mechanisms of multi-drug resistance are associated with ABC transporters, and ABCB7 was found amongst the shared molecules associated with the REM134 RR and the MDA-MB-231 RR EVs (Pan *et al*., 2016). As well as cell cycle regulators and the ABC transporter, twist expression was increased in the content of EVs from RR cancer cells. Twist expression in cancer cells

is associated with stimulation of stem-like phenotypes (Lee *et al.,* 2021) and the activation of EMT. The suppression of EMT occurs by activation of FOXO3a (Jin *et al.,* 2021) which was also found to have decreased expression in the REM134 RR cell line. By comparing the increased and decreased expression of molecules in EVs derived from RR cancer cells, it was found that increased expression was associated with promoting EMT, cell cycle regulator and DDR, whereas decreased proteins were associated with tumour suppressors. This could mean that EVs can have pro-tumourigenic effects in recipient cells, including DDR repair which could confer therapy resistance.

After comparing the EV content from REM134 RR and MDA-MB-231 RR cancer cells that were associated with radioresistance, analyses were performed to identify potential pathways associated with the acquisition of the radioresistant phenotype. Analyses of the canonical pathways that were enriched and activated in the EVs derived from the REM134 RR cells were associated with cell proliferation, survival and motility (Figure 5.4). It was also noted that there was a significant enrichment for wound signalling (Figure 5.4), which also correlates with the results seen in Chapter 4.2.3 (Figure 4.10 A and B). There were only three pathways that were indicated to have decreased expression, which were RHOGDI Signalling, LPS/IL-1 mediated inhibition of RXR function, and PTEN (Figure 5.4). RHOGDI signalling has been shown to be increased in early-stage breast cancer, and decreased in later stage cancers. Downregulation of RHOGDI is associated with increased migration and invasion in malignant tumours (Bozza *et al.,* 2015). Decreased expression of RHOGDI results in the activation of CDC24 which is a known cell cycle division control protein (Johnson *et al*., 1990). The activation of CDC24 also results in COX-2 activation which promotes breast cancer progression (Bozza *et al.,* 2015). RXR is associated with tumour suppression pathways in cancer cells and stem cells through p53 and PI3K/AKT (Zhang *et al.,* 2018), and the LPS/IL-1 mediated inhibition of RXR was decreased in the canonical pathway analysis. PTEN downregulates the PI3K/AKT pathway downregulates the WNT pathway which is associated with inducing stem-like

properties in cancer cells (Vallee *et al.,* 2019). These decreased pathways indicate the protein content in the EVs derived from the RR cell lines is pro-oncogenic.

There was an increased expression of SNARE signalling in the MDA-MB-231 RR content (Figure 5.5), which could indicate a higher level of EV release as SNARE proteins fuse docking vesicles to the cell plasma membrane before release (Xu *et al.,* 2022). This indicates that MDA-MB-231 RR breast cancer cells release more EVs than the nonRR MDA-MB-231 cancer cells which agrees with previous finding in Chapter 3.2.1 in Table 3.2. When comparing the canonical pathway datasets, it appeared that the EV content indicated metabolic differences between the two cell lines, with oxidative phosphorylation being highly expressed in the MDA-MB-231 RR data (Figure 5.5) with very low expression in the REM134 RR dataset when the two were directly compared (Figure 5.6). This means that although both cell lines are radioresistant, there could be subtle differences in the metabolic reprogramming which occurs upon the acquisition of a radioresistant phenotype. There was upregulation of CREB signalling and FAK signalling in EVs from MDA-MB-231 RR and REM134 RR cell lines and wound healing signalling (Figure 5.4). CREB signalling in breast cancer is associated with metastasis to the bone (Jiang *et al*., 2019) and activation of the WNT pathway leads to stimulation of CSC activity (Shima *et al.,* 2019; Eyre *et al.,* 2019), as well as promotion of cellular proliferation, cell survival and differentiation (Stati *et al*., 2021). Interestingly, the expression of estrogen receptor signalling was expressed in both human and canine samples, with a higher expression seen in the human samples, despite these EVs isolated from a triple-negative breast cancer cell line. There was a difference in expression of calcium signalling, with the samples derived from human MDA-MB-231 RR cells having a higher expression compared to REM134 RR samples (Figure 5.6). The canonical pathway analyses indicated that EV content derived from the RR cell lines are likely to promote the growth, proliferation and progression of cancer cells and CSCs, and downregulate canonical pathways that have tumour supressing effects. This means that transfer of EVs from RR cancer cells to nonRR cancer cells may promote cell growth and proliferation of the cancer cells and potentially breast CSC populations which could contribute to the development of a RR phenotype.

EV protein expression from RR cancer cells was normalised to the protein expression levels from the nonRR cancer cells. Expression changes were analysed and ranked from highest to lowest for molecules identified in the EVs derived from the REM134 RR and the MDA-MB-231 RR cell lines. The top 15 increased expressed proteins and the top 15 molecules with decreased expression were analysed. Molecules associated with cell cycle regulation such as CDK9 were increased in the MDA-MB-231 RR EV content. CDK9 is associated with resistance to clinical resistance to CDK inhibitors that are used in metastatic breast cancer (Del Re *et al.,* 2019). Molecules with the lowest decrease in fold expression were mostly associated with tumour suppressing molecules (Table 5.3, Table 5.5). These molecules included ATRX downregulation. ATRX expression inhibits ATM and therefore prevents the activation of DDR (Qin *et al.,* 2022). Given that in these data ATRX is suppressed this will lead to increased activation of the DDR, which is associated with a malignant phenotype. Another feature of acquiring a cancerous phenotype is activation of EMT. PDLIM1 inhibits EMT by promoting the binding of the cell-to-cell adhesion protein E-cadherin (Huang *et al.,* 2020), and was decreased in EVs derived from MDA-MB-231 RR cells.

These findings indicate that EVs derived from REM134 RR and MDA-MB-231 RR breast cancer cells have increased expression of proteins associated with EMT, cell cycle regulation, DDR and CSC activity (Figure 5.5, Figure 5.6) and decreased expression of proteins associated with tumour suppression and inhibitors of CSC phenotypes (Table 5.3, Table 5.5). These data provide a potential insight as to what protein expression changes can occur upon the acquisition of radioresistance in REM134 RR and MDA-MB-231 RR breast cancer cells.

5.3.2 Networks associated with radioresistance in REM134 RR and MDA-MB-231 RR breast were highly similar and indicated the involvement of CSCs, cell cycle manipulation and proteins associated with EMT

After investigating the expression fold change of molecules in the EVs from RR breast cancer cells, radioresistance networks were plotted using the protein molecules in EVs derived from the REM134 RR cell lines and the MDA-MB-231 RR cell lines were highly similar, with both networks showing associations with cyclin D1 (CCND1), a serine/threonine protein kinse (AKT), prion protein (PRNP), human ras protein signal (HRAS), TEA domain transcription factor 1 (TEAD1) and inhibitor of DNA binding 1 (ID1). The content from MDA-MB-231 cells was filtered to the triple-negative subtype and this showed an extra association with CDK4, and BIRC3 when compared to the EV content derived from the REM134 RR cell lines.

An increase in expression of TEAD1 and YAP1 is associated with the induction of an EMT phenotype in breast cancer (Shen *et al.,* 2021). Likewise, an increased expression of ID1 has previously been proposed as a biomarker of breast cancer aggressiveness (Garcia-Esolano *et al.,* 2021), and was increased in both the normalised REM134 RR and MDA-MB-231 RR radioresistance networks (Figure 5.7). This finding could also be associated with the increase in migration rate when nonRR cancer cells were incubated with EVs derived from RR cancer cells, as the EVs from RR cells could be activating the induction of EMT pathways in the recipient cells that may promote their migration which correlates with the other findings of this project in sections 3.2.2 and 4.2.3. This result was also found by Mutchkelnaus *et al.,* (2017) who showed that EVs derived from RR cell lines had a significant increase in AKT content, which could then activate the AKT pathway in recipient cells to promote migration. CCND1 was also highly increased in both EV RR cell content with further association with CDK4. CCND1 is cyclin D1, a known oncogene which promotes progression through the G1/S phase of the cell cycle, which when overexpressed can result in poor patient survival (Chen *et al.,* 2020). CCND1 has shown to be a promoter of cell proliferation and radioresistance in paediatric ependymomas, with

overexpression appearing to increase the rate of HR to correct DNA damage caused by irradiation (Liang *et al.,* 2017). CCND1 also interacts with kinases such as CDK4 to progress through the G1/S phase (Chen *et al.,* 2021) which was also significantly increased in the network associated with radioresistance in EV content derived from the RR cells (Figure 5.7). This also means that EVs derived from RR cells may manipulate the cell cycle in nonRR recipient cells when they take up these EVs.

Baculoviral IAP repeat- containing (BIRC) proteins are inhibitors of apoptosis, in this dataset BIRC3 was increased in the proteins derived from the MDA-MB-231 RR cell lines. BIRC proteins have previously been associated with radiotherapy resistance (Makuch-Kocka *et al.,* 2021). The smallest BIRC protein (BIRC5) is called survivin, and enrichment of survivin in EVs increases the rate of uptake by recipient cells compared to EVs without enriched survivn (Gonda *et al.,* 2018). Once taken up by recipient cells, survivin enriched EVs can inhibit apoptosis in cancer cells, resulting in increased survival following chemotherapy and radiotherapy treatment (Chang *et al.,* 2021). It has also been found that inhibiting survivin can force cancer cells to switch from being in a state of radiation-induced senescence to apoptosis resulting in radiosensitisation (Liu *et al.,* 2018). Therefore, the enrichment of survivin found in the EVs derived from the REM134 RR and MDA-MB-231 RR breast cancer cells indicates these radioresistant cancer cells use survivin signalling as a pro-survival mechanism following radiotherapy. The presence of survivin could also explain the results found in section 4.2.2 where it was identified that EVs derived from REM134 RR and MDA-MB-231 RR cancer cells had an increased uptake when compared to EVs derived from REM134 and MDA-MB-231 cancer cells, this difference could be due to the enrichment of survivin in the EVs from the RR cancer cells. Additionally, the enrichment of survivin in the REM134 RR and MDA-MB-231 RR EVs could also explain the significant increase in cell viability in non-CSCs and CSCs following chemotherapy and radiotherapy seen in sections 4.2.1 – 4.2.7. As once survivn is taken up by recipient cells, apoptotic pathways are inhibited (Gonda *et al.,* 2018). Interestingly, the presence of prion proteins was associated with the tumour radioresistance network (Figure 5.7). Studies have shown ATM can result in the active transcription of PRPN which itself can induce

a CSC like phenotype; resulting in the induction of acquired radioresistance (Bernardino-Sgherri *et al*., 2021).

Further studies could induce chemotherapy resistance by repeated exposure to gradually increasing doses of a chemotherapeutic in MDA-MB-231 and REM134 breast cancer cells. It would be interesting to observe the associated network with chemotherapy resistance, because if the network associated with chemotherapy resistance is highly similar to the one found in this project, the network may point towards a CSC phenotype. This means that both chemotherapy and radiotherapy could be targeted towards the treatment of breast CSC which may reduce the rate of relapse and metastasis as this associated with the presence of breast CSCs.

Additionally, in the networks associated with tumour radioresistance, AKT was shown to be increased in the REM134 RR EV content and the MDA-MB-231 RR EV content. Bioinformatic modelling in IPA indicated that inhibition of AKT and CCND1 may inhibit radioresistance (Figure 5.8). Activation of AKT is associated with inducing EMT, a faster rate of cell migration and promotion of stem-like phenotypes in cancer cells (Huang *et al*., 2021; Lee *et al.,* 2021; Mutchkelnaus *et al.,* 2017). The relation between the CCND1 and the AKT pathway has had very little research as drivers of radioresistance, but a study by Moafian *et al.,* (2021) showed miRNA that could inhibit CCND1 lead to AKT pathway deactivation that inhibited cell proliferation and reversed the EMT process in colon cancer cells. Similar results found by Tortolici *et al.,* (2021) that showed that EVs could induce radioresistance by activating the AKT survival pathway in recipient cells in neuroblastoma cells.

This project showed that EVs derived from REM134 RR and MDA-MB-231 RR cancer cells could increase nonRR and RR recipient cell proliferation and therapy resistance in non-CSCs and breast CSCs (shown in Chapter 4). The findings from the network suggest the mechanism by which radioresistance can be acquired is associated with the induction of CSC features, DDR, cell cycle manipulation and increased expression of EMT. The networks also show high similarities between the canine and human

dataset and these findings should be investigated *in vitro* to confirm the validity of the identified networks.

5.3.3 IPA identified six potential biomarkers of radioresistance in REM134 RR and MDA-MB-231 RR breast cancer cells including AKT, COL1A1, APOC1, CCNH, ALK and CSTB.

Bioinformatic analyses were performed in IPA to identify potential biomarkers of radioresistance. There were six biomarkers identified, one of which was AKT that was also found in the network analyses associated with radioresistance (Figure 5.7). In accordance with these findings, AKT has surfaced as a potential biomarker of radioresistance in nasopharyngeal carcinoma (Chen *et al*., 2020), prostate cancer (Chang *et al*., 2017) and cervical cancer (Kim *et al.,* 2006). AKT was in the top networks associated with the acquisition of an RR phenotype and AKT was also theoretically predicted to be a biomarker of radioresistance in this bioinformatic analyses (Figure 5.9 B). The consistent indication of AKT in the role of radioresistance means that AKT could potentially be both a novel target to inhibit the acquisition of radioresistance in breast cancer, but also as a potential biomarker of the development of acquisition in patients. The identification of such a target/biomarker could potentially personalise medicine for human and veterinary patients that acquire RR tumours, as alternate treatment plans could be used in the case of patients with radioresistance. Radiotherapy is used in veterinary medicine in cases of mammary glioma, sarcomas and CMC, all of which use fractionated radiotherapy of < 2 Gy per week in bi-weekly doses totalling between 36 – 45 Gy (Debreuque *et al.,* 2020; Nolan *et al*., 2012; Rossi *et al.,* 2018).

EV protein content derived from patient serum, plasma and urine have the potential to be profiled and used as biomarkers of cancer diagnosis, progression, and treatment outcome (Theodoraki *et al*., 2021; Guo *et al.,* 2021; Guo *et al.,* 2022). It would be advantageous to human and veterinary medicine to develop a biomarker of radioresistance, as the identification of radioresistance within a tumour means the treatment plan for patients could be altered accordingly. The data analyses of

networks associated with radioresistance in the EVs derived from the REM134 RR and the MDA-MB-231 RR cells indicated that potential biomarkers could be linked to the AKT/MAPK pathway. These include COL1A1 which is associated with radioresistance in nasopharyngeal carcinoma and downregulation of COL1A1 was shown to induce radiosensitivity (Xiao *et al.,* 2021), and has previously shown to promote radioresistance by activation of the Caspase-3/PI3K/AKT to decrease cellular apoptosis (Liu *et al*., 2017).

Additionally, APOC1 is related to increased cell survival, proliferation and migration by activating MAPK and has been proposed as a prognostic marker in colorectal cancer (Ren *et al*., 2019). Likewise, APOC1 has been shown to activate MAPK/AKT via downregulation of miRNA (miR-519) to promote cell survival by also increasing DNA damage repair (Zhang *et al*., 2019). Another biomarker shown to influence DNA repair and regulate the cell cycle was CCNH which activates CDKs (Chou *et al*., 2020), and these were highly enriched in the radioresistance networks (Figure 5.7) and related to knockdown of CCND1 that resulted in the inhibition of the radioresistant phenotype (Figure 5.8). These biomarkers also relate to radioresistance networks identified among the proteomic data (Figure 5.7).

COL1A1 is associated with tumour invasion and migration and has also been identified as a potential biomarker of radioresistance in nasopharyngeal carcinoma (Xiao *et al.,* 2021), cervical cancer (Zhang *et al.,* 2021) and glioblastoma (Serafim *et al.,* 2021), and as far as we are aware, identified for the first time as a biomarker of radioresistance in EVs in BC and CMC in these data. This means that COL1A1 has the potential to be a reliable biomarker due to the consistent findings across cell lines and species. The data indicates that COL1A1 can be present in EVs, future studies could focus on the presence of COL1A1 in patient tumour aspirates, blood or urine in suspected patient cases of radioresistance.

ALK was identified as a potential biomarker from these data. Previous studies have shown that activation of ALK can induce stem-like phenotypes in recipient cells

resulting in radiotherapy resistance (Xu *et al.,* 2020), and in glioblastomas blocking ALK signalling via STAT-3 has shown to induce a radiosensitive phenotype (Xie *et al.,* 2019). The remaining biomarker CSTB, interestingly, was associated with epithelial cell inflammation and has shown to be increased in patients with epithelial cancer (Ventura *et al*., 2021). These biomarkers identified in these datasets are promising candidates for clinically relevant markers of the acquisition of radioresistance, and there was consistency between the findings from this analysis and previous studies. Due to the complex nature of biomarkers, future studies should focus on which biomarkers are consistently identified from EVs derived from radioresistant breast cancer cell lines by western blotting or flow cytometry to confirm an increase or decrease in protein expression, and if these findings can be replicated in EVs isolated from patient biofluids. The identification of such molecules could reveal future novel targets of radioresistance to help the personalisation of patient treatment plans in a clinical setting.

To summarise, EVs derived from REM134 RR and MDA-MB-231 RR cancer cell lines had increased protein expression of cell cycle regulators, DDR and upregulation of EMT. Upregulation of these pro-oncogenic features were also found in functional and canonical pathway analyses. Separate networks associated with radioresistance were plotted based on normalised EV protein expression from REM134 RR and MDA-MB-231 RR cancer cells, and these networks were found to be almost identical with CSC markers and cell cycle regulators being associated with both networks, and AKT and CCND1 upregulation being highlighted as potential drivers of radioresistance. Biomarker analysis also revealed six biomarkers of radioresistance, with AKT being named as one of them. These findings show there is high similarity between networks associated with the acquisition of a phenotype of radioresistance in triple-negative BC and CMC, and although there may be slight metabolic differences, the mechanisms by which radioresistance is developed may be highly similar. This findings may allow novel therapeutic approaches such as AKT or CCND1 inhibitors to be used in conjugation with chemotherapy to be used patients with suspected radioresistance in human and veterinary medicine.

6 Chapter 6: Discussion

The development of radiotherapy resistance results in breast cancer recurrence and treatment failure in human and veterinary medicine. The one health initiative strives to progress medicine for all species, via the use of dogs as models for human diseases, and dogs benefitting from medicines developed for humans. Breast cancer risk factors, causes, development and treatment are highly similar between the two species (Varallo *et al.,* 2019; Antuofermo *et al.,* 2007). The advancement of molecular profiling technologies has allowed for genomic, proteomic and metabolomic comparison studies to confirm high molecular similarities between CMC and BC, highlighting the benefit of using CMC cell lines as reliable *in vitro* models for BC research (Namagerdi *et al.,* 2020). EVs derived from cancer cells have shown to mediate cross-talk between developing cancer cells and the surrounding TME to promote tumour growth in CMC and BC (Lee *et al.,* 2021; Du *et al.,* 2022).

EVs are nanovesicles produced by almost all cells in the range of 30 nm – 150 nm (Lichen *et al*., 2019). EV content reflects the parental cell from which they are derived and content includes active protein, miRNA and lipids which can remodel the genome and proteome of recipient cells (Ham *et al*., 2018; Terlecki-Zaniewicz *et al.,* 2018). There are several studies showing that EVs derived from cancer cells can reprogramme cells in the TME to favour tumour development by nurturing the growth and spread of cancer, as well as chemotherapy resistant cancer cells being able to confer chemotherapy resistance to naïve cancer cells (Zhao *et al.,* 2021). Despite the detrimental effect of the development of radioresistance on patient outcome there are very few studies investigating the role of EVs in the acquisition of radioresistance. Therefore, the hypothesis of this project was that EVs derived from radioresistant breast cancer cells can confer radioresistance to recipient cells. This project was ablet to accept this working hypothesis and proceeded to investigate potential pathways that could be responsible for the induction of a radioresistant phenotype by analysing the protein content of EVs. This could hopefully identify future novel targets or biomarkers for radiotherapy resistance that may be used to

complement or personalise breast cancer treatment plans in human and veterinary medicine to improve patient survival.

6.1 Radioresistant REM134 RR and MDA-MB-231 RR breast cancer cells have increased rates of migration and altered cell cycle distributions compared to their nonRR counterparts

To compare potential tumour cell biology between CMC and BC, the panel of cells used in this project are the REM134 CMC cell line, and the MDA-MB-231 triple-negative BC cell line. There is a clinical unmet need for novel therapies in veterinary medicine, if the biological mechanisms of radiotherapy resistance are similar on a molecular level, this means novel treatments for therapy resistance used in human medicine may also be applicable to veterinary medicine.

The REM134 RR and MDA-MB-231 RR cancer cells were irradiated at 15 Gy every 4-6 weeks to ensure a selection pressure and it was found that the RR cells had a more mesenchymal phenotype (Figure 3.3) with a larger percentage of cells in the G2 phase of the cell cycle (Figure 3.6). The mesenchymal phenotype could also be associated with the induction of a stem-like phenotype (Aschenbrenner *et al.,* 2021). Following cell cycle analyses for the panel of cell lines used for this project, it was found the REM134 RR and the MDA-MB-231 RR cell lines had a higher percentage of cells in the G2 phase of the cell cycle when compared to their non-RR counterparts (Figure 3.6; Table 3.1). This agrees with literature stating that there is an increased percentage of cells in the G2 phase of the cell cycle to promote cell survival due to the increased rate of DNA damage repair required to ensure survival following irradiation that would otherwise kill non-RR cells (Masoudi-Khoram *et al*., 2020). Further studies could look at the effect of EVs derived from RR cells and see if this can increase the G2 phase of the cell cycle in recipient cells. An increased percentage of cells in the G2 phase of the cell cycle is associated with a radioresistant phenotype (Masoudi-Khoram *et al*., 2020), if this radioresistant phenotype can be conferred to

recipient cells it could be a potential phenotype to target to improve the effectiveness of patient radiotherapy treatment plans. These findings could also provide a potential target for altered cancer therapy such as chemo-irradiation and G2 checkpoint regulator inhibitors to specifically target RR cells in the G2/M phase. Cisplatin treatment alongside radiotherapy was found to radiosensitise cells and resulted in an increase in apoptosis in cell lines (Iwata *et al.,* 2020), even in mesenchymal stem cells (Rühle *et al.,* 2017). Similarly, forcing progression from G2 to M phase by activating cell cycle progression inhibitors could specifically target RR cells that are in G2/M phase arrest (PosthumaDeBoer *et al.,* 2011).

6.2 EVs derived from REM134 RR and MDA-MB-231 RR breast cancer cells can induce chemotherapy and radiotherapy resistance potentially by promoting growth and proliferation of breast CSCs

Following the characterisation of cell lines and successful isolation of EVs, the second objective of this project was to determine the effect of EVs derived from non-RR cells and RR cells on recipient cells (Figure 4.1). The results indicated that EVs derived from RR cells are more readily taken up, can increase cell viability and colony forming ability, increase chemoresistance and radioresistance of recipient nonRR and RR cancer cells. The MDA-MB-231 RR cancer cells had a higher baseline resistance to Doxorubicin at 0.001 and 0.01 µM (Figure 4.8 D) compared to the REM134 RR cancer cell line (Figure 4.8 B). Similarly, it was noted during the maintenance of the radioresistant cells that the REM134 RR cancer cells would recover the quickest from irradiation when compared to the MDA-MB-231 RR cells, but would have a larger percentage of cell death. This could potentially explain the differences seen in Figure 4.9 where the REM134 RR appears to have a much higher baseline of resistance at 2.5 Gy and 5 Gy (Figure 4.9, B) when compared to the MDA-MB-231 RR baseline resistance (MDA-MB-231 RR). However, this could be because the assay was finished on day 10 and it was noted that as radiotherapy doses were increased from 8 Gy to 15 Gy that the MDA-MB-231 RR cancer cells had overall cell death but took longer than the REM134 RR cancer cells to recover.

The data showed that EVs derived from RR cells significantly increased the number and size of tumourspheres formed in both nonRR and RR cell types. To analyse potential mechanisms of how EVs could have this effect, the uptake of EVs derived from nonRR and RR cancer cell lines was analysed. This increased uptake of EVs derived from RR cells could also explain the significant increase in the cell viability in all recipient cell lines when treated with EVs derived from RR cells. If more EVs are taken up by the RR recipient cells, the biological effect of promoting proliferation may be further increased when compared to EVs derived from nonRR cells. Similarly, this could also explain the increase in migration rate of recipient cells after the addition of EVs derived from RR cancer cells (Figure 4.7). A few studies have highlighted similar findings in head and neck squamous cell carcinoma in a study by Mutschelknaus *et al*., (2016) who showed that EVs derived from once irradiated cancer cells could increase migration rate in nonRR recipient cells by activating the AKT pathway. They used head and neck squamous cell carcinoma cell lines (FaDu and BHY) and irradiated at doses ranging from 2 Gy to 10 Gy before isolating EVs. The panel of cell lines used in this project are similar as they are also carcinoma cell lines; however, these cell lines are established RR cancer cell lines, not cancer cells that have received just one dose of irradiation. The activation of the AKT pathway has also been identified as an increased pathway in MDA-MB-231 RR and REM134 RR cells (Gray *et al.,* 2019). This aligns with results showing that EVs from the RR cells can increase the rate of migration (Figure 4.7). This could potentially mean that if RR breast cancer cells have activated AKT, that this could potentially be packaged in to EVs derived from RR breast cancer cells, so the addition of these EVs on to RR cells may be able to influence the recipient cells AKT activation to result in an increased rate of migration.

The activation of AKT pathway and increased motility in recipient cells is also associated with metastasis in breast cancer patients (Zhang *et al.,* 2022). AKT has found to induce migration by increasing expression of MMP9 and MMP2 allowing cancer cells to breakdown the extracellular matrix and begin local invasion and

distant metastasis (Xu *et al.,* 2021). EVs derived from irradiated head and neck squamous cell carcinomas have found to increase MMP activity in recipient cells, and clinical breast cancer specimens from patients with metastasis have increased MMP9 expression (Bi *et al.,* 2021). Cellular motility was highlighted to be a characteristic in the REM134 RR and MDA-MB-231 RR cancer cells as per section 5.2.2. Additionally, after performing a network analysis to identify pathways associated with the radioresistant phenotypes in both the REM134 RR and MDA-MB-231 RR cancer cells, AKT was indicated to have an association with the radioresistant phenotype as shown in section 5.2.4. To summarise, EVs from RR cancer cells activate MMPs that are downstream from AKT, resulting in patient metastasis. The use of AKT/MMP2/MMP9 profiling in patients could have the potential to be used in conjugation with the profiling of the G2 phase of the cell cycle to indicate the presence of radioresistant tumour cells. This could mean treatment plans could be tailored to include AKT inhibitors such as capivasertib, which when used in conjugation with chemotherapy can increase the survival of patients with triple-negative breast cancer (Kilock, 2020). Additionally, COL1A1 was found to be a biomarker of radioresistance in breast cancer when comparing pre- and post-irradiation breast cancer tumour samples (Yao *et al.,* 2022). Dysregulated protein activity is associated with a malignant phenotype, CSTB expression has found to be highly increased in the MDA-MB-231 cell line (Salcedo *et al.,* 2021).

After confirming the ability of EVs from RR cells to increase the rate of proliferation and migration of all recipient cells, this project aimed to investigate the effect of EVs derived from RR cell types on chemotherapy and radiotherapy. The results showed that EVs derived from RR cell types were able to increase the chemoresistance in all recipient cell types (Figure 4.8). Other studies have shown that chemoresistance can be transferred from chemotherapy resistant cancer cells via the transfer of ABC transporter in EVs, as the transfer of ABCs to recipient cells allows the increased efflux of chemotherapeutic agents (Jena *et al.,* 2021). It has been proven that EVs containing ABCs result in the increased efflux of chemotherapeutic agents as the increased presence of ABCs in recipient cells cannot be achieved by *de novo* synthesis (Federici *et al.,* 2014; Lv *et al*., 2014). However, the cell panel were

chemotherapy naïve cells, but the transfer of EVs derived from RR cells had the ability to confer chemotherapy resistance to recipient cells (Figure 4.8). Analyses of the EV protein content from REM134 RR cells showed that potentially activated pathways include ATM signalling (Figure 5.5) along with increased expression of DNA ligase 3 (Table 5.3) which senses double and single stranded DNA breaks and performs the final ligation of DNA (Czajkowski *et al.,* 2022). Decreased expression of the DDR inhibitor ATRX was found in EVs derived from MDA-MB-231 RR cells (Table 5.6) along with increased expression of proteins associated with DDR such as ATP2C1 (Table 5.5). Cells treated with chemotherapy accumulate DNA damage as chemotherapeutic agents target enzymes associated with DNA synthesis and repair (Shakya *et al.,* 2022). Such agents include Doxorubicin that intercalates between DNA preventing replication, induce DSBs by trapping topoisomerase II on to DNA and also increases production of ROS (Sahin *et al*., 2022; Mastrangelo *et al.,* 2022; He *et al.,* 2020).

The increased DDR capacity could be transferred from EVs derived from REM134 RR and MDA-MB-231 RR cells, as other studies have shown specifically that EV content from RR cells can increase DNA damage repair in recipient cells (Tortolici *et al.,* 2021). An increase in proteins associated with DDR could also explain the result of EVs derived from RR cells increase radioresistance in all recipient cells (Figure 4.9). Data analyses of the proteomic content of EVs from MDA-MB-231 RR cells showed significant functional expression of proteins associated with free radical scavenging (Figure 5.3). Other studies have shown that the EVs derived from CSCs are highly enriched in proteins that induce stemness in recipient cells such as Notch-1, CD133 and CD44 (Sun *et al.,* 2020; Wang *et al*., 2019), and that cancer cells that have acquired radioresistance also acquired stem-like properties (Bai *et al*., 2021). Analyses of the protein content of EVs derived from REM134 RR cancer cells showed potential increased expression of the transcription regulator TWIST1 (Table 5.3) and decreased expression of FOXA3 which inhibitors stem-like properties (Table 5.4). Likewise, functional expression analyses indicated that embryonic development was enriched in EV protein content derived from REM134 RR cells (Figure 5.2) and MDA-MB-231 RR cells (Figure 5.3). It has been found that EVs derived from irradiated cells

can revert cancer cells to a stem-like state via activation of Notch-1, with additional studies showing these stem-like cells then release pro-oncogenic content in their EVs such as VEGF to induce angiogenesis (Boelens *et al.,* 2014; Treps *et al*., 2017). Further research should investigate if there is a cellular switch towards a more stem-like phenotype, or if the EVs derived from RR cells can revert breast cancer cells to have a more stem-like phenotype alongside increasing the subpopulation of breast CSCs.

The CSC population within a developing tumour can self-renew, have inherent resistance to environmental changes within the TME, and are also inherently resistant to chemotherapy and radiotherapy (Oshimori *et al.,* 2015; Zheng *et al.,* 2021). Therefore, CSCs are associated with promoting tumour cell survival following radiotherapy treatment in patients. Further analyses included the effect of EVs derived from RR cells on the tumoursphere forming ability, and the chemosensitivity and radiosensitivity of the tumoursphere population. The results showed that EVs derived from both non-RR and RR cancer cell types resulted in a significant increase in size and number of tumourspheres formed, but EVs derived from RR cells could significantly increase the size and number of tumoursphere formation in all breast CSCs when compared to EVs derived from nonRR cells (Figure 4.13; Figure 4.14). These findings could mean that during radiotherapy a large percentage of cancer cells die, and considerably less radioresistant cancer cells undergo apoptosis. This means that RR breast cancer cells that survive radiotherapy will produce more EVs (Arscott *et al.,* 2014), and if taken up by remaining breast CSCs, could promote the survival of the tumour by increasing the size and number of tumoursphere formation. The chances of cancer recurrence could also be increased, as EVs from residual RR breast cancer cells could simultaneously increase the chemotherapy and radiotherapy resistance in breast CSCs as shown by the data. The targeting of specific EVs and their content is incredibly complex, and uptake of EVs cannot be inhibited specifically for cancer cells alone. To date, research has shown it is easier to prevent EV release than uptake due to the many mechanisms of EV uptake (described in section 1.8.2). Therefore, inhibitors of EV release target the docking of the MVBs at the cellular membrane to prevent release of EVs in to the extracellular

space (Zhang *et al.,* 2020). However, in the context of cancer therapies, these EV inhibitors would not be specific to cancer cells, and the use of EV release inhibitors could prevent cell to cell communication in all non-cancerous cells (Hao *et al.,* 2021). However, as this project has shown, the significant effect of EVs derived from RR cancer cells on promoting the growth and survival of breast CSCs means that CSCs population should have a greater focus when considering cancer therapy options for advanced stage cancer patients with suspected metastases.

The ability of EVs derived from RR cancer cells to confer radioresistance has not been widely researched, with the few studies that have analysed EV content are mainly from cancer cells that have received only one dose of radiotherapy. These EVs were able to increase cell proliferation in recipient cells which was associated with a change in EV protein content – decreased tumour suppressors and increase in oncogenic content including Notch, Jak-STAT, and cell cycle pathways (Mrowczynski *et al*., 2018; Dai *et al.,* 2019). Expression of Notch is associated with promoting a cancer stem cell phenotype which can result in increased tolerance to environmental changes and resistance to therapy (Fultang *et al.,* 2021); therefore, activation of the Notch pathway may potentially be a pathway increased in breast cancer cells that have a radioresistant phenotype and should be further investigated in the context of the acquisition of radioresistance.

To summarise, the hypothesis of this project was that EVs derived from radioresistant breast cancer cells can confer a radioresistant phenotype. All findings considered, this working hypothesis can be accepted and the effect of EVs from REM134 RR and MDA-MB-231 RR cancer cells have demonstrated their ability to induce therapy resistant biological changes in recipient cells (Figure 6.1).

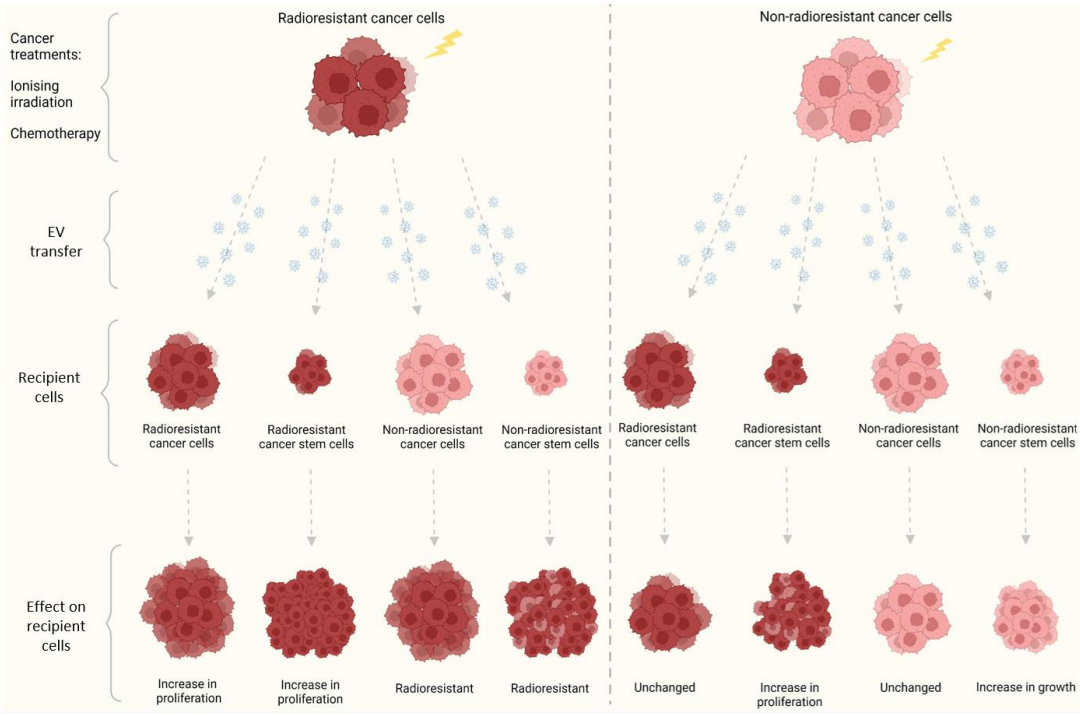


Figure 6.1 EVs derived from radioresistant breast cancer cells can induce radioresistance in recipient cells. *Schematic depicts the biological changes that occur upon the transfer of EVs from nonRR and RR breast cancer cells on breast non-CSCs and breast CSCs. Darker red depicts a radioresistant phenotype and lighter pink depicts a nonRR phenotype (Created in BioRender.com).*

The role of conferring radiotherapy resistance appears to be interlinked with chemotherapy resistance in chemotherapy naïve cells, with findings indicating the effects on the cancer stem cell population as drivers of this resistance. These findings should be considered for future treatments in human and veterinary medicine, as they indicate the need for additional targets that do not primarily focus on DNA damage such as radiotherapy and chemotherapy. Future therapies could be focused towards identifying novel targets for the cancer stem cell population to be used in conjugation with chemotherapy and radiotherapy with the aim to eradicate the cancer cell and cancer stem cell populations in cancer patients.

6.3 Networks associated with radioresistance are DDR, CSCs and the AKT pathway

The analyses completed for this project demonstrated the ability of EVs derived from RR cancer cells to confer radioresistance to non-CSCs and breast CSCs. To identify potential biomarkers of radioresistance, or even potential novel drug targets to radiosensitise cells, EVs were isolated from the established RR cancer cell lines and their nonRR counterparts. The aim of the latter part of this project was to analyse EV content derived from nonRR (REM134 and MDA-MB-231) and RR (REM134 RR and MDA-MB-231 RR) cancer cells to identify potential pathways that could be associated with the acquisition of radioresistance. The protein content of the isolated EVs was analysed by using a "shotgun" method of mass spectrometry. This is where no amino acid labelling techniques are used and any proteins identified from the samples are analysed.

Functional expression analyses found there were expected results such as significant expression of processes associated with cell death and survival and processes involving the cell cycle in both the REM134 RR and MDA-MB-231 RR (Figure 5.3). However, free-radical scavenging was found to significantly increased expression ($p<0.05$) in EVs derived from the REM134 RR (Figure 5.3 A). Due to the REM134 RR cancer cells receiving irradiation, this would result in an increase in free radicals upon the hydrolysis that occurs within the cell, meaning the REM134 RR cancer cells may promote free-radical scavenging mechanisms that are not seen in the MDA-MB-231 RR cancer cells.

Following functional analyses, canonical pathway enrichment was analysed which showed that there were potential metabolic differences between the REM134 RR and the MDA-MB-231 RR cancer cells, as oxidative phosphorylation was the most enriched pathway in EVs from MDA-MB-231 RR cancer cells (Figure 5.5), with ATM signalling being highly enriched ($p<0.001$) which could be attributed to the increased

rate of DDR. This could mean that MDA-MB-231 RR cancer cells do not have a metabolic switch to glycolysis, which results in more DDR, but may still survive radiotherapy due to having increase ATM signalling (Figure 5.5). Whereas the metabolic status of the REM134 RR cancer cells could not be determined from the canonical pathway analyses, but the increased expression of free-radical scavengers could contribute to radioresistance in the REM134 RR cancer cells. The canonical pathway enrichment data and pathway ranking indicates that the REM134 RR cancer cells may be radioresistant by activation of different pathways than compared to the MDA-MB-231 RR breast cancer cells.

Canonical pathway analyses of EV conent derived from the REM134 RR cancer cells showed enrichment for CREB signalling and FAK signalling were the most highly enriched canonical pathways based on the EV protein content from REM134 RR cancer cells (Figure 5.4). CREB signalling and FAK signalling are associated with cell survival, proliferation, differentaiton, migration and survival and FAK signalling has been found to activate the Hippo pathway (Shen *et al.,* 2018). The hippo pathway is associated with the induction of a CSC phenotype and involves two major molecules, YAP and TEAD1 (Yang *et al.,* 2022) which was identified in both REM134 RR and MDA-MB-231 RR networks of molecules that were associated with the radioresistant phenotype. Additionally, there appeared to be differences in metabolic activity with oxidative phosphorylation being highly expressed in the MDA-MB-231 RR data (Figure 5.5) with very low expression in the REM134 RR dataset when the two were directly compared (Figure 5.6). Additionally, there was an increased expression of SNARE signalling only seen in the MDA-MB-231 RR content (Figure 5.5), indicating a higher level of EV release (Xu *et al.,* 2022). This indicates that MDA-MB-231 RR breast cancer cells release more EVs than the nonRR MDA-MB-231 cancer cells which agrees with previous finding in Chapter 3.2.1 in Table 3.2.

Analysis of the mass spectrometry data showed that the content of the EVs from RR cancer cell lines had decreased expression fold changes associated with tumour suppressors and molecules associated with DDR and cell cycle regulators had

increased fold change. A network plot from IPA showed that the simultaneous inhibition of AKT and CCND1 may "inhibit" the RR phenotype. The content of EVs reflects the cell from which it is derived, this means that the RR phenotype seen in the EVs could be the cellular pathway in the parental cell that drives radioresistance. Previous findings have shown that CCND1 is downstream of AKT and CCND1 can form a positive feedback loop between known as the AKT/CCND1/CDK4 survival pathway, and that this pathway is also what provides CSCs with their resistant phenotypes (Shimura *et al.,* 2012). This means that the AKT/CCND1/CDK4 pathway may be the pathway responsible for both intrinsic and acquired radioresistance in cancer cells, which also resonates with other findings in this project previously identifying the potential role of AKT and altered cell cycle regulation being features of RR cancer cells. As AKT and CCND1 appear to be potential drivers of radioresistance, it could also make them ideal novel therapeutics. There are already drug trials using AKT inhibitors (Zhang *et al.,* 2022) and CCND1 inhibitors in BC patients with metastases, that show promising results of prolonging life (Montaudon *et al*., 2020). Future studies could look at the use of dual inhibitors, such as the CDK4/6 inhibitor Palbociclib and AKT inhibitors which have currently been trialled in malignant pleural mesothelioma which is also known to be highly aggressive (Bonelli *et al.,* 2020).

All findings considered, the specific molecular and metabolic pathways by which canine REM134 RR and human MDA-MB-231 RR cancer cells induce radioresistance may differ as indicated by functional expression and canonical pathway analyses. However, the resulting networks activated seems largely associated with DDR, AKT and inducing a breast CSC phenotype which can result in a protective effect (Figure 6.2).

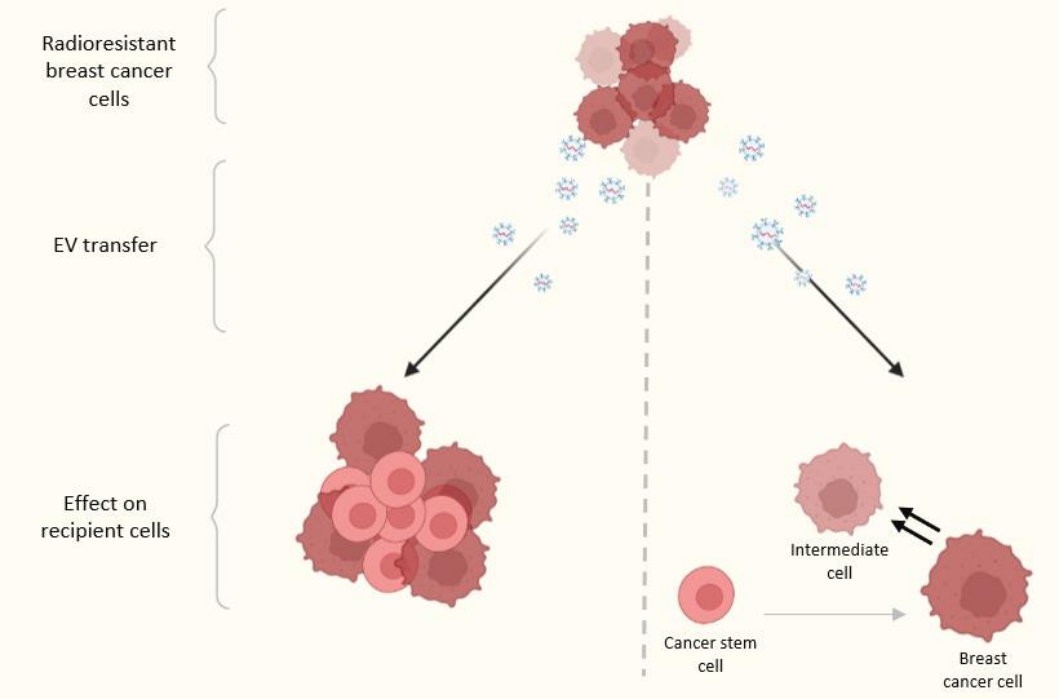


Figure 6.2 Transfer of EVs from radioresistant breast cancer cells appears to be associated with the induction of cancer stem cells. *Diagram showing potential mechanisms that breast CSCs could be induced in recipient cells. Pink spherical cells represent breast CSCs, and red cells represent breast cancer cells (Created in BioRender.com).*

Bioinformatic analyses indicated the inducation of a stem cell-like phenotype (Figure 5.7). A question remains as to how this effect is induced, as EVs transferred to recipient cells could promote growth of breast CSCS (Figure 6.2, left), or if EV transfer could induce CSC-like cellular signalling such as AKT and DDR pathways that somewhat revert the phenotype to an intermediate between a breast CSC and a breast cancer cell (Figure 6.2, right).

These data suggest that proteins in EVs derived from REM134 RR and MDA-MB-231 RR breast cancer cells could contain content that is associated with the induction of a CSC phenotype as indicated by network analyses. Bioinformatic analyses in this project showed theoretical inhibition of CCND1 and AKT could inhibit the phenotype

of radioresistance in both REM134 RR and MDA-MB-231 RR cell lines (Figure 5.8 A, B). These findings need to be confirmed *in vitro* before identifying their true potential as novel targets of radioresistance; however, the repeated identification of the induction of a CSC phenotype cannot be ignored, so should be studied further in the context of breast cancer radioresistance. The networks associated with radioresistance show high homology between the REM134 RR and MDA-MB-231 RR cancer cell EVs and although there may be metabolic differences between the cell lines upon the acquisition of radioresistance, the overall mechanism appears to be highly similar. This outlines the potential applicability of therapy resistant treatment modalities in human medicine to veterinary medicine.

6.4 Biomarkers of radioresistance are associated with pathways such as DDR, AKT and CSCs

The aim of discovering biomarkers of radioresistance could allow the development of personalised treatment plans. The AKT and CCND1 pathways could be used as biomarkers of the development of radioresistance, and AKT was also identified as a potential biomarker of radioresistance by IPA after analyses of the EV content derived from the REM134 RR and MDA-MB-231 RR cancer cells used in this project. Upregulation of CCND1 and AKT have found to be associated with miR-19b, and is a suggested biomarker of breast cancer (Li *et al.,* 2018), and EV miR-19b is associated with inducing radioresistance and stem like phenotypes in colorectal cancer cells by increasing expression of CCND1 (Sun *et al.,* 2021). Therefore, it could be beneficial to review and identify miRNA content that is associated with upregulation of CCND1 and AKT in EVs derived from BC and CMC patients that have developed radioresistance. COL1A1 was also identified as a biomarker of human and veterinary radioresistance following network analyses in IPA. COL1A1 was found to prevent apoptosis in cervical cancer cell lines by affecting caspase-3/PI3K/AKT pathway to regulate cell death, and COL1A1 was found to be indicative of a radioresistant phenotype in clinical specimens (Liu *et al.,* 2017). In breast cancer, COL1A1 has also been suggested to be a biomarker of radiation resistance, as COL1A1 expression was

found to be in increased in data models that analysed profiler breast cancer tumours (Yao *et al.,* 2022). COL1A1 signalling may be associated with radioresistance due to the enhanced ability of EMT seen in radioresistant cells, leading to the association of COL1A1 with breast cancer metastasis to the brain (Wu and Linlin, 2022), and this metastasis being inhibited by silencing of the COL1A1 gene (Liu *et al*., 2018).

APOC1 was also identified as a potential biomarker of radioresistance in this project (Figure 5.9). APOC1 has been shown to activate MAPK/AKT to promote cell survival by also increasing DNA damage repair (Zhang *et al*., 2019). Increased expression of APOC1 has found to be a biomarker of breast cancer in the MDA-MB-231 breast cancer cell line and APOC1 peptides were found to inhibit cell proliferation *in vitro* and tumour growth *in vivo* (Sun *et al.,* 2016). The data analyses showed that EV content from the REM134 RR and MDA-MB-231 RR had increased expression of APOC1 which could indicate the promotion of a pro-oncogenic phenotype and increased activation of AKT.

Additionally, ALK was also identified as a potential biomarker of radioresistance following proteomic analyses of EV content derived from REM134 RR and MDA-MB-231 RR breast cancer cells. There are no studies stating the ALK expression status in canine mammary carcinomas, but one key study showed ALK was overexpressed in 36% of patient tumours with triple-negative breast cacner and was associated with high rates of tumour growth proliferation by the activation of the AKT pathway (Siraj *et al.,* 2015).

The final biomarker of radioresistance identified was CSTB. The increased expression of CSTB is associated with increasing lysosomal activity within the cell. However, there are few studies in the literature showing CSTB as a functional biomarker of radioresistance in cancer. There are no studies stating CSTB as a marker of radioresistance, but there are few studies discussing the potential of CSTB to be a biomarker of the acquisition of a malignant phenotype. One study stated that CSTB

is a marker of lysosomal activity and highlighted increased expression of CSTB as a biomarker in colorectal cancer when used in conjugation with other markers for a poorer overall survival (Sun *et al.,* 2022). Another study stated that CSTB prevents cathepsin leaking from lysosomes and causing uncontrolled proteolysis, and then identified downregulation of CSTB to be a biomarker of the acquisition of a malignant phenotype in oral squamous cell carcinoma tumour samples (Xu *et al.,* 2021). Therefore, the identification of CSTB needs many more validation studies in the context of radiotherapy of cancer cells *in vitro* and in clinical samples.

All data considered, the biomarkers of radioresistance seem to be linked to DDR and the AKT pathway, with some markers such as COL1A1, AKT and CCNH already having some promising clinical data that may endorse further research into their validity as a biomarker of breast cancer radioresistance. However, the biomarkers CSTB and ALK are not as widely researched in breast cancer radioresistance other than their identification in these analyses; therefore, further validation of their potential use as biomarkers needs to be conducted.

6.5 Future studies and directions

The potential novel targets and biomarkers identified in this project could be validated further to begin to explore the development of personalised treatment plans for advanced stage cancer patients who have suspected radioresistance. There are several future directions in terms of experiments and theories that can be derived from the findings in this project. The data from chapter 4 is currently published Payton *et al.,* (2021). However, the data from Chapter 5 is yet to be published, this is because the theoretical findings from the bioinformatic analyses are yet to be confirmed as this could not be completed due to the time restraints of this project. Validation experiments could include obtaining cell lysate samples for REM134, REM134 RR, MDA-MB-231 and MDA-MB-231 RR breast cancer cells and western blotting to confirm expression patterns of AKT and CCND1 identified in Chapter 5. Therefore, if these findings are confirmed, Chapter 5 could be published

as a comparison of the proteomes from EVs of human breast cancer with canine breast cancer EVs in the context of the acquisition of a radioresistant phenotype. Highlighting the key networks that play a role in the acquisition of radioresistance would hopefully allow the development of novel therapies, and demonstrate how novel drugs that are most likely to be utilised in human medicine could also be applicable in veterinary medicine to advance the treatment options available for veterinary cancer patients.

Once the bioinformatic findings of this project have been validated, future studies could explore the use of dual inhibitors to be incorporated to modify personalised treatment plans. Such modifications could include the use of dual inhibitors, altering the treatment course of fractionated radiotherapy (usually lower doses of 2-5 Gy up to 3 weeks totalling around 30 – 40 Gy (Kim *et al.,* 2021) if biomarkers of radioresistance are detected, or altering chemotherapy treatment depending on the patient's side effects. Recently, EVs have shown to have potential as drug nanocarriers and studies have shown that EVs can be loaded with chemotherapy drugs which are delivered to recipient cancer cells, which then show successful killing of cancer cells in several cancer types including glioblastoma and melanoma (Cenik *et al.,* 2021; Liang *et al.,* 2021). Recently nanocarrier vaccines have been developed for triple negative breast cancer, whereby EV derived from cervical cancer HeLa cells were loaded with immunogenic cell death inducer molecules which induced tumour inhibition in triple negative xenograft models and patient-derived human organoids (Huang *et al.,* 2022). These recent experiments are working with the aim of developing the ability to remove patient's EVs, edit their content, and re-inject patients with EVs to allow a nanodrug carrier system.

EVs as nanocarriers have shown promising results when compared to liposomes and artificial nanocarriers, as the small size of EVs means they can pass the blood brain barrier, which could be considered an attractive feature in the context of breast cancer as sites of secondary metastasis include the brain (Altei *et al.,* 2022). Additionally, the double membrane means the EV content remains stable when they

are isolated from patient biofluids and when re-injected *in vivo* (Liang *et al.,* 2021). EVs also have an advantage over other nanocarrier systems because they formed and developed inside the patients own cells, meaning their specific content on their outer double membrane means they are not targeted by the immune system as they are recognised as "self" (Jiang *et al*., 2021).

A potential limitation on expanding on this project to ascertain if EVs derived from patients with suspected radioresistance have any of the expression patterns of biomarkers identified in this study would potentially have to use an alternative method of EV isolation. This is because UC has found to result in a lower yield of EVs from clinical samples such as plasma, with magnetic beads proving to have a more efficient EV isolation (Chen *et al.,* 2018).

Future studies could build on this project to reveal the true potential for developing personalised treatment plans. Firstly, this project showed that the acquisition of chemotherapy and radioresistance after the transfer of EVs from RR cells may be associated with the induction of a cancer stem-like phenotype and this has been demonstrated in the literature (Chen *et al.,* 2020; Liu *et al.,* 2020). If the stem-like state of therapy resistant cells is similar to CSC cells, it could be useful to develop cancer treatments specifically for CSCs, that may also kill cells with radioresistance if the molecular pathways within the cell are similar i.e. are driven by AKT/CCND1/CDK4. Secondly, irradiated cancer cells have also shown to take up more EVs compared to unirradiated cancer cells (Arscott *et al.,* 2013), and the data also showed the same trend. Future studies could determine if EVs derived from RR cancer cells are also preferentially taken up by cancer cells compared to healthy cells. If resistance to therapy is in fact associated with a stem-like state similar to CSCs and is driven by AKT/CCND1, this could provide a focal point for development of cancer therapeutics for cancer patients with radioresistance. If CSCs and cancer cells with radioresistance have developed mechanisms to selectively take up EVs derived from RR cancer cells to promote cell survival, this could be exploited in future cancer therapies. Theoretically, patients with RR cancer could have primary

tumour cells cultured and have the biological content of their EVs edited to contain dual inhibitors or chemotherapy, then isolate the edited EVs that will be injected back in to the cancer patient. In principle the patient's edited EVs could be preferentially taken up by RR cancer cells and cancerous cells, with the lowest uptake by non-cancerous cells if the constituents present on the surface of the double lipid bilayer associated with radioresistance; therefore, selective uptake remain unchanged throughout the EV editing. Then a course of fractionated radiotherapy could be given to patients to promote the uptake of EVs derived from RR cancer cells, alongside injections of therapeutically loaded EVs from that same cancer patient as a novel "trojan horse" method of cancer therapeutics.

Literature has stated that EVs derived from cancer cells with radioresistance have an increased release and uptake of EVs. This project identified that EVs derived from REM134 RR and MDA-MB-231 RR cancer cells are more readily taken up when compared to EVs from REM134 and MDA-MB-231 cancer cells (as per section 4.2.2). In the bioinformatic analyses, there were no definitive identifiers of proteins associated with EV uptake (outlined Figure 1.11); however, the metabolic switch from glycolysis to oxidative phosphorylation is reported to result in a 2-3 fold increase in EV release (Ludwig *et al.,* 2019). It may be that there were pathways associated with EV uptake that were not significant as the cut off for protein expression was set to +/- 1.3 (equivalent of $p<0.05$). Future studies could look at combining more technical repeats as there were n=3 techincal repeats used for mass spec analyses used in this project, whereas using n=3 technical repeats with each technical repeat comprised of n=3 biological repeats may reveal additional pathways that were missed in these analyses.

Finally, further studies could analyse the proteome of nonRR and RR breast cancer cells before and after incubation with EVs from nonRR and RR breast cancer cell lines to compare changes in protein expression and pathways. This project identified the effects of nonRR and RR REM134 and MDA-MB-231 EVs on nonRR and RR REM134 and MDA-MB-231 breast cancer cells (as shown in Chapter 4); however, analysing

the change in protein expression in these recipient cells could confirm the pathways to target for novel therapeutics. It would also be interesting to see if the protein expression differences identified in the REM134 RR and MDA-MB-231 RR EVs in this project (Figure 5.7) also appear in the proteomic dataset of recipient cells.

6.6 Limitations of this study

Firstly, a major limitation of this project was the use of cell lines; although their use allowed the aims to be fulfilled by simplistic experimental design, it minimises the clinical application of the results as 2D cell lines lack the complex TME. The triple-negative BC cell line has most similar receptor status (PR^-, ER^-, $HER2^-$) when compared to the REM134 receptor status (PR^-, ER^-, $HER2^+$) and molecular analyses has shown that when compared to BC cell lines, REM134 has the highest similarities with triple-negative BC (Namagerdi *et al.,* 2020). By using these cell lines in the context of breast cancers and the development of radioresistance, it could reveal the biological similarities and differences that may affect treatment outcomes further down the line. Other models of BC include xenograft mouse models, where human tumours are implanted into mice, although this allows for tumour development in a complex microenvironment, the mouse must be immunocompromised to prevent the implanted tumour being targeted by the immune system. This means that xenograft models are a useful model for tumour progression and metastases, but cancer development is heavily influenced by the immune system which limits the applicability of xenograft models to natural tumour development (Junior *et al.,* 2022). Additionally, organoids can be used as a model of BC. Organoids are derived from a primary tumour, this allows the formation of complex 3D structures when compared to 2D cell lines, but organoids are prone to diverge away from the primary tumour over time which can result in large variation in results when trying to perform experimental repeats (Ebrahimi *et al*., 2021). Although 2D cell culture lacks a TME, this study had a simple aim of identifying the effect EVs derived from RR cancer cells have on the acquisition of radioresistance, by

using 2D cell lines in this project, the complex biology of EVs and cancer radioresistance was simplified allowing the aims of this project to be fulfilled.

The use of the MDA-MB-231 and MDA-MB-231 RR cancer cell line is the most aggressive type of BC (Ovcaricek *et al.,* 2011). This complicated characterisation of the RR phenotype in Chapter 3, as the nonRR MDA-MB-231 cell line also has mesenchymal phenotype. There are currently no officially confirmed markers of radioresistance, which was a major limitation of this project. The main confirmation was that the MDA-MB-231 RR cancer cells could survive the 15 Gy doses of irradiation used to maintain the RR phenotype. Therefore, if more time were given for this project it would have been useful to have detected for expression markers identified as part of the radioresistance network (Figure 5.7). The use of DDR response markers could have been employed throughout the irradiation process and on recipient cells that were considered to have acquired a radioresistant phenotype. Additionally, the protocol for deriving breast CSCs has previously been validated (Pang *et al.,* 2011), if there were less time restrictions in this project it would have been ideal to confirm that the derived CSCs were in fact REM134 CSCs, and human MDA-MB-231 CSCs, therefore analysing for stemness markers such as Oct 3/4 and CD133 to confirm the presence of stem cells. Additionally, the tumourspheres formed could have been paraffin fixed an stained by IHC for markers of a hypoxic core (Gray *et al.,* 2020).

The isolation method of UC may also isolate similarly sized vesicles. Therefore, if more time were allowed in this project, flow cytometry or western blotting could have been used to confirm markers of EVs such as CD81, CD9, CD63, Alix or TSG101, as well as markers of larger vesicles that overlap in size such as ectosomes (Karimi *et al*., 2022; Mizenko *et al.,* 2021). Ectosomes are released from the membrane via outward budding and can be in the size range of 100 nm to 1000 nm and contain miRNA, RNA and proteins. NTA analysis cannot distinguish between EVs and ectosomes; however, TEM analysis of EVs shows a “cup” shape morphology which is not seen in ectosome samples as found in this project (Figure 3.8 D). The samples

analysed in this project appeared to have the classical morphology expected of EVs, but to ensure a majority EV population it would have been benefifical to test for ectosome markers such as annexin 2 (Bras *et al.,* 2022).

EVs from FBS have shown to increase growth and proliferation of HEK293 and HeLa cancer cells *in vitro*; therefore, for *in vitro* experiments it is important to deplete the FBS of EVs (Eitan *et al.,* 2015). However, this can also deplete the FBS of growth hormone which can decrease growth and proliferation of cells grown *in vitro* (Kornilov *et al.,* 2018). In the context of this project, it has been found that EV depleted FBS does not effect cellular responses to DNA damage *in vitro* (Eitan *et al.,* 2015). Data in this project showed that EVs could increased growth and proliferation in recipient cells (as shown in Chapter 4), with mostly significant data. However, the question remains what the true effect would be if complete FBS with no EVs (growth hormones still present) was used in this project.

Secondly, the data showed EVs derived from RR cancer cells are more readily taken up by recipient cells when compared to EVs derived from nonRR cells; however, in retrospect the cell number and incubation time used (45 minutes) was quite short. To determine statistical significance for future experiments it may prove beneficial to use a plate format to drastically increase the number of repeats performed and also incubate EVs with cells for a longer time than 45 minutes, as there would be a greater uptake of EVs when they are incubated with cells for longer, meaning larger numerical differences between background dye and EV samples when analysing the final MFI via flow cytometry. Additionally, it would have been useful to use more appropriate controls to ensure a robust experiment (section 4.2.2). Potential controls that could have been used include the use of boiled EVs that would result in membrane and protein disruption, or even unlabelled EV samples as controls. The use of such controls would have been more valid as a negative control than PBS due to having the same content (EVs) compared to the samples used in this assay.

Thirdly, the use of DMSO can be toxic to cancer cell lines unless used at a final concentration of 1% or less, with studies showing that concentrations less than 0.6-0.15% of DMSO results in no cellular toxicity in MDA-MB-231 breast cancer cells (Dubois *et al*., 2017; Nguyen *et al*., 2020). The highest concentration of DMSO used in cell-based assays in this project would have been 0.03% (as explained in section 2.8). However, it has not been researched what doses of DMSO could be toxic to REM134 cancer cell lines or tumourspheres like the ones used in this project; therefore, it would be useful to have treated cells with the relevant percentage of DMSO as a control along with cells treated with PBS.

Finally, if the time constraints of this project were not a limiting factor, it would have been more clinically relevant to isolate EVs from human or veterinary patient biofluids that have suspected radioresistance as the targets and biomarkers identified in this project would have been more clinically relevant in the context of the development of personalised medicine in CMC and BC. It is also known that the yield of EVs isolated from patient samples causes a bottleneck in the progression of the use of EVs within a clinical setting. Current personalised medicines are being developed by the absence or presence of molecular markers resulting in a "barcode" system, where the patient barcode can predict the potential progression and response to treatment of individual patients; therefore, allowing their therapy to be tailored to improve overall survival (Kim *et al.,* 2022; Patwardhan *et al.,* 2021). In particular relevance to this project, the creation of such a database would have been a great contribution to veterinary medicine in particular, as there is already a vast amount of research towards human patients in comparison to veterinary cancer patients.

6.7 Conclusion

The development of radioresistance in BC and CMC patients is correlated with cancer relapse, metastases and poor survival rates. Recently, EVs have shown to be responsible for modification of the TME in cancers that result in a pro-oncogenic

environment and cancer cell resistance to chemotherapy. Therefore, this project investigated the effect of EVs derived from RR cancer cells on the acquisition of radioresistance. It was found that EVs derived from RR cancer cells can transfer radioresistance to recipient cells, resulting in a more aggressive phenotype associated with an increased rate of migration and increased resistance to chemotherapy and radiotherapy in nonRR and RR cancer cells, potentially by increasing the size and number of the breast CSC population and promoting breast CSC chemotherapy and radiotherapy resistance. To untangle the complex molecular biology involved in the acquisition of radioresistance, EV protein content from the nonRR and RR cancer cells were analysed by mass spectrometry and performed bioinformatic analyses to identify potential novel targets and biomarkers of breast cancer radioresistance. The bioinformatic analyses agreed with the preliminary findings earlier in the project that indicated cancer cells with radioresistance have altered cell cycle regulation, and increased migration rates which similarly studies have identified to be directly associated with activation of AKT (Mutschelknaus *et al.,* 2016). The analyses by IPA identified potential inhibition of radioresistance by simultaneously downregulating expression of AKT and CCND1, and also identified AKT as a potential biomarker of radioresistance based on EV content from REM134 RR and MDA-MB-231 RR cancer cells. This project showed the biological effect of EVs in the context of radioresistance were incredibly similar between the panel of canine and human breast cancer cell lines used, meaning that future development of cancer therapeutics of dual inhibitors, or even EVs as drug nanocarriers could be trialled in dog models, or if already trialled in human medicine could be applicable in veterinary medicine to increase and prolong survival in cancer patients with radioresistance.

Chapter 7: References

ABAD, E., GRAIFER, D. & LYAKHOVICH, A. 2020. DNA damage response and resistance of cancer stem cells. Cancer Lett, 474, 106-117.

ABADIE, J., NGUYEN, F., LOUSSOUARN, D., PENA, L., GAMA, A., RIEDER, N., BELOUSOV, A., BEMELMANS, I., JAILLARDON, L., IBISCH, C. & CAMPONE, M. 2018. Canine invasive mammary carcinomas as models of human breast cancer. Part 2: immunophenotypes and prognostic significance. Breast Cancer Res Treat, 167, 459-468.

ABDELWAHAB YOUSEF, A. J. 2017. Male Breast Cancer: Epidemiology and Risk Factors. Semin Oncol, 44, 267-272.

ABERUYI, N., RAHGOZAR, S., POURABUTALEB, E. & GHAEDI, K. 2021. Selective dysregulation of ABC transporters in methotrexate-resistant leukemia T-cells can confer cross-resistance to cytarabine, vincristine and dexamethasone, but not doxorubicin. Curr Res Transl Med, 69, 103269.

ABDULRAHMAN, G. O., JR. & RAHMAN, G. A. 2012. Epidemiology of breast cancer in europe and Africa. J Cancer Epidemiol, 2012, 915610.

AHN, S., KWON, A., HUH, Y. H., RHEE, S. & SONG, W. K. 2022. Tumor-derived miR-130b-3p induces cancer-associated fibroblast activation by targeting SPIN90 in luminal A breast cancer. Oncogenesis, 11.

AKRIDA, I., BRAVOU, V. & PAPADAKI, H. 2022. The deadly cross-talk between Hippo pathway and epithelial-mesenchymal transition (EMT) in cancer. Molecular Biology Reports, 49, 10065-10076.

AL SAYED, A. D., ELSHENAWY, M. A., TULBAH, A., AL-TWEIGERI, T. & GHEBEH, H. 2019. Complete Response of Chemo-Refractory Metastatic Metaplastic Breast Cancer to Paclitaxel-Immunotherapy Combination. American Journal of Case Reports, 20, 1630-1635.

ALIPOOR, S. D., MORTAZ, E., VARAHRAM, M., MOVASSAGHI, M., KRANEVELD, A. D., GARSSEN, J. & ADCOCK, I. M. 2018. The Potential Biomarkers and Immunological Effects of Tumor-Derived Exosomes in Lung Cancer. Front Immunol, 9, 819.

AL-NEDAWI, K., MEEHAN, B., KERBEL, R. S., ALLISON, A. C. & RAK, J. 2009. Endothelial expression of autocrine VEGF upon the uptake of tumor-derived microvesicles containing oncogenic EGFR. Proc Natl Acad Sci U S A, 106, 3794-9.

ALTEI, W. F., PACHANE, B. C., SOUZA, C., MARQUES, M. M. C. & SELISTRE-DE-ARAUJO, H. 2022. New insights into the discovery of drugs for triple-negative breast cancer metastasis. Expert Opinion on Drug Discovery, 17, 365-376.

AMBROSONE, C. B., AHN, J., SINGH, K. K., REZAISHIRAZ, H., FURBERG, H., SWEENEY, C., COLES, B. & TROVATO, A. 2005. Polymorphisms in genes related to oxidative stress (MPO, MnSOD, CAT) and survival after treatment for breast cancer. Cancer Research, 65, 1105-1111.

AMIRKHANI NAMAGERDI, A., D'ANGELO, D., CIANI, F., IANNUZZI, C. A., NAPOLITANO, F., AVALLONE, L., DE LAURENTIIS, M. & GIORDANO, A. 2020. Triple-Negative Breast Cancer Comparison With Canine Mammary Tumors From Light Microscopy to Molecular Pathology. Front Oncol, 10, 563779.

ANASTASOV, N., HOFIG, I., VASCONCELLOS, I. G., RAPPL, K., BRASELMANN, H., LUDYGA, N., AUER, G., AUBELE, M. & ATKINSON, M. J. 2012. Radiation resistance due to high expression of miR-21 and G2/M checkpoint arrest in breast cancer cells. Radiation Oncology, 7.

ANDRESON, D. 2014. Mammary tumours in the dog and cat (part 2): surgical management. Companion Animal, 19(12), 648-653.

ANDO, S., GELSOMINO, L., PANZA, S., GIORDANO, C., BONOFIGLIO, D., BARONE, I. & CATALANO, S. 2019. Obesity, Leptin and Breast Cancer: Epidemiological Evidence and Proposed Mechanisms. Cancers, 11.

ANTUOFERMO, E., MILLER, M. A., PIRINO, S., XIE, J., BADVE, S. & MOHAMMED, S. I. 2007. Spontaneous mammary intraepithelial lesions in dogs - A model of breast cancer. Cancer Epidemiology Biomarkers & Prevention, 16, 2247-2256.

ARIYOSHI, K., MIURA, T., KASAI, K., FUJISHIMA, Y., NAKATA, A. & YOSHIDA, M. 2019. Radiation-Induced Bystander Effect is Mediated by Mitochondrial DNA in Exosome-Like Vesicles. Scientific Reports, 9.

ARMANDARI, I., ZOMERMAN, W. W., PLASSCHAERT, S. L. A., SMIT, M. J., MARTINI, T. E. I., DE CAMARGO MAGALHAES, E. S., HOGELING, S. M., ROZEMA-HUIZINGA, G. C., LOURENS, H. J., MEEUWSEN-DE BOER, T. G. J., SCHERPEN, F. J. G., DE BONT, E. & BRUGGEMAN, S. W. M. 2021. CREB signaling activity correlates with differentiation and survival in medulloblastoma. Sci Rep, 11, 16077.

ARSCOTT, W. T., TANDLE, A. T., ZHAO, S., SHABASON, J. E., GORDON, I. K., SCHLAFF, C. D., ZHANG, G., TOFILON, P. J. & CAMPHAUSEN, K. A. 2013. Ionizing radiation and glioblastoma exosomes: implications in tumor biology and cell migration. Transl Oncol, 6, 638-48.

ASCHENBRENNER, B., NEGRO, G., SAVIC, D., SOROKIN, M., BUZDIN, A., GANSWINDT, U., CEMAZAR, M., SERSA, G., SKVORTSOV, S. & SKVORTSOVA, I. 2021. Simvastatin is effective in killing the radioresistant breast carcinoma cells. Radiology and Oncology, 55, 305-316.

ASGHARZADEH, M. R., BARAR, J., POURSEIF, M. M., ESKANDANI, M., JAFARI NIYA, M., MASHAYEKHI, M. R. & OMIDI, Y. 2017. Molecular machineries of pH dysregulation in tumor microenvironment: potential targets for cancer therapy. Bioimpacts, 7, 115-133.

ASSANI, G., SEGBO, J., YU, X., YESSOUFOU, A., XIONG, Y., ZHOU, F. & ZHOU, Y. 2019. Downregulation of TMPRSS4 Enhances Triple-Negative Breast Cancer Cell Radiosensitivity Through Cell Cycle and Cell Apoptosis Process Impairment. Asian Pac J Cancer Prev, 20, 3679-3687.

ASSI, H. A., KHOURY, K. E., DBOUK, H., KHALIL, L. E., MOUHIEDDINE, T. H. & EL SAGHIR, N. S. 2013. Epidemiology and prognosis of breast cancer in young women. J Thorac Dis, 5 Suppl 1, S2-8.

AZIMI, I., PETERSEN, R. M., THOMPSON, E. W., ROBERTS-THOMSON, S. J. & MONTEITH, G. R. 2017. Hypoxia-induced reactive oxygen species mediate N-cadherin and SERPINE1 expression, EGFR signalling and motility in MDA-MB-468 breast cancer cells. Scientific Reports, 7.

AZZAM, E. I., DE TOLEDO, S. M., SPITZ, D. R. & LITTLE, J. B. 2002. Oxidative metabolism modulates signal transduction and micronucleus formation in bystander cells from alpha-particle-irradiated normal human fibroblast cultures. Cancer Res, 62, 5436-42.

BAGLIO, S. R., ROOIJERS, K., KOPPERS-LALIC, D., VERWEIJ, F. J., PEREZ LANZON, M., ZINI, N., NAAIJKENS, B., PERUT, F., NIESSEN, H. W., BALDINI, N. & PEGTEL, D. M. 2015. Human bone marrow- and adipose-mesenchymal stem cells secrete exosomes enriched in distinctive miRNA and tRNA species. Stem Cell Res Ther, 6, 127.

BAHR, M. M., AMER, M. S., ABO-EL-SOOUD, K., ABDALLAH, A. N. & EL-TOOKHY, O. S. 2020. Preservation techniques of stem cells extracellular vesicles: a gate for manufacturing of clinical grade therapeutic extracellular vesicles and long-term clinical trials. Int J Vet Sci Med, 8, 1-8.

BAI, X., NI, J., BERETOV, J., WANG, S., DONG, X., GRAHAM, P. & LI, Y. 2021. THOC2 and THOC5 Regulate Stemness and Radioresistance in Triple-Negative Breast Cancer. Adv Sci (Weinh), 8, e2102658.

BARONE, I., GIORDANO, C., BONOFIGLIO, D., ANDO, S. & CATALANO, S. 2020. The weight of obesity in breast cancer progression and metastasis: Clinical and molecular perspectives. Seminars in Cancer Biology, 60, 274-284.

BARKOVSKAYA, A., GOODWIN, C. M., SEIP, K., HILMARSDOTTIR, B., PETTERSEN, S., STALNECKER, C., ENGEBRAATEN, O., BRIEM, E., DER, C. J., MOESTUE, S. A., GUDJONSSON, T., MAELANDSMO, G. M. & PRASMICKAITE, L. 2021. Detection of phenotype-specific therapeutic vulnerabilities in breast cells using a CRISPR loss-of-function screen. Mol Oncol, 15, 2026-2045.

BATENBURG, N. L., WALKER, J. R., COULOMBE, Y., SHERKER, A., MASSON, J. Y. & ZHU, X. D. 2019. CSB interacts with BRCA1 in late S/G2 to promote MRN- and CtIP-mediated DNA end resection. Nucleic Acids Res, 47, 10678-10692.

BAUER, M., KANTELHARDT, E. J., STIEWE, T., NIST, A., MERNBERGER, M., POLITT, K., HANF, V., LANTZSCH, T., ULEER, C., PESCHEL, S., JOHN, J., BUCHMANN, J., WEIGERT, E., BURRIG, K. F., WICKENHAUSER, C., THOMSSEN, C., BARTEL, F. & VETTER, M. 2019. Specific allelic variants of SNPs in the MDM2 and MDMX genes are associated with earlier tumor onset and progression in Caucasian breast cancer patients. Oncotarget, 10, 1975-1992.

BEBELMAN, M. P., BUN, P., HUVENEERS, S., VAN NIEL, G., PEGTEL, D. M. & VERWEIJ, F. J. 2020. Real-time imaging of multivesicular body-plasma membrane fusion to quantify exosome release from single cells. Nature Protocols, 15, 102-121.

BEBELMAN, M. P., JANSSEN, E., PEGTEL, D. M. & CRUDDEN, C. 2021. The forces driving cancer extracellular vesicle secretion. Neoplasia, 23, 149-157.

BELLI, C., ANTONARELLI, G., REPETTO, M., BOSCOLO BIELO, L., CRIMINI, E. & CURIGLIANO, G. 2022. Targeting Cellular Components of the Tumor Microenvironment in Solid Malignancies. Cancers (Basel), 14.

BERKE, T. P., SLIGHT, S. H. & HYDER, S. M. 2022. Role of Reactivating Mutant p53 Protein in Suppressing Growth and Metastasis of Triple-Negative Breast Cancer. Oncotargets and Therapy, 15, 23-30.

BHATTA, B., LUZ, I., KRUEGER, C., TEO, F.X., LANE, D.P., SABAPATHY, K. AND COOKS, T., 2021. Cancer Cells Shuttle Extracellular Vesicles Containing Oncogenic Mutant p53 Proteins to the Tumor Microenvironment. Cancers, 13(12), 2985.

BHOO-PATHY, N., HARTMAN, M., YIP, C. H., SAXENA, N., TAIB, N. A., LIM, S. E., IAU, P., ADAMI, H. O., BULGIBA, A. M., LEE, S. C. & VERKOOIJEN, H. M. 2012. Ethnic differences in survival after breast cancer in South East Asia. PLoS One, 7, e30995.

BI, X., LOU, P., SONG, Y., SHENG, X., LIU, R., DENG, M., YANG, X., LI, G., YUAN, S., ZHANG, H., JIAO, B., ZHANG, B., XUE, L., LIU, Z., PLIKUS, M. V., REN, F., GAO, S., ZHAO, L. & YU, Z. 2021. Msi1 promotes breast cancer metastasis by regulating invadopodia-mediated extracellular matrix degradation via the Timp3-Mmp9 pathway. Oncogene, 40, 4832-4845.

BI, Z., LI, Q., DINGLIN, X., XU, Y., YOU, K., HONG, H., HU, Q., ZHANG, W., LI, C., TAN, Y., XIE, N., REN, W., LI, C., LIU, Y., HU, H., XU, X. & YAO, H. 2020. Nanoparticles (NPs)-Meditated LncRNA AFAP1-AS1 Silencing to Block Wnt/beta-Catenin Signaling Pathway for Synergistic Reversal of Radioresistance and Effective Cancer Radiotherapy. Adv Sci (Weinh), 7, 2000915.

BIAN, R., DANG, W., SONG, X., LIU, L., JIANG, C., YANG, Y., LI, Y., LI, L., LI, X., HU, Y., BAO, R. & LIU, Y. 2021. Rac GTPase activating protein 1 promotes gallbladder cancer via binding DNA ligase 3 to reduce apoptosis. Int J Biol Sci, 17, 2167-2180.

BIDDLE, A., GAMMON, L., LIANG, X., COSTEA, D. E. & MACKENZIE, I. C. 2016. Phenotypic Plasticity Determines Cancer Stem Cell Therapeutic Resistance in Oral Squamous Cell Carcinoma. Ebiomedicine, 4, 138-145.

BILEN, M. A., PAN, T. H., LEE, Y. C., LIN, S. C., YU, G. Y., PAN, J., HAWKE, D., PAN, B. F., VYKOUKAL, J., GRAY, K., SATCHER, R. L., GALLICK, G. E., YU-LEE, L. Y. & LIN, S. H. 2017. Proteomics Profiling of Exosomes from Primary Mouse Osteoblasts under Proliferation versus Mineralization Conditions and Characterization of Their Uptake into Prostate Cancer Cells. Journal of Proteome Research, 16, 2709-2728.

BISCHOFF, J. P., SCHULZ, A. & MORRISON, H. 2022. The role of exosomes in intercellular and inter-organ communication of the peripheral nervous system. FEBS Lett, 596, 655-664.

BOELENS, M. C., WU, T. J., NABET, B. Y., XU, B., QIU, Y., YOON, T., AZZAM, D. J., TWYMAN-SAINT VICTOR, C., WIEMANN, B. Z., ISHWARAN, H., TER BRUGGE, P. J.,

JONKERS, J., SLINGERLAND, J. & MINN, A. J. 2014. Exosome transfer from stromal to breast cancer cells regulates therapy resistance pathways. Cell, 159, 499-513.

BONELLI, M., TERENZIANI, R., ZOPPI, S., FUMAROLA, C., LA MONICA, S., CRETELLA, D., ALFIERI, R., CAVAZZONI, A., DIGIACOMO, G., GALETTI, M. & PETRONINI, P. G. 2020. Dual Inhibition of CDK4/6 and PI3K/AKT/mTOR Signaling Impairs Energy Metabolism in MPM Cancer Cells. Int J Mol Sci, 21.

BOREEL, D. F., SPAN, P. N., HESKAMP, S., ADEMA, G. J. & BUSSINK, J. 2021. Targeting Oxidative Phosphorylation to Increase the Efficacy of Radio- and Immune-Combination Therapy. Clin Cancer Res, 27, 2970-2978.

BONOTTO, M., GERRATANA, L., POLETTO, E., DRIOL, P., GIANGRECO, M., RUSSO, S., MINISINI, A. M., ANDREETTA, C., MANSUTTI, M., PISA, F. E., FASOLA, G. & PUGLISI, F. 2014. Measures of Outcome in Metastatic Breast Cancer: Insights From a Real-World Scenario. Oncologist, 19, 608-615.

BOZZA, W. P., ZHANG, Y., HALLETT, K., RIVERA ROSADO, L. A. & ZHANG, B. 2015. RhoGDI deficiency induces constitutive activation of Rho GTPases and COX-2 pathways in association with breast cancer progression. Oncotarget, 6, 32723-36.

BRAS, I. C., KHANI, M. H., RIEDEL, D., PARFENTEV, I., GERHARDT, E., VAN RIESEN, C., URLAUB, H., GOLLISCH, T. & OUTEIRO, T. F. 2022. Ectosomes and exosomes modulate neuronal spontaneous activity. J Proteomics, 269, 104721.

BRAVI, F., DECARLI, A. & RUSSO, A. G. 2018. Risk factors for breast cancer in a cohort of mammographic screening program: a nested case-control study within the FRiCaM study. Cancer Medicine, 7, 2145-2152.

BRAY, F., FERLAY, J., SOERJOMATARAM, I., SIEGEL, R. L., TORRE, L. A. & JEMAL, A. 2018. Global cancer statistics 2018: GLOBOCAN estimates of incidence and mortality worldwide for 36 cancers in 185 countries. Ca-a Cancer Journal for Clinicians, 68, 394-424.

BRUNETTI, B., BACCI, B., ANGELI, C., BENAZZI, C. & MUSCATELLO, L. V. 2021. p53, ER, and Ki67 Expression in Canine Mammary Carcinomas and Correlation With Pathological Variables and Prognosis. Veterinary Pathology, 58, 325-331.

BRYDSON, R., BROWN, A., HODGES, C., ABELLAN, P. & HONDOW, N. 2015. Microscopy of nanoparticulate dispersions. J Microsc, 260, 238-47.

BUISHAND, F. O., KIK, M. & KIRPENSTEIJN, J. 2010. Evaluation of clinico-pathological criteria and the Ki67 index as prognostic indicators in canine insulinoma. Veterinary Journal, 185, 62-67.

CABRERA-LICONA, A., PEREZ-ANORVE, X. I., FLORES-FORTIS, M., DEL MORAL-HERNANDEZ, O., GONZALEZ-DE LA ROSA, C. H., SUAREZ-SANCHEZ, R., CHAVEZ-SALDANA, M. & ARECHAGA-OCAMPO, E. 2021. Deciphering the epigenetic network in cancer radioresistance. Radiotherapy and Oncology, 159, 48-59.

CAI, S., SHI, G. S., CHENG, H. Y., ZENG, Y. N., LI, G., ZHANG, M., SONG, M., ZHOU, P. K., TIAN, Y., CUI, F. M. & CHEN, Q. 2017. Exosomal miR-7 Mediates Bystander Autophagy in

Lung after Focal Brain Irradiation in Mice. International Journal of Biological Sciences, 13, 1287-1296.

CAILLEAU, R., OLIVE, M. & CRUCIGER, Q. V. J. 1978. Long-Term Human Breast Carcinoma Cell Lines of Metastatic Origin - Preliminary Characterization. In Vitro-Journal of the Tissue Culture Association, 14, 911-915.

CALDERWOOD, S. K., GONG, J. & MURSHID, A. 2016. Extracellular HSPs: The Complicated Roles of Extracellular HSPs in Immunity. Front Immunol, 7, 159.

CAMPANELLA, C., BUCCHIERI, F., MERENDINO, A. M., FUCARINO, A., BURGIO, G., CORONA, D. F., BARBIERI, G., DAVID, S., FARINA, F., ZUMMO, G., DE MACARIO, E. C., MACARIO, A. J. & CAPPELLO, F. 2012. The odyssey of Hsp60 from tumor cells to other destinations includes plasma membrane-associated stages and Golgi and exosomal protein-trafficking modalities. PLoS One, 7, e42008.

CAO, X., WEN, P., FU, Y., GAO, Y., QI, X., CHEN, B., TAO, Y., WU, L., XU, A., LU, H. & ZHAO, G. 2019. Radiation induces apoptosis primarily through the intrinsic pathway in mammalian cells. Cell Signal, 62, 109337.

CARIOLI, G., MALVEZZI, M., RODRIGUEZ, T., BERTUCCIO, P., NEGRI, E. & LA VECCHIA, C. 2018. Trends and predictions to 2020 in breast cancer mortality: Americas and Australasia. Breast, 37, 163-169.

CASSALI, G.D., LAVALLE, G.E., FERREIRA, E., ESTRELA-LIMA, A., DE NARDI, A.B., GHEVER, C., SOBRAL, R.A., AMORIM, R.L., OLIVEIRA, L.O., SUEIRO, F.A.R., BESERRA, H.E.O., BERTAGNOLLI, A.C., GAMBA, C.O., DAMASCENO, K.A., CAMPOS, C.B., ARAUJO, M.R., CAMPOS, L.C., MONTEIRO, L.N., NUNES, F.C., HORTA, R.S., REIS, D.C., LUVIZOTTO, M.C.R., MAGALHÃES, G.M., RAPOSO, J.B., FERREIRA, A.M., TANAKA, N.M., GRANDI, F., UBUKATA, R., BATSCHINSKI, K., TERRA, E.M., SALVADOR, R.C.L., JARK, P.C., DELECORDI, J.E.R., NASCIMENTO, N.A., SILVA, D.N., SILVA, L.P., FERREIRA, K.C.R.S., FREHSE, M.S., SANTIS, G.W., SILVA, E.O., GUIM, T.N., KERR, B., CINTRA, P.P., SILVA, F.B.F., LEITE, J.S., MELLO, M.F.V., FERREIRA, M.L.G., FUKUMASU, H., SALGADO, B.S., TORRES, R. Consensus for the diagnosis, prognosis and treatment of canine mammary tumors. 2014. Braz J Vet Pathol. 7(2), 38–69.

CASSALI, G.D., DAMASCENO, K.A., BERTAGNOLLI, A.C., ESTRELA-LIMA, A., LAVALLE, G.E., DI SANTIS, G.W., DE NARDI, A.B., FERNANDES, C.G., COGLIATI, B., SOBRAL, R. AND AMORIM DA COSTA, F.V. 2017. Consensus regarding the diagnosis, prognosis and treatment of canine mammary tumors: benign mixed tumors, carcinomas in mixed tumors and carcinosarcomas. Brazilian Journal of Veterinary Pathology, 10(3), 87-99.

CENIK, M., ABAS, B. I., KOCABIYIK, B., DEMIRBOLAT, G. M. & CEVIK, O. 2021. Development of a New Drug Delivery System from HELA-Derived EVs and the Effect of Docetaxel-Loaded EVs on Mitochondrial Apoptosis. Journal of Pharmaceutical Innovation.

CHANG, J., SARASWATHIBHATLA, A., SONG, Z., VARMA, S., SANCHEZ, C., SRIVASTAVA, S., LIU, K., BASSIK, M.C., MARINKOVICH, M.P., HODGSON, L. AND SHENOY, V., 2022. Collective invasion of the basement membrane in breast cancer driven by forces from cell volume expansion and local contractility. bioRxiv.

CHANG, W. H., NGUYEN, T. T. T., HSU, C. H., BRYANT, K. L., KIM, H. J., YING, H. Q., ERICKSON, J. W., DER, C. J., CERIONE, R. A. & ANTONYAK, M. A. 2021. KRAS-dependent cancer cells promote survival by producing exosomes enriched in Survivin. Cancer Letters, 517, 66-77.

CHANTELOUP, G., CORDONNIER, M., ISAMBERT, N., BERTAUT, A., HERVIEU, A., HENNEQUIN, A., LUU, M., ZANETTA, S., COUDERT, B., BENGRINE, L., DESMOULINS, I., FAVIER, L., LAGRANGE, A., PAGES, P. B., GUTIERREZ, I., LHERMINIER, J., AVOSCAN, L., JANKOWSKI, C., REBE, C., CHEVRIAUX, A., PADEANO, M. M., COUTANT, C., LADOIRE, S., CAUSERET, S., ARNOULD, L., CHARON-BARRA, C., COTTET, V., BLANC, J., BINQUET, C., BARDOU, M., GARRIDO, C. & GOBBO, J. 2020. Monitoring HSP70 exosomes in cancer patients' follow up: a clinical prospective pilot study. J Extracell Vesicles, 9, 1766192.

CHAPPELL, K., MANNA, K., WASHAM, C. L., GRAW, S., ALKAM, D., THOMPSON, M. D., ZAFAR, M. K., HAZESLIP, L., RANDOLPH, C., GIES, A., BIRD, J. T., BYRD, A. K., MIAH, S. & BYRUM, S. D. 2021. Multi-omics data integration reveals correlated regulatory features of triple-negative breast cancer. Mol Omics, 17, 677-691.

CHEN, F., XU, B., LI, J., YANG, X., GU, J., YAO, X. & SUN, X. 2021. Hypoxic tumour cell-derived exosomal miR-340-5p promotes radioresistance of oesophageal squamous cell carcinoma via KLF10. J Exp Clin Cancer Res, 40, 38.

CHEN, G., HUANG, A. C., ZHANG, W., ZHANG, G., WU, M., XU, W., YU, Z., YANG, J., WANG, B., SUN, H., XIA, H., MAN, Q., ZHONG, W., ANTELO, L. F., WU, B., XIONG, X., LIU, X., GUAN, L., LI, T., LIU, S., YANG, R., LU, Y., DONG, L., MCGETTIGAN, S., SOMASUNDARAM, R., RADHAKRISHNAN, R., MILLS, G., LU, Y., KIM, J., CHEN, Y. H., DONG, H., ZHAO, Y., KARAKOUSIS, G. C., MITCHELL, T. C., SCHUCHTER, L. M., HERLYN, M., WHERRY, E. J., XU, X. & GUO, W. 2018. Exosomal PD-L1 contributes to immunosuppression and is associated with anti-PD-1 response. Nature, 560, 382-386.

CHEN, H., HAN, Z., LUO, Q., WANG, Y., LI, Q., ZHOU, L. & ZUO, H. 2022. Radiotherapy modulates tumor cell fate decisions: a review. Radiat Oncol, 17, 196.

CHEN, H. N., YUAN, K., XIE, N., WANG, K., HUANG, Z., CHEN, Y., DOU, Q., WU, M., NICE, E. C., ZHOU, Z. G. & HUANG, C. 2016. PDLIM1 Stabilizes the E-Cadherin/beta-Catenin Complex to Prevent Epithelial-Mesenchymal Transition and Metastatic Potential of Colorectal Cancer Cells. Cancer Res, 76, 1122-34.

CHEN, J., XU, Y., LU, Y. & XING, W. 2018. Isolation and Visible Detection of Tumor-Derived Exosomes from Plasma. Anal Chem, 90, 14207-14215.

CHEN, J. C., LI, P. L., ZHANG, T. Y., XU, Z. P., HUANG, X. W., WANG, R. M. & DU, L. T. 2022. Review on Strategies and Technologies for Exosome Isolation and Purification. Frontiers in Bioengineering and Biotechnology, 9.

CHEN, L. & BRIGSTOCK, D. R. 2016. Integrins and heparan sulfate proteoglycans on hepatic stellate cells (HSC) are novel receptors for HSC-derived exosomes. FEBS Lett, 590, 4263-4274.

CHEN, M., XU, R., JI, H., GREENING, D. W., RAI, A., IZUMIKAWA, K., ISHIKAWA, H., TAKAHASHI, N. & SIMPSON, R. J. 2016. Transcriptome and long noncoding RNA

sequencing of three extracellular vesicle subtypes released from the human colon cancer LIM1863 cell line. Sci Rep, 6, 38397.

CHEN, M. J., WU, W. Y., YEN, A. M., FANN, J. C., CHEN, S. L., CHIU, S. Y., CHEN, H. H. & CHIOU, S. T. 2016. Body mass index and breast cancer: analysis of a nation-wide population-based prospective cohort study on 1 393 985 Taiwanese women. Int J Obes (Lond), 40, 524-30.

CHEN, W. X., LIU, X. M., LV, M. M., CHEN, L., ZHAO, J. H., ZHONG, S. L., JI, M. H., HU, Q., LUO, Z., WU, J. Z. & TANG, J. H. 2014. Exosomes from Drug-Resistant Breast Cancer Cells Transmit Chemoresistance by a Horizontal Transfer of MicroRNAs. Plos One, 9.

CHEN, X., LIU, J., ZHANG, Q., LIU, B., CHENG, Y., ZHANG, Y., SUN, Y., GE, H. & LIU, Y. 2020. Exosome-mediated transfer of miR-93-5p from cancer-associated fibroblasts confer radioresistance in colorectal cancer cells by downregulating FOXA1 and upregulating TGFB3. J Exp Clin Cancer Res, 39, 65.

CHEN, Y., HUANG, Y., GAO, X., LI, Y., LIN, J., CHEN, L., CHANG, L., CHEN, G., GUAN, Y., PAN, L. K., XIA, X., GUO, Z., PAN, J., XU, Y., YI, X. & CHEN, C. 2020. CCND1 Amplification Contributes to Immunosuppression and Is Associated With a Poor Prognosis to Immune Checkpoint Inhibitors in Solid Tumors. Front Immunol, 11, 1620.

CHEN, Y., XIE, Y., XU, L., ZHAN, S., XIAO, Y., GAO, Y., WU, B. & GE, W. 2017. Protein content and functional characteristics of serum-purified exosomes from patients with colorectal cancer revealed by quantitative proteomics. Int J Cancer, 140, 900-913.

CHEN, Z., YANG, L., CUI, Y., ZHOU, Y., YIN, X., GUO, J., ZHANG, G., WANG, T. & HE, Q. Y. 2016. Cytoskeleton-centric protein transportation by exosomes transforms tumor-favorable macrophages. Oncotarget, 7, 67387-67402.

CHOCTEAU, F., BOULAY, M. M., BESNARD, F., VALEAU, G., LOUSSOUARN, D. & NGUYEN, F. 2019. Proposal for a Histological Staging System of Mammary Carcinomas in Dogs and Cats. Part 2: Feline Mammary Carcinomas. Frontiers in Veterinary Science, 6.

CHOI, H., CHOI, Y., YIM, H. Y., MIRZAAGHASI, A., YOO, J. K. & CHOI, C. 2021. Biodistribution of Exosomes and Engineering Strategies for Targeted Delivery of Therapeutic Exosomes. Tissue Engineering and Regenerative Medicine, 18, 499-511.

CHUN, R. 2009. Lymphoma: Which Chemotherapy Protocol and Why? Topics in Companion Animal Medicine, 24, 157-162.

CIRAVOLO, V., HUBER, V., GHEDINI, G. C., VENTURELLI, E., BIANCHI, F., CAMPIGLIO, M., MORELLI, D., VILLA, A., DELLA MINA, P., MENARD, S., FILIPAZZI, P., RIVOLTINI, L., TAGLIABUE, E. & PUPA, S. M. 2012. Potential role of HER2-overexpressing exosomes in countering trastuzumab-based therapy. J Cell Physiol, 227, 658-67.

CLAYTON, A. & TABI, Z. 2005. Exosomes and the MICA-NKG2D system in cancer. Blood Cells Mol Dis, 34, 206-13.

CLAYTON, A., TURKES, A., DEWITT, S., STEADMAN, R., MASON, M. D. & HALLETT, M. B. 2004. Adhesion and signaling by B cell-derived exosomes: the role of integrins. Faseb Journal, 18, 977-+.

COMMISSO, C., DAVIDSON, S. M., SOYDANER-AZELOGLU, R. G., PARKER, S. J., KAMPHORST, J. J., HACKETT, S., GRABOCKA, E., NOFAL, M., DREBIN, J. A., THOMPSON, C. B., RABINOWITZ, J. D., METALLO, C. M., VANDER HEIDEN, M. G. & BAR-SAGI, D. 2013. Macropinocytosis of protein is an amino acid supply route in Ras-transformed cells. Nature, 497, 633-+.

COUTURE, H. D., WILLIAMS, L. A., GERADTS, J., NYANTE, S. J., BUTLER, E. N., MARRON, J. S., PEROU, C. M., TROESTER, M. A. & NIETHAMMER, M. 2018. Image analysis with deep learning to predict breast cancer grade, ER status, histologic subtype, and intrinsic subtype. Npj Breast Cancer, 4.

CUI, Y. H., KANG, J. H., SUH, Y., ZHAO, Y., YI, J. M., BAE, I. H., LEE, H. J., PARK, D. W., KIM, M. J. & LEE, S. J. 2021. Loss of FBXL14 promotes mesenchymal shift and radioresistance of non-small cell lung cancer by TWIST1 stabilization. Signal Transduct Target Ther, 6, 272.

CURIEL, T. J., COUKOS, G., ZOU, L. H., ALVAREZ, X., CHENG, P., MOTTRAM, P., EVDEMON-HOGAN, M., CONEJO-GARCIA, J. R., ZHANG, L., BUROW, M., ZHU, Y., WEI, S., KRYCZEK, I., DANIEL, B., GORDON, A., MYERS, L., LACKNER, A., DISIS, M. L., KNUTSON, K. L., CHEN, L. P. & ZOU, W. P. 2004. Specific recruitment of regulatory T cells in ovarian carcinoma fosters immune privilege and predicts reduced survival. Nature Medicine, 10, 942-949.

CZAJKOWSKI, D., SZMYD, R. & GEE, H. E. 2022. Impact of DNA damage response defects in cancer cells on response to immunotherapy and radiotherapy. J Med Imaging Radiat Oncol, 66, 546-559.

DAI, X., LIAO, K., ZHUANG, Z., CHEN, B., ZHOU, Z., ZHOU, S., LIN, G., ZHANG, F., LIN, Y., MIAO, Y., LI, Z., HUANG, R., QIU, Y. & LIN, R. 2019. AHIF promotes glioblastoma progression and radioresistance via exosomes. Int J Oncol, 54, 261-270.

DATTA, M., COUSSENS, L. M., NISHIKAWA, H., HODI, F. S. & JAIN, R. K. 2019. Reprogramming the Tumor Microenvironment to Improve Immunotherapy: Emerging Strategies and Combination Therapies. Am Soc Clin Oncol Educ Book, 39, 165-174.

DAWSON, J. C., SERRELS, A., STUPACK, D. G., SCHLAEPFER, D. D. & FRAME, M. C. 2021. Targeting FAK in anticancer combination therapies. Nat Rev Cancer, 21, 313-324.

DE ANDRES, P. J., CACERES, S., ILLERA, J. C., CRESPO, B., SILVAN, G., QUEIROGA, F. L., ILLERA, M. J., PEREZ-ALENZA, M. D. & PENA, L. 2022. Hormonal Homologies between Canine Mammary Cancer and Human Breast Cancer in a Series of Cases. Veterinary Sciences, 9.

DEBREUQUE, M., DE FORNEL, P., DAVID, I., DELISLE, F., DUCERVEAU, M. N., DEVAUCHELLE, P. & THIBAUD, J. L. 2020. Definitive-intent uniform megavoltage fractioned radiotherapy protocol for presumed canine intracranial gliomas: retrospective analysis of survival and prognostic factors in 38 cases (2013-2019). Bmc Veterinary Research, 16.

DEKANEK, E. W., THULL, D. L., MASSART, M., GRUBS, R. E., RAJKOVIC, A. & MAI, P. L. 2020. Knowledge and opinions regarding BRCA1 and BRCA2 genetic testing among primary care physicians. Journal of Genetic Counseling, 29, 122-130.

DENKERT, C., LIEDTKE, C., TUTT, A. & VON MINCKWITZ, G. 2017. Molecular alterations in triple-negative breast cancer-the road to new treatment strategies. Lancet, 389, 2430-2442.

DESANTIS, C. E., MA, J., GODING SAUER, A., NEWMAN, L. A. & JEMAL, A. 2017. Breast cancer statistics, 2017, racial disparity in mortality by state. CA Cancer J Clin, 67, 439-448.

DEVERICKS, E. N., CARSON, M. S., MCCULLOUGH, L. E., COLEMAN, M. F. & HURSTING, S. D. 2022. The obesity-breast cancer link: a multidisciplinary perspective. Cancer and Metastasis Reviews, 41, 607-625.

DHATCHINAMOORTHY, K., COLBERT, J. D. & ROCK, K. L. 2021. Cancer Immune Evasion Through Loss of MHC Class I Antigen Presentation. Front Immunol, 12, 636568.

DIERAS, V., BONNEFOI, H., ALBA, E., AWADA, A., COUDERT, B., PIVOT, X., GLIGOROV, J., JAGER, A., ZAMBELLI, S., LINDEMAN, G. J., CHARPENTIER, E., EMMONS, G. T., GARCIA-RIBAS, I., PARIDAENS, R. & VERWEIJ, J. 2019. Iniparib administered weekly or twice-weekly in combination with gemcitabine/carboplatin in patients with metastatic triple-negative breast cancer: a phase II randomized open-label study with pharmacokinetics. Breast Cancer Res Treat, 177, 383-393.

DINH, T. K., FENDLER, W., CHALUBINSKA-FENDLER, J., ACHARYA, S. S., O'LEARY, C., DERASKA, P. V., D'ANDREA, A. D., CHOWDHURY, D. & KOZONO, D. 2016. Circulating miR-29a and miR-150 correlate with delivered dose during thoracic radiation therapy for non-small cell lung cancer. Radiat Oncol, 11, 61.

DONNARUMMA, E., FIORE, D., NAPPA, M., ROSCIGNO, G., ADAMO, A., IABONI, M., RUSSO, V., AFFINITO, A., PUOTI, I., QUINTAVALLE, C., RIENZO, A., PISCUOGLIO, S., THOMAS, R. & CONDORELLI, G. 2017. Cancer-associated fibroblasts release exosomal microRNAs that dictate an aggressive phenotype in breast cancer. Oncotarget, 8, 19592-19608.

DOROGI, B., UJHELYI, M., KENESSEY, I., IVADY, G. & MATRAI, Z. 2020. Clinicopathological correlations of areola-sparing mastectomies versus nipple-sparing mastectomies: Analysis of the oncological and cosmetic importance of the components of the nipple-areola complex. Breast J.

DU, W. W., LI, X., MA, J., FANG, L., WU, N., LI, F., DHALIWAL, P., YANG, W., YEE, A. J. & YANG, B. B. 2022. Promotion of tumor progression by EV transmission of circular RNA circSKA3. Mol Ther Nucleic Acids, 27, 276-292.

DU, Y., DU, S. F., LIU, L., GAN, F. H., JIANG, X. G., WANGRAO, K. J., LYU, P., GONG, P. & YAO, Y. 2020. Radiation-Induced Bystander Effect can be Transmitted Through EVs Using miRNAs as Effector Molecules. Radiation Research, 194, 89-100.

DUBOIS, C., DUFOUR, R., DAUMAR, P., AUBEL, C., SZCZEPANIAK, C., BLAVIGNAC, C., MOUNETOU, E., PENAULT-LLORCA, F. AND BAMDAD, M. 2017. Development and cytotoxic response of two proliferative MDA-MB-231 and non-proliferative SUM1315 three-dimensional cell culture models of triple-negative basal-like breast cancer cell lines. Oncotarget, 8(56), 95316.

DUDLEY, A. C. 2012. Tumor endothelial cells. Cold Spring Harb Perspect Med, 2, a006536.

EBCTCG, MCGALE, P., TAYLOR, C., CORREA, C., CUTTER, D., DUANE, F., EWERTZ, M., GRAY, R., MANNU, G., PETO, R., WHELAN, T., WANG, Y., WANG, Z. & DARBY, S. 2014. Effect of radiotherapy after mastectomy and axillary surgery on 10-year recurrence and 20-year breast cancer mortality: meta-analysis of individual patient data for 8135 women in 22 randomised trials. Lancet, 383, 2127-35.

EDGE, S. B. & COMPTON, C. C. 2010. The American Joint Committee on Cancer: the 7th edition of the AJCC cancer staging manual and the future of TNM. Ann Surg Oncol, 17, 1471-4.

EGUCHI, T., SOGAWA, C., OKUSHA, Y., UCHIBE, K., IINUMA, R., ONO, K., NAKANO, K., MURAKAMI, J., ITOH, M., ARAI, K., FUJIWARA, T., NAMBA, Y., MURATA, Y., OHYAMA, K., SHIMOMURA, M., OKAMURA, H., TAKIGAWA, M., NAKATSURA, T., KOZAKI, K. I., OKAMOTO, K. & CALDERWOOD, S. K. 2018. Organoids with cancer stem cell-like properties secrete exosomes and HSP90 in a 3D nanoenvironment. PLoS One, 13, e0191109.

EITAN, E., ZHANG, S., WITWER, K. W. & MATTSON, M. P. 2015. Extracellular vesicle-depleted fetal bovine and human sera have reduced capacity to support cell growth. J Extracell Vesicles, 4, 26373.

ELBAKRAWY, E., KAUR BAINS, S., BRIGHT, S., AL-ABEDI, R., MAYAH, A., GOODWIN, E. & KADHIM, M. 2020. Radiation-Induced Senescence Bystander Effect: The Role of Exosomes. Biology (Basel), 9.

ELDH, M., EKSTROM, K., VALADI, H., SJOSTRAND, M., OLSSON, B., JERNAS, M. & LOTVALL, J. 2010. Exosomes communicate protective messages during oxidative stress; possible role of exosomal shuttle RNA. PLoS One, 5, e15353.

ELIA, I. & HAIGIS, M. C. 2021. Metabolites and the tumour microenvironment: from cellular mechanisms to systemic metabolism. Nature Metabolism, 3, 21-32.

ELLIS, T. N. & KUEHN, M. J. 2010. Virulence and immunomodulatory roles of bacterial outer membrane vesicles. Microbiol Mol Biol Rev, 74, 81-94.

ENGINLER, S. O., AKIS, I., TOYDEMIR, T. S. F., OZTABAK, K., HAKTANIR, D., GUNDUZ, M. C., KIRSAN, I. & FIRAT, I. 2014. Genetic variations of BRCA1 and BRCA2 genes in dogs with mammary tumours. Veterinary Research Communications, 38, 21-27.

EUSTACE, A. J., LEE, M. J., COLLEY, G., ROBAN, J., DOWNING, T. & BUCHANAN, P. J. 2022. Aberrant calcium signalling downstream of mutations in TP53 and the PI3K/AKT pathway genes promotes disease progression and therapy resistance in triple negative breast cancer. Cancer Drug Resistance, 5, 560-576.

EYRE, R., ALFEREZ, D. G., SANTIAGO-GOMEZ, A., SPENCE, K., MCCONNELL, J. C., HART, C., SIMOES, B. M., LEFLEY, D., TULOTTA, C., STORER, J., GURNEY, A., CLARKE, N., BROWN, M., HOWELL, S. J., SIMS, A. H., FARNIE, G., OTTEWELL, P. D. & CLARKE, R. B. 2019. Microenvironmental IL1beta promotes breast cancer metastatic colonisation in the bone via activation of Wnt signalling. Nat Commun, 10, 5016.

EZERSKYTE, A., ZAMOKAS, G., GRIGONIS, A. & JUODZIUKYNIENE, N. 2011. The Retrospective Analysis of Mammary Tumors in Dogs. Veterinarija Ir Zootechnika, 53, 3-8.

FABBRI, M., PAONE, A., CALORE, F., GALLI, R., GAUDIO, E., SANTHANAM, R., LOVAT, F., FADDA, P., MAO, C., NUOVO, G. J., ZANESI, N., CRAWFORD, M., OZER, G. H., WERNICKE, D., ALDER, H., CALIGIURI, M. A., NANA-SINKAM, P., PERROTTI, D. & CROCE, C. M. 2012. MicroRNAs bind to Toll-like receptors to induce prometastatic inflammatory response. Proceedings of the National Academy of Sciences of the United States of America, 109, E2110-E2116.

FAN, L., GOSS, P. E. & STRASSER-WEIPPL, K. 2015. Current Status and Future Projections of Breast Cancer in Asia. Breast Care (Basel), 10, 372-8.

FANG, T., LV, H., LV, G., LI, T., WANG, C., HAN, Q., YU, L., SU, B., GUO, L., HUANG, S., CAO, D., TANG, L., TANG, S., WU, M., YANG, W. & WANG, H. 2018. Tumor-derived exosomal miR-1247-3p induces cancer-associated fibroblast activation to foster lung metastasis of liver cancer. Nat Commun, 9, 191.

FARIAS, V. D., O'VALLE, F., SERRANO-SAENZ, S., ANDERSON, P., ANDRES, E., LOPEZ-PENALVER, J., TOVAR, I., NIETO, A., SANTOS, A., MARTIN, F., EXPOSITO, J., OLIVER, F. J. & DE ALMODOVAR, J. M. R. 2018. Exosomes derived from mesenchymal stem cells enhance radiotherapy-induced cell death in tumor and metastatic tumor foci. Molecular Cancer, 17.

FATTAHI, F., SAEEDNEJAD ZANJANI, L., VAFAEI, S., HABIBI SHAMS, Z., KIANI, J., NASERI, M., GHEYTANCHI, E. & MADJD, Z. 2021. Expressions of TWIST1 and CD105 markers in colorectal cancer patients and their association with metastatic potential and prognosis. Diagn Pathol, 16, 26.

FAYAZ, M. S., DEMIAN, G., EL-SHERIFY, M., AZIZ, M. & EISSA, H. 2017. Triple negative breast cancer: 10-year survival update of the applied treatment strategy in Kuwait. Annals of Oncology, 28.

FENG, D., ZHAO, W. L., YE, Y. Y., BAI, X. C., LIU, R. Q., CHANG, L. F., ZHOU, Q. & SUI, S. F. 2010. Cellular Internalization of Exosomes Occurs Through Phagocytosis. Traffic, 11, 675-687.

FERLAY, J., SOERJOMATARAM, I., DIKSHIT, R., ESER, S., MATHERS, C., REBELO, M., PARKIN, D. M., FORMAN, D. & BRAY, F. 2015. Cancer incidence and mortality worldwide: sources, methods and major patterns in GLOBOCAN 2012. Int J Cancer, 136, E359-86.

FOLDI, J., SILBER, A., REISENBICHLER, E., SINGH, K., FISCHBACH, N., PERSICO, J., ADELSON, K., KATOCH, A., HOROWITZ, N., LANNIN, D., CHAGPAR, A., PARK, T., MARCZYK, M., FREDERICK, C., BURRELLO, T., IBRAHIM, E., QING, T., BAI, Y., BLENMAN, K., RIMM, D. L. & PUSZTAI, L. 2021. Neoadjuvant durvalumab plus weekly nab-paclitaxel and dose-dense doxorubicin/cyclophosphamide in triple-negative breast cancer. NPJ Breast Cancer, 7, 9.

FONG, M. Y., ZHOU, W. Y., LIU, L., ALONTAGA, A. Y., CHANDRA, M., ASHBY, J., CHOW, A., O'CONNOR, S. T. F., LI, S. S., CHIN, A. R., SOMLO, G., PALOMARES, M., LI, Z., TREMBLAY, J. R., TSUYADA, A., SUN, G. Q., REID, M. A., WU, X. W., SWIDERSKI, P., REN, X. B., SHI, Y. H., KONG, M., ZHONG, W. W., CHEN, Y. & WANG, S. E. 2015. Breast-cancer-secreted

miR-122 reprograms glucose metabolism in premetastatic niche to promote metastasis. Nature Cell Biology, 17, 183-+.

FULTANG, N., CHAKRABORTY, M. & PEETHAMBARAN, B. 2021. Regulation of cancer stem cells in triple negative breast cancer. Cancer Drug Resistance, 4, 321-342.

GAIKO-SHCHERBAK, A., ESCHENBRUCH, J., KRONENBERG, N. M., TESKE, M., WOLTERS, B., SPRINGER, R., GATHER, M. C., MERKEL, R., HOFFMANN, B. & NOETZEL, E. 2021. Cell Force-Driven Basement Membrane Disruption Fuels EGF- and Stiffness-Induced Invasive Cell Dissemination from Benign Breast Gland Acini. Int J Mol Sci, 22.

GAMPENRIEDER, S. P., RINNERTHALER, G. & GREIL, R. 2013. Neoadjuvant chemotherapy and targeted therapy in breast cancer: past, present, and future. J Oncol, 2013, 732047.

GAO, W. J., WANG, M. M., SU, Y., YU, Z. H., LIU, H. K. & SU, Z. 2023. Self-Assembly Mitochondria-Targeting Donor-Acceptor Type Theranostic Nanosphere Activates ROS Storm for Multimodal Cancer Therapy. ACS Appl Bio Mater.

GARDEN, O. A., VOLK, S. W., MASON, N. J. & PERRY, J. A. 2018. Companion animals in comparative oncology: One Medicine in action. Veterinary Journal, 240, 6-13.

GARRIDO-CASTRO, A. C., LIN, N. U. & POLYAK, K. 2019. Insights into Molecular Classifications of Triple-Negative Breast Cancer: Improving Patient Selection for Treatment. Cancer Discovery, 9, 176-198.

GENER, P., RAFAEL, D., SERAS-FRANZOSO, J., PEREZ, A., PINDADO, L. A., CASAS, G., ARANGO, D., FERNANDEZ, Y., DIAZ-RIASCOS, Z. V., ABASOLO, I. & SCHWARTZ, S., JR. 2019. Pivotal Role of AKT2 during Dynamic Phenotypic Change of Breast Cancer Stem Cells. Cancers (Basel), 11.

GEOFFROY, M., KLEINCLAUSS, A., KUNTZ, S. AND GRILLIER-VUISSOZ, I., 2020. CLAUDIN 1 INHIBITS CELL MIGRATION AND INCREASES INTERCELLULAR ADHESION IN TRIPLE-NEGATIVE BREAST CANCER CELL LINE. *MOLECULAR BIOLOGY REPORTS*, *47*, 7643-7653.

GHONCHEH, M., MOMENIMOVAHED, Z. & SALEHINIYA, H. 2016. Epidemiology, Incidence and Mortality of Breast Cancer in Asia. Asian Pac J Cancer Prev, 17, 47-52.

GHOSSOUB, R., LEMBO, F., RUBIO, A., GAILLARD, C. B., BOUCHET, J., VITALE, N., SLAVIK, J., MACHALA, M. & ZIMMERMANN, P. 2014. Syntenin-ALIX exosome biogenesis and budding into multivesicular bodies are controlled by ARF6 and PLD2. Nat Commun, 5, 3477.

GIULIANO, A. E., CONNOLLY, J. L., EDGE, S. B., MITTENDORF, E. A., RUGO, H. S., SOLIN, L. J., WEAVER, D. L., WINCHESTER, D. J. & HORTOBAGYI, G. N. 2017. Breast Cancer-Major changes in the American Joint Committee on Cancer eighth edition cancer staging manual. CA Cancer J Clin, 67, 290-303.

GONDA, A., KABAGWIRA, J., SENTHIL, G. N., FERGUSON BENNIT, H. R., NEIDIGH, J. W., KHAN, S. & WALL, N. R. 2018. Exosomal survivin facilitates vesicle internalization. Oncotarget, 9, 34919-34934.

GONDA, A., KABAGWIRA, J., SENTHIL, G. N. & WALL, N. R. 2019. Internalization of Exosomes through Receptor-Mediated Endocytosis. Molecular Cancer Research, 17, 337-347.

GONG, J., WENG, D., EGUCHI, T., MURSHID, A., SHERMAN, M. Y., SONG, B. & CALDERWOOD, S. K. 2015. Targeting the hsp70 gene delays mammary tumor initiation and inhibits tumor cell metastasis. Oncogene, 34, 5460-71.

GRANER, M. W., ALZATE, O., DECHKOVSKAIA, A. M., KEENE, J. D., SAMPSON, J. H., MITCHELL, D. A. & BIGNER, D. D. 2009. Proteomic and immunologic analyses of brain tumor exosomes. FASEB J, 23, 1541-57.

GRIGORYEVA, E. S., TASHIREVA, L. A., SAVELIEVA, O. E., ZAVYALOVA, M. V., POPOVA, N. O., KUZNETSOV, G. A., ANDRYUHOVA, E. S. & PERELMUTER, V. M. 2023. The Association of Integrins beta3, beta4, and alphaVbeta5 on Exosomes, CTCs and Tumor Cells with Localization of Distant Metastasis in Breast Cancer Patients. Int J Mol Sci, 24.

GRIMALDI, C., IBRAGHIMOV, A., KIESSLING, A., RATTEL, B., JI, C., FULLER, C. L., BRENNAN, F. R., REGENASS-LECHNER, F., SHENTON, J., PRICE, K. D., PICHE, M. S., STEEVES, M. A., PRELL, R., DUDAL, S., KRONENBERG, S., FREEBERN, W. & BLANSET, D. 2022. Current nonclinical approaches for immune assessments of immuno-oncology biotherapeutics. Drug Discov Today, 28, 103440.

GUERRA, F. & BUCCI, C. 2019. Role of the RAB7 Protein in Tumor Progression and Cisplatin Chemoresistance. Cancers (Basel), 11.

GUO, D. J., TIKOO, S. & HAASS, N. K. 2019. RAB27A-mediated melanoma exosomes: promoters of invasion and metastasis. Translational Cancer Research, 8, 732-735.

GUO, H., HA, C. F., DONG, H., YANG, Z. J., MA, Y. & DING, Y. H. 2019. Cancer-associated fibroblast-derived exosomal microRNA-98-5p promotes cisplatin resistance in ovarian cancer by targeting CDKN1A. Cancer Cell International, 19.

GUO, Y. L., ZHAI, Y. J., WU, L. Y., WANG, Y. Z., WU, P. Z. & XIONG, L. X. 2022. Mesenchymal Stem Cell-Derived Extracellular Vesicles: Pleiotropic Impacts on Breast Cancer Occurrence, Development, and Therapy. International Journal of Molecular Sciences, 23.

HAKKAART, C., PEARSON, J. F., MARQUART, L., DENNIS, J., WIGGINS, G. A. R., BARNES, D. R., ROBINSON, B. A., MACE, P. D., AITTOMAKI, K., ANDRULIS, I. L., ARUN, B. K., AZZOLLINI, J., BALMANA, J., BARKARDOTTIR, R. B., BELHADJ, S., BERGER, L., BLOK, M. J., BOONEN, S. E., BORDE, J., BRADBURY, A. R., BRUNET, J., BUYS, S. S., CALIGO, M. A., CAMPBELL, I., CHUNG, W. K., CLAES, K. B. M., COLLONGE-RAME, M. A., COOK, J., COSGROVE, C., COUCH, F. J., DALY, M. B., DANDIKER, S., DAVIDSON, R., DE LA HOYA, M., DE PUTTER, R., DELNATTE, C., DHAWAN, M., DIEZ, O., DING, Y. C., DOMCHEK, S. M., DONALDSON, A., EASON, J., EASTON, D. F., EHRENCRONA, H., ENGEL, C., EVANS, D. G., FAUST, U., FELIUBADALO, L., FOSTIRA, F., FRIEDMAN, E., FRONE, M., FROST, D., GARBER, J., GAYTHER, S. A., GEHRIG, A., GESTA, P., GODWIN, A. K., GOLDGAR, D. E., GREENE, M. H., HAHNEN, E., HAKE, C. R., HAMANN, U., HANSEN, T. V. O., HAUKE, J., HENTSCHEL, J., HEROLD, N., HONISCH, E., HULICK, P. J., IMYANITOV, E. N., ISAACS, C., IZATT, L., IZQUIERDO, A., JAKUBOWSKA, A., JAMES, P. A., JANAVICIUS, R., JOHN, E. M., JOSEPH, V.,

KARLAN, B. Y., KEMP, Z., KIRK, J., KONSTANTOPOULOU, I., KOUDIJS, M., KWONG, A., LAITMAN, Y., LALLOO, F., LASSET, C., LAUTRUP, C., LAZARO, C., LEGRAND, C., LESLIE, G., LESUEUR, F., MAI, P. L., MANOUKIAN, S., MARI, V., MARTENS, J. W. M., MCGUFFOG, L., MEBIROUK, N., MEINDL, A., MILLER, A., MONTAGNA, M.,. 2022. Copy number variants as modifiers of breast cancer risk for BRCA1/BRCA2 pathogenic variant carriers. Communications Biology, 5.

HALL E.J. & GIACCIA A.J. 2012. Radiobiology for the Radiologist. Lippincott Williams & Wilkins; Philadelphia, PA, USA.

HAM, S., LIMA, L. G., CHAI, E. P. Z., MULLER, A., LOBB, R. J., KRUMEICH, S., WEN, S. W., WIEGMANS, A. P. & MOLLER, A. 2018. Breast Cancer-Derived Exosomes Alter Macrophage Polarization via gp130/STAT3 Signaling. Frontiers in Immunology, 9.

HAN, B. A., ZHANG, H., TIAN, R. N., LIU, H., WANG, Z. S., WANG, Z. Y., TIAN, J. F., CUI, Y. F., REN, S. X., ZUO, X. Y., TIAN, R., NIU, R. F. & ZHANG, F. 2022. Exosomal EPHA2 derived from highly metastatic breast cancer cells promotes angiogenesis by activating the AMPK signaling pathway through Ephrin A1-EPHA2 forward signaling. Theranostics, 12, 4127-4146.

HANAHAN, D. & WEINBERG, R. A. 2000. The hallmarks of cancer. Cell, 100, 57-70.

HANAHAN, D. & WEINBERG, R. A. 2011. Hallmarks of cancer: the next generation. Cell, 144, 646-74.

HANG, Q., ZENG, L., WANG, L., NIE, L., YAO, F., TENG, H., DENG, Y., YAP, S., SUN, Y., FRANK, S. J., CHEN, J. & MA, L. 2021. Non-canonical function of DGCR8 in DNA double-strand break repair signaling and tumor radioresistance. Nat Commun, 12, 4033.

HANNAFON, B. N., CARPENTER, K. J., BERRY, W. L., JANKNECHT, R., DOOLEY, W. C. & DING, W. Q. 2015. Exosome-mediated microRNA signaling from breast cancer cells is altered by the anti-angiogenesis agent docosahexaenoic acid (DHA). Molecular Cancer, 14.

HAO, Y., SONG, H., ZHOU, Z., CHEN, X., LI, H., ZHANG, Y., WANG, J., REN, X. & WANG, X. 2021. Promotion or inhibition of extracellular vesicle release: Emerging therapeutic opportunities. J Control Release, 340, 136-148.

HARADA, H., INOUE, M., ITASAKA, S., HIROTA, K., MORINIBU, A., SHINOMIYA, K., ZENG, L. H., OU, G. F., ZHU, Y. X., YOSHIMURA, M., MCKENNA, W. G., MUSCHEL, R. J. & HIRAOKA, M. 2012. Cancer cells that survive radiation therapy acquire HIF-1 activity and translocate towards tumour blood vessels. Nature Communications, 3.

HARRIS, D. A., PATEL, S. H., GUCEK, M., HENDRIX, A., WESTBROEK, W. & TARASKA, J. W. 2015. Exosomes Released from Breast Cancer Carcinomas Stimulate Cell Movement. Plos One, 10.

HASBAL-CELIKOK, G., AKSOY-SAGIRLI, P., ALTIPARMAK-ULBEGI, G. & CAN, A. 2021. Identification of AKT1/beta-catenin mutations conferring cetuximab and chemotherapeutic drug resistance in colorectal cancer treatment. Oncol Lett, 21, 209.

HASHIMOTO, K., OCHI, H., SUNAMURA, S., KOSAKA, N., MABUCHI, Y., FUKUDA, T., YAO, K., KANDA, H., AE, K., OKAWA, A., AKAZAWA, C., OCHIYA, T., FUTAKUCHI, M., TAKEDA, S. & SATO, S. 2018. Cancer-secreted hsa-miR-940 induces an osteoblastic phenotype in the bone metastatic microenvironment via targeting ARHGAP1 and FAM134A. Proceedings of the National Academy of Sciences of the United States of America, 115, 2204-2209.

HASSAN, M. S. U., ANSARI, J., SPOONER, D. & HUSSAIN, S. A. 2010. Chemotherapy for breast cancer (Review). Oncology Reports, 24, 1121-1131.

HATCH, E. M., FISCHER, A. H., DEERINCK, T. J. & HETZER, M. W. 2013. Catastrophic nuclear envelope collapse in cancer cell micronuclei. Cell, 154, 47-60.

HE, H., WANG, L., QIAO, Y., ZHOU, Q., LI, H. W., CHEN, S. P., YIN, D., HUANG, Q. & HE, M. 2020. Doxorubicin Induces Endotheliotoxicity and Mitochondrial Dysfunction via ROS/eNOS/NO Pathway. Frontiers in Pharmacology, 10.

HENGEL, S. R., SPIES, M. A. & SPIES, M. 2017. Small-Molecule Inhibitors Targeting DNA Repair and DNA Repair Deficiency in Research and Cancer Therapy. Cell Chem Biol, 24, 1101-1119.

HERRERA, M., LLORENS, C., RODRIGUEZ, M., HERRERA, A., RAMOS, R., GIL, B., CANDIA, A., LARRIBA, M. J., GARRE, P., EARL, J., RODRIGUEZ-GARROTE, M., CALDES, T., BONILLA, F., CARRATO, A., GARCIA-BARBERAN, V. & PENA, C. 2018. Differential distribution and enrichment of non-coding RNAs in exosomes from normal and Cancer-associated fibroblasts in colorectal cancer. Mol Cancer, 17, 114.

HIDA, K. 2018. The contribution of tumor endothelial cells in tumor metastasis. Cancer Science, 109, 359-359.

HIGGINBOTHAM, J. N., DEMORY BECKLER, M., GEPHART, J. D., FRANKLIN, J. L., BOGATCHEVA, G., KREMERS, G. J., PISTON, D. W., AYERS, G. D., MCCONNELL, R. E., TYSKA, M. J. & COFFEY, R. J. 2011. Amphiregulin exosomes increase cancer cell invasion. Curr Biol, 21, 779-86.

HINTON, C. P., DOYLE, P. J., BLAMEY, R. W., DAVIES, C. J., HOLLIDAY, H. W. & ELSTON, C. W. 1984. Subcutaneous mastectomy for primary operable breast cancer. Br J Surg, 71, 469-72.

HO, S. S., ZHANG, W. Y., TAN, N. Y., KHATOO, M., SUTER, M. A., TRIPATHI, S., CHEUNG, F. S., LIM, W. K., TAN, P. H., NGEOW, J. & GASSER, S. 2016. The DNA Structure-Specific Endonuclease MUS81 Mediates DNA Sensor STING-Dependent Host Rejection of Prostate Cancer Cells. Immunity, 44, 1177-89.

HORTON, J. K., STEFANICK, D. F., CAGLAYAN, M., ZHAO, M. L., JANOSHAZI, A. K., PRASAD, R., GASSMAN, N. R. & WILSON, S. H. 2018. XRCC1 phosphorylation affects aprataxin recruitment and DNA deadenylation activity. DNA Repair (Amst), 64, 26-33.

HOWLADER, N., CRONIN, K. A., KURIAN, A. W. & ANDRIDGE, R. 2018. Differences in Breast Cancer Survival by Molecular Subtypes in the United States. Cancer Epidemiol Biomarkers Prev, 27, 619-626.

HSU, Y. L., HUNG, J. Y., CHANG, W. A., LIN, Y. S., PAN, Y. C., TSAI, P. H., WU, C. Y. & KUO, P. L. 2017. Hypoxic lung cancer-secreted exosomal miR-23a increased angiogenesis and

vascular permeability by targeting prolyl hydroxylase and tight junction protein ZO-1. Oncogene, 36, 4929-4942.

HU, L., YIN, X., ZHANG, Y., PANG, A., XIE, X., YANG, S., ZHU, C., LI, Y., ZHANG, B., HUANG, Y., TIAN, Y., WANG, M., CAO, W., CHEN, S., ZHENG, Y., MA, S., DONG, F., HAO, S., FENG, S., RU, Y., CHENG, H., JIANG, E. & CHENG, T. 2021. Radiation-induced bystander effects impair transplanted human hematopoietic stem cells via oxidative DNA damage. Blood, 137, 3339-3350.

HU, X., LI, S., JIANG, Y., WEI, W., JI, Y., LI, Q. & JIANG, Z. 2020. Intraoperative ultrasound-guided lumpectomy versus wire-guided excision for nonpalpable breast cancer. J Int Med Res, 48, 300060519896707.

HU, W., TAN, C., HE, Y., ZHANG, G., XU, Y. & TANG, J. 2018. Functional miRNAs in breast cancer drug resistance. Onco Targets Ther, 11, 1529-1541.

HU, Y., YAN, C., MU, L., HUANG, K., LI, X., TAO, D., WU, Y. & QIN, J. 2015. Fibroblast-Derived Exosomes Contribute to Chemoresistance through Priming Cancer Stem Cells in Colorectal Cancer. PLoS One, 10, e0125625.

HUANG, L., RONG, Y., TANG, X., YI, K., QI, P., HOU, J., LIU, W., HE, Y., GAO, X., YUAN, C. & WANG, F. 2022. Engineered EVs as an in situ DC-primed vaccine to boost antitumor immunity in breast cancer. Mol Cancer, 21, 45.

HUANG, Z., ZHOU, J. K., WANG, K., CHEN, H., QIN, S., LIU, J., LUO, M., CHEN, Y., JIANG, J., ZHOU, L., ZHU, L., HE, J., LI, J., PU, W., GONG, Y., LI, J., YE, Q., DONG, D., HU, H., ZHOU, Z., DAI, L., HUANG, C., WEI, X. & PENG, Y. 2020. PDLIM1 Inhibits Tumor Metastasis Through Activating Hippo Signaling in Hepatocellular Carcinoma. Hepatology, 71, 1643-1659.

HUBALEK, M., CZECH, T. & MULLER, H. 2017. Biological Subtypes of Triple-Negative Breast Cancer. Breast Care, 12, 8-14.

HUSSEIN, G. M., MOHAMMED, S. M., FARIS, M., MOHAMMED, A., KADHIM, M. J., AWADH, S. A., AJAM, W. H. & JALIL, A. T. 2022. Find new channel for overcoming chemoresistance in cancers: Role of stem cells-derived exosomal microRNAs. International Journal of Biological Macromolecules, 219, 530-537.

HYDER, Z., HARKNESS, E. F., WOODWARD, E. R., BOWERS, N. L., PEREIRA, M., WALLACE, A. J., HOWELL, S. J., HOWELL, A., LALLOO, F., NEWMAN, W. G., SMITH, M. J. & EVANS, D. G. 2020. Risk of Contralateral Breast Cancer in Women with and without Pathogenic Variants in BRCA1, BRCA2, and TP53 Genes in Women with Very Early-Onset (< 36 Years) Breast Cancer. Cancers, 12.

IONKINA, ANASTASIA A., S. GAIL ECKHARDT, TODD M. PITTS, CAROL SARTORIUS, PETER KABOS, JIYHE KIM, AIK CHOON TAN, JOHN J. TENTLER, AND JENNIFER R. DIAMOND. 2015. "Abstract C34: Senescence as a mechanism of resistance to the Aurora kinase and angiokinase inhibitor, ENMD-2076, in p53 mutated triple-negative breast cancer (TNBC) models." Molecular Cancer Therapeutics 14, no. 12_Supplement_2 C34-C34.

IWATA, H., SHUTO, T., KAMEI, S., OMACHI, K., MORIUCHI, M., OMACHI, C., TOSHITO, T., HASHIMOTO, S., NAKAJIMA, K., SUGIE, C., OGINO, H., KAI, H. & SHIBAMOTO, Y. 2020. Combined effects of cisplatin and photon or proton irradiation in cultured cells:

radiosensitization, patterns of cell death and cell cycle distribution. J Radiat Res, 61, 832-841.

JABER, S., WARNIER, M., LEERS, C., VERNIER, M., GOEHRIG, D., MEDARD, J. J., VINDRIEUX, D., ZIEGLER, D. V. & BERNARD, D. 2023. Targeting chemoresistant senescent pancreatic cancer cells improves conventional treatment efficacy. Mol Biomed, 4, 4.

JASKIEWICZ, M., MOSZYNSKA, A., KROLICZEWSKI, J., CABAJ, A., BARTOSZEWSKA, S., CHARZYNSKA, A., GEBERT, M., DABROWSKI, M., COLLAWN, J. F. & BARTOSZEWSKI, R. 2022. The transition from HIF-1 to HIF-2 during prolonged hypoxia results from reactivation of PHDs and HIF1A mRNA instability. Cell Mol Biol Lett, 27, 109.

JELLA, K. K., RANI, S., O'DRISCOLL, L., MCCLEAN, B., BYRNE, H. J. & LYNG, F. M. 2014. Exosomes Are Involved in Mediating Radiation Induced Bystander Signaling in Human Keratinocyte Cells. Radiation Research, 181, 138-145.

JELONEK, K., WOJAKOWSKA, A., MARCZAK, L., MUER, A., TINHOFER-KEILHOLZ, I., LYSEK-GLADYSINSKA, M., WIDLAK, P. & PIETROWSKA, M. 2015. Ionizing radiation affects protein composition of exosomes secreted in vitro from head and neck squamous cell carcinoma. Acta Biochim Pol, 62, 265-72.

JENA, B. C. & MANDAL, M. 2021. The emerging roles of EVs in anti-cancer drug resistance and tumor progression: An insight towards tumor-microenvironment interaction. Biochimica Et Biophysica Acta-Reviews on Cancer, 1875.

JEPPESEN, D. K., FENIX, A. M., FRANKLIN, J. L., HIGGINBOTHAM, J. N., ZHANG, Q., ZIMMERMAN, L. J., LIEBLER, D. C., PING, J., LIU, Q., EVANS, R., FISSELL, W. H., PATTON, J. G., ROME, L. H., BURNETTE, D. T. & COFFEY, R. J. 2019. Reassessment of Exosome Composition. Cell, 177, 428-445 e18.

JIANG, L., GU, Y., DU, Y., TANG, X., WU, X. & LIU, J. 2021. Engineering EVs Endowed with Targeted Delivery of Triptolide for Malignant Melanoma Therapy. ACS Appl Mater Interfaces, 13, 42411-42428.

JIANG, M., YAN, Y., YANG, K., LIU, Z., QI, J., ZHOU, H., QIAN, N., ZHOU, Q., WANG, T., XU, X., XIAO, X. & DENG, L. 2019. Small molecule nAS-E targeting cAMP response element binding protein (CREB) and CREB-binding protein interaction inhibits breast cancer bone metastasis. J Cell Mol Med, 23, 1224-1234.

JIANG, X. L., HE, S., LIE, Q., QIAN, C. Y., LIU, Z. Q. & LUO, D. Y. 2017. EV microRNA remodels the tumor microenvironment. Peerj, 5.

JIANG, Z. S., SUN, Y. Z., WANG, S. M. & RUAN, J. S. 2017. Epithelial-mesenchymal transition: potential regulator of ABC transporters in tumor progression. J Cancer, 8, 2319-2327.

JOHNSON, D. I. & PRINGLE, J. R. 1990. Molecular characterization of CDC42, a Saccharomyces cerevisiae gene involved in the development of cell polarity. J Cell Biol, 111, 143-52.

JONES, L. B., BELL, C. R., BIBB, K. E., GU, L., COATS, M. T. & MATTHEWS, Q. L. 2018. Pathogens and Their Effect on Exosome Biogenesis and Composition. Biomedicines, 6.

KABAKOV, A. E. & YAKIMOVA, A. O. 2021. Hypoxia-Induced Cancer Cell Responses Driving Radioresistance of Hypoxic Tumors: Approaches to Targeting and Radiosensitizing. Cancers (Basel), 13.

KALLURI, R. & LEBLEU, V. S. 2016. Discovery of Double-Stranded Genomic DNA in Circulating Exosomes. Targeting Cancer, Vol 81, 2016, 81, 275-280.

KAM, W. W. Y. & BANATI, R. B. 2013. Effects of ionizing radiation on mitochondria. Free Radical Biology and Medicine, 65, 607-619.

KAMERKAR, S., LEBLEU, V. S., SUGIMOTO, H., YANG, S., RUIVO, C. F., MELO, S. A., LEE, J. J. & KALLURI, R. 2017. Exosomes facilitate therapeutic targeting of oncogenic KRAS in pancreatic cancer. Nature, 546, 498-503.

KARAYANNOPOULOU, M., KALDRYMIDOU, E., CONSTANTINIDIS, T. C. & DESSIRIS, A. 2001. Adjuvant post-operative chemotherapy in bitches with mammary cancer. Journal of Veterinary Medicine Series a-Physiology Pathology Clinical Medicine, 48, 85-96.

KARAYANNOPOULOU, M. & LAFIONIATIS, S. 2016. Recent advances on canine mammary cancer chemotherapy: A review of studies from 2000 to date. Revue De Medecine Veterinaire, 167, 192-200.

KARIMI, N., DALIRFARDOUEI, R., DIAS, T., LOTVALL, J. & LASSER, C. 2022. Tetraspanins distinguish separate extracellular vesicle subpopulations in human serum and plasma - Contributions of platelet extracellular vesicles in plasma samples. J Extracell Vesicles, 11, e12213.

KAVANAGH, E. L., LINDSAY, S., HALASZ, M., GUBBINS, L. C., WEINER-GORZEL, K., GUANG, M. H. Z., MCGOLDRICK, A., COLLINS, E., HENRY, M., BLANCO-FERNANDEZ, A., P, O. G., FITZPATRICK, P., HIGGINS, M. J., DOWLING, P. & MCCANN, A. 2017. Protein and chemotherapy profiling of extracellular vesicles harvested from therapeutic induced senescent triple negative breast cancer cells. Oncogenesis, 6, e388.

KHAN, S. U., FATIMA, K. & MALIK, F. 2022. Understanding the cell survival mechanism of anoikis-resistant cancer cells during different steps of metastasis. Clinical & Experimental Metastasis, 39, 715-726.

KJENSETH, A., FYKERUD, T.A., SIRNES, S., BRUUN, J., YOHANNES, Z., KOLBERG, M., OMORI, Y., RIVEDAL, E. AND LEITHE, E., 2012. the gap junction channel protein connexin 43 is covalently modified and regulated by sumoylation. journal of biological chemistry, 287, 15851-15861.

KILLOCK, D. 2020. AKT inhibition improves OS in TNBC. Nat Rev Clin Oncol, 17, 135.

KIM, B. R., LEE, S. H., PARK, M. S., SEO, S. H., PARK, Y. M., KWON, Y. J. & RHO, S. B. 2016. MARCKSL1 exhibits anti-angiogenic effects through suppression of VEGFR-2-dependent Akt/PDK-1/mTOR phosphorylation. Oncology Reports, 35, 1041-1048.

KIM, J. Y., KIM, J. K. & KIM, H. 2020. ABCB7 simultaneously regulates apoptotic and non-apoptotic cell death by modulating mitochondrial ROS and HIF1alpha-driven NFkappaB signaling. Oncogene, 39, 1969-1982.

KIM, S., HAN, J., PARK, J. S., KIM, J. H., LEE, E. S., CHA, B. S. & PARK, K. S. 2022. DNA barcode-based detection of EV microRNAs using nucleic acid lateral flow assays for the diagnosis of colorectal cancer. Talanta, 242, 123306.

KIM, S. B., KIM, H. R., PARK, M. C., CHO, S., GOUGHNOUR, P. C., HAN, D., YOON, I., KIM, Y., KANG, T., SONG, E., KIM, P., CHOI, H., MUN, J. Y., SONG, C., LEE, S., JUNG, H. S. & KIM, S. 2017. Caspase-8 controls the secretion of inflammatory lysyl-tRNA synthetase in EVs from cancer cells. J Cell Biol, 216, 2201-2216.

KLOPFLEISCH, R., LENZE, D., HUMMEL, M. & GRUBER, A. D. 2010. Metastatic canine mammary carcinomas can be identified by a gene expression profile that partly overlaps with human breast cancer profiles. Bmc Cancer, 10.

KOBASHIGAWA, S., SUZUKI, K. & YAMASHITA, S. 2011. Ionizing radiation accelerates Drp1-dependent mitochondrial fission, which involves delayed mitochondrial reactive oxygen species production in normal human fibroblast-like cells. Biochemical and Biophysical Research Communications, 414, 795-800.

KOIKE, S. & JAHN, R. 2019. SNAREs define targeting specificity of trafficking vesicles by combinatorial interaction with tethering factors. Nature Communications, 10.

KOJIMA, M., GIMENES-JUNIOR, J. A., LANGNESS, S., MORISHITA, K., LAVOIE-GAGNE, O., ELICEIRI, B., COSTANTINI, T. W. & COIMBRA, R. 2017. Exosomes, not protein or lipids, in mesenteric lymph activate inflammation: Unlocking the mystery of post-shock multiple organ failure. J Trauma Acute Care Surg, 82, 42-50.

KONGE, J., LETEURTRE, F., GOISLARD, M., BIARD, D., MOREL-ALTMEYER, S., VAURIJOUX, A., GRUEL, G., CHEVILLARD, S. & LEBEAU, J. 2018. Breast cancer stem cell-like cells generated during TGFbeta-induced EMT are radioresistant. Oncotarget, 9, 23519-23531.

KORNILOV, R., PUHKA, M., MANNERSTROM, B., HIIDENMAA, H., PELTONIEMI, H., SILJANDER, P., SEPPANEN-KAIJANSINKKO, R. & KAUR, S. 2018. Efficient ultrafiltration-based protocol to deplete extracellular vesicles from fetal bovine serum. J Extracell Vesicles, 7, 1422674.

KORPAL, M., ELL, B. J., BUFFA, F. M., IBRAHIM, T., BLANCO, M. A., CELIA-TERRASSA, T., MERCATALI, L., KHAN, Z., GOODARZI, H., HUA, Y. L., WEI, Y., HU, G. H., GARCIA, B. A., RAGOUSSIS, J., AMADORI, D., HARRIS, A. L. & KANG, Y. B. 2011. Direct targeting of Sec23a by miR-200s influences cancer cell secretome and promotes metastatic colonization. Nature Medicine, 17, 1101-U108.

KOSAKA, N., IGUCHI, H., YOSHIOKA, Y., TAKESHITA, F., MATSUKI, Y. & OCHIYA, T. 2010. Secretory mechanisms and intercellular transfer of microRNAs in living cells. J Biol Chem, 285, 17442-52.

KOULIS, T. A., PHAN, T. & OLIVOTTO, I. A. 2015. Hypofractionated whole breast radiotherapy: current perspectives. Breast Cancer-Targets and Therapy, 7, 363-370.

KOWAL, J., TKACH, M. & THERY, C. 2014. Biogenesis and secretion of exosomes. Curr Opin Cell Biol, 29, 116-25.

KRESOVICH, J. K., XU, Z. L., O'BRIEN, K. M., WEINBERG, C. R., SANDLER, D. P. & TAYLOR, J. A. 2019. Methylation-Based Biological Age and Breast Cancer Risk. Jnci-Journal of the National Cancer Institute, 111, 1051-1058.

KRUGER, S., ABD ELMAGEED, Z. Y., HAWKE, D. H., WORNER, P. M., JANSEN, D. A., ABDEL-MAGEED, A. B., ALT, E. U. & IZADPANAH, R. 2014. Molecular characterization of exosome-like vesicles from breast cancer cells. BMC Cancer, 14, 44.

KUEMMEL, S., HARRACH, H., SCHMUTZLER, R. K., KOSTARA, A., ZIEGLER-LOHR, K., DYSON, M. H., CHIARI, O. & REINISCH, M. 2020. Olaparib for metastatic breast cancer in a patient with a germline PALB2 variant. Npj Breast Cancer, 6.

KUMAR, S., BAL, A., DAS, A., BHATTACHARYYA, S., LAROIYA, I., KHARE, S. & SINGH, G. 2021. Molecular Subtyping of Triple Negative Breast Cancer by Surrogate Immunohistochemistry Markers. Applied Immunohistochemistry & Molecular Morphology, 29, 251-257.

LAI, R. C., ARSLAN, F., LEE, M. M., SZE, N. S., CHOO, A., CHEN, T. S., SALTO-TELLEZ, M., TIMMERS, L., LEE, C. N., EL OAKLEY, R. M., PASTERKAMP, G., DE KLEIJN, D. P. & LIM, S. K. 2010. Exosome secreted by MSC reduces myocardial ischemia/reperfusion injury. Stem Cell Res, 4, 214-22.

LAN, J., LU, H. Q., SAMANTA, D., SALMAN, S., LU, Y. & SEMENZA, G. L. 2018. Hypoxia-inducible factor 1-dependent expression of adenosine receptor 2B promotes breast cancer stem cell enrichment. Proceedings of the National Academy of Sciences of the United States of America, 115, E9640-E9648.

LAN, J., SUN, L., XU, F., LIU, L., HU, F., SONG, D., HOU, Z., WU, W., LUO, X., WANG, J., YUAN, X., HU, J. & WANG, G. 2019. M2 Macrophage-Derived Exosomes Promote Cell Migration and Invasion in Colon Cancer. Cancer Res, 79, 146-158.

LE, M., FERNANDEZ-PALOMO, C., MCNEILL, F. E., SEYMOUR, C. B., RAINBOW, A. J. & MOTHERSILL, C. E. 2017. Exosomes are released by bystander cells exposed to radiation-induced biophoton signals: Reconciling the mechanisms mediating the bystander effect. Plos One, 12.

LEAL-ORTA, E., RAMIREZ-RICARDO, J., GARCIA-HERNANDEZ, A., CORTES-REYNOSA, P. & SALAZAR, E. P. 2022. Extracellular vesicles from MDA-MB-231 breast cancer cells stimulated with insulin-like growth factor 1 mediate an epithelial-mesenchymal transition process in MCF10A mammary epithelial cells. Journal of Cell Communication and Signaling, 16, 531-546.

LEE, C. H., YU, C. C., WANG, B. Y. & CHANG, W. W. 2016. Tumorsphere as an effective in vitro platform for screening anticancer stem cell drugs. Oncotarget, 7, 1215-1226.

LEE, H. D., KIM, Y. H. & KIM, D. S. 2014. Exosomes derived from human macrophages suppress endothelial cell migration by controlling integrin trafficking. European Journal of Immunology, 44, 1156-1169.

LEE, H., PARK, J.H., JUNG, K.H., LIM, J.H. AND HONG, S.S., 2022. HS-173, a novel PI3K inhibitor enhances radiosensitivity of breast cancer cells. International Journal of Radiation Research, 20(2), 347-352.

LEE, J. 2019. A Meta-analysis of the Association Between Physical Activity and Breast Cancer Mortality. Cancer Nursing, 42, 271-285.

LEHMANN, B. D., BAUER, J. A., CHEN, X., SANDERS, M. E., CHAKRAVARTHY, A. B., SHYR, Y. & PIETENPOL, J. A. 2011. Identification of human triple-negative breast cancer subtypes and preclinical models for selection of targeted therapies. Journal of Clinical Investigation, 121, 2750-2767.

LEHUEDE, C., LI, X., DAUVILLIER, S., VAYSSE, C., FRANCHET, C., CLEMENT, E., ESTEVE, D., LONGUE, M., CHALTIEL, L., LE GONIDEC, S., LAZAR, I., GENESTE, A., DUMONTET, C., VALET, P., NIETO, L., FALLONE, F. & MULLER, C. 2019. Adipocytes promote breast cancer resistance to chemotherapy, a process amplified by obesity: role of the major vault protein (MVP). Breast Cancer Res, 21, 7.

LEI, S. Y., ZHENG, R. S., ZHANG, S. W., WANG, S. M., CHEN, R., SUN, K. X., ZENG, H. M., ZHOU, J. C. & WEI, W. Q. 2021. Global patterns of breast cancer incidence and mortality: A population-based cancer registry data analysis from 2000 to 2020. Cancer Communications, 41, 1183-1194.

LI, B., LI, C., ZHU, M., ZHANG, Y., DU, J., XU, Y., LIU, B., GAO, F., LIU, H., CAI, J. & YANG, Y. 2017. Hypoxia-Induced Mesenchymal Stromal Cells Exhibit an Enhanced Therapeutic Effect on Radiation-Induced Lung Injury in Mice due to an Increased Proliferation Potential and Enhanced Antioxidant Ability. Cell Physiol Biochem, 44, 1295-1310.

LI, C. I., MALONE, K. E. & DALING, J. R. 2002. Differences in breast cancer hormone receptor status and histology by race and ethnicity among women 50 years of age and older. Cancer Epidemiol Biomarkers Prev, 11, 601-7.

LI, C. S., ZHANG, J. W., MA, Z. L., ZHANG, F. & YU, W. L. 2018. miR-19b serves as a prognostic biomarker of breast cancer and promotes tumor progression through PI3K/AKT signaling pathway. Oncotargets and Therapy, 11, 4087-4095

LI, H., QI, Z., NIU, Y., YANG, Y., LI, M., PANG, Y., LIU, M., CHENG, X., XU, M. & WANG, Z. 2021. FBP1 regulates proliferation, metastasis, and chemoresistance by participating in C-MYC/STAT3 signaling axis in ovarian cancer. Oncogene, 40, 5938-5949.

LI, H. S., ZHOU, Y. N., LI, L., LI, S. F., LONG, D., CHEN, X. L., ZHANG, J. B., FENG, L. & LI, Y. P. 2019. HIF-1 alpha protects against oxidative stress by directly targeting mitochondria. Redox Biology, 25.

LI, L., YANG, W. T., ZHENG, P. S. & LIU, X. F. 2018. SOX17 restrains proliferation and tumor formation by down-regulating activity of the Wnt/ss-catenin signaling pathway via trans-suppressing ss-catenin in cervical cancer. Cell Death & Disease, 9.

LI, N., LI, Y., GAO, H., LI, J., MA, X., LIU, X., GONG, P., CUI, X. & LI, Y. 2020. Forkhead-box A3 (FOXA3) represses cancer stemness and partially potentiates chemosensitivity by targeting metastasis-associated in colon cancer 1 (MACC1) signaling pathway in colorectal cancer cells. Curr Cancer Drug Targets.

LI, Q., HU, J., SHI, Y., XIAO, M., BI, T., WANG, C., YAN, L. & LI, X. 2021. Exosomal lncAY927529 enhances prostate cancer cell proliferation and invasion through regulating bone microenvironment. Cell Cycle, 20, 2531-2546.

LIANG, M. L., HSIEH, T. H., LIU, Y. R., CHEN, Y. W., LEE, Y. Y., CHANG, F. C., LIN, S. C., HUANG, M. C., DONALD MING-TAK, H., WONG, T. T., YEN, Y. & YANG, M. H. 2018. Significance of cyclin D1 overexpression in progression and radio-resistance of pediatric ependymomas. Oncotarget, 9, 2527-2542.

LIANG, S., XU, H. & YE, B. C. 2022. Membrane-Decorated EVs for Combination Drug Delivery and Improved Glioma Therapy. Langmuir, 38, 299-308.

LICHEN, C.A.O., BAOXING, T.I.A.N., FEILIN, Q.U., QINGHUA, Z.H.A.N.G. AND SHANYU, G.U.O., 2019. Study on serum exosome proteins in metastatic breast cancer patients. Journal of Surgery Concepts & Practice, 24(02), 141.

LIEBER, M. R. 2010. The Mechanism of Double-Strand DNA Break Repair by the Nonhomologous DNA End-Joining Pathway. Annual Review of Biochemistry, Vol 79, 79, 181-211.

LIM, H. Y., IM, K. S., KIM, N. H., KIM, H. W., SHIN, J. I. & SUR, J. H. 2015. Obesity, expression of adipocytokines, and macrophage infiltration in canine mammary tumors. Veterinary Journal, 203, 326-331.

LIN, H. H., LI, X., CHEN, J. L., SUN, X., COOPER, F. N., CHEN, Y. R., ZHANG, W., CHUNG, Y., LI, A., CHENG, C. T., YANG, L., DENG, X., LIU, X., YEN, Y., JOHNSON, D. L., SHIH, H. M., YANG, A. & ANN, D. K. 2012. Identification of an AAA ATPase VPS4B-dependent pathway that modulates epidermal growth factor receptor abundance and signaling during hypoxia. Mol Cell Biol, 32, 1124-38.

LINDBLAD-TOH, K., WADE, C. M., MIKKELSEN, T. S., KARLSSON, E. K., JAFFE, D. B., KAMAL, M., CLAMP, M., CHANG, J. L., KULBOKAS, E. J., ZODY, M. C., MAUCELI, E., XIE, X. H., BREEN, M., WAYNE, R. K., OSTRANDER, E. A., PONTING, C. P., GALIBERT, F., SMITH, D. R., DEJONG, P. J., KIRKNESS, E., ALVAREZ, P., BIAGI, T., BROCKMAN, W., BUTLER, J., CHIN, C. W., COOK, A., CUFF, J., DALY, M. J., DECAPRIO, D., GNERRE, S., GRABHERR, M., KELLIS, M., KLEBER, M., BARDELEBEN, C., GOODSTADT, L., HEGER, A., HITTE, C., KIM, L., KOEPFLI, K. P., PARKER, H. G., POLLINGER, J. P., SEARLE, S. M. J., SUTTER, N. B., THOMAS, R., WEBBER, C., LANDER, E. S. & PLAT, B. I. G. S. 2005. Genome sequence, comparative analysis and haplotype structure of the domestic dog. Nature, 438, 803-819.

LIU, H., LEI, C., HE, Q., PAN, Z., XIAO, D. & TAO, Y. 2018. Nuclear functions of mammalian MicroRNAs in gene regulation, immunity and cancer. Mol Cancer, 17, 64.

LIU, L., ZHANG, Z., ZHOU, L., HU, L., YIN, C., QING, D., HUANG, S., CAI, X. & CHEN, Y. 2020. Cancer associated fibroblasts-derived exosomes contribute to radioresistance through promoting colorectal cancer stem cells phenotype. Exp Cell Res, 391, 111956.

LIU, L. Z., LI, C. Y., CHEN, Q., JING, Y., CARPENTER, R., JIANG, Y., KUNG, H. F., LAI, L. H. & JIANG, B. H. 2011. MiR-21 Induced Angiogenesis through AKT and ERK Activation and HIF-1 alpha Expression. Plos One, 6.

LIU, Q., GUAN, C. C., LIU, C., LI, H. Y., WU, J. B. & SUN, C. G. 2022. Targeting hypoxia-inducible factor-1alpha: A new strategy for triple-negative breast cancer therapy. Biomedicine & Pharmacotherapy, 156.

LIU, Q., PALMGREN, V. A. C., DANEN, E. H. & LE DEVEDEC, S. E. 2022. Acute vs. chronic vs. intermittent hypoxia in breast Cancer: a review on its application in in vitro research. Mol Biol Rep, 49, 10961-10973.

LIU, X., CHEN, H., XU, X., YE, M., CAO, H., XU, L., HOU, Y., TANG, J., ZHOU, D., BAI, Y. & MA, X. 2018. Insulin-like growth factor-1 receptor knockdown enhances radiosensitivity via the HIF-1alpha pathway and attenuates ATM/H2AX/53BP1 DNA repair activation in human lung squamous carcinoma cells. Oncol Lett, 16, 1332-1340.

LIU, X. H., ZHAO, Y. H., ZHANG, W. N., GAO, Y., HUO, M. M., LIU, M., XIAO, Z. F., LIANG, S. F., XU, N. Z. & ZHU, H. X. 2018. Inhibition of survivin enhances radiosensitivity of esophageal cancer cells by switching radiation-induced senescence to apoptosis. Oncotargets and Therapy, 11, 3087-3100.

LIU, Y. P., ZHENG, C. C., HUANG, Y. N., HE, M. L., XU, W. W. & LI, B. 2021. Molecular mechanisms of chemo- and radiotherapy resistance and the potential implications for cancer treatment. Medcomm, 2, 315-340.

LOH, Z. H., DOUMY, G., ARNOLD, C., KJELLSSON, L., SOUTHWORTH, S. H., AL HADDAD, A., KUMAGAI, Y., TU, M. F., HO, P. J., MARCH, A. M., SCHALLER, R. D., BIN MOHD YUSOF, M. S., DEBNATH, T., SIMON, M., WELSCH, R., INHESTER, L., KHALILI, K., NANDA, K., KRYLOV, A. I., MOELLER, S., COSLOVICH, G., KORALEK, J., MINITTI, M. P., SCHLOTTER, W. F., RUBENSSON, J. E., SANTRA, R. & YOUNG, L. 2020. Observation of the fastest chemical processes in the radiolysis of water. Science, 367, 179-182.

LOTVALL, J., HILL, A. F., HOCHBERG, F., BUZAS, E. I., DI VIZIO, D., GARDINER, C., GHO, Y. S., KUROCHKIN, I. V., MATHIVANAN, S., QUESENBERRY, P., SAHOO, S., TAHARA, H., WAUBEN, M. H., WITWER, K. W. & THERY, C. 2014. Minimal experimental requirements for definition of extracellular vesicles and their functions: a position statement from the International Society for Extracellular Vesicles. J Extracell Vesicles, 3, 26913.

LU, C. W., LO, Y. H., CHEN, C. H., LIN, C. Y., TSAI, C. H., CHEN, P. J., YANG, Y. F., WANG, C. H., TAN, C. H., HOU, M. F. & YUAN, S. F. 2017. VLDL and LDL, but not HDL, promote breast cancer cell proliferation, metastasis and angiogenesis. Cancer Lett, 388, 130-138.

LU, H. Q., SAMANTA, D., XIANG, L. S., ZHANG, H. M., HU, H. X., CHEN, I., BULLEN, J. W. & SEMENZA, G. L. 2015. Chemotherapy triggers HIF-1-dependent glutathione synthesis and copper chelation that induces the breast cancer stem cell phenotype. Proceedings of the National Academy of Sciences of the United States of America, 112, E4600-E4609.

LU, K., LIU, G. Y., YANG, L., LIU, F., GAO, L. B., SHI, J. X., DENG, X. L., LI, Q. F., XU, D. H. & SHI, S. L. 2016. Sustainable inflammation transforms hepatic cells by causing oxidative stress injury and potential epithelial-mesenchymal transition. International Journal of Oncology, 49, 971-980.

LUDWIG, N., YERNENI, S. S., MENSHIKOVA, E. V., GILLESPIE, D. G., JACKSON, E. K. & WHITESIDE, T. L. 2020. Simultaneous Inhibition of Glycolysis and Oxidative Phosphorylation Triggers a Multi-Fold Increase in Secretion of Exosomes: Possible Role of 2'3'-cAMP. Sci Rep, 10, 6948.

LUTZ, S. T., JONES, J. & CHOW, E. 2014. Role of radiation therapy in palliative care of the patient with cancer. J Clin Oncol, 32, 2913-9.

LV, M. M., ZHU, X. Y., CHEN, W. X., ZHONG, S. L., HU, Q., MA, T. F., ZHANG, J., CHEN, L., TANG, J. H. & ZHAO, J. H. 2014. EVs mediate drug resistance transfer in MCF-7 breast cancer cells and a probable mechanism is delivery of P-glycoprotein. Tumor Biology, 35, 10773-10779.

LV, Y., MA, X., DU, Y. & FENG, J. 2021. Understanding Patterns of Brain Metastasis in Triple-Negative Breast Cancer and Exploring Potential Therapeutic Targets. Onco Targets Ther, 14, 589-607.

MA, T., FU, B., YANG, X., XIAO, Y. & PAN, M. 2019. Adipose mesenchymal stem cell-derived exosomes promote cell proliferation, migration, and inhibit cell apoptosis via Wnt/beta-catenin signaling in cutaneous wound healing. J Cell Biochem, 120, 10847-10854.

MACIAS, M., REBMANN, V., MATEOS, B., VARO, N., PEREZ-GRACIA, J. L., ALEGRE, E. & GONZALEZ, A. 2019. Comparison of six commercial serum exosome isolation methods suitable for clinical laboratories. Effect in cytokine analysis. Clinical Chemistry and Laboratory Medicine, 57, 1539-1545.

MAKUCH-KOCKA, A., KOCKI, J., BRZOZOWSKA, A., BOGUCKI, J., KOLODZIEJ, P., PLACHNO, B. J. & BOGUCKA-KOCKA, A. 2021. The BIRC Family Genes Expression in Patients with Triple-negative Breast Cancer. Int J Mol Sci, 22.

MANDAL, R., BECKER, S. & STREBHARDT, K. 2021. Targeting CDK9 for Anti-Cancer Therapeutics. Cancers (Basel), 13.

MASOUDI-KHORAM, N., ABDOLMALEKI, P., HOSSEINKHAN, N., NIKOOFAR, A., MOWLA, S. J., MONFARED, H. & BALDASSARRE, G. 2020. Differential miRNAs expression pattern of irradiated breast cancer cell lines is correlated with radiation sensitivity. Scientific Reports, 10.

MASTRANGELO, S., ATTINA, G., TRIARICO, S., ROMANO, A., MAURIZI, P. AND RUGGIERO, A., 2022. The DNA-topoisomerase Inhibitors in Cancer Therapy. Biomedical and Pharmacology Journal, 15(2).

MASUDA, N., LEE, S. J., OHTANI, S., IM, Y. H., LEE, E. S., YOKOTA, I., KUROI, K., IM, S. A., PARK, B. W., KIM, S. B., YANAGITA, Y., OHNO, S., TAKAO, S., AOGI, K., IWATA, H., JEONG, J., KIM, A., PARK, K. H., SASANO, H., OHASHI, Y. & TOI, M. 2017. Adjuvant Capecitabine for Breast Cancer after Preoperative Chemotherapy. N Engl J Med, 376, 2147-2159.

MATHESON, C. J., BACKOS, D. S. & REIGAN, P. 2016. Targeting WEE1 Kinase in Cancer. Trends in Pharmacological Sciences, 37, 872-881.

MATTHAEUS, C., LAHMANN, I., KUNZ, S., JONAS, W., MELO, A. A., LEHMANN, M., LARSSON, E., LUNDMARK, R., KERN, M., BLUHER, M., OLSCHOWSKI, H., KOMPA, J., BRUGGER, B., MULLER, D. N., HAUCKE, V., SCHURMANN, A., BIRCHMEIER, C. & DAUMKE, O. 2020. EHD2-mediated restriction of caveolar dynamics regulates cellular fatty acid uptake. Proceedings of the National Academy of Sciences of the United States of America, 117, 7471-7481.

MCKENZIE, F., FERRARI, P., FREISLING, H., CHAJES, V., RINALDI, S., DE BATLLE, J., DAHM, C. C., OVERVAD, K., BAGLIETTO, L., DARTOIS, L., DOSSUS, L., LAGIOU, P., TRICHOPOULOS,

D., TRICHOPOULOU, A., KROGH, V., PANICO, S., TUMINO, R., ROSSO, S., BUENO-DE-MESQUITA, H. B., MAY, A., PEETERS, P. H., WEIDERPASS, E., BUCKLAND, G., SANCHEZ, M. J., NAVARRO, C., ARDANAZ, E., ANDERSSON, A., SUND, M., ERICSON, U., WIRFALT, E., KEY, T. J., TRAVIS, R. C., GUNTER, M., RIBOLI, E., VERGNAUD, A. C. & ROMIEU, I. 2015. Healthy lifestyle and risk of breast cancer among postmenopausal women in the European Prospective Investigation into Cancer and Nutrition cohort study. International Journal of Cancer, 136, 2640-2648.

MEEHAN, J., GRAY, M., MARTINEZ-PEREZ, C., KAY, C., PANG, L. Y., FRASER, J. A., POOLE, A. V., KUNKLER, I. H., LANGDON, S. P., ARGYLE, D. & TURNBULL, A. K. 2020. Precision Medicine and the Role of Biomarkers of Radiotherapy Response in Breast Cancer. Front Oncol, 10, 628.

MEILLAN, N., VERNEREY, D., LEFEVRE, J. H., MANCEAU, G., SVRCEK, M., AUGUSTIN, J., FLEJOU, J. F., LASCOLS, O., SIMON, J. M., COHEN, R., MAINGON, P., BACHET, J. B. & HUGUET, F. 2019. Mismatch Repair System Deficiency Is Associated With Response to Neoadjuvant Chemoradiation in Locally Advanced Rectal Cancer. International Journal of Radiation Oncology Biology Physics, 105, 824-833.

MELVIN, J. C., WULANINGSIH, W., HANA, Z., PURUSHOTHAM, A. D., PINDER, S. E., FENTIMAN, I., GILLETT, C., MERA, A., HOLMBERG, L. & VAN HEMELRIJCK, M. 2016. Family history of breast cancer and its association with disease severity and mortality. Cancer Med, 5, 942-9.

MENG, Y. C., XU, Q. F., CHEN, L., WANG, L. F. & HU, X. C. 2020. The function of SOX2 in breast cancer and relevant signaling pathway. Pathology Research and Practice, 216.

METCALFE, K. A., FINCH, A., POLL, A., HORSMAN, D., KIM-SING, C., SCOTT, J., ROYER, R., SUN, P. & NAROD, S. A. 2009. Breast cancer risks in women with a family history of breast or ovarian cancer who have tested negative for a BRCA1 or BRCA2 mutation. British Journal of Cancer, 100, 421-425.

METCALFE, K. A., PRICE, M. A., MANSFIELD, C., HALLETT, D. C., LINDEMAN, G. J., FAIRCHILD, A., POSNER, J., FRIEDMAN, S., SNYDER, C., LYNCH, H. T., EVANS, D. G., NAROD, S. A., LIEDE, A. & CONSORTIUM, K. C. F. 2020. Predictors of long-term cancer-related distress among female BRCA1 and BRCA2 mutation carriers without a cancer diagnosis: an international analysis. British Journal of Cancer.

MILLER, E. R., WILSON, C., CHAPMAN, J., FLIGHT, I., NGUYEN, A. M., FLETCHER, C. & RAMSEY, L. 2018. Connecting the dots between breast cancer, obesity and alcohol consumption in middle-aged women: ecological and case control studies. Bmc Public Health, 18.

MISDORP, W., 1999. Histological classification of the mammary tumors of the dog and the cat. World Health Organization International Histological Classification of Tumors of Domestic Animals second series, 7, 1-59.

MITTELBRUNN, M., GUTIERREZ-VAZQUEZ, C., VILLARROYA-BELTRI, C., GONZALEZ, S., SANCHEZ-CABO, F., GONZALEZ, M. A., BERNAD, A. & SANCHEZ-MADRID, F. 2011. Unidirectional transfer of microRNA-loaded exosomes from T cells to antigen-presenting cells. Nat Commun, 2, 282.

MIZENKO, R. R., BROSTOFF, T., ROJALIN, T., KOSTER, H. J., SWINDELL, H. S., LEISEROWITZ, G. S., WANG, A. & CARNEY, R. P. 2021. Tetraspanins are unevenly distributed across single extracellular vesicles and bias sensitivity to multiplexed cancer biomarkers. J Nanobiotechnology, 19, 250.

MLADENOV, E., FAN, X., DUEVA, R., SONI, A. & ILIAKIS, G. 2019. Radiation-dose-dependent functional synergisms between ATM, ATR and DNA-PKcs in checkpoint control and resection in G2-phase. Sci Rep, 9, 8255.

MONAKHOVA, P. A., SHALAEV, P. V. & BONDINA, E. V. 2021. A Comparative Study of Different Software Packages for Nanoparticle Tracking Analysis. Proceedings of the 2021 Ieee Conference of Russian Young Researchers in Electrical and Electronic Engineering (Elconrus), 2832-2835.

MONTAUDON, E., NIKITOROWICZ-BUNIAK, J., SOURD, L., MORISSET, L., EL BOTTY, R., HUGUET, L., DAHMANI, A., PAINSEC, P., NEMATI, F., VACHER, S., CHEMLALI, W., MASLIAH-PLANCHON, J., CHATEAU-JOUBERT, S., REGA, C., LEAL, M. F., SIMIGDALA, N., PANCHOLI, S., RIBAS, R., NICOLAS, A., MESEURE, D., VINCENT-SALOMON, A., REYES, C., RAPINAT, A., GENTIEN, D., LARCHER, T., BOHEC, M., BAULANDE, S., BERNARD, V., DECAUDIN, D., COUSSY, F., LE ROMANCER, M., DUTERTRE, G., TARIQ, Z., COTTU, P., DRIOUCH, K., BIECHE, I., MARTIN, L. A. & MARANGONI, E. 2020. PLK1 inhibition exhibits strong anti-tumoral activity in CCND1-driven breast cancer metastases with acquired palbociclib resistance. Nat Commun, 11, 4053.

MROWCZYNSKI, O. D., MADHANKUMAR, A. B., SUNDSTROM, J. M., ZHAO, Y., KAWASAWA, Y. I., SLAGLE-WEBB, B., MAU, C., PAYNE, R. A., RIZK, E. B., ZACHARIA, B. E. & CONNOR, J. R. 2018. Exosomes impact survival to radiation exposure in cell line models of nervous system cancer. Oncotarget, 9, 36083-36101.

MROZIK, K. M., BLASCHUK, O. W., CHEONG, C. M., ZANNETTINO, A. C. W. & VANDYKE, K. 2018. N-cadherin in cancer metastasis, its emerging role in haematological malignancies and potential as a therapeutic target in cancer. Bmc Cancer, 18.

MULLER, I., STROZYK, E., SCHINDLER, S., BEISSERT, S., OO, H. Z., SAUTER, T., LUCARELLI, P., RAETH, S., HAUSSER, A., AL NAKOUZI, N., FAZLI, L., GLEAVE, M. E., LIU, H., SIMON, H. U., WALCZAK, H., GREEN, D. R., BARTEK, J., DAUGAARD, M. & KULMS, D. 2020. Cancer Cells Employ Nuclear Caspase-8 to Overcome the p53-Dependent G2/M Checkpoint through Cleavage of USP28. Molecular Cell, 77, 970-+.

MURPHY, J. E. J., NUGENT, S., SEYMOUR, C. & MOTHERSILL, C. 2005. Mitochondrial DNA point mutations and a novel deletion induced by direct low-LET radiation and by medium from irradiated cells. Mutation Research-Genetic Toxicology and Environmental Mutagenesis, 585, 127-136.

NAKAMURA, R., ISHII, H., ENDO, K., HOTTA, A., FUJII, E., MIYAZAWA, K. & SAITOH, M. 2018. Reciprocal expression of Slug and Snail in human oral cancer cells. PLoS One, 13, e0199442.

NANBO, A., KAWANISHI, E., YOSHIDA, R. & YOSHIYAMA, H. 2013. Exosomes Derived from Epstein-Barr Virus-Infected Cells Are Internalized via Caveola-Dependent

Endocytosis and Promote Phenotypic Modulation in Target Cells. Journal of Virology, 87, 10334-10347.

NGUYEN, S.T., NGUYEN, H.T.L. AND TRUONG, K.D. 2020. Comparative cytotoxic effects of methanol, ethanol and DMSO on human cancer cell lines. Biomedical Research and Therapy, 7(7), 3855-3859.

NICOLETTO, R. E. & OFNER, C. M. 2022. Cytotoxic mechanisms of doxorubicin at clinically relevant concentrations in breast cancer cells. Cancer Chemotherapy and Pharmacology, 89, 285-311.

NISHIO, M., TERANISHI, Y., MORIOKA, K., YANAGIDA, A. & SHOJI, A. 2020. Real-time assay for exosome membrane fusion with an artificial lipid membrane based on enhancement of gramicidin A channel conductance. Biosensors & Bioelectronics, 150.

NOLAN, M. W., KOGAN, L., GRIFFIN, L. R., CUSTIS, J. T., HARMON, J. F., BILLER, B. J. & LARUE, S. M. 2012. Intensity-Modulated and Image-Guided Radiation Therapy for Treatment of Genitourinary Carcinomas in Dogs. Journal of Veterinary Internal Medicine, 26, 987-995.

NOZAKI, Y., MOTOMURA, H., TAMORI, S., KIMURA, Y., ONAGA, C., KANAI, S., ISHIHARA, Y., OZAKI, A., HARA, Y., HARADA, Y., MANO, Y., SATO, T., SATO, K., SASAKI, K., ISHIGURO, H., OHNO, S. & AKIMOTO, K. 2020. High PKClambda expression is required for ALDH1-positive cancer stem cell function and indicates a poor clinical outcome in late-stage breast cancer patients. PLoS One, 15, e0235747.

NWOKWU, C. D., ISHRAQ BARI, S. M., HUTSON, K. H., BRAUSELL, C. & NESTOROVA, G. G. 2022. ExoPRIME: Solid-phase immunoisolation and OMICS analysis of surface-marker-specific exosomal subpopulations. Talanta, 236, 122870.

OBERKERSCH, R. E., PONTARIN, G., ASTONE, M., SPIZZOTIN, M., ARSLANBAEVA, L., PONTARIN, G., PANIERI, E., RICCIARDI, S., ALLEGA, M. F., BROSSA, A., GRUMATI, P., BUSSOLATI, B., BIFFO, S., TARDITO, S. & SANTORO, M. M. 2022. Aspartate metabolism in endothelial cells activates the mTORC1 pathway to initiate translation during angiogenesis. Developmental Cell, 57, 1241-+.

OGUNSEITAN, O.A., 2022. One health and the environment: from conceptual framework to implementation science. Environment: Science and Policy for Sustainable Development, 64(2), 11-21.

OSHIMORI, N., ORISTIAN, D. & FUCHS, E. 2015. TGF-beta promotes heterogeneity and drug resistance in squamous cell carcinoma. Cell, 160, 963-976.

OSTROWSKI, M., CARMO, N. B., KRUMEICH, S., FANGET, I., RAPOSO, G., SAVINA, A., MOITA, C. F., SCHAUER, K., HUME, A. N., FREITAS, R. P., GOUD, B., BENAROCH, P., HACOHEN, N., FUKUDA, M., DESNOS, C., SEABRA, M. C., DARCHEN, F., AMIGORENA, S., MOITA, L. F. & THERY, C. 2010. Rab27a and Rab27b control different steps of the exosome secretion pathway. Nat Cell Biol, 12, 19-30; sup pp 1-13.

OSUKA, S., ZHU, D., ZHANG, Z. B., LI, C. X., STACKHOUSE, C. T., SAMPETREAN, O., OLSON, J. J., GILLESPIE, G. Y., SAYA, H., WILLEY, C. D. & VAN MEIR, E. G. 2021. IGF1/N-

cadherin/b-catenin/Clusterin signaling axis can mediates adaptive radioresistance in glioblastoma. Cancer Research, 81.

PALAZZOLO, G., ALBANESE, N. N., DI CARA, G., GYGAX, D., VITTORELLI, M. L. & PUCCI-MINAFRA, I. 2012. Proteomic Analysis of Exosome-like Vesicles Derived from Breast Cancer Cells. Anticancer Research, 32, 847-860.

PANJWANI, B., SINGH, V., RANI, A. & MOHAN, V. 2021. Optimum multi-drug regime for compartment model of tumour: cell-cycle-specific dynamics in the presence of resistance. J Pharmacokinet Pharmacodyn, 48, 543-562.

PANJWANI, M. K., ATHERTON, M. J., MALONEYHUSS, M. A., HARAN, K. P., XIONG, A., GUPTA, M., KULIKOVSAYA, I., LACEY, S. F. & MASON, N. J. 2020. Establishing a model system for evaluating CAR T cell therapy using dogs with spontaneous diffuse large B cell lymphoma. Oncoimmunology, 9.

PAOLONI, M., DAVIS, S., LANA, S., WITHROW, S., SANGIORGI, L., PICCI, P., HEWITT, S., TRICHE, T., MELTZER, P. & KHANNA, C. 2009. Canine tumor cross-species genomics uncovers targets linked to osteosarcoma progression. BMC Genomics, 10, 625.

PAPAZOGLOU, L.G., BASDANI, E., RABIDI, S., PATSIKAS, M.N. & KARAYIANNOPOULOU, M. 2014. Current surgical options for mammary tumor removal in dogs. J Vet Sci Med, 2(1), 2-7.

PARK, M. H., CHOI, J. E., KIM, J. R. & BAE, Y. K. 2021. Immunohistochemical Expressions of Senescence-Associated Secretory Phenotype and Its Association With Immune Microenvironments and Clinicopathological Factors in Invasive Breast Cancer. Pathol Oncol Res, 27, 1609795.

PAROLINI, I., FEDERICI, C., RAGGI, C., LUGINI, L., PALLESCHI, S., DE MILITO, A., COSCIA, C., IESSI, E., LOGOZZI, M., MOLINARI, A., COLONE, M., TATTI, M., SARGIACOMO, M. & FAIS, S. 2009. Microenvironmental pH is a key factor for exosome traffic in tumor cells. J Biol Chem, 284, 34211-22.

PATWARDHAN, G. A., MARCZYK, M., WALI, V. B., STERN, D. F., PUSZTAI, L. & HATZIS, C. 2021. Treatment scheduling effects on the evolution of drug resistance in heterogeneous cancer cell populations. NPJ Breast Cancer, 7, 60.

PAWLOWSKI, K. M., MACIEJEWSKI, H., DOLKA, I., MOL, J. A., MOTYL, T. & KROL, M. 2013. Gene expression profiles in canine mammary carcinomas of various grades of malignancy. BMC Vet Res, 9, 78.

PAYTON, C., PANG, L.Y., GRAY, M. AND ARGYLE, D.J., 2021. Exosomes derived from radioresistant breast cancer cells promote therapeutic resistance in naive recipient cells. Journal of personalized medicine, 11, 1310.

PEINADO, H., ALECKOVIC, M., LAVOTSHKIN, S., MATEI, I., COSTA-SILVA, B., MORENO-BUENO, G., HERGUETA-REDONDO, M., WILLIAMS, C., GARCIA-SANTOS, G., GHAJAR, C., NITADORI-HOSHINO, A., HOFFMAN, C., BADAL, K., GARCIA, B. A., CALLAHAN, M. K., YUAN, J., MARTINS, V. R., SKOG, J., KAPLAN, R. N., BRADY, M. S., WOLCHOK, J. D., CHAPMAN, P. B., KANG, Y., BROMBERG, J. & LYDEN, D. 2012. Melanoma exosomes

educate bone marrow progenitor cells toward a pro-metastatic phenotype through MET. Nat Med, 18, 883-91.

PENG, Y., FU, S., HU, W., QIU, Y., ZHANG, L., TAN, R. & SUN, L. Q. 2020. Glutamine synthetase facilitates cancer cells to recover from irradiation-induced G2/M arrest. Cancer Biol Ther, 21, 43-51.

PETROVA, V., ANNICCHIARICO-PETRUZZELLI, M., MELINO, G. & AMELIO, I. 2018. The hypoxic tumour microenvironment. Oncogenesis, 7, 10.

PHAN, T. K., FONSEKA, P., TIXEIRA, R., PATHAN, M., ANG, C. S., OZKOCAK, D. C., MATHIVANAN, S. & POON, I. K. H. 2021. Pannexin-1 channel regulates nuclear content packaging into apoptotic bodies and their size. Proteomics.

PHUYAL, S., HESSVIK, N. P., SKOTLAND, T., SANDVIG, K. & LLORENTE, A. 2014. Regulation of exosome release by glycosphingolipids and flotillins. Febs Journal, 281, 2214-2227.

PINHO, S. S., CARVALHO, S., CABRAL, J., REIS, C. A. & GARTNER, F. 2012. Canine tumors: a spontaneous animal model of human carcinogenesis. Transl Res, 159, 165-72.

POSTHUMADEBOER, J., WURDINGER, T., GRAAT, H. C., VAN BEUSECHEM, V. W., HELDER, M. N., VAN ROYEN, B. J. & KASPERS, G. J. 2011. WEE1 inhibition sensitizes osteosarcoma to radiotherapy. BMC Cancer, 11, 156.

PRADA, I. & MELDOLESI, J. 2016. Binding and Fusion of Extracellular Vesicles to the Plasma Membrane of Their Cell Targets. International Journal of Molecular Sciences, 17.

PRAT, A., ADAMO, B., CHEANG, M. C. U., ANDERS, C. K., CAREY, L. A. & PEROU, C. M. 2013. Molecular Characterization of Basal-Like and Non-Basal-Like Triple-Negative Breast Cancer. Oncologist, 18, 123-133.

PUSTOVALOVA, M., ALHADDAD, L., BLOKHINA, T., SMETANINA, N., CHIGASOVA, A., CHUPROV-NETOCHIN, R., EREMIN, P., GILMUTDINOVA, I., OSIPOV, A. N. & LEONOV, S. 2021. The CD44high Subpopulation of Multifraction Irradiation-Surviving NSCLC Cells Exhibits Partial EMT-Program Activation and DNA Damage Response Depending on Their p53 Status. Int J Mol Sci, 22.

QI, M., XIA, Y., WU, Y., ZHANG, Z., WANG, X., LU, L., DAI, C., SONG, Y., XU, K., JI, W. & ZHAN, L. 2022. Lin28B-high breast cancer cells promote immune suppression in the lung pre-metastatic niche via exosomes and support cancer progression. Nat Commun, 13, 897.

QIAO, X. B., ZHANG, Y. X., SUN, L. S., MA, Q. T., YANG, J., AI, L. P., XUE, J. Q., CHEN, G. L., ZHANG, H., JI, C., GU, X., LEI, H. X., YANG, Y. L. & LIU, C. G. 2021. Association of human breast cancer CD44(-)/CD24(-) cells with delayed distant metastasis. Elife, 10.

QIN, F., FAN, Q., YU, P. K. N., ALMAHI, W. A., KONG, P., YANG, M., CAO, W., NIE, L., CHEN, G. & HAN, W. 2021. Properties and gene expression profiling of acquired radioresistance in mouse breast cancer cells. Ann Transl Med, 9, 628.

QIN, X., GUO, H., WANG, X., ZHU, X., YAN, M., WANG, X., XU, Q., SHI, J., LU, E., CHEN, W. & ZHANG, J. 2019. EV miR-196a derived from cancer-associated fibroblasts confers

cisplatin resistance in head and neck cancer through targeting CDKN1B and ING5. Genome Biol, 20, 12.

QUACKENBUSH, K., AMINI, A., FISHER, C. M. & RABINOVITCH, R. 2017. Regression of a Fungating Tumor After Hypofractionated Radiation Therapy in a Patient With Metastatic Breast Cancer. Cureus, 9.

QUEZADA, C., TORRES, A., NIECHI, I., URIBE, D., CONTRERAS-DUARTE, S., TOLEDO, F., SAN MARTIN, R., GUTIERREZ, J. & SOBREVIA, L. 2018. Role of extracellular vesicles in glioma progression. Mol Aspects Med, 60, 38-51.

RAMOS-CARDONA, X. E., LUO, W. C. & MOHAMMED, S. I. 2022. Advances and challenges of CAR T therapy and suitability of animal models (Review). Molecular and Clinical Oncology, 17.

RANA, S. & ZOLLER, M. 2011. Exosome target cell selection and the importance of exosomal tetraspanins: a hypothesis. Biochemical Society Transactions, 39, 559-562.

RAO, N. A., VAN WOLFEREN, M. E., GRACANIN, A., BHATTI, S. F., KROL, M., HOLSTEGE, F. C. & MOL, J. A. 2009. Gene expression profiles of progestin-induced canine mammary hyperplasia and spontaneous mammary tumors. J Physiol Pharmacol, 60 Suppl 1, 73-84.

RAPOSO, G., NIJMAN, H. W., STOORVOGEL, W., LIEJENDEKKER, R., HARDING, C. V., MELIEF, C. J. & GEUZE, H. J. 1996. B lymphocytes secrete antigen-presenting vesicles. J Exp Med, 183, 1161-72.

RAUCH, E.F. AND DUFT, A., 2005. orientation maps derived from tem diffraction patterns collected with an external ccd camera. in *materials science forum* (vol. 495, pp. 197-202). trans tech publications ltd.

RASOTTO, R., BERLATO, D., GOLDSCHMIDT, M. H. & ZAPPULLI, V. 2017. Prognostic Significance of Canine Mammary Tumor Histologic Subtypes: An Observational Cohort Study of 229 Cases. Vet Pathol, 54, 571-578.

RECLUSA, P., TAVERNA, S., PUCCI, M., DURENDEZ, E., CALABUIG, S., MANCA, P., SERRANO, M. J., SOBER, L., PAUWELS, P., RUSSO, A. & ROLFO, C. 2017. Exosomes as diagnostic and predictive biomarkers in lung cancer. Journal of Thoracic Disease, 9, S1373-S1382.

RICCI, E., MATTEI, E., DUMONTET, C., EATON, C. L., HAMDY, F., VAN DER PLUIJE, G., CECCHINI, M., THALMANN, G., CLEZARDIN, P. & COLOMBEL, M. 2013. Increased Expression of Putative Cancer Stem Cell Markers in the Bone Marrow of Prostate Cancer Patients Is Associated With Bone Metastasis Progression. Prostate, 73, 1738-1746.

RIVERA, P., MELIN, M., BIAGI, T., FALL, T., HAGGSTROM, J., LINDBLAD-TOH, K. & VON EULER, H. 2009. Mammary Tumor Development in Dogs Is Associated with BRCA1 and BRCA2. Cancer Research, 69, 8770-8774.

RIVERA, P. & VON EULER, H. 2011. Molecular biological aspects on canine and human mammary tumors. Vet Pathol, 48, 132-46.

ROHRDANZ, E. & KAHL, R. 1998. Alterations of antioxidant enzyme expression in response to hydrogen peroxide. Free Radical Biology and Medicine, 24, 27-38.

RONTOGIANNI, S., SYNADAKI, E., LI, B., LIEFAARD, M. C., LIPS, E. H., WESSELING, J., WU, W. & ALTELAAR, M. 2019. Proteomic profiling of extracellular vesicles allows for human breast cancer subtyping. Commun Biol, 2, 325.

ROOMAN, I., PINHO, A., PHILLIPS, P., BIANKIN, A. & WU, J. 2017. Altered Slit-Robo signalling activates TGF-beta signalling and stroma remodelling in the pancreas. Pancreatology, 17, 6-7.

RUDT, S. & MULLER, R. H. 1993. In-Vitro Phagocytosis Assay of Nanoparticles and Microparticles by Chemiluminescence .3. Uptake of Differently Sized Surface-Modified Particles, and Its Correlation to Particle Properties and in-Vivo Distribution. European Journal of Pharmaceutical Sciences, 1, 31-39.

RUGAMBA, A., KANG, D. Y., SP, N., JO, E. S., LEE, J. M., BAE, S. W. & JANG, K. J. 2021. Silibinin Regulates Tumor Progression and Tumorsphere Formation by Suppressing PD-L1 Expression in Non-Small Cell Lung Cancer (NSCLC) Cells. Cells, 10.

RUHLAND, M. K., LOZA, A. J., CAPIETTO, A. H., LUO, X. M., KNOLHOFF, B. L., FLANAGAN, K. C., BELT, B. A., ALSPACH, E., LEAHY, K., LUO, J. Q., SCHAFFER, A., EDWARDS, J. R., LONGMORE, G., FACCIO, R., DENARDO, D. G. & STEWART, S. A. 2016. Stromal senescence establishes an immunosuppressive microenvironment that drives tumorigenesis. Nature Communications, 7.

RUHLE, A., PEREZ, R. L., GLOWA, C., WEBER, K. J., HO, A. D., DEBUS, J., SAFFRICH, R., HUBER, P. E. & NICOLAY, N. H. 2017. Cisplatin radiosensitizes radioresistant human mesenchymal stem cells. Oncotarget, 8, 87809-87820.

RUNZ, S., KELLER, S., RUPP, C., STOECK, A., ISSA, Y., KOENSGEN, D., MUSTEA, A., SEHOULI, J., KRISTIANSEN, G. & ALTEVOGT, P. 2007. Malignant ascites-derived exosomes of ovarian carcinoma patients contain CD24 and EpCAM. Gynecol Oncol, 107, 563-71.

RUSHTON, J., NIELSEN, L. R., CORNELSEN, L., QUEENAN, K., RUEGG, S. R. & HASLER, B. 2018. Evaluation of integrated approaches to health with a focus on One Health. Integrated Approaches to Health: A Handbook for the Evaluation of One Health, 14-21.

RUSIDZÉ, M., ADLANMÉRINI, M., & CHANTALAT, E. 2021. Estrogen receptor-α signaling in post-natal mammary development and breast cancers. Cell. Mol. Life Sci. 78, 5681–5705.

RUTLEDGE, B. S., CHOY, W. Y. & DUENNWALD, M. L. 2022. Folding or holding?-Hsp70 and Hsp90 chaperoning of misfolded proteins in neurodegenerative disease. J Biol Chem, 298, 101905.

SABA, C., PAOLONI, M., MAZCKO, C., KISSEBERTH, W., BURTON, J. H., SMITH, A., WILSON-ROBLES, H., ALLSTADT, S., VAIL, D., HENRY, C., LANA, S., EHRHART, E. J., CHARLES, B., KENT, M., LAWRENCE, J., BURGESS, K., BORGATTI, A., SUTER, S., WOODS, P., GORDON, I., VRIGNAUD, P., KHANNA, C. & LEBLANC, A. K. 2016. A Comparative Oncology Study of Iniparib Defines Its Pharmacokinetic Profile and Biological Activity in a Naturally-Occurring Canine Cancer Model. Plos One, 11.

SABOL, R. A., VILLELA, V. A., DENYS, A., FREEMAN, B. T., HARTONO, A. B., WISE, R. M., HARRISON, M. A. A., SANDLER, M. B., HOSSAIN, F., MIELE, L. & BUNNELL, B. A. 2020.

Obesity-Altered Adipose Stem Cells Promote Radiation Resistance of Estrogen Receptor Positive Breast Cancer through Paracrine Signaling. Int J Mol Sci, 21.

SAHIN AKDENIZ, E. & SELCUKI, C. 2022. Investigation of interactions of doxorubicin with purine nucleobases by molecular modeling. J Mol Model, 28, 69.

SAHOO, S., KLYCHKO, E., THORNE, T., MISENER, S., SCHULTZ, K. M., MILLAY, M., ITO, A., LIU, T., KAMIDE, C., AGRAWAL, H., PERLMAN, H., QIN, G., KISHORE, R. & LOSORDO, D. W. 2011. Exosomes from human CD34(+) stem cells mediate their proangiogenic paracrine activity. Circ Res, 109, 724-8.

SAIFULLAH & TSUKAHARA, T. 2022. Integrated analysis of the clinical consequence and associated gene expression of ALK in ALK-positive human cancers. Heliyon, 8, e09878.

SAKAI, O., YAMAMOTO, H., IGASE, M. & MIZUNO, T. 2022. Optimization of Culture Conditions for the Generation of Canine CD20-CAR-T Cells for Adoptive Immunotherapy. In Vivo, 36, 764-772.

SALCEDO, E. C., WINTER, M. B., KHURI, N., KNUDSEN, G. M., SALI, A. & CRAIK, C. S. 2021. Global Protease Activity Profiling Identifies HER2-Driven Proteolysis in Breast Cancer. ACS Chem Biol, 16, 712-723.

SALCEDO, E. C., WINTER, M. B., KHURI, N., KNUDSEN, G. M., SALI, A. & CRAIK, C. S. 2021. Global Protease Activity Profiling Identifies HER2-Driven Proteolysis in Breast Cancer. Acs Chemical Biology, 16, 712-723.

SANDVIG, K., KAVALIAUSKIENE, S. & SKOTLAND, T. 2018. Clathrin-independent endocytosis: an increasing degree of complexity. Histochemistry and Cell Biology, 150, 107-118.

SANSONE, P., SAVINI, C., KURELAC, I., CHANG, Q., AMATO, L. B., STRILLACCI, A., STEPANOVA, A., IOMMARINI, L., MASTROLEO, C., DALY, L., GALKIN, A., THAKUR, B. K., SOPLOP, N., URYU, K., HOSHINO, A., NORTON, L., BONAFE, M., CRICCA, M., GASPARRE, G., LYDEN, D. & BROMBERG, J. 2017. Packaging and transfer of mitochondrial DNA via exosomes regulate escape from dormancy in hormonal therapy-resistant breast cancer. Proc Natl Acad Sci U S A, 114, E9066-E9075.

SANTANDER, A. M., LOPEZ-OCEJO, O., CASAS, O., AGOSTINI, T., SANCHEZ, L., LAMAS-BASULTO, E., CARRIO, R., CLEARY, M. P., GONZALEZ-PEREZ, R. R. & TORROELLA-KOURI, M. 2015. Paracrine Interactions between Adipocytes and Tumor Cells Recruit and Modify Macrophages to the Mammary Tumor Microenvironment: The Role of Obesity and Inflammation in Breast Adipose Tissue. Cancers, 7, 143-178.

SAĞLAM-UÇAR, Ö., DEĞIRMENCI, İ., HALBUTOĞULLARI, Z.S., PÖSTEKI, G., SUBAŞI-DEMIRCI, C., ERMAN, G., KARAÖZ, E. AND UTKAN, N.Z., 2022. The effect of mesenchymal stromal cells ın the microenvironment on cancer development. Medical Oncology, 39(8), 1-10.

SAVINA, A., FADER, C. M., DAMIANI, M. T. & COLOMBO, M. I. 2005. Rab11 promotes docking and fusion of multivesicular bodies in a calcium-dependent manner. Traffic, 6, 131-43.

SCHIFFMAN, J. D. & BREEN, M. 2015. Comparative oncology: what dogs and other species can teach us about humans with cancer. Philosophical Transactions of the Royal Society B-Biological Sciences, 370.

SCHON, K. & TISCHKOWITZ, M. 2018. Clinical implications of germline mutations in breast cancer: TP53. Breast Cancer Research and Treatment, 167, 417-423.

SEO, N., AKIYOSHI, K. & SHIKU, H. 2018. Exosome-mediated regulation of tumor immunology. Cancer Sci, 109, 2998-3004.

SHAH, A., HAIDER, G., ABRO, N., BHUTTO, S., BAQAI, T. I., AKHTAR, S. & ABBAS, K. 2022. Correlation Between Age and Hormone Receptor Status in Women With Breast Cancer. Cureus, 14, e21652.

SHAKYA, A. K. & NAIK, R. R. 2022. The Chemotherapeutic Potentials of Compounds Isolated from the Plant, Marine, Fungus, and Microorganism: Their Mechanism of Action and Prospects. J Trop Med, 2022, 5919453.

SHARMA, A., DHAKATE, M.S. & UPADHYE, S.V. 2020. Chemotheraputic Management of Canine Mammary Tumors. Vet Scan| Online Veterinary Medical Journal, 5(1).

SHEFER, A., YALOVAYA, A. & TAMKOVICH, S. 2022. Exosomes in Breast Cancer: Involvement in Tumor Dissemination and Prospects for Liquid Biopsy. International Journal of Molecular Sciences, 23.

SHEN, Y. J., LE BERT, N., CHITRE, A. A., KOO, C. X., NGA, X. H., HO, S. S., KHATOO, M., TAN, N. Y., ISHII, K. J. & GASSER, S. 2015. Genome-derived cytosolic DNA mediates type I interferon-dependent rejection of B cell lymphoma cells. Cell Rep, 11, 460-73.

SHIMA, E. K., LISTYORINI, D., SUSANTO, H., WISNUBROTO, J. D. P., PRACEPTIN, P. K. H., ARDANA, I. K. K. G., WARDANA, Z. O., ARIYADHINY, M., NISA, S. A. R. & KHASNA, E. N. 2019. WNT5A and CREB Genetic Profiling from Breast Cancer Patients: A Case Study of Malang Population. International Conference on Biology and Applied Science (Icobas), 2120.

SHIMAOKA, M., KAWAMOTO, E., GAOWA, A., OKAMOTO, T. & PARK, E. J. 2019. Connexins and Integrins in Exosomes. Cancers (Basel), 11.

SHIMURA, T., KAKUDA, S., OCHIAI, Y., NAKAGAWA, H., KUWAHARA, Y., TAKAI, Y., KOBAYASHI, J., KOMATSU, K. & FUKUMOTO, M. 2010. Acquired radioresistance of human tumor cells by DNA-PK/AKT/GSK3beta-mediated cyclin D1 overexpression. Oncogene, 29, 4826-37.

SHIMURA, T., NOMA, N., OIKAWA, T., OCHIAI, Y., KAKUDA, S., KUWAHARA, Y., TAKAI, Y., TAKAHASHI, A. & FUKUMOTO, M. 2012. Activation of the AKT/cyclin D1/Cdk4 survival signaling pathway in radioresistant cancer stem cells. Oncogenesis, 1, e12.

SHIMURA, T., NOMA, N., OIKAWA, T., OCHIAI, Y., KAKUDA, S., KUWAHARA, Y., TAKAI, Y., TAKAHASHI, A. & FUKUMOTO, M. 2012. Activation of the AKT/cyclin D1/Cdk4 survival signaling pathway in radioresistant cancer stem cells. Oncogenesis, 1, e12.

SIEGEL, R. L., MILLER, K. D. & JEMAL, A. 2019. Cancer statistics, 2019. CA Cancer J Clin, 69, 7-34.

SILVA, M. & MELO, S. A. 2015. Non-coding RNAs in Exosomes: New Players in Cancer Biology. Curr Genomics, 16, 295-303.

SIMON, D., SCHOENROCK, D., BAUMGARTNER, W. & NOLTE, I. 2006. Postoperative adjuvant treatment of invasive malignant mammary gland tumors in dogs with doxorubicin and docetaxel. J Vet Intern Med, 20, 1184-90.

SINHA, S., HOSHINO, D., HONG, N. H., KIRKBRIDE, K. C., GREGA-LARSON, N. E., SEIKI, M., TYSKA, M. J. & WEAVER, A. M. 2016. Cortactin promotes exosome secretion by controlling branched actin dynamics. J Cell Biol, 214, 197-213.

SONG, F., WANG, C., WANG, C., WANG, J., WU, Y., WANG, Y., LIU, H., ZHANG, Y. & HAN, L. 2022. Multi-Phenotypic Exosome Secretion Profiling Microfluidic Platform for Exploring Single-Cell Heterogeneity. Small Methods, 6, e2200717.

SONG, M., WANG, Y., SHANG, Z. F., LIU, X. D., XIE, D. F., WANG, Q., GUAN, H. & ZHOU, P. K. 2016. Bystander autophagy mediated by radiation-induced exosomal miR-7-5p in non-targeted human bronchial epithelial cells. Scientific Reports, 6.

SONG, Y., BARRY, W. T., SEAH, D. S., TUNG, N. M., GARBER, J. E. & LIN, N. U. 2020. Patterns of recurrence and metastasis in BRCA1/BRCA2-associated breast cancers. Cancer, 126, 271-280.

SOUNG, Y. H., NGUYEN, T., CAO, H., LEE, J. & CHUNG, J. 2016. Emerging roles of exosomes in cancer invasion and metastasis. BMB Rep, 49, 18-25.

SPRING, F. A., GRIFFITHS, R. E., MANKELOW, T. J., AGNEW, C., PARSONS, S. F., CHASIS, J. A. & ANSTEE, D. J. 2013. Tetraspanins CD81 and CD82 facilitate alpha4beta1-mediated adhesion of human erythroblasts to vascular cell adhesion molecule-1. PLoS One, 8, e62654.

STATI, G., PASSARETTA, F., GINDRAUX, F., CENTURIONE, L. & DI PIETRO, R. 2021. The Role of the CREB Protein Family Members and the Related Transcription Factors in Radioresistance Mechanisms. Life (Basel), 11.

STEINBICHLER, T. B., DUDAS, J., SKVORTSOV, S., GANSWINDT, U., RIECHELMANN, H. & SKVORTSOVA, II 2018. Therapy resistance mediated by cancer stem cells. Semin Cancer Biol, 53, 156-167.

STRIETZ, J., STEPPUTTIS, S. S., FOLLO, M., BRONSERT, P., STICKELER, E. & MAURER, J. 2021. Human Primary Breast Cancer Stem Cells Are Characterized by Epithelial-Mesenchymal Plasticity. Int J Mol Sci, 22.

STUFFERS, S., SEM WEGNER, C., STENMARK, H. & BRECH, A. 2009. Multivesicular endosome biogenesis in the absence of ESCRTs. Traffic, 10, 925-37.

SUBBALAKSHMI, A. R., SAHOO, S., BISWAS, K. & JOLLY, M. K. 2021. A Computational Systems Biology Approach Identifies SLUG as a Mediator of Partial Epithelial-Mesenchymal Transition (EMT). Cells Tissues Organs.

SUETA, A., FUJIKI, Y., GOTO-YAMAGUCHI, L., TOMIGUCHI, M., YAMAMOTO-IBUSUKI, M., IWASE, H. & YAMAMOTO, Y. 2021. Exosomal miRNA profiles of triple-negative breast cancer in neoadjuvant treatment. Oncology Letters, 22.

SUN, R., ZENG, Y., FAN, Y., LIN, D., DU, S. AND WANG, X., 2022. A new post-operative prognostic System Combining CEA and CA199 for locally advanced rectal cancer patients undergoing neoadjuvant chemoradiotherapy followed by total mesorectal excision, Research Square 1- 19.

SUN, T., YIN, Y. F., JIN, H. G., LIU, H. R. & TIAN, W. C. 2022. Exosomal microRNA-19b targets FBXW7 to promote colorectal cancer stem cell stemness and induce resistance to radiotherapy. Kaohsiung J Med Sci, 38, 108-119.

SUN, Z. H., CHEN, C., KUANG, X. W., SONG, J. L., SUN, S. R. & WANG, W. X. 2021. Breast surgery for young women with early-stage breast cancer Mastectomy or breast-conserving therapy? Medicine, 100.

SUNG, B. H., KETOVA, T., HOSHINO, D., ZIJLSTRA, A. & WEAVER, A. M. 2015. Directional cell movement through tissues is controlled by exosome secretion. Nature Communications, 6.

SUNG, H., FERLAY, J., SIEGEL, R. L., LAVERSANNE, M., SOERJOMATARAM, I., JEMAL, A. & BRAY, F. 2021. Global cancer statistics 2020: GLOBOCAN estimates of incidence and mortality worldwide for 36 cancers in 185 countries. Ca-a Cancer Journal for Clinicians, 71, 209-249.

SZATMARI, T., PERSA, E., KIS, E., BENEDEK, A., HARGITAI, R., SAFRANY, G. & LUMNICZKY, K. 2018. Extracellular vesicles mediate low dose ionizing radiation-induced immune and inflammatory responses in the blood. International Journal of Radiation Biology, 95, 12-22.

TACCONI, E. M., LAI, X., FOLIO, C., PORRU, M., ZONDERLAND, G., BADIE, S., MICHL, J., SECHI, I., ROGIER, M., MATIA GARCIA, V., BATRA, A. S., RUEDA, O. M., BOUWMAN, P., JONKERS, J., RYAN, A., REINA-SAN-MARTIN, B., HUI, J., TANG, N., BRUNA, A., BIROCCIO, A. & TARSOUNAS, M. 2017. BRCA1 and BRCA2 tumor suppressors protect against endogenous acetaldehyde toxicity. EMBO Mol Med, 9, 1398-1414.

TACHON, G., CORTES, U., GUICHET, P. O., RIVET, P., BALBOUS, A., MASLIANTSEV, K., BERGER, A., BOISSONNADE, O., WAGER, M. & KARAYAN-TAPON, L. 2018. Cell Cycle Changes after Glioblastoma Stem Cell Irradiation: The Major Role of RAD51. International Journal of Molecular Sciences, 19.

TAKAHASHI, K., CHIDA, S., SUWATTHANARAK, T., IIDA, M., ZHANG, M., FUKUYAMA, M., MAEKI, M., ISHIDA, A., TANI, H., YASUI, T., BABA, Y., HIBARA, A., OKOCHI, M. & TOKESHI, M. 2022. Non-competitive fluorescence polarization immunosensing for CD9 detection using a peptide as a tracer. Lab Chip, 22, 2971-2977.

TAN, S. S., YIN, Y., LEE, T., LAI, R. C., YEO, R. W., ZHANG, B., CHOO, A. & LIM, S. K. 2013. Therapeutic MSC exosomes are derived from lipid raft microdomains in the plasma membrane. J Extracell Vesicles, 2.

TANG, Z., DOKIC, I., KNOLL, M., CIAMARONE, F., SCHWAGER, C., KLEIN, C., CEBULLA, G., HOFFMANN, D. C., SCHLEGEL, J., SEIDEL, P., RUTENBERG, C., BRONS, S., HEROLD-MENDE, C., WICK, W., DEBUS, J., LEMKE, D. & ABDOLLAHI, A. 2022. Radioresistance and Transcriptional Reprograming of Invasive Glioblastoma Cells. Int J Radiat Oncol Biol Phys, 112, 499-513.

TENG, F. & FUSSENEGGER, M. 2020. Shedding Light on Extracellular Vesicle Biogenesis and Bioengineering. Adv Sci (Weinh), 8, 2003505.

TENG, Y., REN, Y., HU, X., MU, J., SAMYKUTTY, A., ZHUANG, X., DENG, Z., KUMAR, A., ZHANG, L., MERCHANT, M. L., YAN, J., MILLER, D. M. & ZHANG, H. G. 2017. MVP-mediated exosomal sorting of miR-193a promotes colon cancer progression. Nat Commun, 8, 14448.

TERLECKI-ZANIEWICZ, L., LAMMERMANN, I., LATREILLE, J., BOBBILI, M. R., PILS, V., SCHOSSERER, M., WEINMULLNER, R., DELLAGO, H., SKALICKY, S., PUM, D., ALMARAZ, J. C. H., SCHEIDELER, M., MORIZOT, F., HACKL, M., GRUBER, F. & GRILLARI, J. 2018. Small extracellular vesicles and their miRNA cargo are anti-apoptotic members of the senescence-associated secretory phenotype. Aging-Us, 10, 1103-1132.

TESI, M., MILLANTA, F., POLI, A., MAZZETTI, G., PASQUINI, A., PANZANI, D., ROTA, A. & VANNOZZI, I. 2020. Role of body condition score and adiponectin expression in the progression of canine mammary carcinomas. Vet Med Sci.

THAKUR, P., SEAM, R. K., GUPTA, M. K., GUPTA, M., SHARMA, M. & FOTEDAR, V. 2017. Breast cancer risk factor evaluation in a Western Himalayan state: A case-control study and comparison with the Western World. South Asian J Cancer, 6, 106-109.

THAYANITHY, V., BABATUNDE, V., DICKSON, E. L., WONG, P., OH, S., KE, X., BARLAS, A., FUJISAWA, S., ROMIN, Y., MOREIRA, A. L., DOWNEY, R. J., STEER, C. J., SUBRAMANIAN, S., MANOVA-TODOROVA, K., MOORE, M. A. & LOU, E. 2014. Tumor exosomes induce tunneling nanotubes in lipid raft-enriched regions of human mesothelioma cells. Exp Cell Res, 323, 178-88.

THERY, C., WITWER, K. W., AIKAWA, E., ALCARAZ, M. J., ANDERSON, J. D., ANDRIANTSITOHAINA, R., ANTONIOU, A., ARAB, T., ARCHER, F., ATKIN-SMITH, G. K., AYRE, D. C., BACH, J. M., BACHURSKI,D., BAHARVAND, H., BALAJ, L., BALDACCHINO, S., BAUER, N. N., BAXTER, A. A., BEBAWY, M., BECKHAM, C., BEDINA ZAVEC, A., BENMOUSSA, A., BERARDI, A. C., BERGESE, P., BIELSKA, E., BLENKIRON, C., BOBIS-WOZOWICZ, S., BOILARD, E., BOIREAU, W., BONGIOVANNI, A., BORRAS, F. E., BOSCH, S., BOULANGER, C. M., BREAKEFIELD, X., BREGLIO, A. M., BRENNAN, M. A., BRIGSTOCK, D. R., BRISSON, A., BROEKMAN, M. L., BROMBERG, J. F., BRYL-GORECKA, P., BUCH, S., BUCK, A. H., BURGER, D., BUSATTO, S., BUSCHMANN, D., BUSSOLATI, B., BUZAS, E. I., BYRD, J. B., CAMUSSI, G., CARTER, D. R., CARUSO, S., CHAMLEY, L. W., CHANG, Y. T., CHEN, C., CHEN, S., CHENG, L., CHIN, A. R., CLAYTON, A., CLERICI, S. P., COCKS, A., COCUCCI, E., COFFEY, R. J., CORDEIRO-DA-SILVA, A., COUCH, Y., COUMANS, F. A., COYLE, B., CRESCITELLI, R., CRIADO, M. F., D'SOUZA-SCHOREY, C., DAS, S., DATTA CHAUDHURI, A., DE CANDIA, P., DE SANTANA, E. F., DE WEVER, O., DEL PORTILLO, H. A., DEMARET, T., DEVILLE, S., DEVITT, A., DHONDT, B., DI VIZIO, D., DIETERICH, L. C., DOLO, V., DOMINGUEZ RUBIO, A. P., DOMINICI, M., DOURADO, M. R., DRIEDONKS, T. A., DUARTE, F. V., DUNCAN, H. M., EICHENBERGER, R. M., EKSTROM, K., EL ANDALOUSSI, S., ELIE-CAILLE, C., ERDBRUGGER, U., FALCON-PEREZ, J. M., FATIMA, F., FISH, J. E., FLORES-BELLVER, M., FORSONITS, A., FRELET-BARRAND, A., 2018. Minimal information for studies of extracellular vesicles 2018 (MISEV2018): a position statement of the International Society for Extracellular Vesicles and update of the MISEV2014 guidelines. J Extracell Vesicles, 7, 1535750.

THOMAS, S. N., LIAO, Z., CLARK, D., CHEN, Y., SAMADANI, R., MAO, L., ANN, D. K., BAULCH, J. E., SHAPIRO, P. & YANG, A. J. 2013. Exosomal Proteome Profiling: A Potential Multi-Marker Cellular Phenotyping Tool to Characterize Hypoxia-Induced Radiation Resistance in Breast Cancer. Proteomes, 1, 87-108.

THUMSER-HENNER, P., NYTKO, K. J. & BLEY, C. R. 2020. Mutations of BRCA2 in canine mammary tumors and their targeting potential in clinical therapy. Bmc Veterinary Research, 16.

TIAN, T., ZHU, Y. L., ZHOU, Y. Y., LIANG, G. F., WANG, Y. Y., HU, F. H. & XIAO, Z. D. 2014. Exosome Uptake through Clathrin-mediated Endocytosis and Macropinocytosis and Mediating miR-21 Delivery. Journal of Biological Chemistry, 289, 22258-22267.

TIAN, Y. H., XIE, G. Z., REN, C., SUN, Q. Q., SUN, A. M., LIU, Y. & YUAN, Y. W. 2011. [Radiation-induced G2 phase arrest may contribute to the radioresistance of breast cancer stem cells]. Nan Fang Yi Ke Da Xue Xue Bao, 31, 53-6.

TODOROVIC, V., PREVC, A., ZAKELJ, M. N., SAVARIN, M., BROZIC, A., GROSELJ, B., STROJAN, P., CEMAZAR, M. & SERSA, G. 2019. Mechanisms of different response to ionizing irradiation in isogenic head and neck cancer cell lines. Radiat Oncol, 14, 214.

TOLOUEE, M., HENDRIKS, K. D. W., LIE, F. F., GARTZKE, L. P., GORIS, M., HOOGSTRA-BERENDS, F., BERGINK, S. & HENNING, R. H. 2022. Cooling of Cells and Organs Confers Extensive DNA Strand Breaks Through Oxidative Stress and ATP Depletion. Cell Transplant, 31, 9636897221108705.

TOME-GARCIA, J., ERFANI, P., NUDELMAN, G., TSANKOV, A. M., KATSYV, I., TEJERO, R., BIN, Z., WALSH, M., FRIEDEL, R. H., ZASLAVSKY, E. & TSANKOVA, N. M. 2018. Analysis of chromatin accessibility uncovers TEAD1 as a regulator of migration in human glioblastoma. Nat Commun, 9, 4020.

TOMINAGA, N., KOSAKA, N., ONO, M., KATSUDA, T., YOSHIOKA, Y., TAMURA, K., LOTVALL, J., NAKAGAMA, H. & OCHIYA, T. 2015. Brain metastatic cancer cells release microRNA-181c-containing extracellular vesicles capable of destructing blood-brain barrier. Nature Communications, 6.

TOMITA, M., MAEDA, M., KOBAYASHI, K. & MATSUMOTO, H. 2013. Dose response of soft X-ray-induced bystander cell killing affected by p53 status. Radiat Res, 179, 200-7.

TORTOLICI, F., VUMBACA, S., INCOCCIATI, B., DAYAL, R., AQUILANO, K., GIOVANETTI, A. & RUFINI, S. 2021. Ionizing Radiation-Induced Extracellular Vesicle Release Promotes AKT-Associated Survival Response in SH-SY5Y Neuroblastoma Cells. Cells, 10.

TOSS, A. AND CORTESI, L., 2013. Molecular mechanisms of PARP inhibitors in BRCA-related ovarian cancer. J. Cancer Sci. Ther, 5(11).

TRAJKOVIC, K., HSU, C., CHIANTIA, S., RAJENDRAN, L., WENZEL, D., WIELAND, F., SCHWILLE, P., BRUGGER, B. & SIMONS, M. 2008. Ceramide triggers budding of exosome vesicles into multivesicular endosomes. Science, 319, 1244-7.

TRAN, C. M., MOORE, A. S. & FRIMBERGER, A. E. 2016. Surgical treatment of mammary carcinomas in dogs with or without postoperative chemotherapy. Vet Comp Oncol, 14, 252-62.

TREPS, L., PERRET, R., EDMOND, S., RICARD, D. & GAVARD, J. 2017. Glioblastoma stem-like cells secrete the pro-angiogenic VEGF-A factor in extracellular vesicles. Journal of Extracellular Vesicles, 6.

TSENG, L. M., CHIU, J. H., LIU, C. Y., TSAI, Y. F., WANG, Y. L., YANG, C. W. & SHYR, Y. M. 2017. A comparison of the molecular subtypes of triple-negative breast cancer among non-Asian and Taiwanese women. Breast Cancer Research and Treatment, 163, 241-254.

TUNCER, G. S., DEMIR, H., IZMIRLI, M., CAKIR, T., YILMAZER, G. & DEMIR, C. 2022. Effect of radiotherapy on erythrocyte catalase, and carbonic anhydrase activities, serum levels of some trace elements and heavy metals (Zn, Cu, Pb, Cd, Mn, Fe, Mg and Co) in cancer patients. International Journal of Radiation Research, 20, 97-102.

TURNA, O., UVEZ, A., BAYKAL, A., DEVELI, E. S., DIRAMALI, M., SONMEZ, K., KARAKAS, D., KASIKCI, G., ARMUTAK, E. I. & ULUKAYA, E. 2022. Evidence for heterogeneity in response to treatment in mammary tumors of dogs as happens in humans. Veterinary Research Communications.

TUTANOV, O., ORLOVA, E., PROSKURA, K., GRIGOR'EVA, A., YUNUSOVA, N., TSENTALOVICH, Y., ALEXANDROVA, A. & TAMKOVICH, S. 2020. Proteomic Analysis of Blood EVs from Healthy Females and Breast Cancer Patients Reveals an Association between Different EV Bioactivity on Non-tumorigenic Epithelial Cell and Breast Cancer Cell Migration in Vitro. Biomolecules, 10.

VALERO, M. G., MOO, T. A., MUHSEN, S., ZABOR, E. C., STEMPEL, M., PUSIC, A., GEMIGNANI, M. L., MORROW, M. & SACCHINI, V. 2020. Use of bilateral prophylactic nipple-sparing mastectomy in patients with high risk of breast cancer. British Journal of Surgery.

VAN BEIJNUM, J. R., HUIJBERS, E. J. M., VAN LOON, K., BLANAS, A., AKBARI, P., ROOS, A., WONG, T. J., DENISOV, S. S., HACKENG, T. M., JIMENEZ, C. R., NOWAK-SLIWINSKA, P. & GRIFFIOEN, A. W. 2022. Extracellular vimentin mimics VEGF and is a target for anti-angiogenic immunotherapy. Nature Communications, 13.

VAN DALEN, E. C., VAN DER PAL, H. J. H. & KREMER, L. C. M. 2016. Different dosage schedules for reducing cardiotoxicity in people with cancer receiving anthracycline chemotherapy. Cochrane Database of Systematic Reviews.

VAN DER POL, E., BOING, A. N., HARRISON, P., STURK, A. & NIEUWLAND, R. 2012. Classification, Functions, and Clinical Relevance of Extracellular Vesicles. Pharmacological Reviews, 64, 676-705.

VAN DONGEN, H. M., MASOUMI, N., WITWER, K. W. & PEGTEL, D. M. 2016. Extracellular Vesicles Exploit Viral Entry Routes for Cargo Delivery. Microbiology and Molecular Biology Reviews, 80, 369-386.

VAN NIEL, G., CHARRIN, S., SIMOES, S., ROMAO, M., ROCHIN, L., SAFTIG, P., MARKS, M. S., RUBINSTEIN, E. & RAPOSO, G. 2011. The Tetraspanin CD63 Regulates ESCRT-Independent and -Dependent Endosomal Sorting during Melanogenesis. Developmental Cell, 21, 708-721.

VAQUERO, J., GUEDJ, N., CLAPERON, A., NGUYEN HO-BOULDOIRES, T. H., PARADIS, V. & FOUASSIER, L. 2017. Epithelial-mesenchymal transition in cholangiocarcinoma: From clinical evidence to regulatory networks. J Hepatol, 66, 424-441.

VARALLO, G. R., GELALETI, G. B., MASCHIO-SIGNORINI, L. B., MOSCHETTA, M. G., LOPES, J. R., DE NARDI, A. B., TINUCCI-COSTA, M., ROCHA, R. M. & DE CAMPOS ZUCCARI, D. A. P. 2019. Prognostic phenotypic classification for canine mammary tumors. Oncol Lett, 18, 6545-6553.

VASCELLARI, M., CAPELLO, K., CARMINATO, A., ZANARDELLO, C., BAIONI, E. & MUTINELLI, F. 2016. Incidence of mammary tumors in the canine population living in the Veneto region (Northeastern Italy): Risk factors and similarities to human breast cancer. Prev Vet Med, 126, 183-9.

VILLARROYA-BELTRI, C., BAIXAULI, F., GUTIERREZ-VAZQUEZ, C., SANCHEZ-MADRID, F. & MITTELBRUNN, M. 2014. Sorting it out: regulation of exosome loading. Semin Cancer Biol, 28, 3-13.

VILLARROYA-BELTRI, C., BAIXAULI, F., MITTELBRUNN, M., FERNANDEZ-DELGADO, I., TORRALBA, D., MORENO-GONZALO, O., BALDANTA, S., ENRICH, C., GUERRA, S. & SANCHEZ-MADRID, F. 2016. ISGylation controls exosome secretion by promoting lysosomal degradation of MVB proteins. Nat Commun, 7, 13588.

VON EULER, H., KHOSHNOUD, R., HE, Q. M., KHOSHNOUD, A., FORNANDER, T., RUTQVIST, L. E. & SKOG, S. 2005. Time-dependent RNA degradation affecting cDNA array quality in spontaneous canine tumours sampled using standard surgical procedures. International Journal of Molecular Medicine, 16, 979-985.

VORSELEN, D., PIONTEK, M. C., ROOS, W. H. & WUITE, G. J. L. 2020. Mechanical Characterization of Liposomes and Extracellular Vesicles, a Protocol. Frontiers in Molecular Biosciences, 7.

WAN, H., LI, Z., WANG, H., CAI, F. & WANG, L. 2021. ST8SIA1 inhibition sensitizes triple negative breast cancer to chemotherapy via suppressing Wnt/beta-catenin and FAK/Akt/mTOR. Clin Transl Oncol, 23, 902-910.

WANG, C., XU, J., YUAN, D., BAI, Y., PAN, Y., ZHANG, J. & SHAO, C. 2020. Exosomes carrying ALDOA and ALDH3A1 from irradiated lung cancer cells enhance migration and invasion of recipients by accelerating glycolysis. Mol Cell Biochem, 469, 77-87.

WANG, K. & TEPPER, J. E. 2021. Radiation Therapy-Associated Toxicity: Etiology, Management, and Prevention. Ca-a Cancer Journal for Clinicians, 71, 437-454.

WANG, M., JI, S., SHAO, G., ZHANG, J., ZHAO, K., WANG, Z. & WU, A. 2018. Effect of exosome biomarkers for diagnosis and prognosis of breast cancer patients. Clinical & Translational Oncology, 20, 906-911.

WANG, S., LI, F., YE, T., WANG, J., LYU, C., QING, S., DING, Z., GAO, X., JIA, R., YU, D., REN, J., WEI, W. & MA, G. 2021. Macrophage-tumor chimeric exosomes accumulate in lymph node and tumor to activate the immune response and the tumor microenvironment. Sci Transl Med, 13, eabb6981.

WANG, T., GILKES, D. M., TAKANO, N., XIANG, L. S., LUO, W. B., BISHOP, C. J., CHATURVEDI, P., GREEN, J. J. & SEMENZA, G. L. 2014. Hypoxia-inducible factors and RAB22A mediate formation of microvesicles that stimulate breast cancer invasion and metastasis. Proceedings of the National Academy of Sciences of the United States of America, 111, E3234-E3242.

WANG, W. L. W., SOROKIN, I., ALEKSIC, I., FISHER, H., KAUFMAN, R. P., WINER, A., MCNEILL, B., GUPTA, R., TILKI, D., FLESHNER, N., KLOTZ, L., DIRIENZO, A. G. & TENNISWOOD, M. 2020. Expression of Small Noncoding RNAs in Urinary Exosomes Classifies Prostate Cancer into Indolent and Aggressive Disease. Journal of Urology, 204, 466-474.

WANG, Z., SUN, H. X., PROVAZNIK, J., HACKERT, T. & ZOLLER, M. 2019. Pancreatic cancer-initiating cell exosome message transfer into noncancer-initiating cells: the importance of CD44v6 in reprogramming. Journal of Experimental & Clinical Cancer Research, 38.

WEBBER, J. P., SPARY, L. K., SANDERS, A. J., CHOWDHURY, R., JIANG, W. G., STEADMAN, R., WYMANT, J., JONES, A. T., KYNASTON, H., MASON, M. D., TABI, Z. & CLAYTON, A. 2015. Differentiation of tumour-promoting stromal myofibroblasts by cancer exosomes. Oncogene, 34, 319-331.

WEBER, W. P., HAUG, M., KURZEDER, C., BJELIC-RADISIC, V., KOLLER, R., REITSAMER, R., FITZAL, F., BIAZUS, J., BRENELLI, F., URBAN, C., PAULINELLI, R. R., BLOHMER, J. U., HEIL, J., HOFFMANN, J., MATRAI, Z., CATANUTO, G., GALIMBERTI, V., GENTILINI, O., BARRY, M., HADAR, T., ALLWEIS, T. M., OLSHA, O., CARDOSO, M. J., GOUVEIA, P. F., RUBIO, I. T., DE BONIFACE, J., SVENSJO, T., BUCHER, S., DUBSKY, P., FARHADI, J., FEHR, M. K., FULCO, I., GANZ-BLATTLER, U., GUNTHERT, A., HARDER, Y., HAUSER, N., KAPPOS, E. A., KNAUER, M., LANDIN, J., MECHERA, R., MEANI, F., MONTAGNA, G., RITTER, M., SACCILOTTO, R., SCHWAB, F. D., STEFFENS, D., TAUSCH, C., ZEINDLER, J., SOYSAL, S. D., LOHSIRIWAT, V., KOVACS, T., TANSLEY, A., WYLD, L., ROMICS, L., EL-TAMER, M., PUSIC, A. L., SACCHINI, V. & GNANT, M. 2018. Oncoplastic Breast Consortium consensus conference on nipple-sparing mastectomy. Breast Cancer Res Treat, 172, 523-537.

WEI, D. H., ZHAN, W. X., GAO, Y., HUANG, L. Y., GONG, R., WANG, W., ZHANG, R. H., WU, Y. Z., GAO, S. & KANG, T. B. 2021. RAB31 marks and controls an ESCRT-independent exosome pathway. Cell Research, 31, 157-177.

WEINMAN, M. A., RAMSEY, S. A., LEEPER, H. J., BRADY, J. V., SCHLUETER, A., STANISHEUSKI, S., MAIER, C. S., MILLER, T., RUBY, C. E. & BRACHA, S. 2021. EV proteomic signatures correlate with drug resistance and carboplatin treatment outcome in a spontaneous model of canine osteosarcoma. Cancer Cell International, 21.

WEN, S. Y., ALI, A., HUANG, I. C., LIU, J. S., CHEN, P. Y., PADMA VISWANADHA, V., HUANG, C. Y. & KUO, W. W. 2023. Doxorubicin induced ROS-dependent HIF1alpha activation mediates blockage of IGF1R survival signaling by IGFBP3 promotes cardiac apoptosis. Aging (Albany NY), 15, 164-178.

WESTBROOK, R. L., BRIDGES, E., ROBERTS, J., ESCRIBANO-GONZALEZ, C., EALES, K. L., VETTORE, L. A., WALKER, P. D., VERA-SIGUENZA, E., RANA, H., CUOZZO, F., ESKLA, K. L., VELLAMA, H., SHAABAN, A., NIXON, C., LUUK, H., LAVERY, G. G., HODSON, D. J., HARRIS,

A. L. & TENNANT, D. A. 2022. Proline synthesis through PYCR1 is required to support cancer cell proliferation and survival in oxygen-limiting conditions. Cell Reports, 38.

WHEELER, D. A., SRINIVASAN, M., EGHOLM, M., SHEN, Y., CHEN, L., MCGUIRE, A., HE, W., CHEN, Y. J., MAKHIJANI, V., ROTH, G. T., GOMES, X., TARTARO, K., NIAZI, F., TURCOTTE, C. L., IRZYK, G. P., LUPSKI, J. R., CHINAULT, C., SONG, X. Z., LIU, Y., YUAN, Y., NAZARETH, L., QIN, X., MUZNY, D. M., MARGULIES, M., WEINSTOCK, G. M., GIBBS, R. A. & ROTHBERG, J. M. 2008. The complete genome of an individual by massively parallel DNA sequencing. Nature, 452, 872-6.

WHITESIDE, T. L. 2017. The effect of tumor-derived exosomes on immune regulation and cancer immunotherapy. Future Oncology, 13, 2583-2592.

WINER, E. P., LIPATOV, O., IM, S. A., GONCALVES, A., MUNOZ-COUSELO, E., LEE, K. S., SCHMID, P., TAMURA, K., TESTA, L., WITZEL, I., OHTANI, S., TURNER, N., ZAMBELLI, S., HARBECK, N., ANDRE, F., DENT, R., ZHOU, X., KARANTZA, V., MEJIA, J., CORTES, J. & INVESTIGATORS, K.-. 2021. Pembrolizumab versus investigator-choice chemotherapy for metastatic triple-negative breast cancer (KEYNOTE-119): a randomised, open-label, phase 3 trial. Lancet Oncology, 22, 499-511.

WOLF, P. 1967. The nature and significance of platelet products in human plasma. Br J Haematol, 13, 269-88.

WONG, G. L., ABU JALBOUSH, S. & LO, H. W. 2020. Exosomal MicroRNAs and Organotropism in Breast Cancer Metastasis. Cancers (Basel), 12.

WOOLSTON, C. M., AL-ATTAR, A., STORR, S. J., ELLIS, I. O., MORGAN, D. A. L. & MARTIN, S. G. 2011. Redox Protein Expression Predicts Radiotherapeutic Response in Early-Stage Invasive Breast Cancer Patients. International Journal of Radiation Oncology Biology Physics, 79, 1530-1540.

WOOLSTON, C. M., STORR, S. J., ELLIS, I. O., MORGAN, D. A. L. & MARTIN, S. G. 2011. Expression of thioredoxin system and related peroxiredoxin proteins is associated with clinical outcome in radiotherapy treated early stage breast cancer. Radiotherapy and Oncology, 100, 308-313.

WORSLEY, C. M., VEALE, R. B. & MAYNE, E. S. 2022. The acidic tumour microenvironment: Manipulating the immune response to elicit escape. Human Immunology, 83, 399-408.

WU, H. J., HAO, M. G., YEO, S. K. & GUAN, J. L. 2020. FAK signaling in cancer-associated fibroblasts promotes breast cancer cell migration and metastasis by exosomal miRNAs-mediated intercellular communication. Oncogene, 39, 2539-2549.

XIAO, D. Y., BARRY, S., KMETZ, D., EGGER, M., PAN, J. M., RAI, S. N., QU, J. F., MCMASTERS, K. M. & HAO, H. Y. 2016. Melanoma cell-derived EVs promote epithelial-mesenchymal transition in primary melanocytes through paracrine/autocrine signaling in the tumor microenvironment. Cancer Letters, 376, 318-327.

XIAO, H. & XU, Y. 2021. Overexpression of Apolipoprotein C1 (APOC1) in Clear Cell Renal Cell Carcinoma and Its Prognostic Significance. Med Sci Monit, 27, e929347.

XIN, Y., WANG, J. J., WU, Y. H., LI, Q. Q., DONG, M. Y., LIU, C., HE, Q. J., WANG, R. F., WANG, D., JIANG, S., XIAO, W., TIAN, Y. & ZHANG, W. W. 2022. Identification of Nanog as a novel inhibitor of Rad51. Cell Death & Disease, 13.

XU, B., CHEN, H., XU, Z., YAO, X., SUN, X. & CHENG, H. 2021. CDCA2 promotes tumorigenesis and induces radioresistance in oesophageal squamous cell carcinoma cells. Mol Med Rep, 24.

XU, M., JI, J., JIN, D., WU, Y., WU, T., LIN, R., ZHU, S., JIANG, F., JI, Y., BAO, B. AND LI, M., 2022. The biogenesis and secretion of exosomes and multivesicular bodies (MVBs): Intercellular shuttles and implications in human diseases. Genes & Diseases.

XU, S., HUANG, H., TANG, D., XING, M., ZHAO, Q., LI, J., SI, J., GAN, L., MAO, A. & ZHANG, H. 2021. Diallyl Disulfide Attenuates Ionizing Radiation-Induced Migration and Invasion by Suppressing Nrf2 Signaling in Non-small-Cell Lung Cancer. Dose Response, 19, 15593258211033114.

XU, T. T., ZENG, X. W., WANG, X. H., YANG, L. X., LUO, G. & YU, T. 2021. Cystatin-B Negatively Regulates the Malignant Characteristics of Oral Squamous Cell Carcinoma Possibly Via the Epithelium Proliferation/Differentiation Program. Frontiers in Oncology, 11.

YADAV, P. & SHANKAR, B. S. 2019. Radio resistance in breast cancer cells is mediated through TGF-beta signalling, hybrid epithelial-mesenchymal phenotype and cancer stem cells. Biomedicine & Pharmacotherapy, 111, 119-130.

YAMAMORI, T., IKE, S., BO, T., SASAGAWA, T., SAKAI, Y., SUZUKI, M., YAMAMOTO, K., NAGANE, M., YASUI, H. & INANAMI, O. 2015. Inhibition of the mitochondrial fission protein dynamin-related protein 1 (Drp1) impairs mitochondrial fission and mitotic catastrophe after x-irradiation. Molecular Biology of the Cell, 26, 4607-4617.

YAMASHITA, T., TAKAHASHI, Y., NISHIKAWA, M. & TAKAKURA, Y. 2016. Effect of EV isolation methods on physicochemical properties of EVs and clearance of EVs from the blood circulation. Eur J Pharm Biopharm, 98, 1-8.

YAN, J., KIM, Y. S., YANG, X. P., LI, L. P., LIAO, G., XIA, F. & JETTEN, A. M. 2007. The ubiquitin-interacting motif containing protein RAP80 interacts with BRCA1 and functions in DNA damage repair response. Cancer Res, 67, 6647-56.

YANG, H., REN, S., YU, S., PAN, H., LI, T., GE, S., ZHANG, J. & XIA, N. 2020. Methods Favoring Homology-Directed Repair Choice in Response to CRISPR/Cas9 Induced-Double Strand Breaks. Int J Mol Sci, 21.

YANG, J., ANTIN, P., BERX, G., BLANPAIN, C., BRABLETZ, T., BRONNER, M., CAMPBELL, K., CANO, A., CASANOVA, J., CHRISTOFORI, G., DEDHAR, S., DERYNCK, R., FORD, H. L., FUXE, J., GARCIA DE HERREROS, A., GOODALL, G. J., HADJANTONAKIS, A. K., HUANG, R. Y. J., KALCHEIM, C., KALLURI, R., KANG, Y., KHEW-GOODALL, Y., LEVINE, H., LIU, J., LONGMORE, G. D., MANI, S. A., MASSAGUE, J., MAYOR, R., MCCLAY, D., MOSTOV, K. E., NEWGREEN, D. F., NIETO, M. A., PUISIEUX, A., RUNYAN, R., SAVAGNER, P., STANGER, B., STEMMLER, M. P., TAKAHASHI, Y., TAKEICHI, M., THEVENEAU, E., THIERY, J. P., THOMPSON, E. W., WEINBERG, R. A., WILLIAMS, E. D., XING, J., ZHOU, B. P., SHENG, G. &

ASSOCIATION, E. M. T. I. 2020. Guidelines and definitions for research on epithelial-mesenchymal transition. Nat Rev Mol Cell Biol, 21, 341-352.

YANG, L., SHEN, C., ESTRADA-BERNAL, A., ROBB, R., CHATTERJEE, M., SEBASTIAN, N., WEBB, A., MO, X., CHEN, W., KRISHNAN, S. & WILLIAMS, T. M. 2021. Oncogenic KRAS drives radioresistance through upregulation of NRF2-53BP1-mediated non-homologous end-joining repair. Nucleic Acids Res, 49, 11067-11082.

YANG, S. S., MA, S., DOU, H., LIU, F., ZHANG, S. Y., JIANG, C., XIAO, M. & HUANG, Y. X. 2020. Breast cancer-derived EVs regulate cell invasion and metastasis in breast cancer via miR-146a to activate cancer associated fibroblasts in tumor microenvironment. Exp Cell Res, 391, 111983.

YANG, Y. Y., BUCAN, V., BAEHRE, H., VON DER OHE, J., OTTE, A. & HASS, R. 2015. Acquisition of new tumor cell properties by MSC-derived EVs. International Journal of Oncology, 47, 244-252.

YE, Z., ZHANG, T., HE, W., JIN, H., LIU, C., YANG, Z. & REN, J. 2018. Methotrexate-Loaded Extracellular Vesicles Functionalized with Therapeutic and Targeted Peptides for the Treatment of Glioblastoma Multiforme. ACS Appl Mater Interfaces, 10, 12341-12350.

YING, X., WU, Q. F., WU, X. L., ZHU, Q. Y., WANG, X. J., JIANG, L., CHEN, X. & WANG, X. P. 2016. Epithelial ovarian cancer-secreted exosomal miR-222-3p induces polarization of tumor-associated macrophages. Oncotarget, 7, 43076-43087.

YOKOI, A., VILLAR-PRADOS, A., OLIPHINT, P. A., ZHANG, J., SONG, X., DE HOFF, P., MOREY, R., LIU, J., ROSZIK, J., CLISE-DWYER, K., BURKS, J. K., O'HALLORAN, T. J., LAURENT, L. C. & SOOD, A. K. 2019. Mechanisms of nuclear content loading to EVs. Sci Adv, 5, eaax8849.

YONG, T., ZHANG, X., BIE, N., ZHANG, H., ZHANG, X., LI, F., HAKEEM, A., HU, J., GAN, L., SANTOS, H. A. & YANG, X. 2019. Tumor exosome-based nanoparticles are efficient drug carriers for chemotherapy. Nat Commun, 10, 3838.

YOSHIKAWA, Y., MORIMATSU, M., OCHIAI, K., ISHIGURO-OONUMA, T., WADA, S., ORINO, K. & WATANABE, K. 2015. Reduced canine BRCA2 expression levels in mammary gland tumors. BMC Vet Res, 11, 159.

YOULDEN, D. R., CRAMB, S. M., YIP, C. H. & BAADE, P. D. 2014. Incidence and mortality of female breast cancer in the Asia-Pacific region. Cancer Biol Med, 11, 101-15.

YU, L. L., ZHU, J., LIU, J. X., JIANG, F., NI, W. K., QU, L. S., NI, R. Z., LU, C. H. & XIAO, M. B. 2018. A Comparison of Traditional and Novel Methods for the Separation of EVs from Human Samples. Biomed Res Int, 2018, 3634563.

YU, Y., WANG, W., LU, W., CHEN, W. & SHANG, A. 2021. Inhibin beta-A (INHBA) induces epithelial-mesenchymal transition and accelerates the motility of breast cancer cells by activating the TGF-beta signaling pathway. Bioengineered, 12, 4681-4696.

ZAMBRANO-ESTRADA, X., LANDAVERDE-QUIROZ, B., DUENAS-BOCANEGRA, A. A., DE PAZ-CAMPOS, M. A., HERNANDEZ-ALBERTO, G., SOLORIO-PERUSQUIA, B., TREJO-MANDUJANO, M., PEREZ-GUERRERO, L., DELGADO-GONZALEZ, E., ANGUIANO, B. & ACEVES, C. 2018. Molecular iodine/doxorubicin neoadjuvant treatment impair invasive

capacity and attenuate side effect in canine mammary cancer. Bmc Veterinary Research, 14.

ZECCHIN, A., KALUCKA, J., DUBOIS, C. & CARMELIET, P. 2017. How endothelial Cells Adapt Their Metabolism to Form vessels in Tumors. Frontiers in Immunology, 8.

ZENG, X., LIU, C., YAO, J., WAN, H., WAN, G., LI, Y. & CHEN, N. 2021. Breast cancer stem cells, heterogeneity, targeting therapies and therapeutic implications. Pharmacol Res, 163, 105320.

ZEVIAN, S. C., JOHNSON, J. L., WINTERWOOD, N. E., WALTERS, K. S., HERNDON, M. E., HENRY, M. D. & STIPP, C. S. 2015. CD151 promotes alpha3beta1 integrin-dependent organization of carcinoma cell junctions and restrains collective cell invasion. Cancer Biol Ther, 16, 1626-40.

ZHANG, H., DENG, T., LIU, R., BAI, M., ZHOU, L., WANG, X., LI, S., WANG, X., YANG, H., LI, J., NING, T., HUANG, D., LI, H., ZHANG, L., YING, G. & BA, Y. 2017. Exosome-delivered EGFR regulates liver microenvironment to promote gastric cancer liver metastasis. Nat Commun, 8, 15016.

ZHANG, H. R., LU, J., LIU, J., ZHANG, G. & LU, A. P. 2020. Advances in the discovery of exosome inhibitors in cancer. Journal of Enzyme Inhibition and Medicinal Chemistry, 35, 1322-1330.

ZHANG, H. Y., FREITAS, D., KIM, H. S., FABIJANIC, K., LI, Z., CHEN, H. Y., MARK, M. T., MOLINA, H., MARTIN, A. B., BOJMAR, L., FANG, J., RAMPERSAUD, S., HOSHINO, A., MATEI, I., KENIFIC, C. M., NAKAJIMA, M., MUTVEI, A. P., SANSONE, P., BUEHRING, W., WANG, H. J., JIMENEZ, J. P., COHEN-GOULD, L., PAKNEJAD, N., BRENDEL, M., MANOVA-TODOROVA, K., MAGALHAES, A., FERREIRA, J. A., OSORIO, H., SILVA, A. M., MASSEY, A., CUBILLOS-RUIZ, J. R., GALLETTI, G., GIANNAKAKOU, P., CUERVO, A. M., BLENIS, J., SCHWARTZ, R., BRADY, M. S., PEINADO, H., BROMBERG, J., MATSUI, H., REIS, C. A. & LYDEN, D. 2018. Identification of distinct nanoparticles and subsets of extracellular vesicles by asymmetric flow field-flow fractionation. Nature Cell Biology, 20, 332-+.

ZHANG, L., ZHAN, S. Y., YAO, J., LOWERY, F. J., ZHANG, Q. L., HUANG, W. C., LI, P., LI, M., WANG, X., ZHANG, C. Y., WANG, H., ELLIS, K., CHEERATHODI, M., MCCARTY, J. H., PALMIERI, D., SAUNUS, J., LAKHANI, S., HUANG, S. Y., SAHIN, A. A., ALDAPE, K. D., STEEG, P. S. & YU, D. H. 2015. Microenvironment-induced PTEN loss by exosomal microRNA primes brain metastasis outgrowth. Nature, 527, 100-104.

ZHANG, L. L., YAN, T., WANG, W. M., WU, Q., LI, G. Y., LI, D. D., STOVALL, D. B., WANG, Y. X., LI, Y. H. & SUI, G. C. 2021. AKT1 is positively regulated by G-quadruplexes in its promoter and 3 '-UTR. Biochemical and Biophysical Research Communications, 561, 93-100.

ZHANG, T. C., LI, X., HE, Y. N., WANG, Y. H., SHEN, J. J., WANG, S. L., YOU, Q., ZHAI, J. & SHEN, L. Z. 2022. Cancer-associated fibroblasts-derived HAPLN1 promotes tumour invasion through extracellular matrix remodeling in gastric cancer. Gastric Cancer, 25, 346-359.

ZHANG, W., YANG, S., CHEN, D., YUWEN, D., ZHANG, J., WEI, X., HAN, X. & GUAN, X. 2022. SOX2-OT induced by PAI-1 promotes triple-negative breast cancer cells metastasis by sponging miR-942-5p and activating PI3K/Akt signaling. Cell Mol Life Sci, 79, 59.

ZHAO, WENYAN, MING SUN, SHUQIANG LI, ZHAOFU CHEN, AND DONGHUA GENG. 2018. "Transcription factor ATF 3 mediates the radioresistance of breast cancer." Journal of cellular and molecular medicine 22(10), 4664-4675.

ZHAO, H., YANG, L., BADDOUR, J., ACHREJA, A., BERNARD, V., MOSS, T., MARINI, J. C., TUDAWE, T., SEVIOUR, E. G., SAN LUCAS, F. A., ALVAREZ, H., GUPTA, S., MAITI, S. N., COOPER, L., PEEHL, D., RAM, P. T., MAITRA, A. & NAGRATH, D. 2016. Tumor microenvironment derived exosomes pleiotropically modulate cancer cell metabolism. Elife, 5, e10250.

ZHAO, Y., CHEN, Y., WANG, J. & LIU, L. 2021. Effects of ATP-binding cassette transporter G2 in extracellular vesicles on drug resistance of laryngeal cancer cells in in vivo and in vitro. Oncol Lett, 21, 364.

ZHOU, S., LAN, Y., LI, Y., LI, Z., PU, J. & WEI, L. 2022. Hypoxic Tumor-Derived Exosomes Induce M2 Macrophage Polarization via PKM2/AMPK to Promote Lung Cancer Progression. Cell Transplant, 31, 9636897221106998.

ZHU, M. J., XIE, S., XIE, Q., ZHU, J. L. & HUANG, Y. Z. 2021. Effecacy of Biejia (Carapax Trionycis) and Ezhu (Rhizoma Curcumae Phaeocaulis) couplet medicine on epithelial-mesenchymal transition, invasion and migration of MDA-MB-231 triple negative breast cancer cells via PI3K/Akt/mTOR signaling pathway. J Tradit Chin Med, 41, 853-861.

ZHU, Y.G., SHI, M.M., MONSEL, A., DAI, C.X., DONG, X., SHEN, H., LI, S.K., CHANG, J., XU, C.L., LI, P. AND WANG, J., 2022. nebulized exosomes derived from allogenic adipose tissue mesenchymal stromal cells in patients with severe covid-19: a pilot study. stem cell research & therapy, 13, 1-10.

ZIMTA, A. A., TIGU, A. B., MUNTEAN, M., CENARIU, D., SLABY, O. & BERINDAN-NEAGOE, I. 2019. Molecular Links between Central Obesity and Breast Cancer. International Journal of Molecular Sciences, 20.

Chapter 8: Appendix

Cell line datasheets

Public Health England

General Cell Collection Detail

ECACC General Cell Collection: REM 134

Supplied by:	European Collection of Authenticated Cell Cultures (ECACC)
Culture Type:	Cell line
Collection:	ECACC General Collection
Catalogue No.:	12122002
Cell Line Name:	REM 134
Citation Guidance:	If use of this culture results in a scientific publication, it should be cited in the publication as: REM 134 (ECACC 12122002)
Keywords:	Mammary, carcinoma, canine
Cell Line Description:	REM 134 is a canine mammary carcinoma cell line derived from a spontaneous primary tumour.
Species:	Canine
Tissue of Origin:	Mammary
CellType:	mixed population of polygonal cells
Growth Mode:	Adherent
Biosafety Information:	Unless specified otherwise, at the European Collection of Authenticated Cell Cultures (ECACC) we routinely handle all of our cell lines at containment level 2 in accordance with the ACDP guidelines. ACDP = Advisory Committee on Dangerous Pathogens (UK) All cell cultures have the potential to carry as yet unidentified adventitious agents. It is the responsibility of the end user to ensure that their facilities comply with biosafety regulations for their own country. ACDP Guidance: Biological agents: Managing the risks in laboratories and healthcare premises. Hyperlinks to MSDS documents: Frozen cell cultures Material Safety Data Sheet Growing cell cultures Material Safety Data Sheet Nucleic acids derived from cell cultures Material Safety Data Sheet
Subculture Routine:	Split sub-confluent cultures (70-80%) seed new cultures at 2-4x10,000 cells/cm² using 0.05% trypsin or trypsin/EDTA; 5% CO_2; 37°C.
Culture Medium:	EMEM + 2mM Glutamine + 10% Foetal Bovine Serum (FBS).
Depositor:	Professor RW Else, University of Edinburgh, Royal (Dick) School of Veterinary Studies, Easter Bush Veterinary Centre, Easter Bush, Midlothian, EH25 9RG.
Originator:	Yes
Country:	UK
References:	Else RW, Norval M, Neill WA.1982 The characteristics of a canine mammary carcinoma cell line, REM 134. Br J Cancer.46(4):675-81. PMID: 7138772

Public Health England

General Cell Collection Detail

ECACC General Cell Collection: MDA-MB-231

Supplied by:	European Collection of Authenticated Cell Cultures (ECACC)
Culture Type:	Cell line
Collection:	ECACC General Collection
Catalogue No.:	92020424
Cell Line Name:	MDA-MB-231
Citation Guidance:	If use of this culture results in a scientific publication, it should be cited in the publication as: MDA-MB-231 (ECACC 92020424)
Keywords:	Human Caucasian breast adenocarcinoma
Cell Line Description:	MDA-MB-231 was established from a pleural effusion of a 51 year old woman with metastatic breast cancer.
Species:	Human
Tissue of Origin:	Breast
CellType:	Epithelial
Growth Mode:	Adherent
DNA Profile:	STR-PCR Data: Amelogenin: X CSF1PO: 12,13 D13S317: 13 D16S539: 12 D5S818: 12 D7S820: 8,9 THO1: 7,9.3 TPOX: 8,9 vWA: 15,18
Karyotype:	Range 52-68, Modal number 64, near triploid
Biosafety Information:	Unless specified otherwise, at the European Collection of Authenticated Cell Cultures (ECACC) we routinely handle all of our cell lines at containment level 2 in accordance with the ACDP guidelines. ACDP = Advisory Committee on Dangerous Pathogens (UK) All cell cultures have the potential to carry as yet unidentified adventitious agents. It is the responsibility of the end user to ensure that their facilities comply with biosafety regulations for their own country. ACDP Guidance: Biological agents: Managing the risks in laboratories and healthcare premises. Hyperlinks to MSDS documents: Frozen cell cultures Material Safety Data Sheet Growing cell cultures Material Safety Data Sheet Nucleic acids derived from cell cultures Material Safety Data Sheet
Subculture Routine:	Split sub-confluent cultures (70-80%) 1:3 to 1:6, i.e. seeding at 1-3 x10,000 cells/cm² using 0.05% trypsin or trypsin/EDTA; 37°C. CO_2 is not required.
Culture Medium:	L15 + 2mM Glutamine + 15% Foetal Bovine Serum (FBS).

Continued overleaf…

Continued…

Depositor:	The University of Texas M. D. Anderson Cancer Center Office of Technology Commercialization 7515 S. Main, Suite 490, Unit 0510 Houston, Texas 77030
Originator:	Yes
Country:	USA
References:	Cailleau R, Young R, Olivé M, Reeves WJ Jr 1974 Breast tumor cell lines from pleural effusions. J Natl Cancer Inst. 53(3):661-74. PMID: 4412247.
Additional Bibliography:	Cruciger QV, Pathak S, Cailleau R.1976 Human breast carcinomas: marker chromosomes involving 1q in seven cases. Cytogenet Cell Genet. 17(4):231-5. PMID: 1001030. Cailleau R, Olivé M, Cruciger QV 1978 Long-term human breast carcinoma cell lines of metastatic origin: preliminary characterization. In Vitro. 14(11):911-5.PMID: 730202. Brinkley BR, Beall PT, Wible LJ, Mace ML, Turner DS, Cailleau RM 1980 Variations in cell form and cytoskeleton in human breast carcinoma cells in vitro. Cancer Res.;40(9):3118-29.PMID: 7000337. Siciliano MJ, Barker PE, Cailleau R 1979 Mutually exclusive genetic signatures of human breast tumor cell lines with a common chromosomal marker. Cancer Res.39(3):919-22. PMID: 427779. Huguet EL, McMahon JA, McMahon AP, Bicknell R, Harris AL 1994 Differential expression of human Wnt genes 2, 3, 4, and 7B in human breast cell lines and normal and disease states of human breast tissue. Cancer Res. 54(10):2615-21. PMID: 8168088. Bates SE, Valverius EM, Ennis BW, Bronzert DA, Sheridan JP, Stampfer MR, Mendelsohn J, Lippman ME, Dickson RB 1990 Expression of the transforming growth factor-alpha/epidermal growth factor receptor pathway in normal human breast epithelial cells. Endocrinology. 126(1):596-607. PMID: 2294006. Satya-Prakash KL, Pathak S, Hsu TC, Olivé M, Cailleau R.1981 Cytogenetic analysis on eight human breast tumor cell lines: high frequencies of 1q, 11q and HeLa-like marker chromosomes.Cancer Genet Cytogenet. 3(1):61-73. PMID: 7272986. Littlewood-Evans AJ, Bilbe G, Bowler WB, Farley D, Wlodarski B, Kokubo T, Inaoka T, Sloane J, Evans DB, Gallagher JA.1997 The osteoclast-associated protease cathepsin K is expressed in human breast carcinoma. Cancer Res. 57(23):5386-90. PMID: 9393764. Abaan OD, Polley EC, Davis SR, Zhu YJ, Bilke S, Walker RL, Pineda M, Gindin Y, Jiang Y, Reinhold WC, Holbeck SL, Simon RM, Doroshow JH, Pommier Y, Meltzer PS.2013 The exomes of the NCI-60 panel: a genomic resource for cancer biology and systems pharmacology. Cancer Res. 73(14):4372-82. PMID: 23856246.
Patents:	None specified by Depositor
Release Conditions:	Yes - commercial organisations are required to complete the 'Cell Line Release Authorisation for Research Use in Commercial Organisations' release conditions form.

Chapter 9: Publicatinos

Payton, C., Pang, L.Y., Gray, M. and Argyle, D.J., 2021. Exosomes Derived from Radioresistant Breast Cancer Cells Promote Therapeutic Resistance in Naïve Recipient Cells. *Journal of personalized medicine*, *11*(12), p.1310.